REACTIONS, ADSORPTION AND DIFFUSION IN FCC CATALYSTS

by

Wafa Mahaly

A Thesis Presented to the Faculty of the
American University of Sharjah
College of Engineering
in Partial Fulfillment
of the Requirements
for the Degree of

Master of Science in
Chemical Engineering

Sharjah, United Arab Emirates

June 2013

Approval Signatures

We, the undersigned, approve the Master's Thesis of Wafa Mahaly.

Thesis Title: Reactions, Adsorption and Diffusion in FCC Catalyst

Signature	**Date of Signature**
_____	_____
Dr. Kevin Francis Loughlin Professor, Department of Chemical Engineering Thesis Advisor	
_____	_____
Dr. Rachid Chebbi Professor, Department of Chemical Engineering Thesis Committee Member	
_____	_____
Dr. Yehya A. El-Sayed Assistant Professor, Department of Biology, Chemistry and Environmental Sciences Thesis Committee Member	
_____	_____
Dr. Naif Darwish Head, Department of Chemical Engineering	
_____	_____
Dr. Hany El Kadi Associate Dean, College of Engineering	
_____	_____
Dr. Leland Blank Interim Dean, College of Engineering	
_____	_____
Dr. Khaled Assaleh Director of Graduate Studies	

Acknowledgements

I would like to start with the name of Allah most Merciful, most Gracious. First and foremost, I would like to thank Allah for all the blessings He has bestowed on me. I am most grateful to get the opportunity to pursue my Master degree and complete this work successfully.

After that, I would like to thank my advisor, Dr. Kevin Loughlin who was abundantly helpful and offered invaluable assistance, support and guidance. He inspired me greatly to work in this thesis. His willingness to motivate me contributed tremendously to my thesis. I wish to express my sincere gratitude to my committee members, Dr. Rachid Chebbi from the Chemical Engineering Department and Dr. Yehya A. El-Sayed from the Department of Biology, Chemistry and Environmental Sciences for their constructive criticism. I would also like to thank the Department of Chemical Engineering at the American University of Sharjah for offering me the opportunity to attain my master degree and recognize the joy of research.

This thesis would not have been possible without the support of my parents. I wish to express my deepest gratitude to my parents for their endless love and support. Special thanks to my siblings, relatives and friends for their help and support through the duration of my studies. Finally, I would like to thank all the people who have been helpful in the successful completion of this thesis.

Abstract

The objective of this MS thesis is to study the reactions, adsorption and diffusion in FCC catalysts. The effects of different parameters on catalytic cracking are studied. Three main cases are considered: isothermal reactions with adsorption and diffusion, nonisothermal reactions with adsorption and diffusion and isothermal reactions with adsorption and diffusion in an active matrix. In each case, the conditions are varied and the effects of different parameters are studied.

It is concluded that for an isothermal process the conversion increases with Thiele modulus and Biot number and decreases with the ratio of bulk to solids volumes and degree of nonlinearity. For a nonisothermal process, the conversion decreases if the heat transfer resistance is the controlling step. When diffusion and adsorption processes occur simultaneously in the macropore and micropore, macropore processes slow the diffusion and therefore reduce the conversion. The conversion is further decreased if the three resistances are significant: external fluid film resistance, macropore and micropore diffusion.

The models developed are applied to gas oil data and to 1,3,5-triisopropylbenzene (1,3,5-TIPB) data at two different temperatures. The finite volume model with external fluid film resistance gives the best fit for the gas oil data. Different reaction sets are considered for 1,3,5-TIPB and it is found that the parallel reactions of 1,3-diisopropylbenzene (1,3-DIPB) at 400 ℃ gives the best fit while the second order reaction for cumene gives the best fit at 550℃. It was checked that the optimized Thiele moduli follow Arrhenius equation. To find the reaction constants, diffusivities and adsorption constants should be measured experimentally.

Keywords: reactions, adsorption, diffusion, FCC, gas oil, 1,3,5-TIPB, zeolite, modeling, Thiele modulus.

Table of Contents

List of Figures

List of Tables

Abbreviations

a	Order of the reaction
A	Orthogonal collocation matrix
b	Langmuir equilibrium constant (Pa^{-1})
b_0	Pre-exponential of Langmuir constant (Pa^{-1})
B	Orthogonal collocation matrix
Bi_m	Mass transfer Biot number
Bi	Biot number
C	Concentration in bulk vapor (mol/m^3) Concentration of the bulk phase in the macropore (mol/m^3) (Chapter 5)
C_∞	Concentration as $t \rightarrow \infty$ (mol/m^3)
C_s	Surface concentration (mol/m^3)
C_s	Concentration of the adsorbed phase in the macropore (mol/m^3) (Chapter 5)
C_p	Heat capacity (kJ/kmol.K)
D	Diffusivity (m^2/s)
D_0	Corrected diffusivity (m^2/s)
D_c	Micropore diffusivity (m^2/s)
D_e	Effective diffusivity (m^2/s)
D_p	Macropore diffusivity (m^2/s)
$\mathcal{D}_p$	Effective Macropore diffusivity (m^2/s)
E	Activation energy (kJ/mol)
E_D	Diffusional activation energy (kJ/mol)

ΔG	Gibbs free energy (kJ/mol)
H	Heat transfer coefficient ($W/m^2.K$)
ΔH	Heat of adsorption (kJ/mol) (Chapter 2)
ΔH_{ad}	Heat of adsorption (kJ/mol)
ΔH_{rxn}	Heat of reaction (kJ/mol)
J	Diffusive flux ($mol/m^2.s$)
k	Reaction rate constant (s^{-1} for first order reaction)
k	Thermal conductivity (W/m.K) (Chapter 4)
k_0	Pre-exponential of Arrhenius law (s^{-1} for first order reaction)
k_f	Film mass transfer coefficient (m/s)
K	Henry's law constant
K'	Henry's law constant in terms of partial pressure ($mol/m^3.Pa$)
K_0	Pre-exponential of Henry's law
K_c	Henry's law constant in the micropore
K_p	Henry's law constant in the macropore
Le	Lewis number
M_c	Concentration in the micropore at t (mol/m^3) (Chapter 5)
M_p	Concentration in the macropore at t (mol/m^3) (Chapter 5)
M_t	Total concentration in the particle at t (mol/m^3) (Chapter 5)
MW	Molecular weight (g/mol)
N	Number of catalyst particles
N	Number of collocation points

P	Pressure (Pa)
q	Concentration of the adsorbed phase (mol/m^3) Concentration of the bulk phase in the micropore (mol/m^3) (Chapter 5)
q_∞	Adsorbed phase concentration as $t \rightarrow \infty$ (mol/m^3)
q_0	Initial adsorbed phase concentration (mol/m^3)
q_s	Saturation limit in Langmuir isotherm (mol/m^3)
q_s	Concentration of the adsorbed phase in the micropore (mol/m^3) (Chapter 5)
$\dot{q}$	Heat generated (W/m^3)
r	Radial distance in the micropore (m)
r_A	Reaction rate ($mol/m^3.s$ for first order reaction)
r_c	Radius of zeolite crystal (m)
R	Radial distance in the macropore (m)
R_p	Radius of the particle (m)
R	Gas constant (J/mol.K)
ΔS	Entropy (J/mol.K)
S_p	Surface area of the macropore (m^2)
t	Time (s)
T	Temperature (K)
T_0	Reference temperature (K)
T_i	Initial temperature (K)
T_∞	Temperature of the surrounding fluid (K)
V	Volume of the bulk fluid (m^3)
V_s	Volume of the solid particles (m^3)

W	Weight fractions in orthogonal collocation
x	Distance (m)
y_A	Mass fraction of component A

Greek letters

α	Thermal diffusivity (m^2/s)
α	Ratio of the diffusional time constants (Chapter 5)
β	Dimensionless parameter (Chapter 5)
γ	Ratio of micropore and macropore diffusional time constant
γ_{ad}	Dimensionless heat of adsorption
γ_{rxn}	Dimensionless heat of reaction
ϵ_c	Micropore porosity of adsorbent particle
ϵ_p	Macropore porosity of adsorbent particle
η	Effectiveness factor
θ	Fractional saturation
λ	Deactivation parameter
λ	Degree of isotherm nonlinearity (Chapter 3)
Λ	Ratio of the bulk to solids volumes
τ	Tortuosity
ϕ	Deactivation function
φ	Thiele modulus

Abbreviations

1,3,5-TIPB	1,3,5-triisopropylbenzene
1,3-DIPB	1,3-diisopropylbenzene
1,2,4-TMB	1,2,4-trimethylbenzene
1,2,3-TMB	1,2,3-trimethylbenzene
1,3,5-TMB	1,3,5-trimethylbenzene
1,2,3,4-TeMB	1,2,3,4-tetramethylbenzene
1,2,3,5-TeMB	1,2,3,5-tetramethylbenzene
1,2,4,5-TeMB	1,2,4,5-tetramethylbenzene
CAT-SC	Small crystallite zeolite
CAT-LC	Large crystallite zeolite

Chapter 1. Introduction

1.1 FCC

Crude oil is a natural complex mixture of hydrocarbons that exists as gaseous, liquid or solid state in the earth in addition to other elements such as sulfur, nitrogen, heavy metals and salts. Crude oil has no significant value in its original state; therefore, it has to be refined. Petroleum refining is converting crude oil to valuable marketable products through different physical and chemical processes. One of these processes is fluid catalytic cracking [1].

Fluid catalytic cracking breaks the large molecules into lighter molecules in the presence of catalysts. The feed to fluid catalytic cracking is atmospheric and vacuum unit gas oils and coker gas oil whereas the products are liquefied petroleum gas (LPG), gasoline and middle distillate components [1]. In FCC, the preheated gas oil is fed to the bottom of the riser where it contacts the catalyst. The reaction occurs immediately in the riser. The reactants and products flow up the riser where the reaction is completed. The products and catalyst are separated in a cyclone. The catalyst is sent to a regenerator where the deposited coke is burnt. The regenerated catalyst is recycled back to the riser. Figure 1 shows the typical configuration of FCC unit [2]. Make-up catalyst is added regularly to account for the loss of activity. The FCC reaction is endothermic and the needed heat for the reaction is supplied by the regenerator where the combustion of coke is an exothermic process [3]. The average temperature in the riser varies from 480 to 566 °C, whereas the average temperature in the regenerator varies from 650 to 815 °C [1].

FCC is considered a major unit in most refineries. The necessity of FCC arises from the fact that the crude distillation cannot meet the demand for the most valuable and needed petroleum products, which are transportation fuels. Figure 2 shows the effect of FCC on refinery yields. FCC provides the greatest potential for increasing the profitability among all refining processes. Small improvements can increase the yield of gasoline which results in a significant economic gain. Therefore, the incentives for better understanding of FCC process, chemistry and catalyst are immense [4].

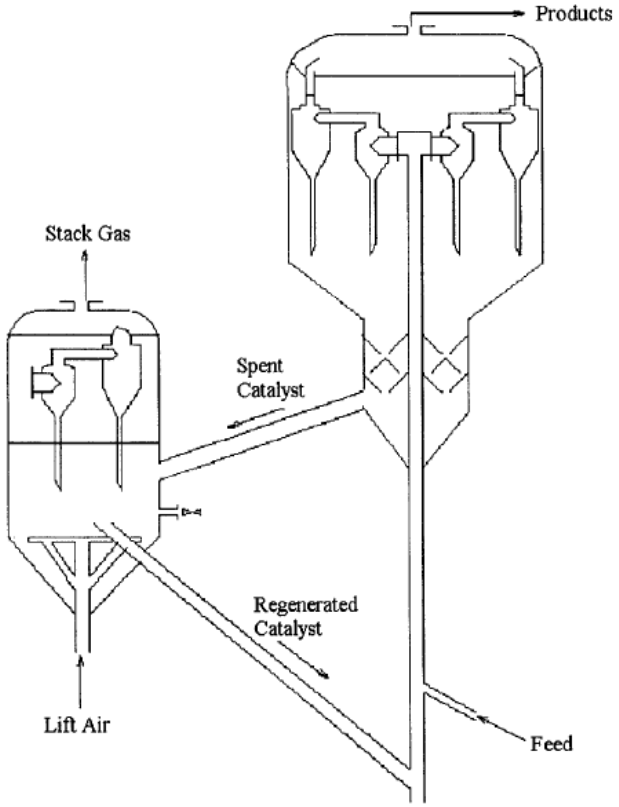

Figure 1: Typical configuration of FCC unit [2]

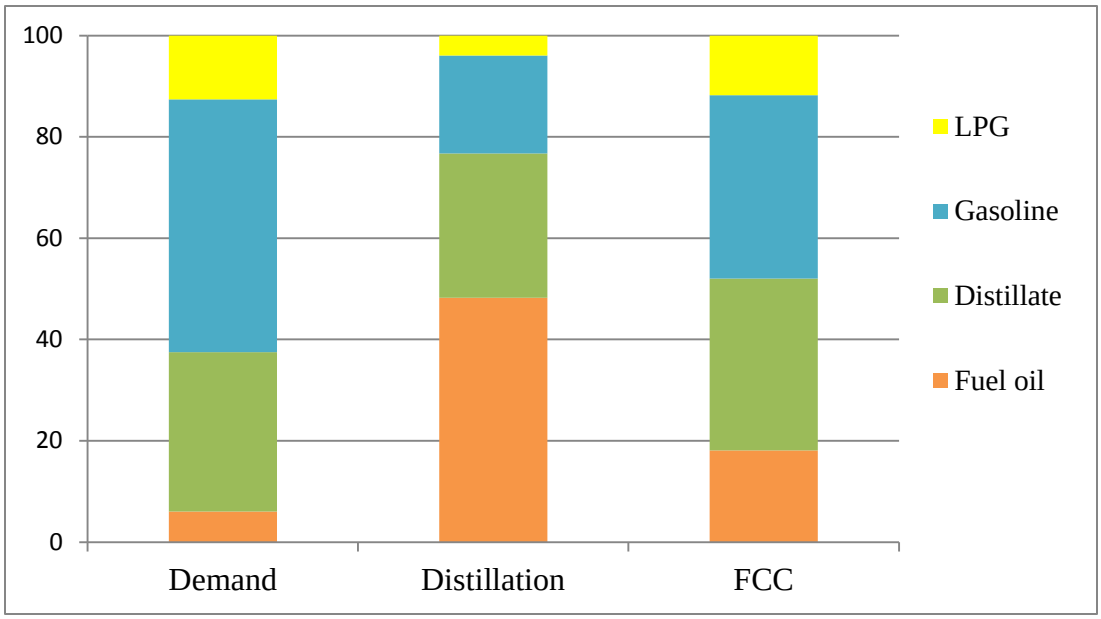

Figure 2: Effect of FCC on refinery yield (30% of crude fed to FCC) [1]

1.2 FCC catalyst

The introduction of zeolite catalysts in the early 1960s was a boost for the catalytic cracking field. Zeolite catalysts replaced the amorphous silica-alumina catalysts that were used before in FCC after Plank and Rosinski discovered that the incorporation of a small amount of zeolite in a matrix of silica-alumina produces a catalyst that meets the severe requirements of catalytic cracking [5]. FCC catalyst consist of approximately 20% Y zeolite crystals embedded in an 80% alumina matrix [6].

Gasoline, the most important product of FCC, is rated based on the octane number which measures the tendency for knocking. The octane rating is affected by three factors: feedstock, process variables and catalyst. Aromatics have the higher octane number while paraffins have the lower. Therefore, a feedstock rich in aromatics will have a higher octane number. The octane number is affected by different process variables. It increases with increasing the conversion, reaction temperature, coke on regenerated catalyst and decreases with increasing oil partial pressure and contact time. Moreover, the octane number is affected by the catalyst used. Octane FCC catalysts are catalyst designed to increase the octane rating [7].

Octane FCC catalysts are composed of two major components: zeolite and matrix. Some octane FCC catalysts include a third component which is an octane-boosting additive. The zeolite is the component responsible for the catalyst's activity, stability and selectivity. The zeolite used in octane FCC catalyst is modified Y zeolite [8] which is a synthetic version of naturally occurring faujasites zeolite [9]. Figure 3 below shows the elementary cell of faujasites.

Y zeolite has the framework structure shown in Figure 4 below. The crystallographic unit cell consists of an array of eight cages containing a total of 192 AlO_2 and SiO_2 tetrahedral units. The tetrahedral of sodalite units are connected through six-membered oxygen bridges. The resulting structure is very open with each cage connected to four other cages through a twelve-membered oxygen rings of free diameter of 7.4 Å. Large molecules such as neopentane and tertiary butyl amine can penetrate these pores [8].

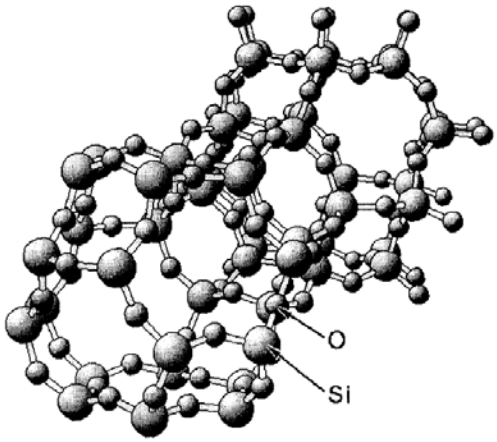

Figure 3: Faujasites elementary cell [2]

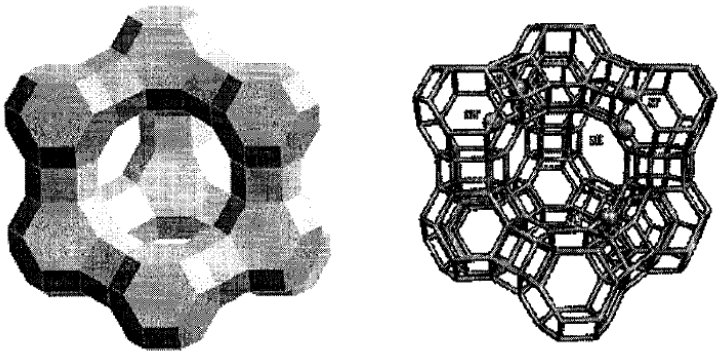

Figure 4: Framework structure of Y zeolite [2]

In Y zeolite the silica to alumina ratio is between 1.5 and 3. The number of exchangeable univalent cations varies with the Si/Al ratio and it can reach 6 for high silica Y. the distribution of cations between sites depends on the nature and number of cations and the presence of traces of moisture. The adsorption properties of Y zeolite can be modified by ion exchange and selectivity can be improved by using mixed cations [8]. The typical chemical composition for Y zeolite is $Na_{56}[(AlO_2)_{56}(SiO_2)_{136}].250\ H_2O$. Each tetrahedral aluminum atom in the framework carries a negative charge that is balanced by a positive charge carried on the cation. When cations occupy the various sites, two types of acidic hydroxyl groups are formed: α-cage hydroxyls and β-cage hydroxyls. The α-cage hydroxyls are very acidic and accessible to different sorbates, while the β-cage hydroxyls are less acidic but able to interact with α-cage restricted sorbates [7].

Modified Y zeolite is dealuminated Y zeolite. Removing some of the aluminum from the framework and therefore increasing the Si/Al ratio, affects the phsico-chemical properties of the zeolite and increases the catalyst's activity, selectivity, stability, capacity and gasoline octane rating. Dealumination can be achieved by thermal and hydrothermal modification, chemical modification and combination of both [7].

An increase of the zeolite content increases the catalytic activity regardless of the zeolite type (conventional Y or high-silica Y). As the Si/Al ratio increases, the conversion decreases. Therefore, the zeolite content should increase as the Si/Al ratio increases to maintain a desired conversion. Although high-silica zeolites are less active than conventional Y zeolites, they can preserve the activity under severe hydrothermal treatment. Furthermore, LPG selectivity increases and coke selectivity decreases with increasing Si/Al ratio [7].

In octane FCC catalyst the zeolite is embedded in the catalyst matrix. Most matrices used in octane FCC catalysts have the same composition as the catalyst used in FCC prior to zeolite such as acid leached clays and synthetic silica-alumina gels. These materials became the matrix components in octane FCC catalyst. The catalyst matrix performs several physical functions. One of the major functions of a matrix is binding the zeolites together to withstand interparticle and reactor wall collisions. The matrix also serves as a diffusion medium for the reactants and products. Therefore, it is required to have a pore structure that allows diffusion of hydrocarbon molecules and survives the severe hydrothermal treatment of the catalyst. Moreover, the matrix acts as a diluting medium for zeolite particles, hence moderating zeolite activity and avoiding excessive cracking. In addition, matrices can operate as a sink for sodium ions which increase the thermal and hydrothermal stability of zeolite and as a heat carrier which facilitate heat transfer during cracking and regeneration [7].

Besides the physical functions, FCC catalyst matrix performs a number of catalytic functions. The activity of the matrix is related to the surface area, surface acidity and steam-stable pores. Although the matrix has a lower activity than zeolite, the matrix component can improve gasoline octane because the hydrogen transfer rate is lower than the cracking rate. Matrices can also improve bottoms upgrading by cracking the large

molecules that cannot diffuse into the zeolite. Moreover, the matrix can protect the zeolite structure from damages caused by vanadium since the matrix cracks the heavy metal-containing molecules and binds them. It also protects the zeolite from nitrogen poisoning by reacting with nitrogen compounds in the feed. When the matrix contains active alumina, it facilitates SO_x abatement thus reducing SO_x emissions from the regenerator. Active matrix catalysts are used to achieve higher conversion and improved gasoline octane under milder operating conditions; however, the gasoline selectivity decreases [7].

The addition of small amounts of ZSM-5 additive to a FCC catalyst increases the octane rating of gasoline, but decrease the gasoline yield. ZSM-5 can be either used as a separate component or incorporated into the catalyst particle. ZSM-5 is one of the pentasil high-silica zeolites. It is used in different applications due to its unusual properties. It contains $T(Si,Al)O_4$ tetrahedral units linked into five-membered rings which are joined together to form two types of intersecting channels with ten-membered rings. The properties of ZSM-5 vary with the Si/Al ratio which can range from 20 to 8000 [7].

1.3 Reactions in FCC

Catalytic cracking involves both primary and secondary reactions. The first step of catalytic cracking is the formation of a carbenium ion ($R\text{-}CH_2^+$) as a result of the reaction of hydrocarbons molecules with the acidic sites on the catalyst. The primary reactions are those involving the breakage of carbon-carbon bond and immediate neutralization of the carbenium ion. They occur at a higher rate in olefins. The primary cracking reactions form smaller molecules by the successive cracking of the formed carbenium. Moreover, the olefins can undergo cracking after being converted to a carbenium ion through hydrogen addition. Although successive cracking occur, the cracking rate decreases as the hydrocarbon chain becomes smaller [10].

Catalytic cracking yields more LPG (C_3 and C_4) than lighter gases because the carbenium ion is usually secondary or tertiary and when the bond attached to the charged carbon breaks, it will form a hydrocarbon molecule with at least three carbon atoms [10].

The secondary reactions have a major influence on the products properties and yield. The secondary reactions involve hydrogen transfer, isomerization and dehydrogenation [10]. The hydrogen transfer occurs at the surface of the catalyst and involves the transfer of hydrogen atoms to more hydrogen deficient molecules. Hydrogen transfer reactions produce higher yield of and more stable gasoline. On the other hand, they decrease the octane rating of gasoline, the amount of LPG produced and the olefin level in the light gasoline fraction [2]. Isomerization reactions convert less stable carbenium ions into the most stable tertiary carbenium ions that produce monobranched molecules [10]. Isomerization results in higher octane rating and higher products in the C_3/C_4 fraction that are used to produce methyl tertiary butyl ether (MTBE) [1]. Cyclization produces naphthenes from straight chain olefins. The produced naphthenes can be further transferred to aromatics by hydrogen transfer. Therefore, if the feed to FCC contains paraffins only, it is possible to have aromatic products [10]. The last secondary cracking reaction is dehydrogenation which results from contaminants such as nickel, copper and iron. These contaminants deposited on the catalyst increasing the yield of hydrogen, the formation of aromatics and the yield of coke [10]. The dehydrogenation rate of naphthenes is greater than the rate of the primary reaction at temperatures below 540℃ [1].

1.4 Adsorption in FCC catalyst

Adsorption of reactants on the catalyst surface is the first chemical step in any catalytic reaction. Adsorption is responsible for the preactivation of reactants, which result in a decrease of the activation energy of the process. The apparent differences in activation energies are due to the different adsorption heats. The heat of adsorption is affected by two factors: the van der Waals interactions and the electron transfer [11]. Adsorption and desorption are usually rapid enough not to limit the reactivity of the catalyst. The adsorption in FCC catalyst is evidenced by the difference in reactant gas-phase concentrations between thermal and catalytic experiments performed under the same operating condition [12].

Despite the importance of adsorption in FCC catalyst, many simulations use models that neglect adsorption. Few studies were devoted to quantify hydrocarbon adsorption in FCC [13]. It was found that the rates of adsorption and desorption are the same for the FCC catalyst as for the pure zeolite implying that mass transport in the matrix component of FCC catalyst is rapid and not rate limiting step in the desorption process. The knowledge of adsorption and desorption kinetics is important in FCC to understand the chemical reactions, to design the riser in which adsorption of heavy compounds could in principle be a limiting step and to design the stripper in which desorption of hydrocarbons is desired [14]. Moreover, adsorption affects the feed reactivity, product selectivity, reaction kinetics and catalyst decay [11].

1.5 Diffusion in FCC catalyst

Diffusion is a significant phenomenon in porous solids such as catalysts and adsorbents. Although zeolite catalysts have better activity, selectivity and stability than amorphous silica alumina, zeolite catalysts are affected by diffusional limitations that can control the overall rate of reaction [15]. In FCC, the feedstock molecules diffuse through the matrix of the catalyst then through the zeolite reaching an active site. The reaction occurs in the active sites and the products diffuse out of the zeolite and the matrix to the gas stream. FCC catalyst involves different mechanism of diffusion, micropores in Y zeolite and mesopores and macropores in alumina matrix [6].

Catalytic cracking is influenced by the mass diffusion in the zeolite because the diffusivities in the matrix are larger than in the zeolite [2]. Moreover, larger hydrocarbon molecules may hinder the diffusion of smaller molecules causing lighter products to be trapped or delayed in the zeolite pore network already filled with sorbed heavier molecules [16]. Diffusion in zeolite is affected by the type of zeolite, molecular structure, nature of sorbate molecules and temperature [2]. The diffusional limitations become more limiting with increasing molecular size [17]; however, Barrie et al. [14] suggests that the pore diffusion of zeolite influence the observed activity even for small molecules such as n-hexane. It was shown by Al-Khattaf et al. [18] that diffusional limitations have a major impact on primary cracking reactions but no apparent impact on secondary reactions.

The decrease in conversion is the first sign to mass transfer limitations. Factors affecting mass limitations can be grouped into unit design factors like contact time and feed effects like feed density and carbon content. The disadvantage of mass transfer limited operation is the lack of response to independent variable manipulation to improve conversion and selectivity [2]. Nevertheless, diffusional limitations can be decreased by reducing the size of zeolite crystals but that will result in a decrease of the yield and difficulty in handling nanometer-sized particles. Another way to decrease the diffusional limitations is by synthesizing large-pore zeolites which are expensive [19].

1.6 Literature Review

Many studies were done of FCC catalysts. Different studies used different models to calculate different data. Two methods were used to describe the catalytic cracking of gas oil. The first method lumped large numbers of components into smaller number of pseudocomponents [4]. The second method is studying pure components that behave as gas oil.

One of the studies that considered lump models is by Weekman et al. [20] who evaluated the reaction parameters of a three lump model consisting of the feed (Gas oil), gasoline boiling fraction and the remaining carbons (Gases and coke). Lee et al. [3] calculated the reaction parameters for a four lump model consisting of gas oil, gasoline, coke and gases, while Bollas et al. [21] calculated the parameters for a five lump model by separating the gases lump to dry gas lump and LPG lump. Ancheyta-Juarez et al. [4] estimated the reaction parameters for three, four and five lump models. In addition, Al-Khattaf et al. [17] considered diffusion and reaction in a four lump model with constant diffusivity of gas oil.

Other studies investigated the cracking of pure components. Barrie et al. [14] modeled the adsorption of n-hexane, n-heptane, n-octane, toluene and p-xylene in FCC catalyst. Two models where used: the first model assumes that the particle boundary transport is the limiting step affecting the adsorption kinetics, while the second model assumes that diffusion in zeolite is the limiting step. Barrie at al. found that n-hexane, n-heptane and n-octane can be only fitted to the first model whereas for toluene and p-

xylene can be fitted tolerably to the second model. This study indicate the limitations of assuming local equilibrium between vapor and adsorbed phase at the edge of the catalyst particle in the non-dilute system since the rate of transport between these phases can be rate limiting step which will affect adsorption kinetics. Puente et al. [22] estimated the apparent adsorption constants for n-hexane, n-decane and toluene assuming the applicability of Henry's law, while Avila et al. [23] used a nonlinear diffusion-adsorption model based on Langmuir isotherm to estimate adsorption and micropore diffusion data for n-hexane, n-decane and toluene. Moreover, Bidabehere et al. [13] analyzed simultaneous reaction, adsorption and diffusion in FCC catalyst using n-hexadecane as the reactant. The model assumes micropore diffusion in zeolite as the rate limiting step with constant diffusivity. It also assumes the applicability of Henry's law, isothermal system and neglects mass transfer, adsorption and reaction in the matrix. Corma et al. [11] considered adsorption-reaction system with Langmuir-Hinshelwood model for some pure hydrocarbons such as n-hexadecane, decalin, tetralin and 1-octene and reported reaction and adsorption parameters for those hydrocarbons.

One of the studies that included a component that can describe the cracking of gas oil is by Al-Khattaf et al. [24] who modeled the catalytic cracking of 1,3,5-triisopropylbenzene. 1,3,5-TIPB was reacted using Y-zeolite catalyst (small and large crystals) in a 48 cm^3 CREC riser simulator. The riser simulator is a novel bench scale unit invented by de Lasa which overcomes the technical problems of the standard micro-activity test. The catalyst had the following composition: 30 wt% zeolite, 50 wt% kaoline, and 20 wt% silica sol. Table 1 summarizes the properties of the catalysts used.

Table 1: Properties of the small (CAT-SC) and large (CAT-LC) zeolite crystal [24]

	CAT-SC	CAT-LC
Na_2O (wt%)	4.1	0.25
SiO_2/Al_2O_3 (mol/mol)	5.6	5.7
Unit cell size (Å)	24.49	24.51
Crystal size (μm)	0.4	0.9

The conversion of 1,3,5-TIPB at several temperatures (350, 400, 450, 500, 525, 550 °C) and reaction time (3-10 s) was obtained. The model used by Al-Khattaf et al. [24] made the following assumptions: a) Isothermal process, b) Quasi-steady state inside the zeolite, c) Instantaneous vaporization, d) Inert matrix to adsorption-reaction processes, e) Negligible transport limitations around the particle and inside the matrix, f) Linear equilibrium isotherm and g) Linear diffusivity. Al-Khattaf et al. [24] concluded that diffusion controls at low temperatures (350-450 °C), while chemical reaction controls at higher temperatures (500-550 °C).

The assumptions made by Al-Khattaf et al. [24] are not accurate. The process cannot be isothermal because the catalytic reaction is endothermic and the adsorption of large molecules like 1,3,5-TIPB process is highly exothermic. Al-Khattaf et al. [24] showed that the process is quasi-steady state inside the zeolite for reaction times greater than 1 s. Figure 5 shows the change of effectiveness factor with time using unsteady and quasi-steady state inside the zeolite.

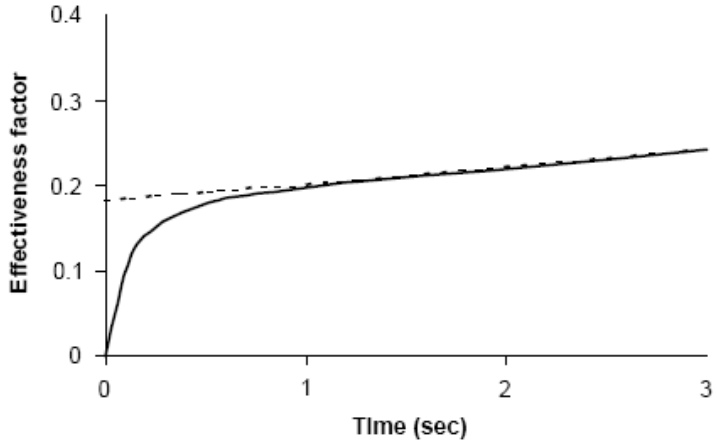

Figure 5: Changes of effectiveness factor with time. The solid line is the unsteady state process. The broken line is the quasi-steady state process [24]

The matrix of FCC catalyst is active and adsorption occurs in the matrix as proved by Zaman et al. [6]. The proof will be discussed in the subsequent paragraphs. Therefore, the assumption of inert matrix is inadequate. Furthermore, macropore diffusion is present in the matrix and should be taken into account. Assumption f is not valid at high concentrations and for large molecules, while assumption g is valid when the change in concentration is small.

In addition, Atias et al. [25] modeled catalytic cracking of 1,2,4-trimethylbenzene assuming no diffusional limitations to exist in the system. The model also assumed the matrix to be inert to adsorption-reaction processes and that linear equilibrium isotherm applies. Atias et al. [25] used the CREC riser simulator to react 1,2,4-TMB using small and large zeolite crystals. The composition of the catalyst is: 30 wt% zeolite, 50 wt% kaoline, and 20 wt% silica sol. The properties of the catalysts are similar to those in Table 1. Again, the assumptions made by Atias et al. [25] were not accurate. The critical diameter for 1,2,4-TMB is close to 7.4 Å which is the size of zeolite window opening; therefore, diffusional limitations exists.

Moreover, Al-Sabawi et al. [26] modeled the catalytic cracking of methylcyclohexane. The model assumes non-diffusional limitations, inert matrix to adsorption-reaction processes, isothermal process and the applicability of Henry's law.

Although most studies done on FCC catalyst neglect adsorption in the alumina matrix, Zaman et al. [6] found that both Y zeolite and the matrix have high adsorption capacity for oil mixtures. Zaman et al. modeled catalytic cracking in 1,3,5-TIPB assuming linear adsorption equilibrium isotherm and isothermal operation. Zaman et al. found that the plots of dimensionless concentration of 1,3,5-TIPB for FCC catalyst are lower than that of zeolitic adsorbents, thus significant amount of 1,3,5-TIPB is adsorbed on the alumina matrix. Moreover, it was found that micropore diffusion is the rate-limiting step.

Despite the several studies done of fluid catalytic cracking, there are some drawbacks that need to be taken into account. The main drawback is assuming an inert matrix of the FCC catalyst. Zaman et al. [6] proved that the matrix is active and adsorption in the matrix should be considered. Most studies used linear adsorption equilibrium isotherm but the linearity assumption in the adsorption isotherm is not generally valid especially for strongly adsorbed molecules [6]. Most studies assume isothermal process thus neglecting the thermal effect on catalytic cracking. The reaction time in FCC is 1 to 3 seconds [1], however, most studies model catalytic cracking for reaction times greater than 3 seconds.

1.7 Proposed research

As mentioned earlier, FCC plays a major role in increasing the profitability of any refinery. Major improvements on FCC come from understanding the reaction chemistry and enhancing the catalyst [27]. Therefore, better modeling of catalytic cracking is essential.

To account for some of the drawbacks in the literature, the objectives of this research are as follows:

1. Account for macropore diffusion in the matrix.
2. Use a localized adsorption equilibrium isotherm (Langmuir isotherm).
3. Study the thermal effects on catalytic cracking.
4. Model catalytic cracking for FCC reaction times.
5. Model catalytic cracking including for reaction, adsorption and diffusion in FCC catalyst with active matrix.

The research will study the effects of the different parameters on the catalytic cracking reactions. In addition, the research aims to develop models for the catalytic cracking of the pure component 1,3,5-TIPB and the catalytic cracking of gas oil using a four lump model. Modeling catalytic cracking in pure components will facilitate modeling gas oil and will give an insight on the role of reaction, adsorption and diffusion in catalytic cracking. 1,3,5-TIPB was chosen because it is an important compound to study diffusion and reaction in FCC catalysts. This compound can be considered a typical gas oil molecule and it has a critical diameter of 9.5 Å which is significantly larger than the 7.4 Å opening of Y zeolite thus diffusional limitations can be studied. Also, the reaction pathway of 1,3,5-TIPB can be easily followed.

The data that will be modeled are obtained from Al-Khattaf [28] and shown in Figures 6 to 8.

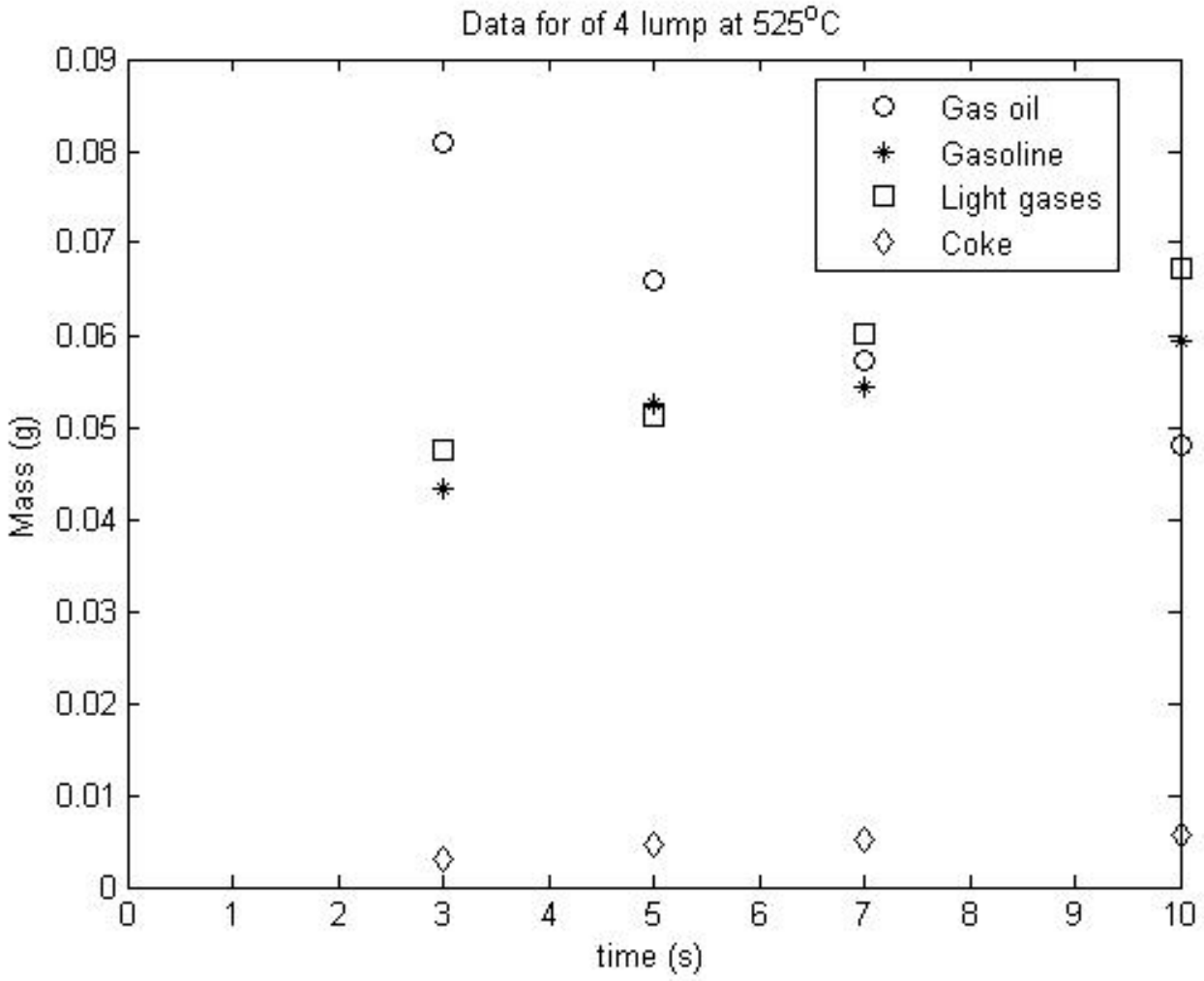

Figure 6: Data for gas oil (4 lump model) at 525℃ (CAT-SC)

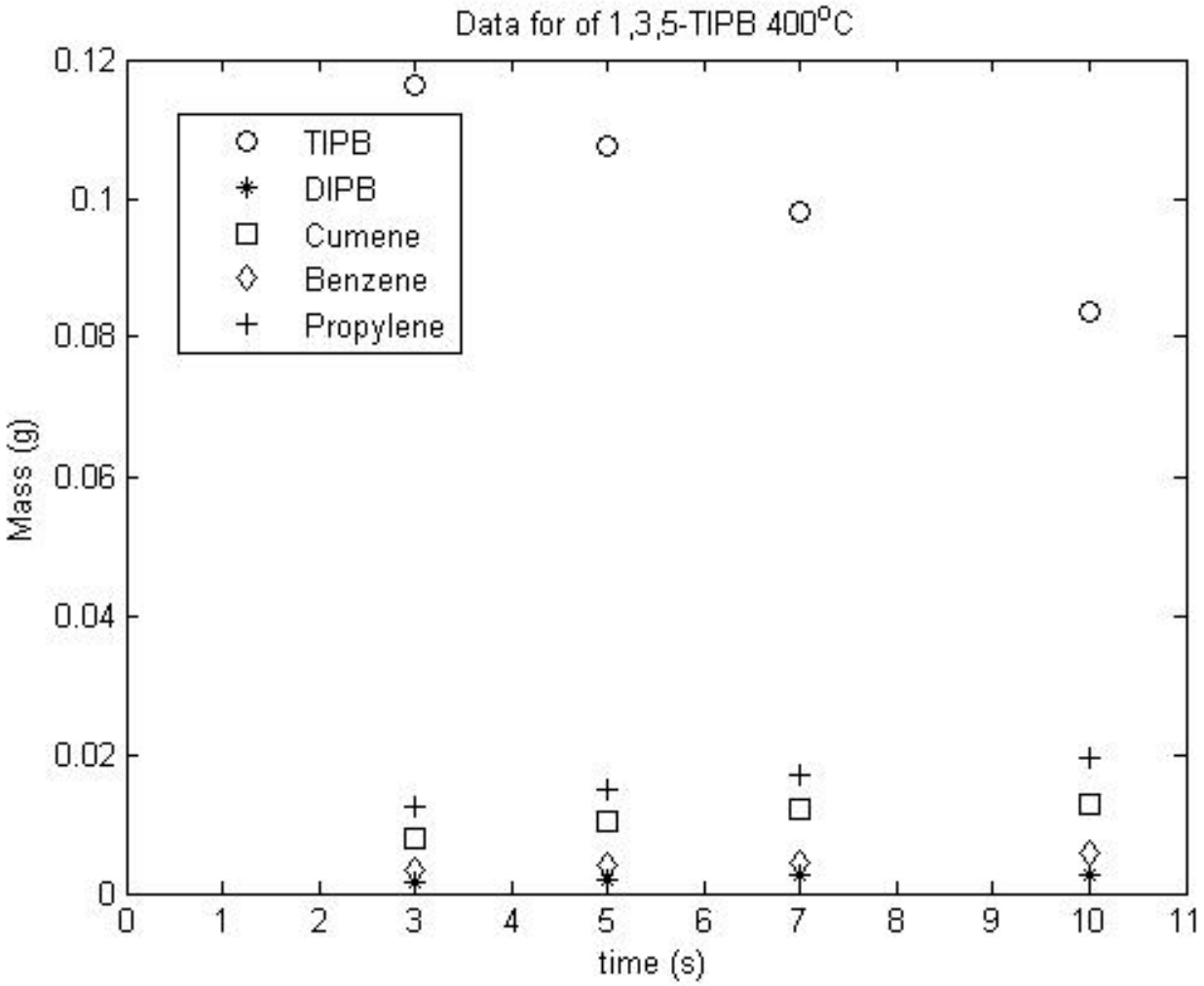

Figure 7: Data for 1,3,5-TIPB at 400℃ (CAT-SC)

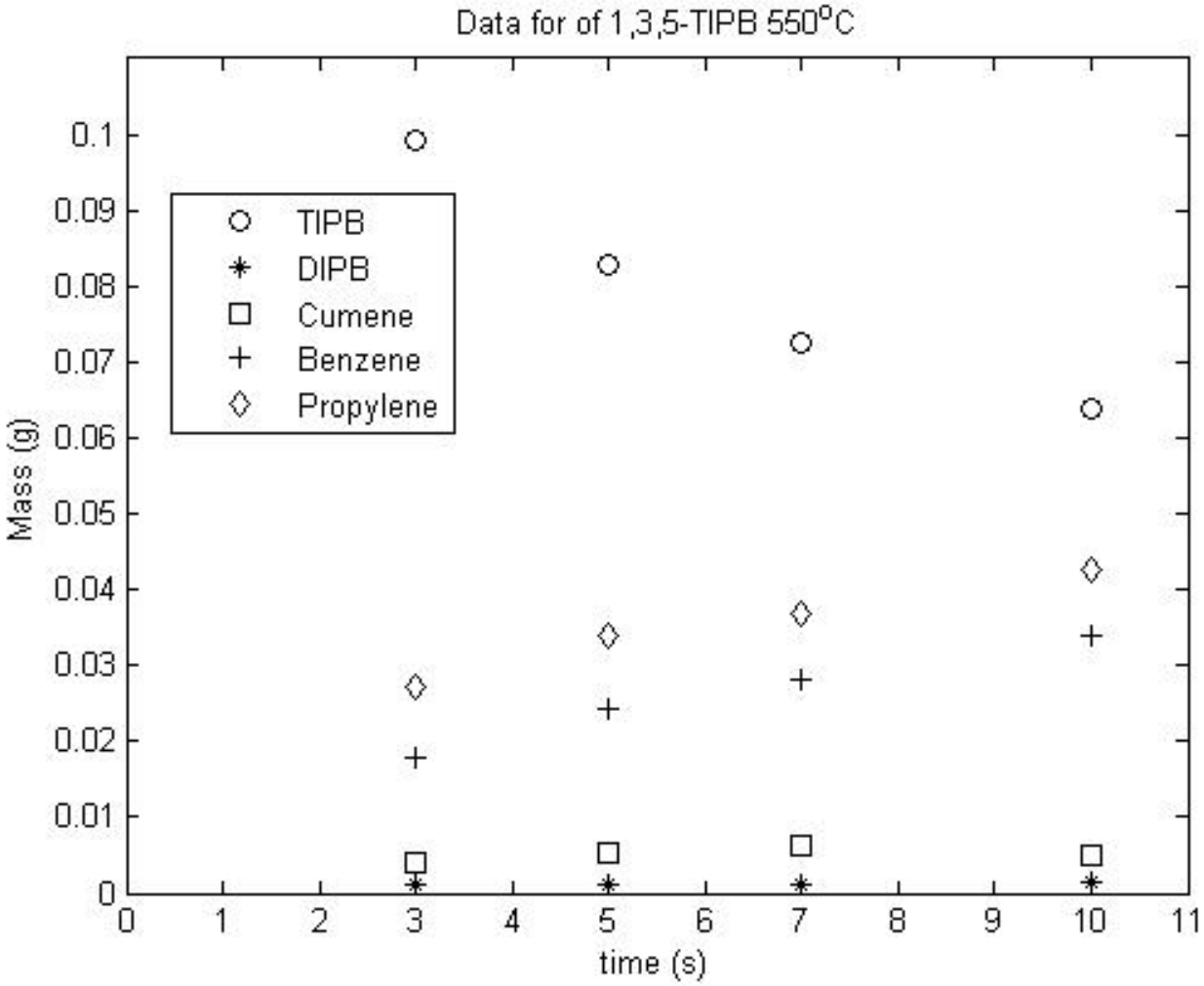

Figure 8: Data for 1,3,5-TIPB at 550℃ (CAT-SC)

Chapter 2. Theory

In heterogeneous catalytic reactions, reactants transfer from the bulk fluid to the external surface of the pellet, then into and through the pores within the pellet. Reaction occurs only on the catalytic surface of the pores [29]. Figure 9 shows the steps for a heterogeneous catalytic reaction to occur. The seven steps are:

1. Transport of reactants from the bulk fluid to the catalyst pellet surface.
2. Transport of reactants into and through the catalyst pores.
3. Adsorption of reactants on the catalytic site.
4. Surface chemical reaction between adsorbed atoms or molecules.
5. Desorption of products.
6. Transport of the products from the catalyst pores to the catalyst pellet surface.
7. Transport of the products to the bulk fluid stream [30].

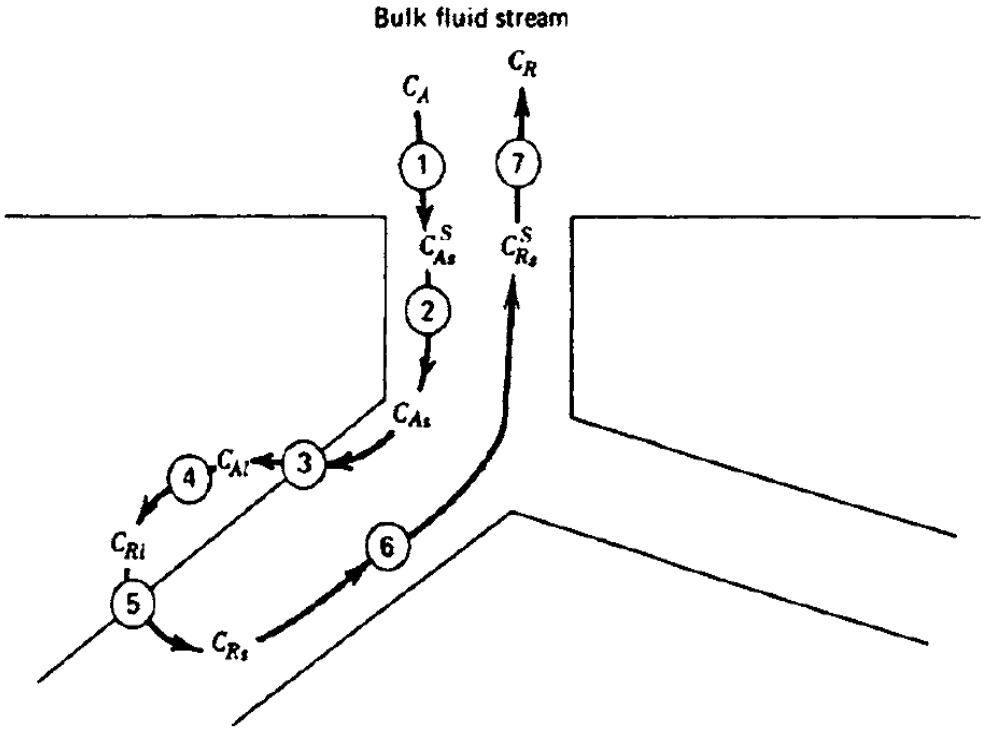

Figure 9: Steps involved heterogeneous catalytic reaction [30]

The theory of the previous steps will be discussed for 1,3,5-TIPB, 1,2,4-TMB and gas oil.

2.1 Reactions

Reactions can be quantified by a rate law which is an algebraic equation that is a function of reactants' properties and reaction conditions [29]. For single reactant A with catalyst activity decay, the rate law can be expressed as:

$$-r_A = k\ \phi\ C_A^a \qquad 2.1$$

where k is the reaction constant, ϕ is the catalyst activity decay function and a is the order of the reaction. The reaction constant dependence on the temperature follows Arrhenius law:

$$k = k_0 \exp\left(\frac{-E}{RT}\right) \qquad 2.2$$

where k_0 is the pre-exponential factor and E is the activation energy.

2.1.1 Reactions for 1,3,5-TIPB.

The catalytic cracking of 1,3,5-TIPB starts by the dealkylation to 1,3-diisopropylbenzene and propylene. This is followed by the dealkylation of 1,3-DIPB to cumene and propylene. Cumene also reacts to form benzene and propylene through alkylation reaction [24]. Figure 10 below shows a schematic description of the catalytic cracking of 1,3,5-TIPB.

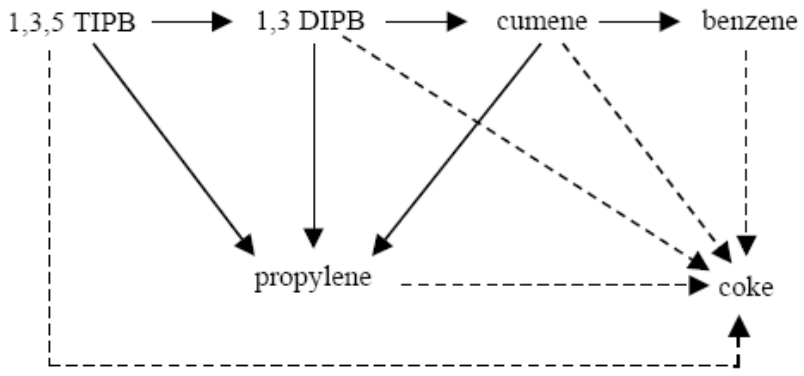

Figure 10: Schematic description of the catalytic cracking of 1,3,5-TIPB [24]

Other reactions such as disproportionation, isomerization and condensation may also occur, however, the alkylation reactions are dominant. The catalyst activity decay function can be related to the reactant conversion through the following relation [24]:

$$\phi = \exp\left(-\lambda(1 - y_A)\right) \qquad 2.3$$

where λ is a constant and y_A is the mass fraction of reactant A.

Atias et al. [12] performed experiments to study the catalytic cracking of 1,3,5-TIPB and found intrinsic kinetics constants over small (CAT-SC) and large (CAT-LC) zeolite crystallites. The data are shown in Table 2 below:

Table 2: Intrinsic kinetics constants for 1,3,5-TIPB [12]

Catalyst	$k_0' \times 10^3$ (1/s) At 450 °C	E_R (kJ/mol)	λ
CAT-LC	4.89	73.3	6.03
CAT-SC	5.33	73.29	4.98

2.1.2 Reactions for 1,2,4-TMB.

The primary reactions of 1,2,4-trimethylbenzene catalytic cracking involve the isomerization of 1,2,4-trimethylbenzene to 1,2,3-trimethylbenzene and 1,3,5-trimethylbenzene and the disproportionation of 1,2,4-trimethylbenzene to 1,2,3,4-tetramethylbenzene, 1,2,3,5-tetramethylbenzene, 1,2,4,5-tetramethylbenzene and xylene isomers [25]. Figure 11 below shows the different reactions:

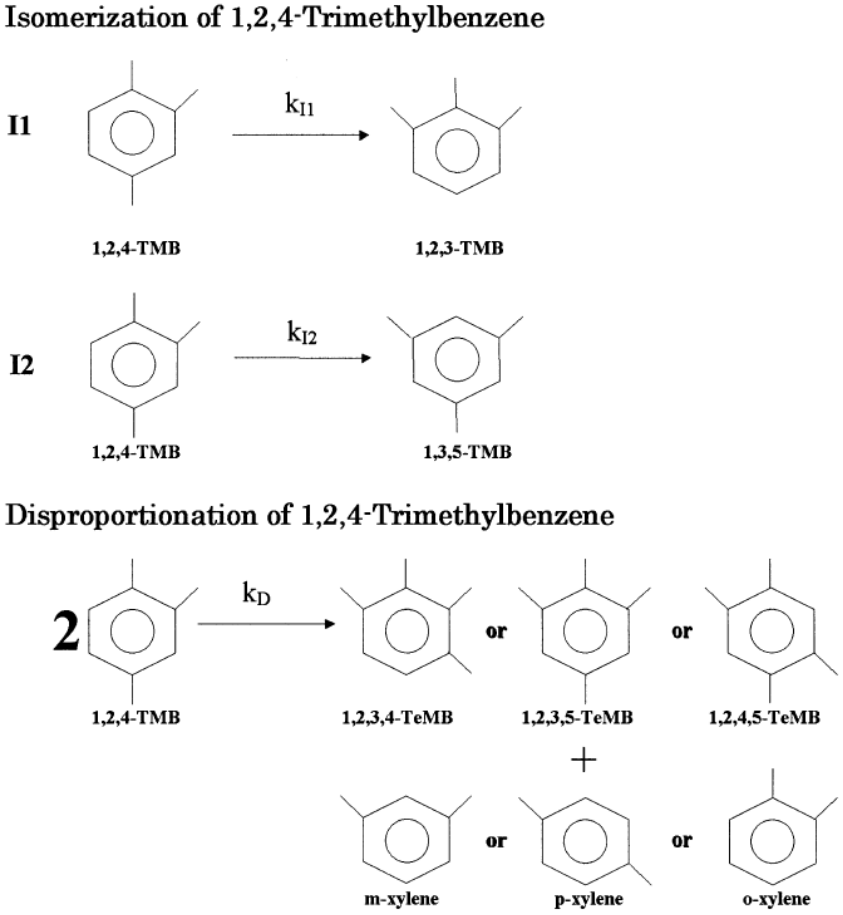

Figure 11: Primary reactions of 1,2,4-TMB catalytic conversion [25]

Kikuchi et al. [31] and Ko [32] proposed that the isomerization reactions are first order while the disproportionation reaction is second order. The rate of the reactions can be expressed as:

$$-r_A = -r_{A1} - r_{A2} - r_{A3} = k_{I1} C_A \phi^I + k_{I2} C_A \phi^I + 2\, k_D C_A^2 \phi^D \quad (2.4)$$

$$-r_B = -k_{I1} C_A \phi^I \quad (2.5)$$

$$-r_C = -k_{I2} C_A \phi^I \quad (2.6)$$

$$-r_X = -k_D C_A^2 \phi^D \quad (2.7)$$

where A, B ,C and X represent 1,2,4-TMB, 1,2,3-TMB, 1,3,5-TMB and xylenes, respectively.

The deactivation function can be expressed in terms of the reactant conversion. The isomerization activation function is related to the fraction formed of TMB isomers, while the disproportionation deactivation function is related to the fraction formed of xylene isomers as follows [25]:

$$\phi^I = \exp[-\lambda^I (y_B + y_C)] \quad (2.8)$$

$$\phi^D = \exp(-\lambda^D y_X) \quad (2.9)$$

Atias et al. [25] performed experiments and found the kinetics parameters as summarized in Table 3 below:

Table 3: Reaction parameters for 1,2,4-TMB at 450 °C [25]

Parameter	CAT-SC	CAT-LC
k_{I0} (1/s)	0.341	0.454
E_I (kJ/mol)	52.73	47.36
λ^I	20.8	18.7
k_{D0} (kg of crystallite/mol s)	0.552	0.586
E_D (kJ/mol)	15.43	15.59
λ^D	4.7	5

2.1.3 Reactions for gas oil.

As mentioned earlier, fluid catalytic cracking can be described using lump model. The number of lumps has been increased to obtain detailed prediction of product distribution. In this section, reactions in 3, 4 and 5 lumps model will be discussed.

In the three lumps model, gas oil reacts to produce gasoline and gas plus coke according to the reaction shown in Figure 12 below:

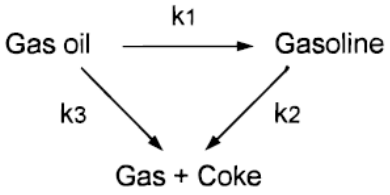

Figure 12: 3-Lump kinetic model [4]

It is assumed that gas oil cracking is second order. The rate of the reaction is expressed as:

$$\frac{dy_1}{dt} = -k_0 y_1^2 \phi \qquad 2.10$$

where y_1 is the gas oil mole fraction and $k_0 = k_1+k_3$

Gasoline also reacts to form gas and coke. The reaction is assumed to be first order:

$$\frac{dy_2}{dt} = (k_1 y_1^2 - k_2 y_2)\phi \qquad 2.11$$

The gas plus coke lump can be determined as follows:

$$\frac{dy_3}{dt} = (k_3 y_1^2 + k_2 y_2)\phi \qquad 2.12$$

In the four lumps model, the cracking of gas oil is shown in Figure 13 below:

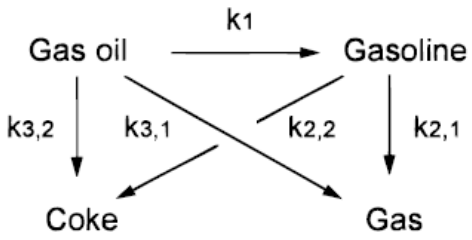

Figure 13: 4-Lump kinetic model [4]

Gas oil and gasoline rates are similar to the previous equations with:

$$k_0 = k_1 + k_3$$

$$k_3 = k_{3,1} + k_{3,2}$$

$$k_2 = k_{2,1} + k_{2,2}$$

The gas (y_3) and coke (y_4) production are determined from the following relations:

$$\frac{dy_3}{dt} = (k_{3,1}y_1^2 + k_{2,1}y_2)\phi \quad 2.13$$

$$\frac{dy_4}{dt} = (k_{3,2}y_1^2 + k_{2,2}y_2)\phi \quad 2.14$$

In the five lumps model, gas oil reacts according to the reaction shown in Figure 14 below:

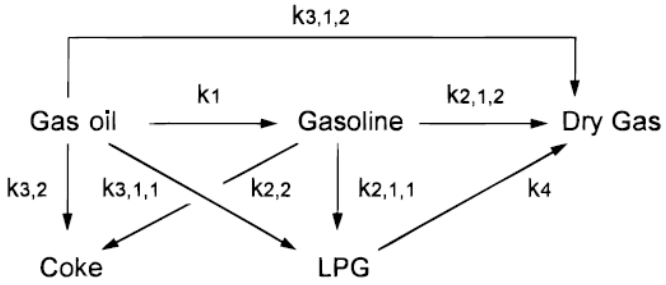

Figure 14: 5-Lump kinetic model [4]

The gas oil, gasoline and coke rates are similar to those in the 4-lump model with:

$$k_0 = k_1 + k_3$$

$$k_3 = k_{3,1} + k_{3,2}$$

$$k_{3,1} = k_{3,1,1} + k_{3,1,2}$$

$$k_2 = k_{2,1} + k_{2,2}$$

$$k_{2,1} = k_{2,1,1} + k_{2,2,2}$$

The rates for LPG (y_3) and dry gas (y_5) can be determined as follows:

$$\frac{dy_3}{dt} = (k_{3,1,1}y_1^2 + k_{2,1,1}y_2 - k_4y_3)\phi \quad 2.15$$

$$\frac{dy_5}{dt} = (k_{3,1,2}y_1^2 + k_{2,1,2}y_2 - k_4 y_3)\phi \quad 2.16$$

The deactivation function can be represented by an exponential law as following:

$$\phi = e^{-k_d t_c} \quad 2.17$$

where k_d is the deactivation constant (s^{-1}) and t_c is the catalyst residence time (s).

Ancheyta-Juarez et al. [4] calculated the parameters for each model. Kinetics parameters at 500 °C are shown in Table 4:

Table 4: Reaction parameters for the three models at 500°C [4]

Parameter	Reaction	3 lump	4 lump	5 lump
k_1	GO → Gasoline	0.1942	0.1942	0.1942
k_2	Gasoline → gas + coke	0.0093		
$k_{2,1}$	Gasoline → gas		0.0093	
$k_{2,1,1}$	Gasoline → LPG			0.0061
$k_{2,1,2}$	Gasoline → dry gas			0.0032
$k_{2,2}$	Gasoline → coke		2×10^{-8}	2×10^{-8}
k_3	GO → gas + coke	0.0488		
$k_{3,1}$	GO → gas		0.0348	
$k_{3,1,1}$	GO → LPG			0.0357
$k_{3,1,2}$	GO → dry gas			0.0001
$k_{3,2}$	GO → coke		0.0140	0.0140
k_4	LPG → dry gas			0.0020
k_d		0.0875	0.0875	0.0875

Moreover, [4] provided the activation energies which are shown in Table 5 below:

Table 5: Activation energies for the three models [4]

Parameter	Reaction	3 lump	4 lump	5 lump
k_1	GO → Gasoline	13.7	13.7	13.7
k_2	Gasoline → gas + coke	15.7		
$k_{2,1}$	Gasoline → gas		15.7	
$k_{2,1,1}$	Gasoline → LPG			17.5
$k_{2,1,2}$	Gasoline → dry gas			10.8
$k_{2,2}$	Gasoline → coke		15.9	15.9
k_3	GO → gas + coke	11.1		
$k_{3,1}$	GO → gas		12.6	
$k_{3,1,1}$	GO → LPG			12.5
$k_{3,1,2}$	GO → dry gas			11.8
$k_{3,2}$	GO → coke		7.6	7.6
k_4	LPG → dry gas			9.6

2.2 Adsorption

Adsorption is an important phenomenon in porous solids. Physical adsorption is characterized by the relatively weak intermolecular forces, while chemisorption involves the formation of a chemical bond between the sorbate and the surface of the adsorption. Due to its reversibility, almost all adsorptive separation processes depend on physical adsorption. The heat of adsorption measures the strength of the bonding between the sorbate and surface. Adsorption is an exothermic process because the free energy change on adsorption ΔG must be negative and the entropy change on adsorption ΔS is also negative and according to the following equation ΔH should be negative [8]:

$$\Delta G = \Delta H - T\Delta S \tag{2.18}$$

There is no change in molecular state on adsorption for physical adsorption. Therefore, at low concentrations, the equilibrium relation between the fluid phase and adsorbed phase concentrations is linear. This linear relation is referred to as Henry's law. The Henry's law can be expressed in terms of concentrations or pressures [8]:

$$q = Kc \;\; or \; q = K'p \tag{2.19}$$

where q and c are number of moles per unit volume in the adsorbed and fluid phases, respectively.

The dependence of Henry's constant (K) on temperature follows the van't Hoff equation:

$$K = K_0 \exp\left(-\frac{\Delta H}{RT}\right) \tag{2.20}$$

Monolayer adsorption occurs when adsorption has a definite saturation limit that corresponds to filling the micropores completely. The simplest model representing monolayer adsorption is Langmuir. Langmuir isotherm is based on the following assumptions [8]:

1. Localized adsorption.
2. One adsorbed molecule is held by each site.
3. All sites have the same energy.
4. No interactions between molecules adsorbed on neighboring sites are present.

The Langmuir isotherm can be expressed in terms of the pressure at equilibrium as follow:

$$\theta = \frac{q}{q_s} = \frac{bP}{1 + bP} \qquad 2.21$$

where q_s is the saturation capacity and b is the adsorption equilibrium constant and its dependence on temperature follows the van't Hoff equation:

$$b = b_0 \exp\left(-\frac{\Delta H}{RT}\right) \qquad 2.22$$

Since adsorption is exothermic, the adsorption constant decreases with increasing temperature. Although the assumption of localized adsorption is not accurate for physical adsorption and deviations from the Langmuir isotherm exist for most real systems, Langmuir isotherm provides a reasonably good fit for many experimental isotherms over quite wide concentration ranges [8].

2.2.1 Adsorption of 1,3,5-TIPB:

The difference in reactant gas-phase concentration between thermal and catalytic experiments performed under the same operating condition proves that adsorption of 1,3,5-TIPB occurs on FCC catalyst. Adsorption of 1,3,5-TIPB is assumed to apply Henry's law [12]. The Adsorption constant follows van't Hoff equation:

$$K_i = K_{i0} \exp\left[-\frac{\Delta H_i}{R}\left(\frac{1}{T} - \frac{1}{T_0}\right)\right] \qquad 2.23$$

where ΔH_i is the heat of adsorption and K_{i0} is the pre-exponential factor.

Heat of adsorption and adsorption constants for 1,3,5-TIPB reported in [12] are summarized in Table 6 below:

Table 6: Heat of adsorption and adsorption constants for 1,3,5-TIPB [12]

	CAT-SC	CAT-LC
$-\Delta H_i$ (kJ/mol)	67	69
$K_{i0} \times 10^3$ at 450 °C (m^3/kg of crystallite)	19	22

2.2.2 Adsorption of 1,2,4-TMB:

Atias et al. [25] performed several experiments with different ratios of catalyst to 1,2,4-TMB reactant and observed that the adsorption isotherm suggest a linear function similar to Henry's law with the amount of 1,2,4-TMB adsorbed increasing almost linearly with 1,2,4-TMB partial pressures in the operating range of interest. Atias et al. [25] also examined the dependence of adsorption constant on temperature and found that the constant of adsorption for CAT-SC is slightly lower than that for CAT-LC. Atias et al. [25] attributed the differences to the minor differences in specific surface area. Heat of adsorption and adsorption constants for 1,2,4-TMB reported in [25] are summarized in Table 7 below:

Table 7: Heat of adsorption and adsorption constants for 1,2,4-TMB [25]

	CAT-SC	CAT-LC
$-\Delta H_i$ (kJ/mol)	3.74	3.82
$K_{i0} \times 10^3$ at 450 °C (m^3/kg of crystallite)	11.4	11.8

2.2.3 Adsorption of gas oil:

Atias [2] calculated the adsorption parameters for 4-lump model. Heat of adsorption and adsorption constants for gas oil reported in [2] are summarized in Table 8 below where coke is assumed to be adsorbed on the catalyst:

Table 8: Heat of adsorption and adsorption constants for gas oil [2]

Lump	K_i at 450 °C (cm^3/kg)	$-\Delta H_i$ (kJ/mol)
Light Gases	3.42	29.46
Gasoline	8.03	54.32
Gas oil	26.56	69.32

2.3 Diffusion:

Diffusivity is defined in terms of Fick's first equation:

$$J = -D(c)\frac{\partial c}{\partial x} \qquad 2.24$$

From Fick's first equation, diffusivity is dependent on concentration gradient but may depend on concentration. The driving force for diffusion is differences in chemical potentials. Pore diffusion occurs by different mechanisms depending on the pore size. In micropores or intracrystalline pores, the diffusing molecules do not escape from the force field of the adsorbent surface and transport occurs by an activated process involving jumps between adsorption sites. This mechanism is called micropore or intracrystalline diffusion. Diffusion in larger pores where the molecules can escape from the surface field is called macropore diffusion [8].

Concentration dependence of diffusivity varies according to Darken's relationship [33]:

$$D(q) = D_0\frac{d\ lnP}{d\ lnq} \qquad 2.25$$

If Henry's law is obeyed and the concentrations of the adsorbed and bulk phases are related linearly, then d lnP/d lnq = 1 and diffusivity approaches a constant limiting value. If Langmuir isotherm is obeyed then [33]:

$$D(q) = D_0\frac{d\ lnP}{d\ lnq} = \frac{D_0}{1-\frac{q}{q_s}} \qquad 2.26$$

2.3.1 Diffusion in macropores:

Macropore diffusion has four distinct mechanisms: molecular diffusion, Knudsen diffusion, Poiseuille flow and surface diffusion. The effective macropore diffusivity often includes contributions from more than one mechanism. The transport in macropore diffusion is assumed to occur only through the pores not through the solids. Moreover, random orientation of the pores and lower concentration gradient in the direction of flow lower the diffusivity through pores. To account for these effects, tortuosity factor is introduced such that [8]:

$$D_p = \frac{D}{\tau} \tag{2.27}$$

If macropore diffusion controls the system, the following differential mass balance applies for macropore diffusivity independent of concentration for isothermal process [8]:

$$\left(1-\epsilon_p\right)\frac{\partial q}{\partial t} + \epsilon_p \frac{\partial c}{\partial t} = \epsilon_p D_p \left(\frac{\partial^2 c}{\partial R^2} + \frac{2}{R}\frac{\partial c}{\partial R}\right) \tag{2.28}$$

If Henry's law applies [8]:

$$\frac{\partial c}{\partial t} = \frac{\epsilon_p D_p}{\epsilon_p + \left(1-\epsilon_p\right)K}\left(\frac{\partial^2 c}{\partial R^2} + \frac{2}{R}\frac{\partial c}{\partial R}\right) \tag{2.29}$$

2.3.2 Diffusion in micropores:

The relationship between sorbate activity and concentration for zeolitic systems is highly nonlinear approaching Henry's law at very low concentration. The factor $\frac{d\ lnP}{d\ lnC}$ is large approaching infinity in the saturation region of the isotherm. In micropore diffusion, self-diffusivity or corrected diffusivity is considered rather than transport diffusivity. Micropore diffusion is an activated process and its dependence on temperature follows Eyring relation [8]:

$$D_c = D_0 \exp\left(-\frac{E_D}{RT}\right) \tag{2.30}$$

where E_D is the diffusional activation energy which depends on the diameter of the sorbate molecule relative to the sieve window.

Micropore diffusivity decreases with sorbate concentration, however, corrected diffusivity D_0 found using Darkens equation (2.25) are essentially independent of concentration.

If micropore diffusion controls the system, the following differential mass balance applies for isothermal process [8]:

$$\frac{\partial q}{\partial t} = \frac{1}{r^2}\frac{\partial}{\partial r}\left(r^2 D_c \frac{\partial q}{\partial r}\right) \tag{2.31}$$

Ruthven and Loughlin [6] developed a criterion to determine the importance of diffusion mechanisms

$$\gamma = \left(\frac{D_c}{r_c^2}\right)\frac{(1+K)}{D_p/R_p^2} \qquad 2.32$$

If $\gamma > 10$, then macropore diffusion controls, whereas if $\gamma < 0.1$, then micropore diffusion controls. For $0.1 < \gamma < 10$, both diffusion mechanisms should be taken into consideration.

2.3.3 Diffusion of 1,3,5-TIPB.

Atias et al. [12] considered micropore diffusion because the size of the 1,3,5-TIPB is nearly the size of the zeolite pore. Configuration diffusion is a strong function of temperature and the dependence on temperature can be expressed by the Eyring expression:

$$\mathrm{D} = D_0 \exp\left(-\frac{E_D}{RT}\right) \qquad 2.33$$

where D_0 is the pre-exponential factor and E_D is the activation energy for diffusion.

Atias et al. [12] estimated the diffusion parameters for 1,3,5-TIPB and found that Activation energies for micropore diffusion are comparable or higher than activation energies for intrinsic reactions. These parameters are presented in Table 9 below:

Table 9: Diffusion parameters for 1,3,5-TIPB at 450°C [12]

Diffusion parameter	CAT-SC	CAT-LC
D_{eff} (m^2/s) 10^{13}	1.76	0.82
E_D (kJ/mol)	165.89	113.11

Zaman et al. [6] considered diffusion in micropore and macropore. Zaman et al. [6] found the data in Table 10 for the diffusion parameter in the zeolite and the matrix:

Table 10: Diffusion parameter in the zeolite and the matrix [6]

T (°C)	D/r^2 sec^{-1}	D_{ap}/R^2 sec^{-1}
150	1.74×10^{-5}	1.33×10^{-5}
170	8.35×10^{-5}	7.17×10^{-5}
190	3.14×10^{-4}	2.90×10^{-4}
210	1.13×10^{-3}	1.40×10^{-3}

2.3.4 Diffusion of 1,2,4-TMB

The critical diameter for 1,2,4-TMB is close to 7.4 Å which is the size of USY zeolite window opening. Therefore, it is assumed that there are no diffusion limitations in 1,2,4-TMB [25].

2.3.5 Diffusion of gas oil:

Atias [2] assumed that the diffusion coefficient of gas oil is comparable to the diffusion of 1,3,5-TIPB, while [17] assumed that the effective gas oil diffusivity at 525°C is 6×10^{-14} m^2/s.

2.4 Effectiveness factor

When diffusion and reaction occur in a porous spherical solid, a quantity called Thiele modulus can be defined, φ^2. The Thiele modulus is the ratio of a surface reaction rate to the diffusion rate. Therefore, it can be used to determine the rate limiting step. If Thiele modulus is large, diffusion limits the overall rate of reaction; while if Thiele modulus is small, the surface reaction is usually rate-limiting. The Thiele modulus is defined by [29]:

$$\varphi^2 = \frac{k_n R^2 C_A^{n-1}}{D_{eff}} \qquad 2.34$$

where k is the rate constant, R is the radius, n is the order of the reaction and D_{eff} is the effective diffusivity.

The importance of diffusion and reaction limitations is depicted by the effectiveness factor. The effectiveness factor is the ratio of actual overall rate of reaction to the rate of reaction in absence of diffusional limitations [29]. The effectiveness factor is expressed in terms of Thiele modulus as [29]:

$$\eta = \frac{\tanh(\varphi)}{\varphi} \qquad 2.35$$

Effectiveness factor η equals to 1 represents no diffusional limitations while η equals to 0 represents infinite diffusive resistance which occurs when the molecule size is larger than a given cut off point defined by the pore size and molecules cannot diffuse in the pores.

Chapter 3. Modeling Isothermal Reaction, Adsorption and Diffusion in FCC Catalyst with Inert Matrix

3.1 Introduction

As in any heterogeneous catalytic reaction, when cracking reactions occur on the catalytic surface of the FCC catalyst, diffusion and adsorption processes are taken into account. Physical adsorption is an extremely rapid process. Therefore, the reactions in porous catalyst are always controlled by mass or heat transfer resistances or reaction kinetics.

As discussed previously, FCC catalyst consists of the zeolite and the matrix. This chapter assumes that adsorption and reaction processes do not occur in the matrix, thus the matrix is inert. Moreover, the diffusivities in the matrix are more rapid than the diffusivities in the zeolite. Hence, diffusion in the zeolite is the controlling mass transfer resistance.

In addition, this chapter assumes isothermal process so the heat transfer resistance is negligible and micropore diffusion in the zeolite is the rate limiting step. Adsorption is an exothermic process while cracking reaction is an endothermic process. The catalyst will remain isothermal if the effect of both processes is comparable or if the rate of heat dissipation by conduction, convection and radiation is higher than the adsorption and reaction rates [8].

This chapter considers different systems for diffusion-reaction processes with different boundary conditions. The chapter starts with the simplest case and proceeds by reducing the assumptions in each section. The main objective of this chapter is to study the effect of different parameters on diffusion-reaction processes to attain the best conditions that increases the yield.

3.2 Linear infinite volume system:

In this section, the diffusion-reaction equation is solved for an infinite volume system. Infinite volume system is a valid assumption when the uptake within the catalyst is very small compared to the capacity of the system. A linear system is a system where the diffusivity is a constant and independent on concentration which is a valid approximation when the change in concentration is small [8].

3.2.1 The model:

When micropore diffusion is rate controlling, the uptake rate is given by the solution of transient diffusion-reaction equation for a spherical particle. The diffusion-reaction equation may be written for reactant A in the following form if transport limitations in the matrix are neglected:

$$\frac{\partial q_A}{\partial t} = \frac{1}{r^2}\frac{\partial}{\partial r}\left(r^2 D_c \frac{\partial q_A}{\partial r}\right) + r_A \qquad 3.2.1$$

The model will be applied to the following reaction:

$$A \rightarrow B$$

The following assumptions will be applied to the model:

1. Linear equilibrium isotherm (Henry's law).

$$q_A = K_A C_A \qquad 3.2.2$$

2. First order reaction with a constant deactivation function.

$$r_A = -k_{int}\,\phi_{int} q_A \qquad 3.2.3$$

3. Constant diffusivity.

Applying these assumptions to Equation 3.2.1 gives the following equation:

$$\frac{\partial q_A}{\partial t} = \frac{D_c}{r^2}\frac{\partial}{\partial r}\left(r^2 \frac{\partial q_A}{\partial r}\right) - k_{int}\phi_{int}\, q_A \qquad 3.2.4$$

For a step change in concentration at time zero, the initial and boundary conditions are:

$$q_A(r, 0) = 0 \qquad 3.2.5$$

$$\left(\frac{\partial q_A}{\partial r}\right)_{r=0} = 0 \tag{3.2.6}$$

$$q_A(r_c, t) = K_A C_\infty \tag{3.2.7}$$

Equation 3.2.4 is the partial differential equation that describes linear micropore diffusion with a first order reaction. Solving this equation with the preceding initial and boundary conditions yields the uptake rate.

3.2.2 Normalization:

To find the solution of the partial differential equation, normalization should be performed. Normalization is a useful tool to simplify the model, reduce the number of parameters and generalize the solution.

The first step in normalization is introducing dimensionless variables as follows:

Let
$$\bar{q}_A = \frac{q_A}{q_0}, \qquad \bar{r} = \frac{r}{r_0}, \qquad \bar{t} = \frac{t}{t_0} \tag{3.2.8}$$

Therefore,
$$\frac{\partial q_A}{\partial t} = \frac{q_0}{t_0}\frac{\partial \bar{q}_A}{\partial \bar{t}} \tag{3.2.9}$$

$$\frac{\partial q_A}{\partial r} = \frac{q_0}{r_0}\frac{\partial \bar{q}_A}{\partial \bar{r}} \tag{3.2.10}$$

Substitute the dimensionless variables in equation 3.2.4:

$$\frac{q_0}{t_0}\frac{\partial \bar{q}_A}{\partial \bar{t}} = \frac{D_c}{r_0^2 \bar{r}^2}\frac{q_0}{r_0}\frac{\partial}{r_0 \partial \bar{r}}\left(r_0^2 \bar{r}^2 \ \frac{\partial \bar{q}_A}{\partial \bar{r}}\right) - k_{int}\phi_{int} q_0 \ \bar{q}_A \tag{3.2.11}$$

$$\frac{\partial \bar{q}_A}{\partial \bar{t}} = \frac{D_c \ t_0}{r_0^2}\frac{1}{\bar{r}^2}\ \frac{\partial}{\partial \bar{r}}\left(\bar{r}^2 \ \frac{\partial \bar{q}_A}{\partial \bar{r}}\right) - k_{int}\phi_{int} \ t_0 \bar{q}_A \tag{3.2.12}$$

Now the value of the quantities t_0, r_0 and q_0 should be determined. The selection should be based on either the physical significance of the quantity or on the mathematical simplification.

Due to physical significance, let:

$$r_0 = r_c \tag{3.2.13}$$

$$q_0 = q_\infty = K_A C_\infty \tag{3.2.14}$$

Due to the mathematical simplification, let:

$$\frac{D_c\, t_0}{r_0^2} = 1 \;\rightarrow t_0 = \frac{r_c^2}{D_c} \tag{3.2.15}$$

$$\varphi^2 = k_{int}\phi_{int}\, t_0 = \frac{k_{int}\phi_{int}\, r_c^2}{D_c} \tag{3.2.16}$$

where φ^2 is the Thiele modulus for the first order reaction.

Substitution in equation 3.2.12 yields:

$$\frac{\partial \bar{q}_A}{\partial \bar{t}} = \frac{1}{\bar{r}^2}\,\frac{\partial}{\partial \bar{r}}\left(\bar{r}^2\,\frac{\partial \bar{q}_A}{\partial \bar{r}}\right) - \varphi^2 \bar{q}_A \tag{3.2.17}$$

Equation 3.2.17 is the dimensionless form of the diffusion-reaction equation (Equation 3.2.4).

The relevant initial and boundary conditions have to be normalized as well:

$$\left(\frac{\partial q_A}{\partial r}\right)_{r=0} = 0 \;\rightarrow \left(\frac{\partial \bar{q}_A}{\partial \bar{r}}\right)_{\bar{r}=0} = 0 \tag{3.2.18}$$

$$q_A(r_c, t) = K_A C_\infty \rightarrow\; \bar{q}_A(1, \bar{t}) = 1 \tag{3.2.19}$$

$$\bar{q}_A(\bar{r}, 0) = 0 \tag{3.2.20}$$

Equation 3.2.17 with the initial and boundary conditions Equations 3.2.18-3.2.20 are ready to be solved.

3.2.3 Orthogonal Collocation

To solve the previous partial differential equation, orthogonal collocation is used. Orthogonal collocation method chooses collocation points as roots of orthogonal polynomials. The two often used orthogonal polynomials are the shifted Legendre polynomials and the Jacobi polynomials. The shifted Legendre polynomials are used for non-symmetric problems; whereas the Jacobi polynomials are used for problems with symmetry [34]. Since equation 3.2.17 is symmetrical, Jacobi polynomials will be used.

Orthogonal collocation transforms a partial differential equation into a system of ordinary differential equations. To apply orthogonal collocation, the following relations are used for spherical coordinates [34]:

$$\frac{\partial y}{\partial r} = \sum_{i=1}^{N+1} A_{ji}\ y_i \qquad 3.2.21$$

$$\frac{1}{r^2}\frac{\partial}{\partial r}\left(r^2\frac{\partial y}{\partial r}\right) = \sum_{i=1}^{N+1} B_{ji}\ y_i \qquad 3.2.22$$

where A and B are matrices with the dimension (N+1, N+1), the index j denote the dependent variable at the collocation points, and N refers to the number of collocation points [34]. Matrices A and B are given in Appendix A.1 for N = 7 and N = 14.

Substituting these relations into the partial differential equation transform it into an ordinary differential equation. The ordinary differential equation was then solved using ODE solver in Matlab. The numerical solution will depend on the number of collocation points. Higher numbers of collocation points will increase the accuracy of the solution. After solving different examples with different number of collocation points, it was found that seven points is a good choice that results in accurate solution. Appendix B compares the solutions for N = 7 and N = 14 for different cases.

Applying orthogonal collocation to equation 3.2.17:

For i = 1 to N:

$$\frac{\partial \bar{q}_i}{\partial \bar{t}} = \sum_{j=1}^{N+1} B_{ij}\,\bar{q}_j - \varphi^2 \bar{q}_i \qquad 3.2.23$$

For i=N+1:

$$\bar{q}_{N+1} = 1 \qquad 3.2.24$$

After solving for the concentration at the orthogonal points, the total concentration as a function of time is given by:

$$\bar{q} = 3\sum_{i=1}^{N+1} W_i\,\bar{q}_i \qquad 3.2.25$$

where W is the weight fraction of each orthogonal point.

Equations 3.2.23-3.2.25 were solved using Matlab for different values of Thiele modulus. The Matlab code is presented in Appendix A.2.

3.2.4 Results:

Figure 15 below shows the uptake for reactant A for different values of Thiele modulus.

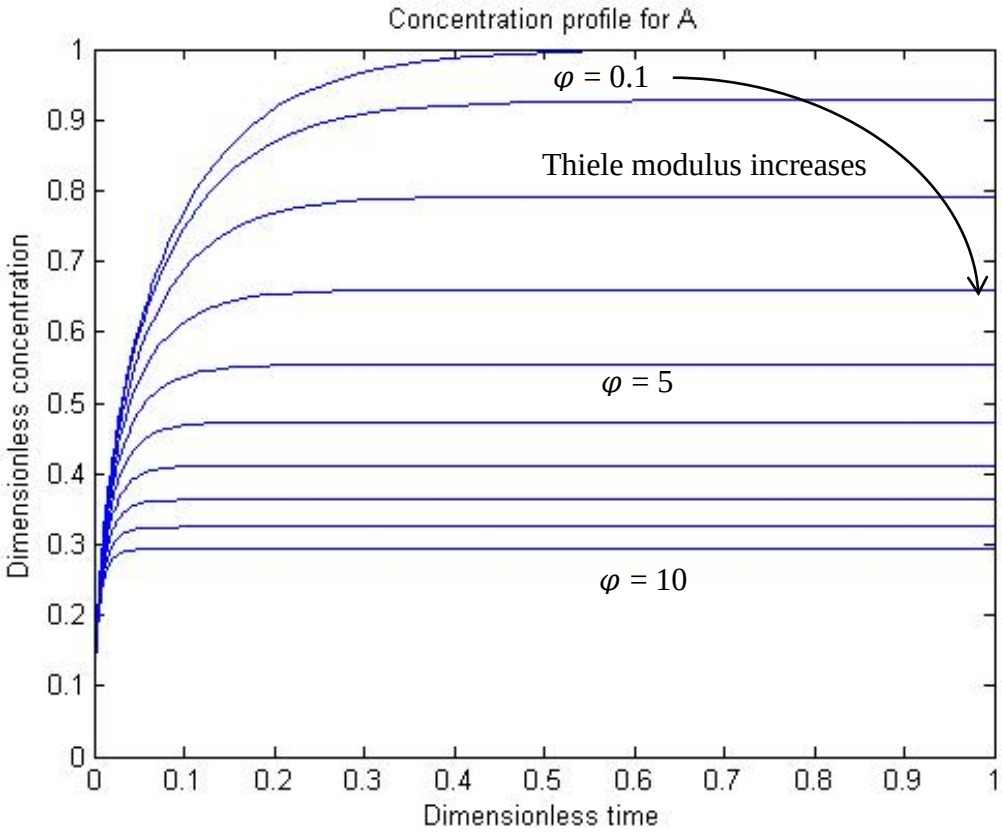

Figure 15: Concentration profile for reactant A

As observed from Figure 15, the concentration of the reactant decreases as the Thiele modulus increases. Therefore, higher conversion is achieved for higher Thiele modules. The Thiele modulus is the ratio of intrinsic reaction to diffusion. Therefore, high Thiele modulus represents regimes where intrinsic reaction controls the overall system. Whereas, low Thiele modulus represents regimes where diffusional limitations affect and lower the reaction rate.

If the model was applied to product B, then the diffusion-reaction equation becomes:

$$\frac{\partial q_B}{\partial t} = \frac{D_c}{r^2}\frac{\partial}{\partial r}\left(r^2\frac{\partial q_B}{\partial r}\right) + k_{int}\phi_{int}\, q_A \qquad 3.2.26$$

For a step change in concentration at time zero, the initial and boundary conditions are:

$$q_B(r,0) = 0 \qquad 3.2.27$$

$$\left(\frac{\partial q_B}{\partial r}\right)_{r=0} = 0 \qquad 3.2.28$$

$$q_B(r_c,t) = 0 \qquad 3.2.29$$

Equation 3.2.26 can be solved using the same steps as for equation 3.1.4. The solution yields the rate uptake for product B. Figure 16 shows the concentration profile for different values of B.

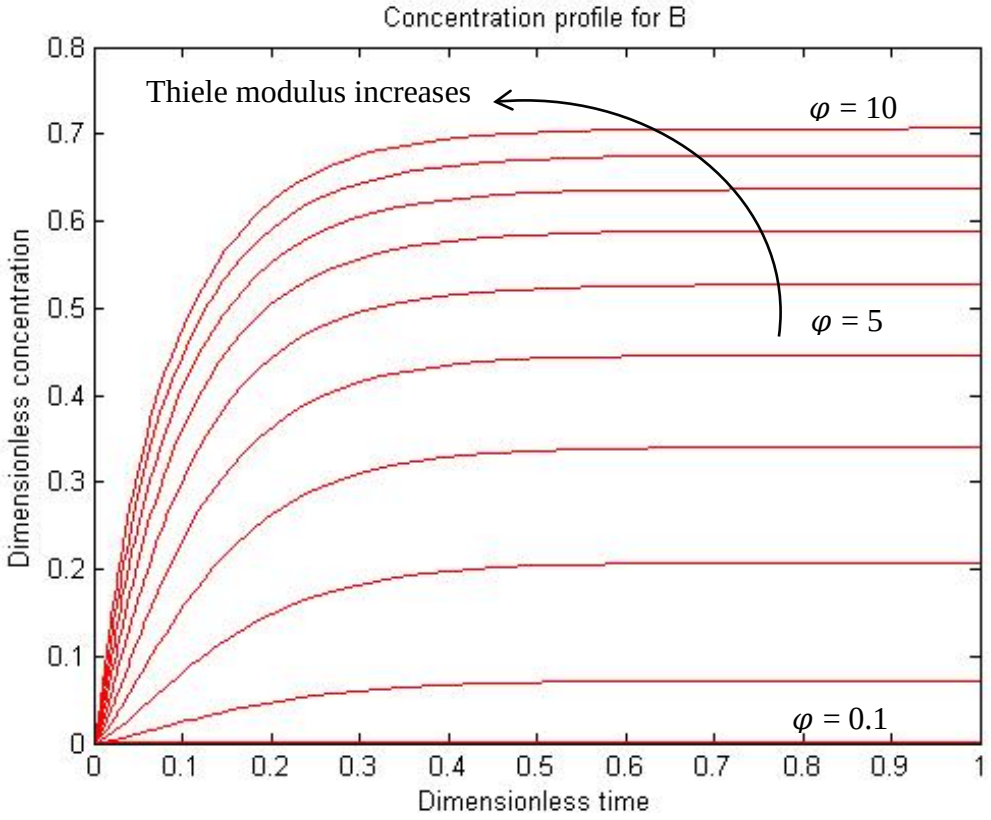

Figure 16: Concentration profile for product B

As illustrated from the figure, the concentration of the product increases as Thiele modulus increases.

Figure 17 shows the Concentration profile for the reactant for different values of Thiele modulus:

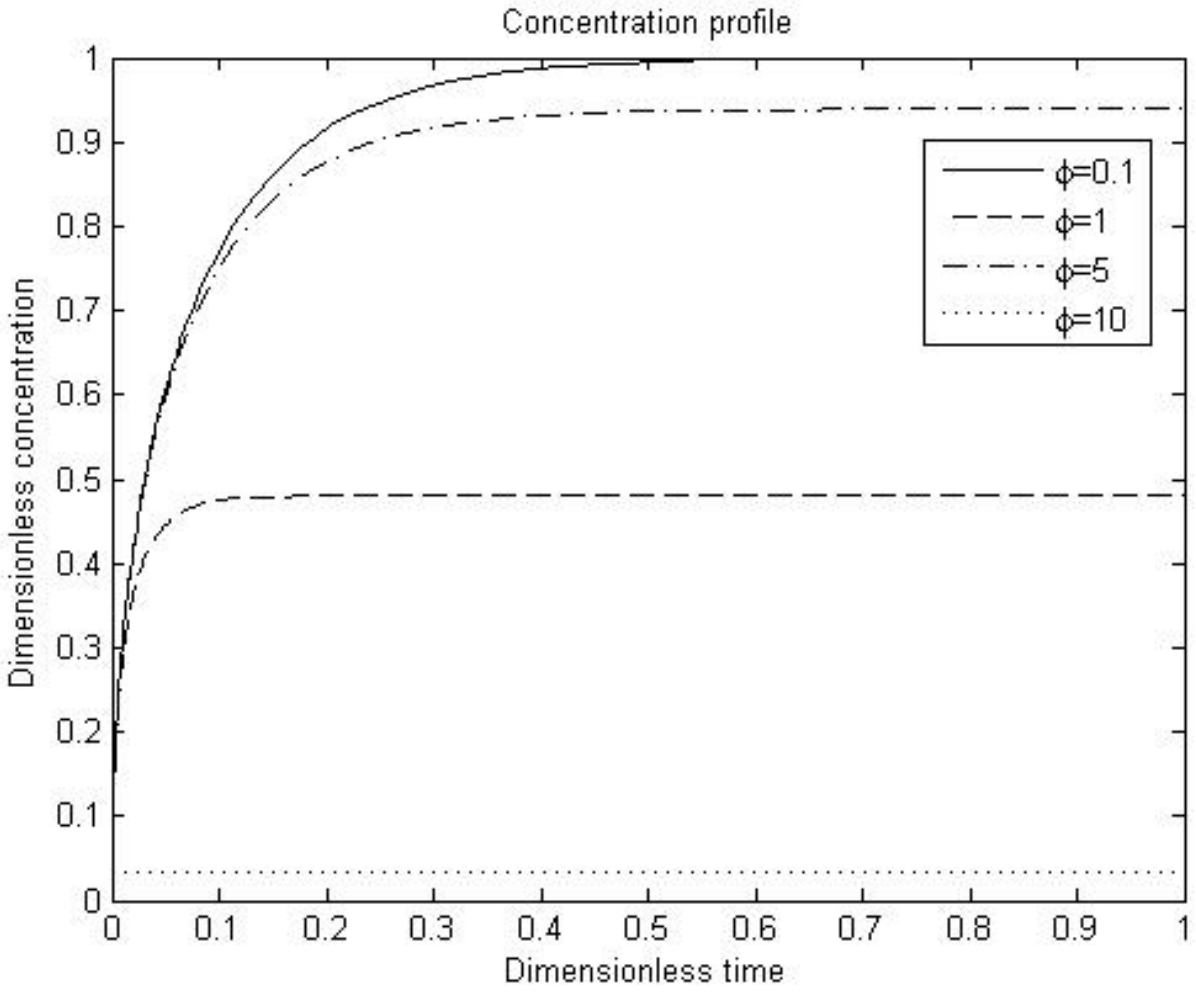

Figure 17: Concentration profile for the reactant for different Thiele modulus

Figure 18 shows the Concentration profile for the product for different values of Thiele modulus:

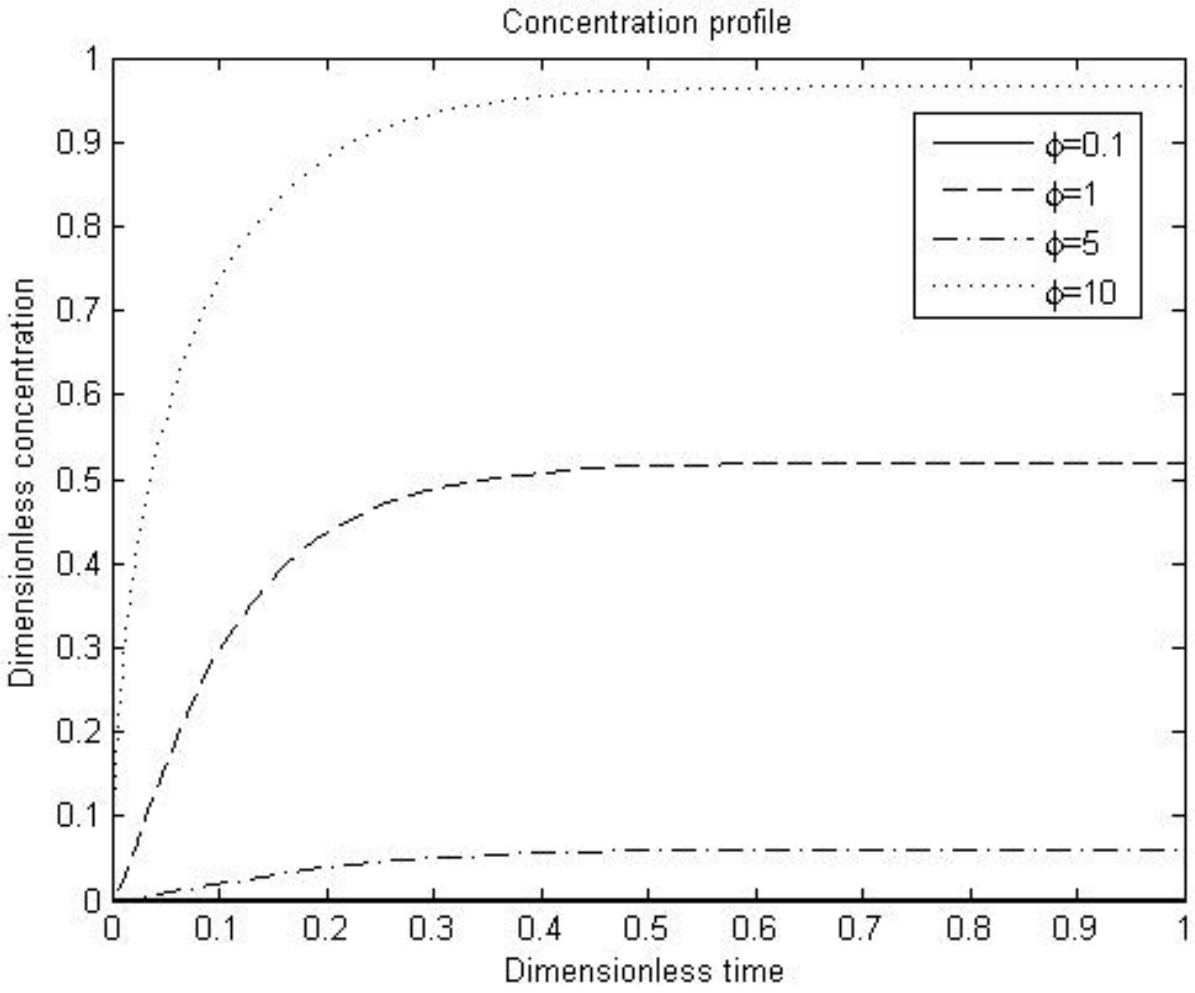

Figure 18: Concentration profile for the product for different Thiele modulus

For the case $\varphi = 0.1$, the intrinsic reaction is hindered by diffusional limitations. Thus, no product is produced. For the case $\varphi = 1$, the rate of intrinsic reaction equals the rate of diffusion. A small amount of the product is produced because the amount of reactant entering the micropore is limited by diffusion. For φ larger than one, the intrinsic reaction is controlling and the conversion is higher for higher values of φ. The concentration of the product exceeds the concentration of the reactant after a short time. Since there is one reactant and one product, the sum of the concentrations in all cases is equal to one.

3.3 Nonlinear infinite volume:

In this section, the diffusion-reaction equation is solved for nonlinear infinite system. For a large concentration step, the system is considered nonlinear. Nonlinear systems are systems where the diffusivity is dependent on the concentration.

For micropore diffusion, the concentration dependency is approximated by Darken's relationship (Equation 2.25).

3.3.1 The model:

Starting from the diffusion-reaction equation:

$$\frac{\partial q_A}{\partial t} = \frac{1}{r^2}\frac{\partial}{\partial r}\left(r^2 D_c \frac{\partial q_A}{\partial r}\right) + r_A \qquad 3.3.1$$

The following assumptions can be applied:

1. Nonlinear equilibrium isotherm (Langmuir isotherm)

$$q_A = \frac{q_s\, b\, C_A}{1 + bC_A} \qquad 3.3.2$$

2. First order reaction with constant deactivation function.

$$r_A = -k_{int}\, \phi_{int} q_A \qquad 3.3.3$$

Applying Darken's relationship with Langmuir isotherm, gives Equation 2.26. Substituting Equation 2.26 in 3.3.1 gives:

$$\frac{\partial q_A}{\partial t} = \frac{D_0}{r^2}\frac{\partial}{\partial r}\left(\frac{r^2}{1-\frac{q}{q_s}}\frac{\partial q_A}{\partial r}\right) - k_{int}\, \phi_{int}\, q_A \qquad 3.3.4$$

Expanding equation 3.3.4 gives:

$$\frac{\partial q_A}{\partial t} = \frac{D_0}{r^2}\left[\frac{1}{1-\frac{q}{q_s}}\frac{\partial}{\partial r}\left(r^2\frac{\partial q_A}{\partial r} + \frac{r^2(-1)\left(-\frac{1}{q_s}\right)}{\left(1-\frac{q_A}{q_s}\right)^2}\left(\frac{\partial q_A}{\partial r}\right)^2\right)\right] - k_{int}\, \phi_{int}\; q_A \qquad 3.3.5$$

The relevant initial and boundary conditions are:

$$\left(\frac{\partial q_A}{\partial r}\right)_{r=0} = 0 \tag{3.3.6}$$

$$q_A(r_c, t) = \frac{q_s\, b\, C_\infty}{1 + bC_\infty} \tag{3.3.7}$$

$$q_A(r, 0) = 1 \tag{3.3.8}$$

Equation 3.3.5 is the diffusion-reaction equation for nonlinear systems.

3.3.2 Normalization

To normalize equation 3.3.5 and the relevant initial and boundary condition, define the following dimensionless variables:

$$\bar{q}_A = \frac{q_A}{q_0}, \qquad \bar{r} = \frac{r}{r_0}, \qquad \bar{t} = \frac{t}{t_0} \tag{3.3.9}$$

Therefore,

$$\frac{\partial q_A}{\partial t} = \frac{q_0}{t_0}\frac{\partial \bar{q}_A}{\partial \bar{t}} \tag{3.3.10}$$

$$\frac{\partial^2 q_A}{\partial r^2} = \frac{q_0}{r_0^2}\frac{\partial^2 \bar{q}_A}{\partial \bar{r}^2} \tag{3.3.11}$$

Substitute in equation 3.3.5:

$$\frac{\partial \bar{q}_A}{\partial \bar{t}} = \frac{D_0 t_0}{r_0^2 \bar{r}^2}\frac{1}{\left(1 - \frac{q_0 \bar{q}_A}{q}\right)}\ \frac{\partial}{\partial \bar{r}}\left(\bar{r}^2\ \frac{\partial \bar{q}_A}{\partial \bar{r}}\right) + \frac{D_0 t_0 q_0}{q_s r_0^2 \left(1 - \frac{q_0 \bar{q}_A}{q_s}\right)^2}\left(\frac{\partial \bar{q}_A}{\partial \bar{r}}\right)^2 - k_{int}\, \phi_{int} t_0 \bar{q}_A \tag{3.3.12}$$

Due to physical significance, let

$$r_0 = r_c \tag{3.3.13}$$

$$\lambda = \frac{q_0}{q_s} \tag{3.3.14}$$

$$q_0 = \frac{q_s\, b\, C_\infty}{1 + b\, C_\infty} = \lambda q_s \tag{3.3.15}$$

where λ is the degree of isotherm nonlinearity.

Due to mathematical simplification, let:

$$\frac{D_0\, t_0}{r_0^2} = 1 \;\rightarrow t_0 = \frac{r_c^2}{D_0} \qquad 3.3.16$$

$$\varphi^2 = k_{int}\, \phi_{int}\, t_0 = \frac{k_{int}\phi_{int}\, r_c^2}{D_0} \qquad 3.3.17$$

Substituting in Equation 3.3.12:

$$\frac{\partial \bar{q}_A}{\partial \bar{t}} = \frac{1}{(1-\lambda \bar{q}_A)}\; \frac{\partial}{\partial \bar{r}}\left(\bar{r}^2\; \frac{\partial \bar{q}_A}{\partial \bar{r}}\right) + \frac{\lambda}{(1-\lambda \bar{q}_A)^2}\left(\frac{\partial \bar{q}_A}{\partial \bar{r}}\right)^2 - \varphi^2 \bar{q}_A \qquad 3.3.18$$

Equation 3.3.18 is the normalized diffusion-reaction for nonlinear system.

Normalization of the boundary and initial conditions gives:

$$\left(\frac{\partial q_A}{\partial r}\right)_{r=0} = 0 \;\rightarrow \left(\frac{\partial \bar{q}_A}{\partial \bar{r}}\right)_{\bar{r}=0} = 0 \qquad 3.3.19$$

$$q_A(r_c, t) = \frac{q_s\, b\, C_A}{1 + b\, C_A} \rightarrow\; \bar{q}_A(1, \bar{t}) = 1 \qquad 3.3.20$$

$$\bar{q}_A(\bar{r}, 0) = 0 \qquad 3.3.21$$

Equation 3.318 with the initial and boundary conditions Equations 3.3.19-3.3.21 are solved using orthogonal collocation.

3.3.3 Orthogonal Collocation:

Applying orthogonal collocation:

For i = 1 to N:

$$\frac{\partial \bar{q}_i}{\partial \bar{t}} = \frac{1}{(1-\lambda \bar{q}_i)}\; \sum_{j=1}^{N+1} B_{ij}\, \bar{q}_j + \frac{\lambda}{(1-\lambda\, \bar{q}_i)^2}\left(\sum_{j=1}^{N+1} A_{ij}\, \bar{q}_j\right)^2 - \varphi^2 \bar{q}_i \qquad 3.3.22$$

For i = N+1:

$$\bar{q}_{N+1} = 1 \qquad 3.3.23$$

Equations 3.3.22-3.3.23 were solved in Matlab. The program is presented in Appendix A.3.

3.3.4 Results:

The concentration profile was found by solving Equation 3.3.23 in Matlab. Figure 19 below shows the concentration profile for reactant A for different values of the degree of isotherm nonlinearity (λ) for Thiele modulus $\varphi = 5$:

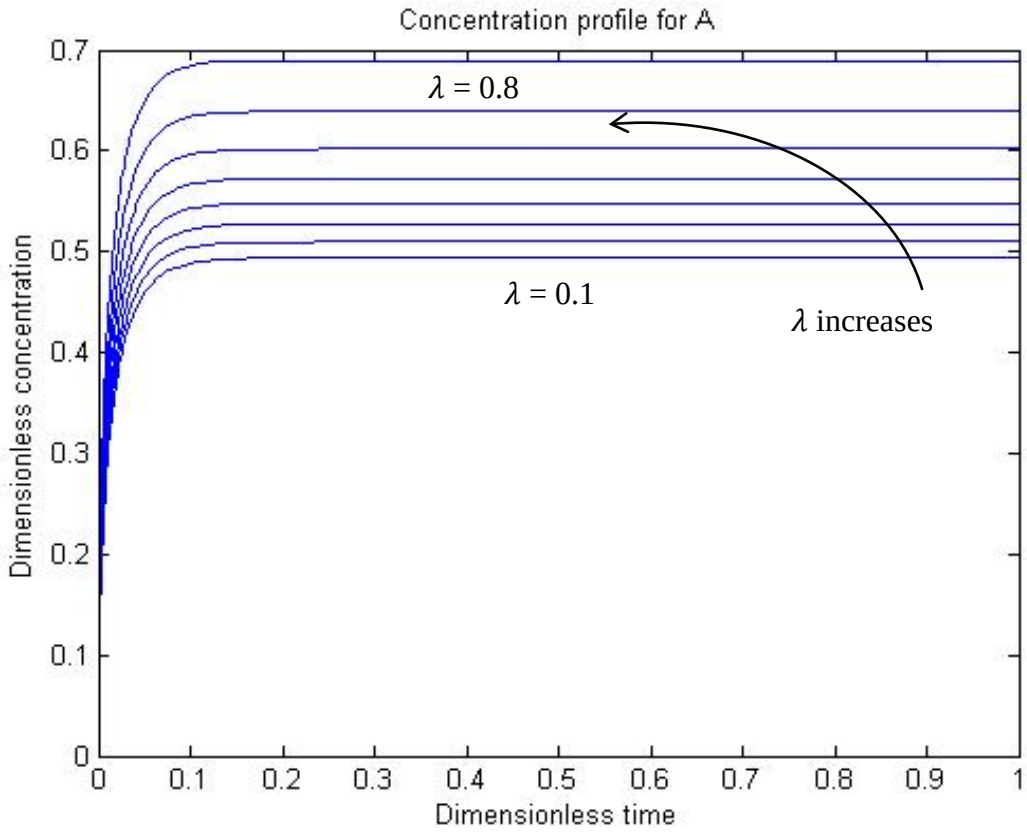

Figure 19: Concentration profile for A for different λ and φ=5

As shown in Figure 19, as the degree of isotherm nonlinearity increases, the concentration of reactant A increases which means that the conversion decreases. This result implies that a linear system will yield a higher conversion than a nonlinear system.

Figure 20 shows the concentration profile for reactant A for linear and nonlinear systems with λ = 0.5 and Thiele modulus $\varphi = 5$:

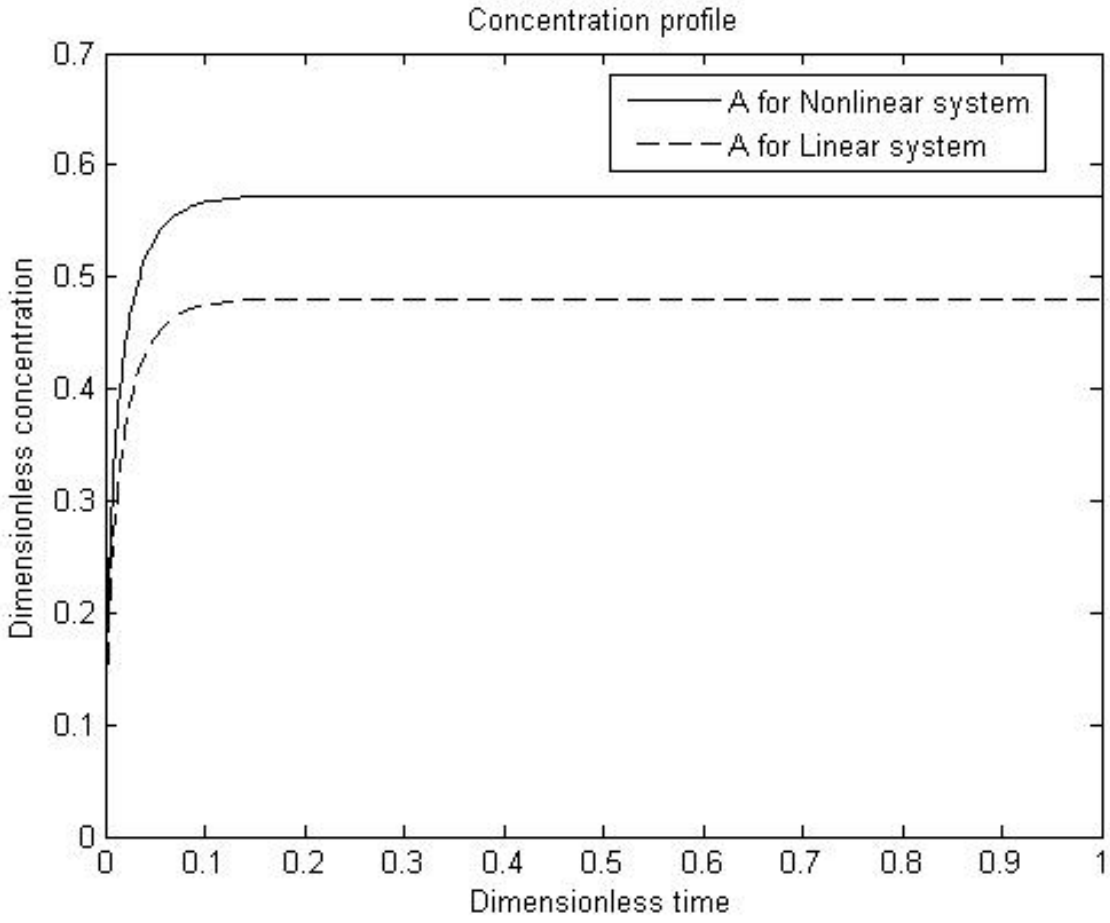

Figure 20: Concentration profile for A for Nonlinear and linear systems

Figure 20 shows that for a degree of isotherm nonlinearity λ = 0.5, the dimensionless concentration of reactant A increases from 0.48 for the linear system to 0.57.

3.4 Linear infinite volume with external fluid film resistance:

In this section, the diffusion-reaction equation is solved for a system that combines micropore diffusion and external fluid film resistance.

3.4.1 The model

Since within the pore only micropore diffusion is present, the diffusion-reaction equation is the same as equation 3.2.4.

$$\frac{\partial q_A}{\partial t} = \frac{D_c}{r^2}\frac{\partial}{\partial r}\left(r^2 \frac{\partial q_A}{\partial r}\right) - k_{int}\phi_{int}\, q_A \qquad 3.2.4$$

The initial and the boundary condition at the center of the catalyst will remain the same. However, the boundary condition at the surface will change.

Equation 3.2.7 will be replaced by the following equation [33]:

$$D_c\left(\frac{\partial q_A}{\partial r}\right)_{r_c} = k_f(C_\infty - C_s) \qquad 3.4.1$$

where k_f is the film mass transfer coefficient, C_∞ is the bulk fluid concentration and C_s is the bulk concentration at the surface. For linear system 3.2.2 is applicable:

$$D_c\left(\frac{\partial q_A}{\partial r}\right)_{r_c} = \frac{k_f}{K_A}(q_\infty - q_{r_c}) \qquad 3.4.2$$

Equation 3.2.4 with the initial condition 3.2.5 and the boundary conditions 3.2.6 and 3.4.2 represents the model for diffusion-reaction system with external fluid film resistance. The external fluid film resistance will affect the reactants only as they diffuse into the particle.

3.4.2 Normalization:

Only Equation 3.4.2 needs to be normalized since the other equations were normalized in the previous sections. Using the same dimensionless variables that were used to normalize Equation 3.2.4:

$$D_c \frac{q_0}{r_0}\left(\frac{\partial \bar{q}_A}{\partial \bar{r}}\right)_{\bar{r}=1} = \frac{k_f}{K_A}(q_\infty - q_0 \bar{q}_{A\bar{r}=1}) \quad 3.4.3$$

$$\left(\frac{\partial \bar{q}_A}{\partial \bar{r}}\right)_{\bar{r}=1} = \frac{k_f\, r_c}{D_c K_A}(1 - (\bar{q}_A)_{\bar{r}=1}) \quad 3.4.4$$

$$\left(\frac{\partial \bar{q}_A}{\partial \bar{r}}\right)_{\bar{r}=1} = Bi_m(1 - (\bar{q}_A)_{\bar{r}=1})) \quad 3.4.5$$

where Bi_m is a dimensionless quantity called the mass transfer Biot number which the ratio of mass transfer resistance inside and at the surface of the catalyst.

Equation 3.2.17 with the initial and boundary conditions 3.2.18, 3.2.20 and 3.4.5 were solved using orthogonal collocation.

3.4.3 Orthogonal collocation:

Applying orthogonal collocation:

For i = 1 to N:

Equation 3.2.23 is still valid.

For i=N+1:

$$\sum_{j=1}^{N+1} A_{N+1,j} q_j = Bi_m(1 - q_{N+1}) \quad 3.4.6$$

Therefore,

$$q_{N+1} = \frac{Bi_m - \sum_{j=1}^{N} A_{ij} q_j}{Bi_m + A_{N+1,N+1}} \quad 3.4.7$$

Equations 3.2.23 and 3.4.7 were solved in Matlab. The code is presented in Appendix A.4

3.4.4 Results:

The previous model was applied to reactant A and the concentration profile is shown in Figure 21 for different values of the mass transfer Biot number with no reaction.

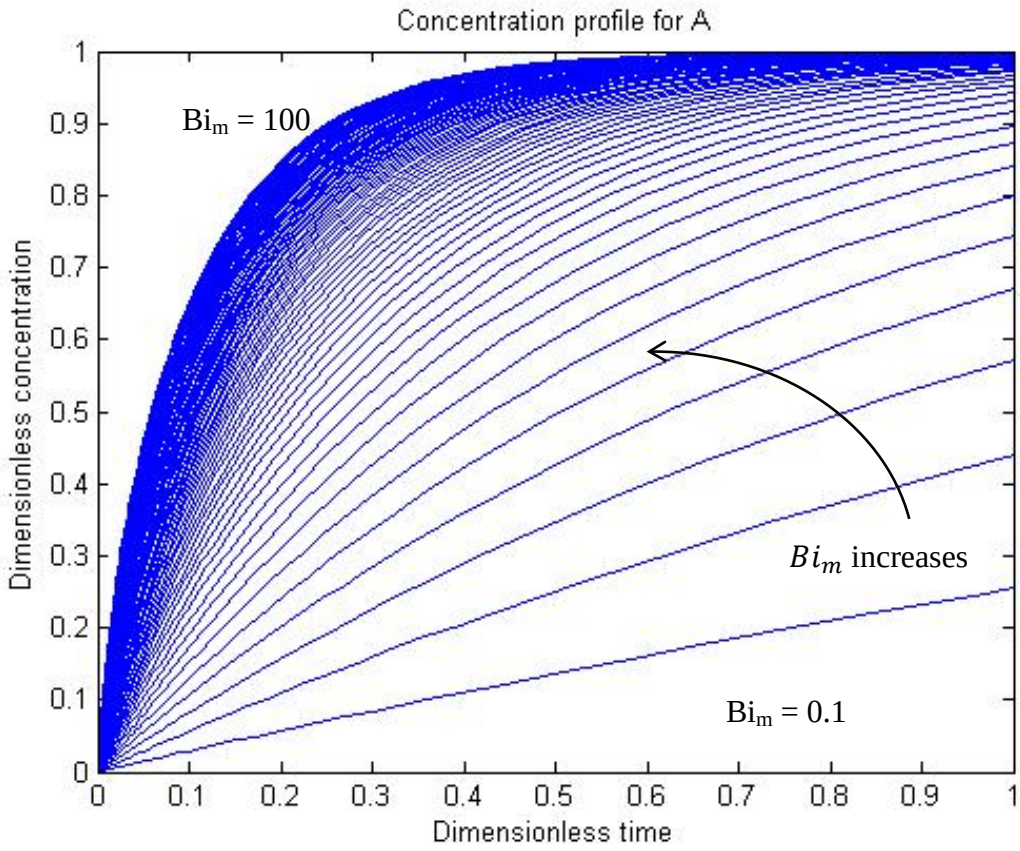

Figure 21: Concentration profile for different values of Biot number

Figure 21 shows that as the mass transfer Biot number decreases, the concentration of reactant A inside the catalyst decreases. Therefore, less reactant is present inside the catalyst and the yield of products is lower.

For large Biot number, micropore diffusion controls the system, whereas, for small Biot number, the external film resistance controls. From the previous figure, micropore diffusion is preferred as the controlling step.

Figure 22 below compares the concentration of reactant A and product B for two values of Biot number and Thiele modulus $\varphi = 5$.

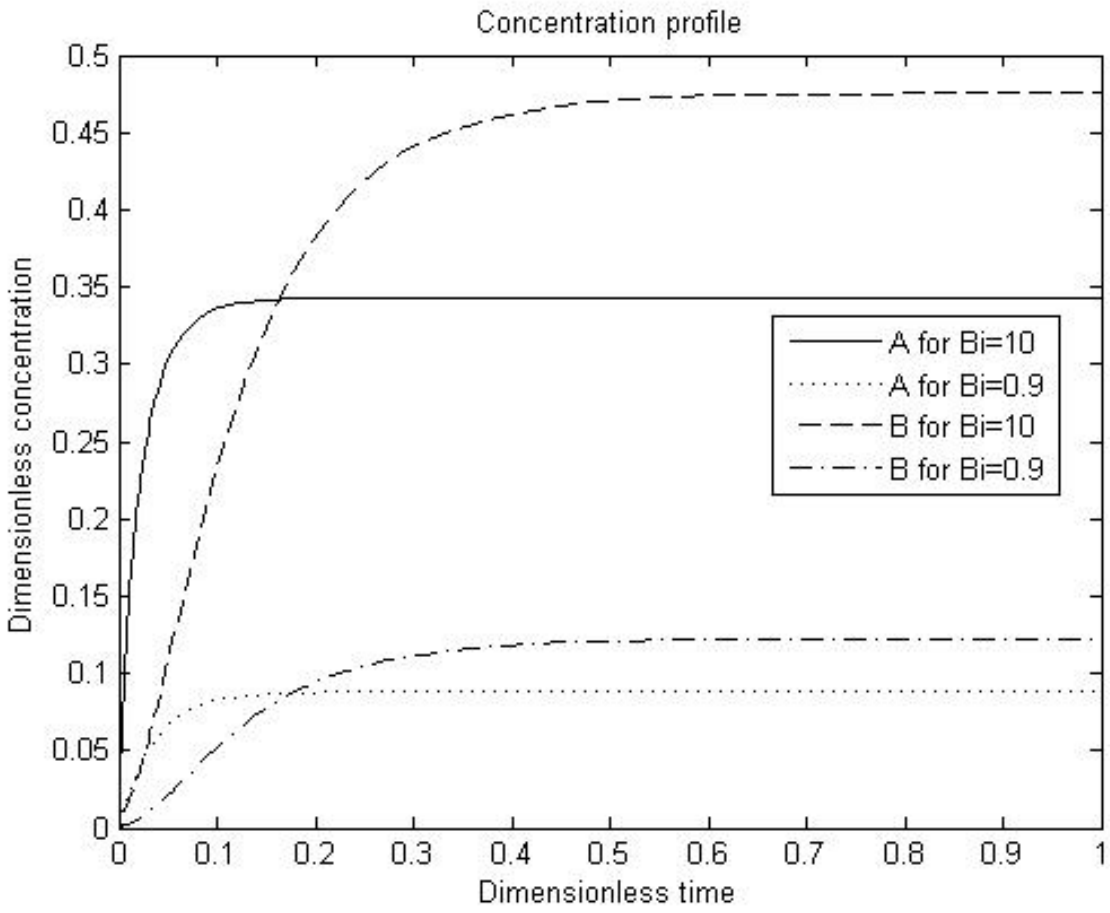

Figure 22: Concentration profile for A and B for different Bi number

From Figure 22, a large mass transfer Biot number (Diffusion controls) results in a higher conversion because more reactant is available for the reaction.

Figure 23 compares the concentration profile for reactant A for Biot number equals to 10, 1 and 0.1 and the case if no external fluid film resistance is present. The Thiele modulus is set to 5.

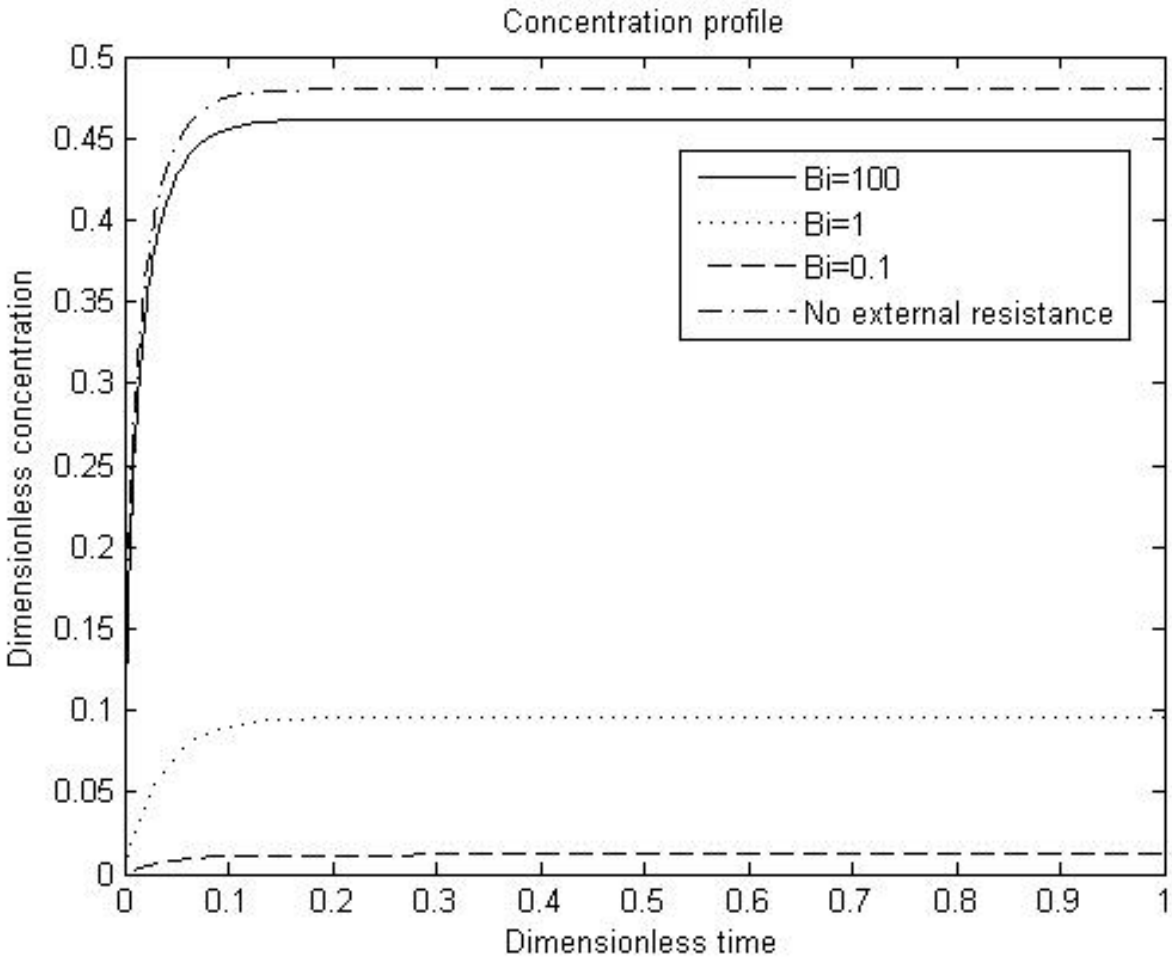

Figure 23: Concentration profile for A for different Biot number

Figure 23 shows that even for a large Biot number as 100, the concentration of reactant A is less than the concentration if external fluid film resistance is not present. When the rate of external fluid film resistance equals the rate of diffusion, the concentration of reactant A is approximately 20% of the concentration if external fluid film resistance is not present. For the case when Biot number is equals to 0.1, approximately no reactant is present.

3.5 Linear finite volume:

This section relaxes the assumption of infinite volume. For constant volume reactors such as the CREC Riser Simulator and for strongly adsorbed species, the assumption of infinite volume is invalid.

3.5.1 Model:

The diffusion-reaction equation for this system is the same as equation 3.2.4.

$$\frac{\partial q_A}{\partial t} = \frac{D_c}{r^2}\frac{\partial}{\partial r}\left(r^2 \frac{\partial q_A}{\partial r}\right) - k_{int}\phi_{int}\, q_A \qquad 3.2.4$$

The initial and the boundary condition at the center of the catalyst will remain the same. However, the boundary condition at the surface will change.

In the CREC, the concentration of the bulk fluid is uniform and dependent only on the time because the CREC is well stirred. The total mass transferring across the surface per unit time is equal to the rate of increasing the total mass in the spherical catalyst:

$$-4\,\pi\, N\, r_c^2\, D_c \left(\frac{\partial q_A(r,t)}{\partial r}\right)_{r=rc} = V \left(\frac{\partial C_A(r,t)}{\partial t}\right)_{r=r_c} \qquad 3.5.1$$

where V is the volume of the fluid and N is the number of solid particles.

Substituting Equation 3.2.2:

$$-4\,\pi\, N\, r_c^2\, D_c \left(\frac{\partial q_A(r,t)}{\partial r}\right)_{r=rc} = \frac{V}{K_A}\left(\frac{\partial q_A(r,t)}{\partial t}\right)_{r=r_c} \qquad 3.5.2$$

Equation 3.2.4 with the initial condition 3.2.5 and the boundary conditions 3.2.6 and 3.5.2 represents the model for diffusion-reaction system with finite volume.

3.5.2 Normalization:

Only the boundary condition at the surface needs to be normalized. Substituting the previous dimensionless variables into equation 3.5.2:

$$-4\,\pi\, N\, r_c^2 D_c \frac{K_A}{V}\frac{q_0}{r_0}\left(\frac{\partial \bar{q}_A}{\partial \bar{r}}\right)_{\bar{r}=1} = \frac{q_0}{t_0}\left(\frac{\partial \bar{q}_A}{\partial \bar{t}}\right)_{\bar{r}=1} \qquad 3.5.3$$

Substitute equation 3.2.15 into equation 3.5.3:

$$-4\,\pi\,N\,r_c^3\,\frac{K_A}{V}\left(\frac{\partial \bar{q}_A}{\partial \bar{r}}\right)_{\bar{r}=1} = \left(\frac{\partial \bar{q}_A}{\partial \bar{t}}\right)_{\bar{r}=1} \qquad 3.5.4$$

Define Λ as the ratio of the volume of the bulk fluid to that of the sphere. Therefore:

$$\Lambda = \frac{V}{\frac{4}{3}\,\pi\,N\,r_c^3 K_A} \qquad 3.5.5$$

Therefore, equation 3.5.3 becomes:

$$\left(\frac{\partial \bar{q}}{\partial \bar{t}}\right)_{\bar{r}=1} = -\frac{3}{\Lambda}\left(\frac{\partial \bar{q}}{\partial \bar{r}}\right)_{\bar{r}=1} \qquad 3.5.6$$

Equation 3.5.6 is the boundary condition for the case of finite volume.

The model of diffusion-reaction of a reactant in limited volume is equation 3.2.17 with the boundary conditions 3.2.18 and 3.5.6 and the initial condition 3.2.20.

3.5.3 Orthogonal collocation:

Applying orthogonal collocation:

For i = 1 to N:

Equation 3.2.23 is still valid.

For i=N+1:

$$\left(\frac{\partial \bar{q}}{\partial \bar{t}}\right)_{N+1} = -\frac{3}{\Lambda}\sum_{j=1}^{N+1} A_{N+1,j}\,\bar{q}_j \qquad 3.5.7$$

where $\bar{q}_{N+1}$is defined as:

For t = 0

$$q_{N+1} = 1 \qquad 3.5.8$$

For t > 0

$$\bar{q}_{N+1} = \frac{\left[\left(\frac{\partial \bar{q}}{\partial \bar{t}}\right)_{N+1} + \frac{3}{\Lambda}\Sigma_{i=1}^{N} A_{N+1,i}\,\bar{q}_i\right]}{-\frac{3}{\Lambda}A_{N+1,N+1}} \qquad 3.5.9$$

Equations 3.2.23 and 3.5.7 were solved in Matlab. The code is presented in Appendix A.5

3.5.4 Results:

Figure 24 below shows the concentration profile for reactant A for different values of Λ with no reaction.

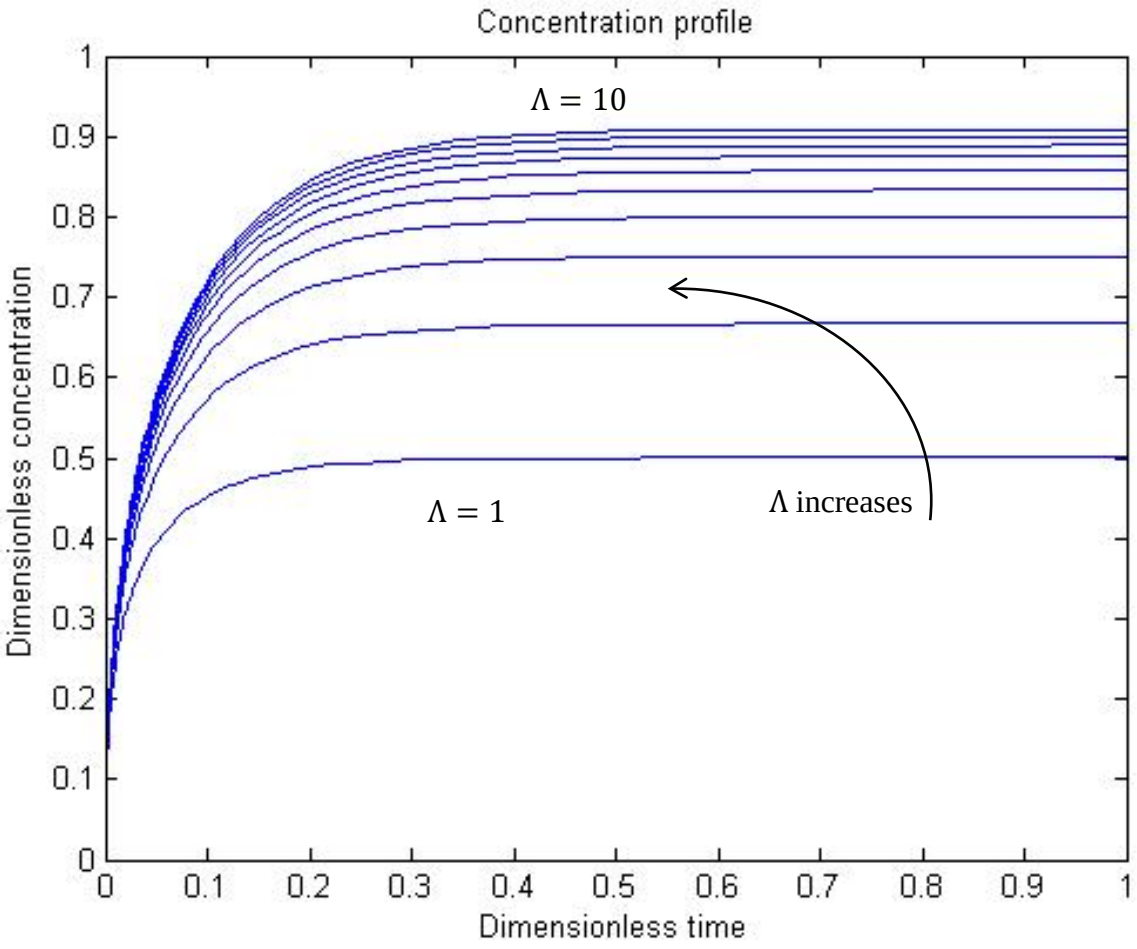

Figure 24: Concentration profile for reactant A for different values of Λ

From Figure 24, as the ratio of the volumes of solution and spheres increase, the concentration of the reactant increases. High Λ is desired to increase the conversion.

Figure 25 below shows the concentration profile for reactant A for different values of Λ with Thiele modulus $\varphi = 5$.

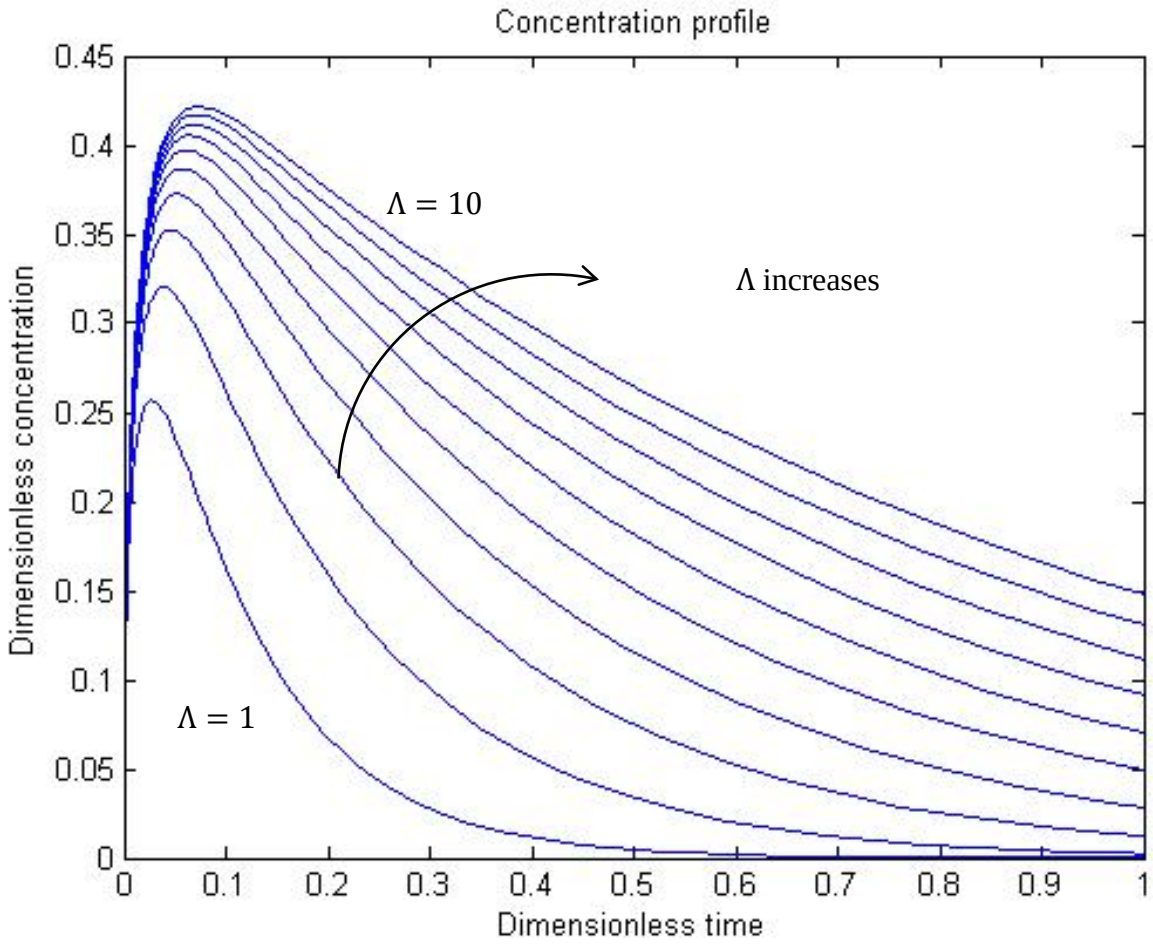

Figure 25: Concentration profile for reactant A for different values of Λ with Thiele modulus φ=5

As shown in Figure 25, the concentration of reactant A initially increases and after a short time, the concentration decreases rapidly. This behavior occurs because reactant A is consumed in the reaction and due to the limited volume, reactant A cannot be replenished so 100% conversion is achieved.

Figure 26 shows the concentration profile for product B for different values of Λ with Thiele modulus $\varphi = 5$.

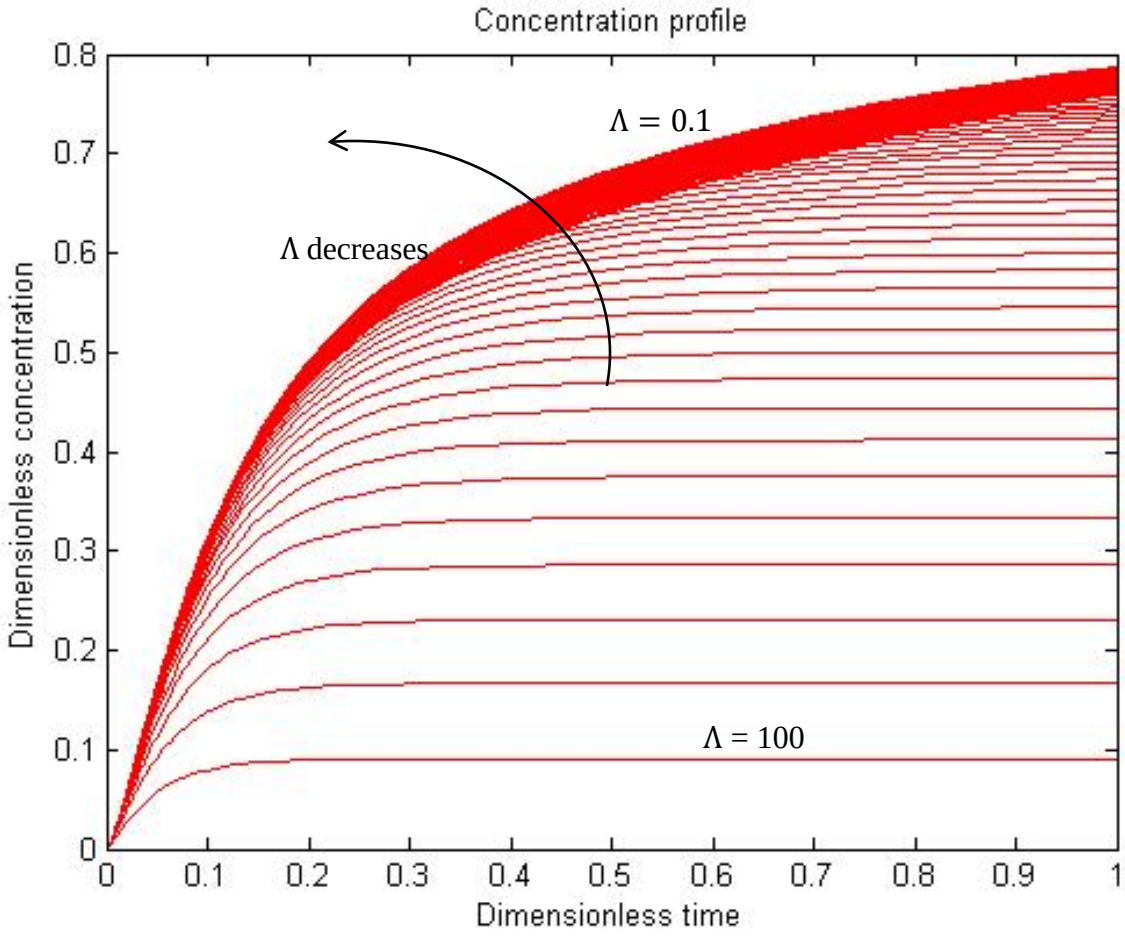

Figure 26: Concentration profile for product B for different values of Λ with Thiele modulus φ=5

Figure 26 shows that as Λ decreases, the concentration of the product increases.

Figure 27 compares the reactant concentration profile for infinite and finite volumes with no reaction for Λ = 100 and Thiele modulus $\varphi = 0$

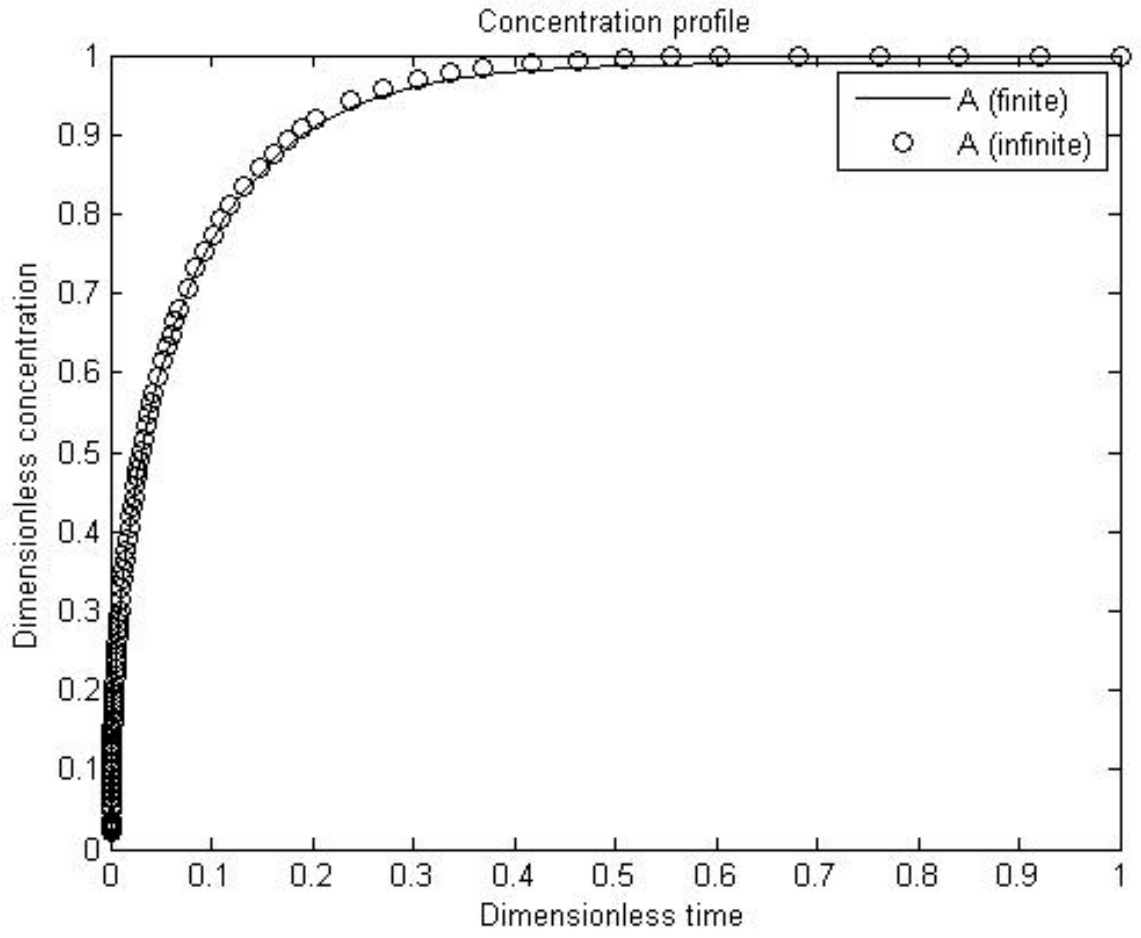

Figure 27: Concentration profile for infinite and finite volumes with no reaction for Λ = 100

As shown from Figure 27, when the ratio of the volumes of fluid and solids is Λ = 100, the concentration of reactant A is the same as the concentration resulted from an infinite volume system.

Figure 28 compares the reactant and product concentration profile for infinite and finite volumes for Λ = 100 and Thiele modulus $\varphi = 5$

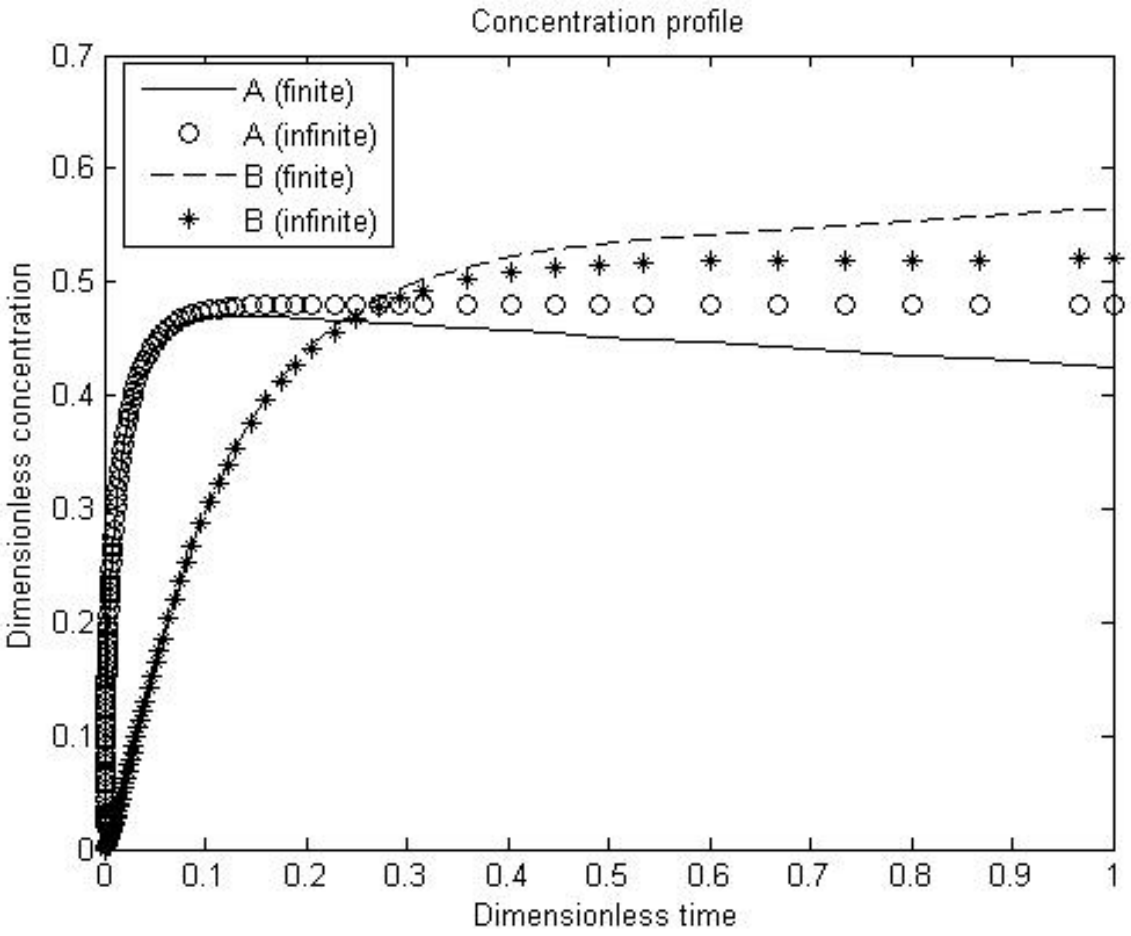

Figure 28: Concentration profile for infinite and finite volumes for Λ = 100 and $\varphi = 5$

As shown from Figure 28, when the ratio of the volumes of fluid and solids is Λ = 100 and there is a reaction, the concentration of reactant A in a finite system is initially the same as the concentration of reactant A in an infinite system but it decreases after a short time rapidly. The concentration of product B is higher in the finite volume than in the infinite volume systems. Figure 28 demonstrates the short time solution for finite volume. As the reaction proceeds, the concentration of the product will reach 1 while the concentration of the reactant will reach 0.

Figure 29 compares the reactant and product concentration profile for infinite and finite volumes with for $\Lambda = 10$ with no reaction.

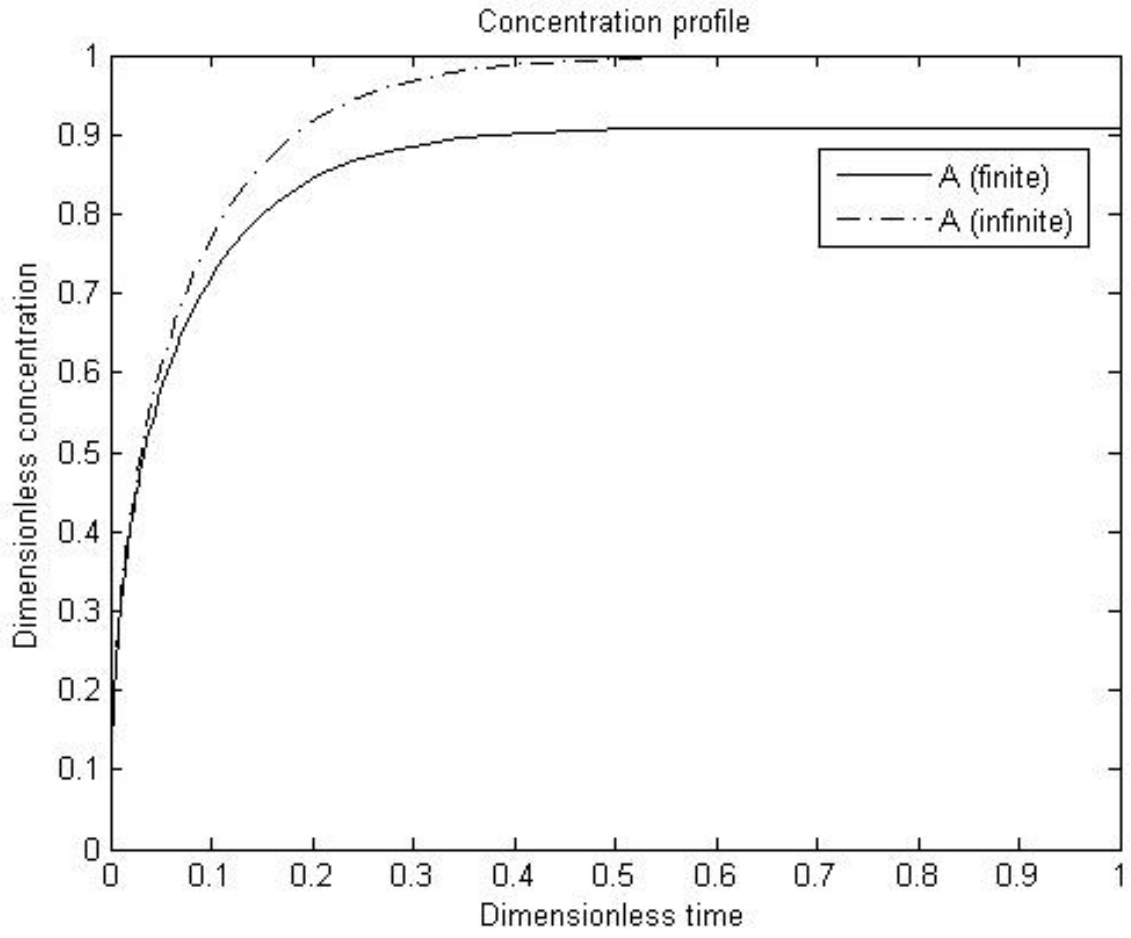

Figure 29: Concentration profile for infinite and finite volumes for $\Lambda = 10$ with no reaction

Figure 29 shows that when the ratio of the volumes of fluid and solids is $\Lambda = 10$ and no reaction is present; the concentration of reactant A in a finite system is almost 90% of that of the infinite volume.

Figure 30 compares the reactant and product concentration profile for infinite and finite volumes with for Λ = 10 and Thiele modulus $\varphi = 5$

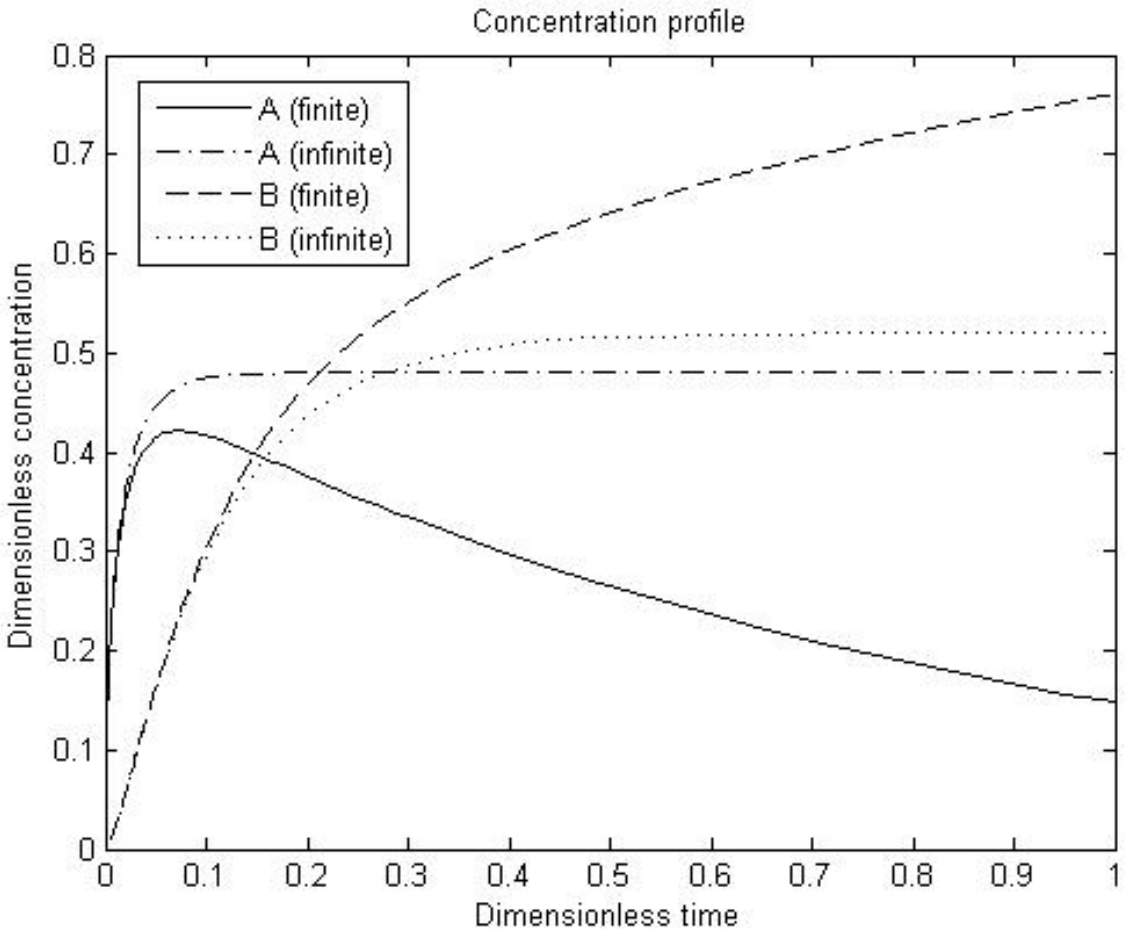

Figure 30: Concentration profile for infinite and finite volumes for Λ = 10 and $\varphi = 5$

As shown from Figure 30, when the ratio of the volumes of fluid and solids is Λ = 10 and the Thiele modulus $\varphi = 5$, the concentration of reactant A in a finite system decreases as the reaction proceeds. The concentration of product B is higher when the volume is finite.

3.6 Linear finite volume with external fluid film resistance:

This section solves the diffusion-reaction equation for a finite volume system where two resistances are present: micropore diffusion and external fluid film resistances.

3.6.1 The model:

Since within the pore only micropore diffusion is present, the diffusion-reaction equation is the same as equation 3.2.4.

$$\frac{\partial q_A}{\partial t} = \frac{D_c}{r^2}\frac{\partial}{\partial r}\left(r^2 \frac{\partial q_A}{\partial r}\right) - k_{int}\phi_{int}\, q_A \qquad 3.2.4$$

The initial and the boundary condition at the center of the catalyst will remain the same. However, the boundary condition at the surface will change.

Since the system has a limited volume, Equation 3.5.2 is applied:

$$-4\,\pi\, N\, r_c^2\, D_c \left(\frac{\partial q_A}{\partial r}\right)_{r=rc} = \frac{V}{K_A}\left(\frac{\partial q_A}{\partial t}\right)_{r=r_c} \qquad 3.5.2$$

Also, Equation 3.4.8 is applied due to the external fluid film resistance:

$$D_c \left(\frac{\partial q_A}{\partial r}\right)_{r_c} = k_f (C_\infty - C_s) \qquad 3.4.8$$

For a linear system, Equation 3.4.9 is obtained:

$$D_c \left(\frac{\partial q_A}{\partial r}\right)_{r_c} = \frac{k_f}{K_A}(q_\infty - q_{r_c}) \qquad 3.4.9$$

Combining the two equation yields,

$$\left(\frac{\partial q_A}{\partial t}\right)_{r=r_c} = \frac{-4\,\pi\, N\, r_c^2 k_f}{V}(q_\infty - q_{r_c}) \qquad 3.6.1$$

Equation 3.6.1 is the boundary condition at the surface for limited volume system with external fluid film resistance.

3.6.2 Normalization:

Only the boundary condition at the surface needs to be normalized. Substituting the previous dimensionless variables into equation 3.6.1:

$$\left(\frac{\partial \bar{q}_A}{\partial \bar{t}}\right)_{\bar{r}=1} = -\frac{3}{\Lambda}\, Bi_m \left(\frac{q_\infty}{q_0} - (\bar{q}_A)_{\bar{r}=1}\right) \qquad 3.6.2$$

Since the volume of the system is limited, $q_\infty \neq q_0$. To find the relation between q_∞ and q_0, a mass balance around the total volume is performed:

The mass of the system initially is equal to the total mass inside the catalyst.

$$V\, C_0 = V\, C_\infty + V_s\, q_\infty \qquad 3.6.3$$

$$C_0 = C_\infty \left(1 + \frac{V_s K}{V}\right) \qquad 3.6.4$$

Substituting Equation 3.5.5:

$$C_\infty = \frac{\Lambda}{1 + \Lambda}\, C_0 \qquad 3.6.5$$

$$\frac{q_\infty}{q_0} = \frac{\Lambda}{1 + \Lambda} \qquad 3.6.6$$

Substitute Equation 3.6.6 into Equation 3.6.2:

$$\left(\frac{\partial \bar{q}_A}{\partial \bar{t}}\right)_{\bar{r}=1} = -\frac{3}{\Lambda}\, Bi_m \left(\frac{\Lambda}{1 + \Lambda} - (\bar{q}_A)_{\bar{r}=1}\right) \qquad 3.6.7$$

Equation 3.6.7 is the normalized boundary condition at the surface for limited volume system with external fluid film resistance. Therefore, the model of diffusion-reaction equation for this system is equation 3.2.17 with the boundary conditions 3.2.18 and 3.6.7 and the initial condition 3.2.20.

3.6.3 Orthogonal collocation:

Applying orthogonal collocation:

For i = 1 to N:

Equation 3.2.23 is still valid.

For i=N+1:

Equation 3.5.7 is valid:

$$\left(\frac{\partial \bar{q}}{\partial \bar{t}}\right)_{N+1} = -\frac{3}{\Lambda}\sum_{j=1}^{N+1} A_{N+1,j}\,\bar{q}_j \qquad 3.5.7$$

where $\bar{q}_{N+1}$is defined as in Equations 3.4.11:

$$\bar{q}_{N+1} = \frac{Bi_m - \sum_{j=1}^{N} A_{ij}\bar{q}_j}{Bi_m + A_{N+1,N+1}} \qquad 3.4.11$$

Equations 3.2.23 and 3.5.7 were solved in Matlab. The code is presented in Appendix A.6

3.6.4 Results:

The diffusion-reaction equation was solved for this system using Matlab. Figure 31 shows the concentration profile for reactant A and product B for the case when Thiele modulus φ=5, the ratio of the volumes Λ=10 and the mass transfer Biot number Bi_m=10.

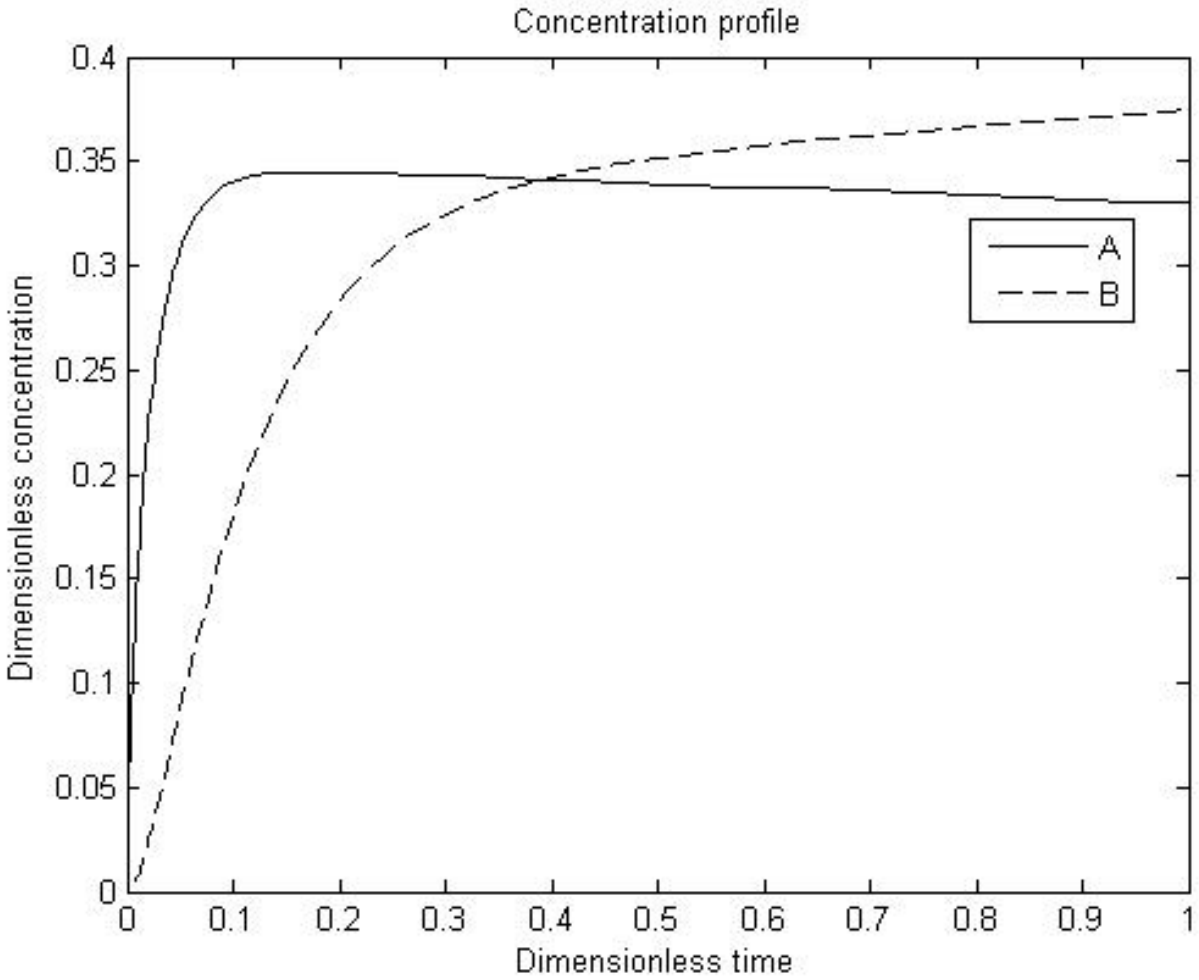

Figure 31: Concentration profile for finite volume with external fluid film resistance

Comparing Figure 31 with Figure 30, initially the concentration of reactant A is higher for Figure 30. However after a short time, the concentration of reactant A in Figure 30 decreases rapidly. The external mass transfer resistance eliminates this decrease as shown in Figure 31.

Figure 32 shows the concentration profile for reactant A and product B for the case when Thiele modulus φ=5, the ratio of the volumes Λ=1 and the mass transfer Biot number Bi_m=10.

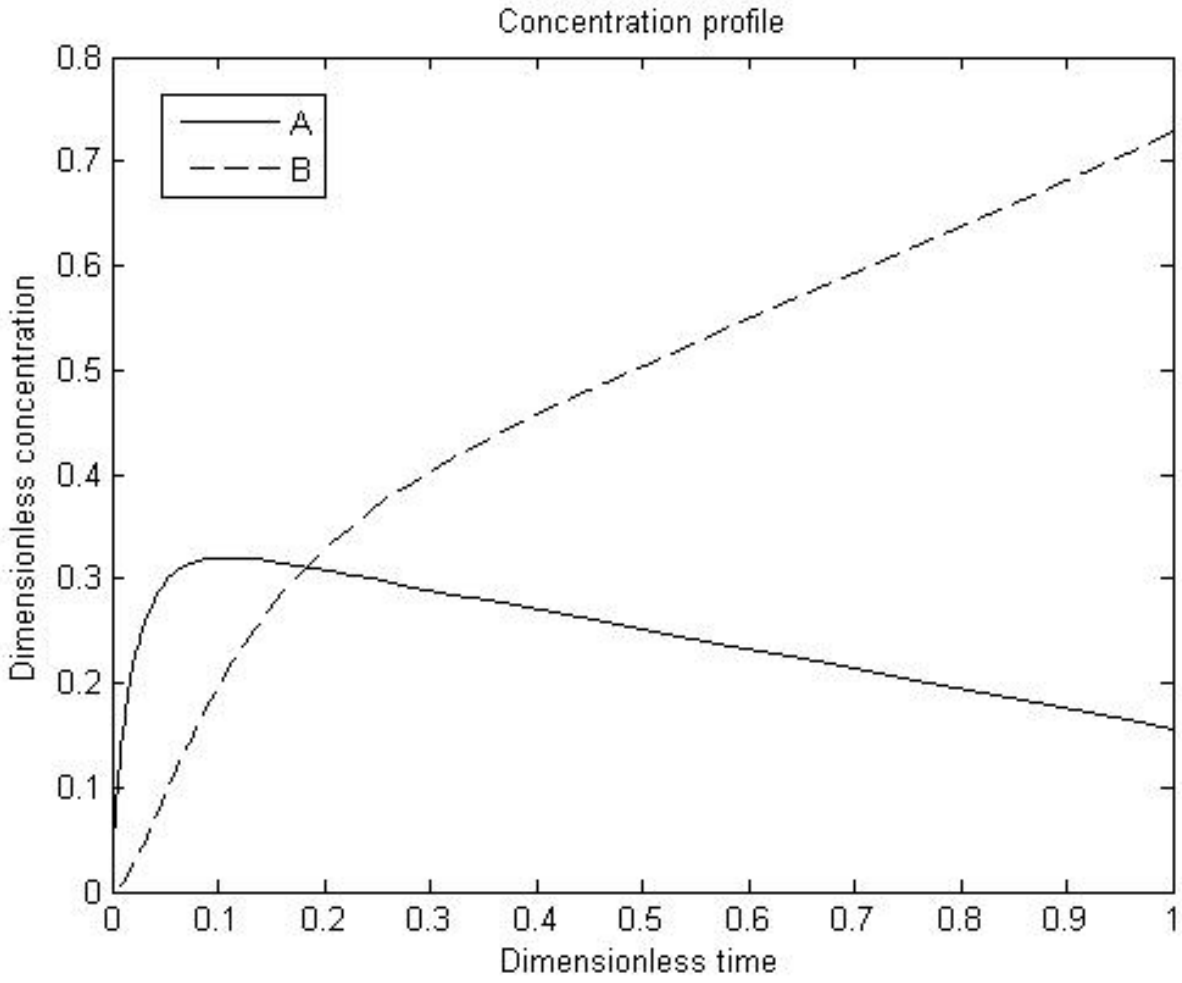

Figure 32: Concentration profile for finite volume with external fluid film resistance

Comparing Figure 32 with Figure 31, both graphs have almost the same profile. However, the ratio of the fluid and solids volumes is decreased to 1. Therefore, introducing the effect of external fluid film resistance created the same effect of 10 times higher ratio (Λ).

Figure 33 shows the concentration profile for reactant A and product B for the case when Thiele modulus φ=5, the ratio of the volumes Λ=10 and the mass transfer Biot number Bi_m=1.

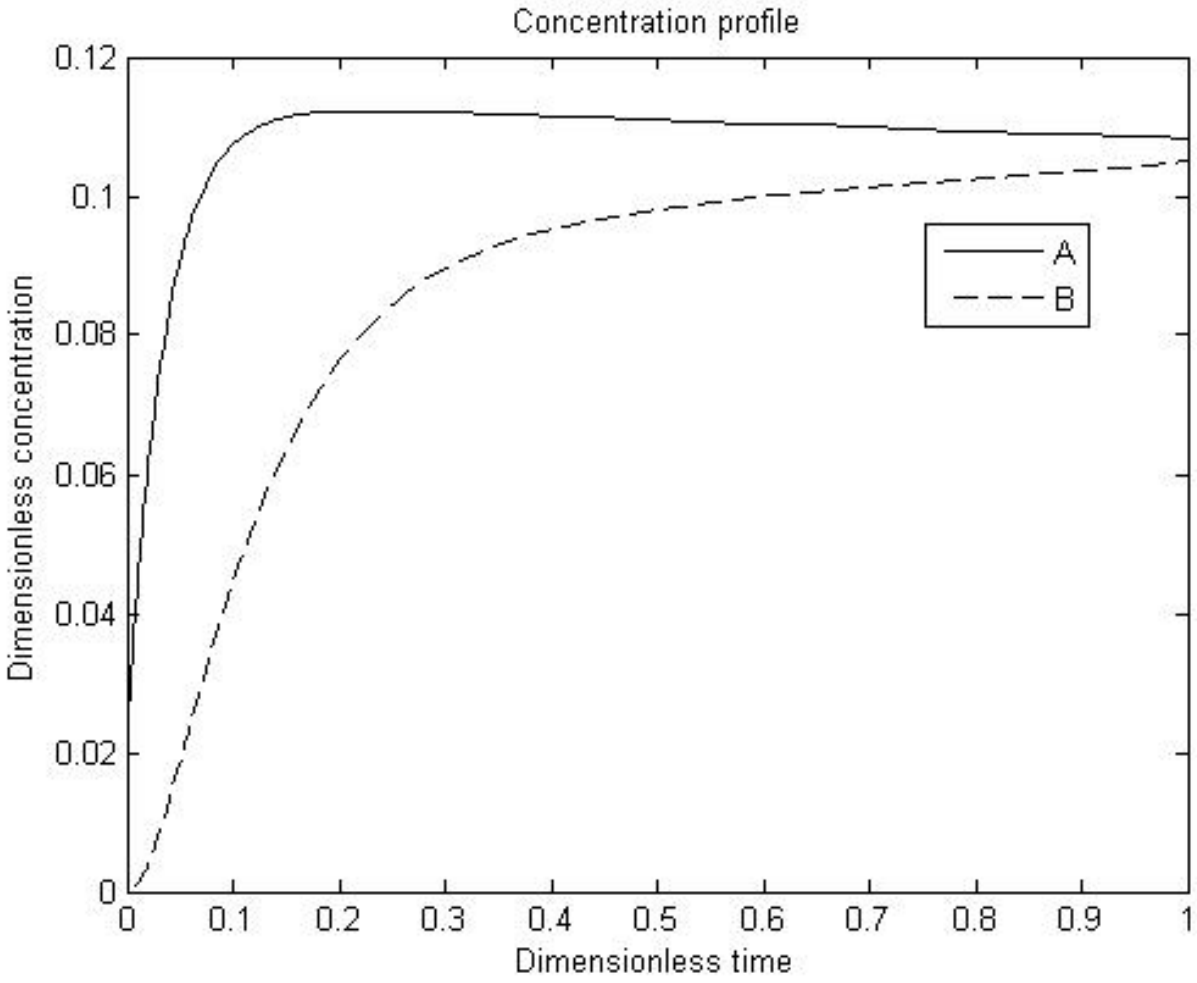

Figure 33: Concentration profile for finite volume with external fluid film resistance

Figure 33 shows that a low ratio (Λ) and a low Biot number (Bi_m) produce a very low yield. This establishes that external fluid film resistance should be eliminated if possible while finite volume systems are preferred.

Figure 34 shows the concentration profile for reactant A and product B for the case when Thiele modulus φ=5, the ratio of the volumes Λ=100 and the mass transfer Biot number Bi_m=100.

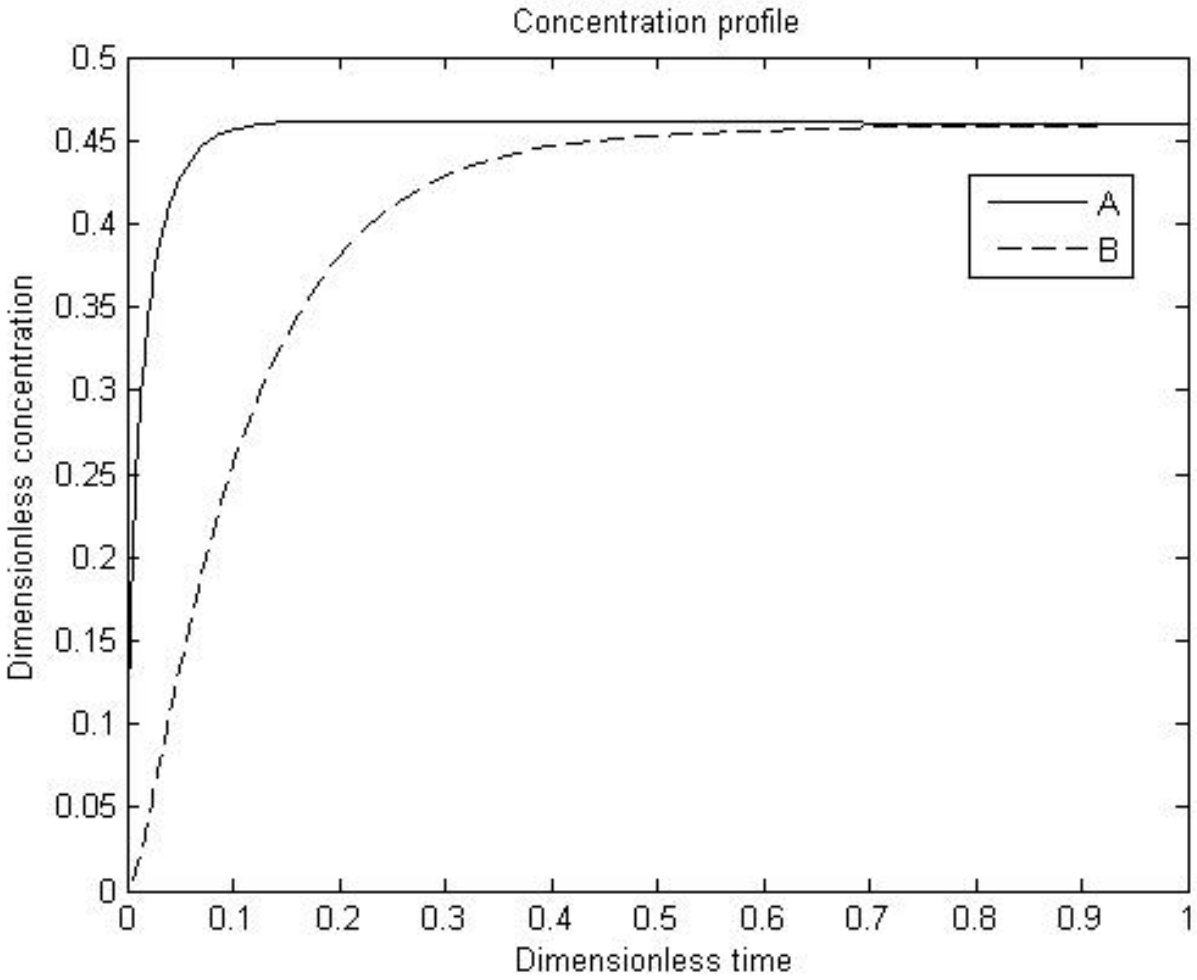

Figure 34: Concentration profile for finite volume with external fluid film resistance

Figure 34 shows that a high ratio (Λ) and a high Biot number (Bi_m) produce the almost the same profile as an infinite volume with no external fluid film resistance.

3.7 Deactivation function:

In all the previous sections, the deactivation function was assumed to be constant. In this section, this assumption is reviewed. The catalyst deactivation function can be related to the reactant conversion through the following relation [24]:

$$\phi_{int} = \exp\left(-\lambda(1 - y_A)\right) \quad 2.3$$

where λ is a constant and y_A is the mass fraction of reactant A.

The new deactivation function will be applied to the case of linear finite volume.

3.7.1 Model

The diffusion-reaction equation for this system is the same as equation 3.2.4.

$$\frac{\partial q_A}{\partial t} = \frac{D_c}{r^2}\frac{\partial}{\partial r}\left(r^2 \frac{\partial q_A}{\partial r}\right) - k_{int}\phi_{int}\, q_A \quad 3.2.4$$

where

$$\phi_{int} = \exp\left(-\lambda(1 - y_A)\right) \quad 2.3$$

$$y_A = \frac{q_A}{q_A + q_B} \quad 3.7.1$$

With the following initial and boundary conditions:

$$q_A(r, 0) = 0 \quad 3.2.5$$

$$\left(\frac{\partial q_A}{\partial r}\right)_{r=0} = 0 \quad 3.2.6$$

$$-4\,\pi\, N\, r_c^2\, D_c \left(\frac{\partial q_A(r,t)}{\partial r}\right)_{r=rc} = \frac{V}{K_A}\left(\frac{\partial q_A(r,t)}{\partial t}\right)_{r=r_c} \quad 3.5.10$$

3.7.2 Normalization:

Equation 3.2.4 is normalized as discussed before to give Equation 3.2.31

$$\frac{\partial \bar{q}_A}{\partial \bar{t}} = \frac{1}{\bar{r}^2}\,\frac{\partial}{\partial \bar{r}}\left(\bar{r}^2\,\frac{\partial \bar{q}_A}{\partial \bar{r}}\right) - \varphi^2 \bar{q}_A \quad 3.2.17$$

with

$$\varphi^2 = {\varphi_1}^2 \phi_{int} = \frac{k_{int}\, r_c^2}{D_c}\,\exp\left(-\lambda(1 - y_A)\right) \quad 3.7.2$$

With the normalized initial and boundary conditions:

$$\left(\frac{\partial q_A}{\partial r}\right)_{r=0} = 0 \rightarrow \left(\frac{\partial \bar{q}_A}{\partial \bar{r}}\right)_{\bar{r}=0} = 0 \qquad 3.2.18$$

$$\left(\frac{\partial \bar{q}}{\partial \bar{t}}\right)_{\bar{r}=1} = -\frac{3}{\Lambda}\left(\frac{\partial \bar{q}}{\partial \bar{r}}\right)_{\bar{r}=1} \qquad 3.5.6$$

$$\bar{q}_A(\bar{r}, 0) = 0 \qquad 3.2.20$$

3.7.3 Orthogonal collocation:

For i = 1 to N:

Equation 3.2.23 is still valid.

For i= N+1

Equations 3.5.7 with 3.5.9 are valid

3.7.4 Results

The previous equations were solved using Matlab with the deactivation function defined in Equation 2.1. The constant λ was set to 6.03 which is the value of λ for 1,3,5-TIPB for CAT-LC as shown earlier in Table 2.

Figure 35 compares the concentration profile for reactant A with constant and variable deactivation function with Thiele modulus φ_1 = 5 and Λ = 100.

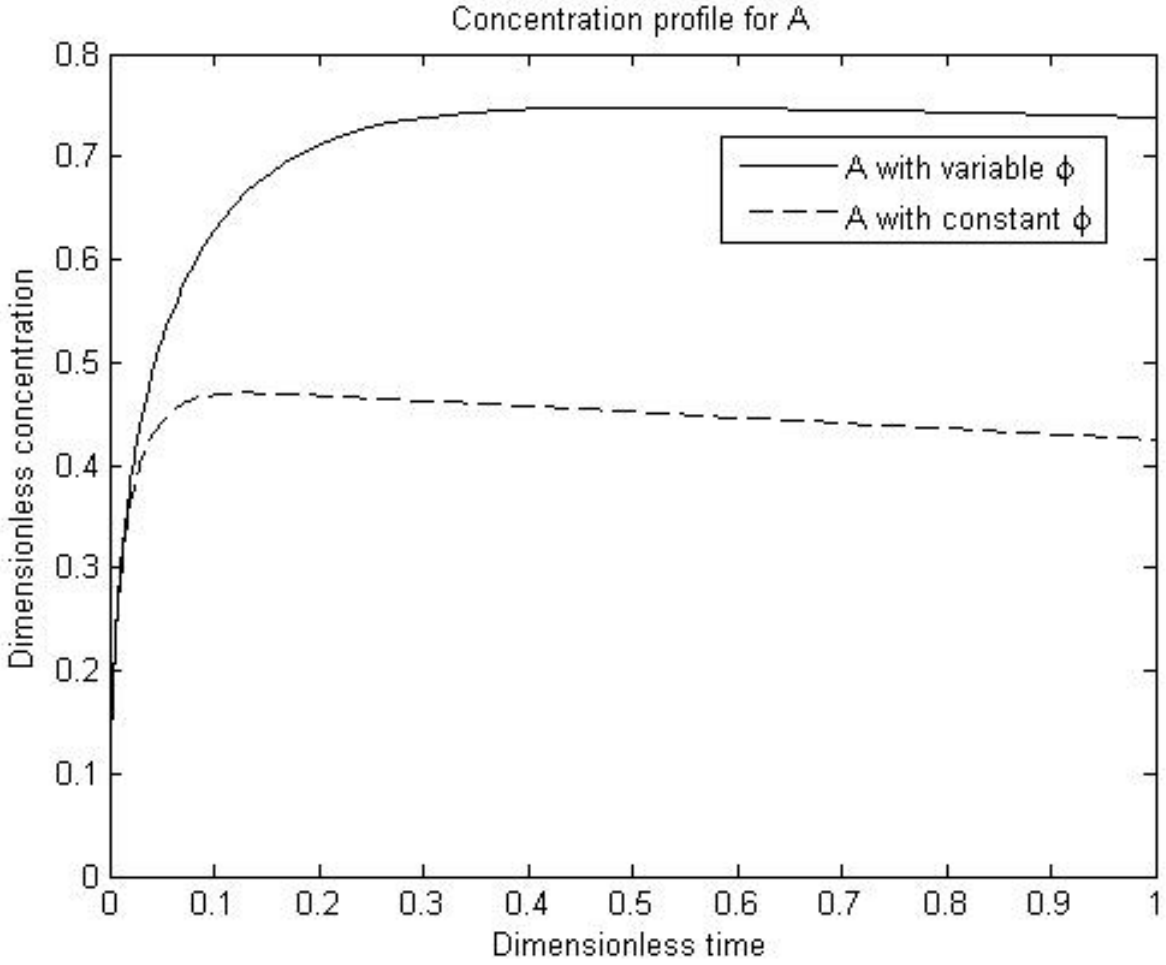

Figure 35: Concentration profile for A with constant and variable deactivation function

Figure 35 shows that the concentration of reactant A is higher when the deactivation function is included. This is because as the reaction proceeds, the mole fraction of reactant A decreases so the value of the deactivation function and Thiele modulus decreases and less reactant is converted to product.

Figure 36 compares the concentration profile for product B with constant and variable deactivation function with Thiele modulus φ_1 = 5 and Λ = 100.

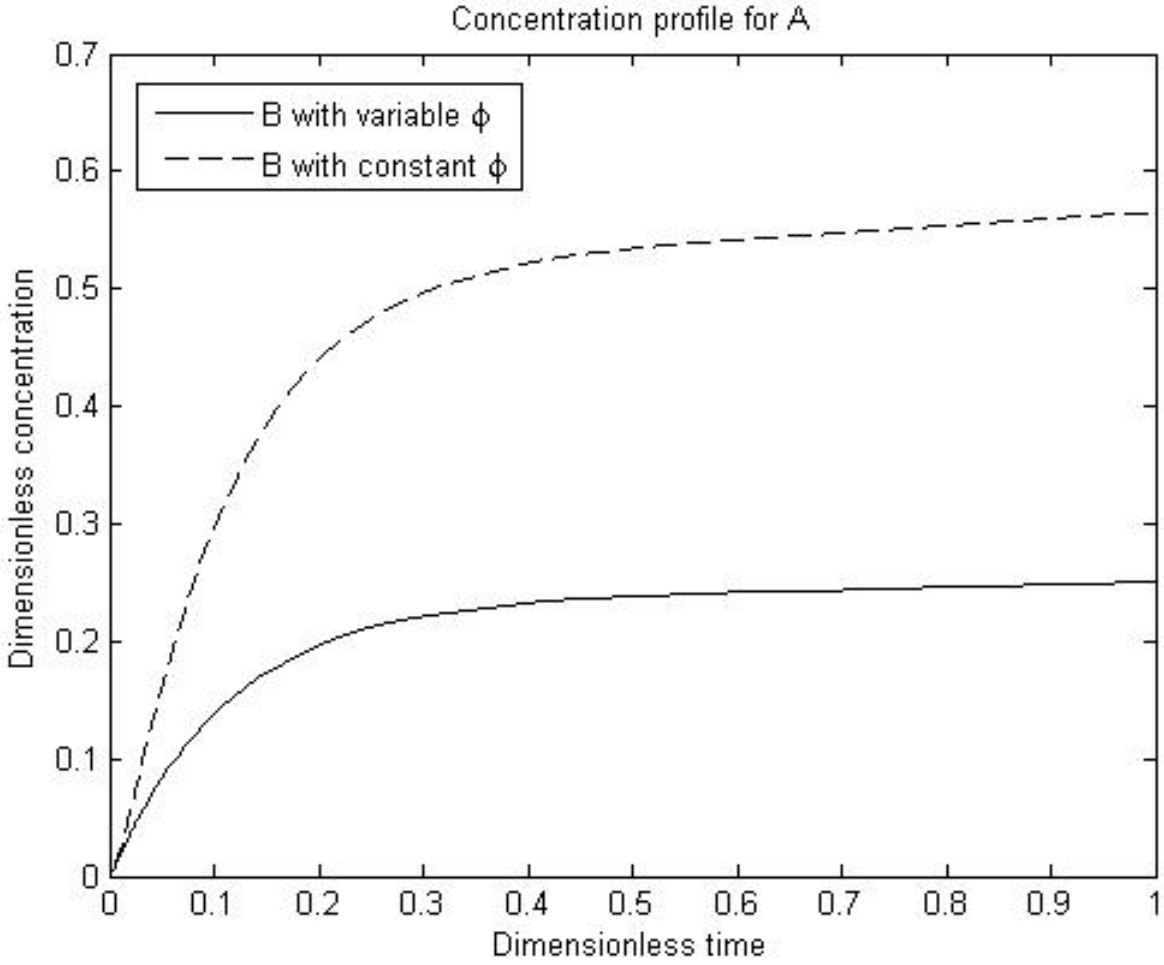

Figure 36: Concentration profile for A with constant and variable deactivation function

Figure 36 shows that the concentration of product B is lower when the deactivation function is included.

3.8 Conclusion

In summary, this chapter considered different systems for diffusion-reaction processes. By solving different cases, the best conditions that increase the yield can be identified. Higher Thiele modulus increases the conversion. A high Thiele modulus can be obtained either by increasing the reaction rate or decreasing the diffusion. A high degree of isotherm nonlinearity decreases the conversion. Thus, a linear isotherm which can be obtained at low temperatures is preferred. A higher Biot number increases the conversion. Thus the effect of external fluid film resistance should be eliminated. Limited volume systems have higher conversion than infinite volume systems. The ratio of the volume of fluid and solids should be decreased if possible. Finally, the activity of the catalyst represented as the deactivation function decreases as the reaction proceeds which result in less conversion.

Chapter 4. Modeling Nonisothermal Reaction, Adsorption and Diffusion in FCC Catalyst with Inert Matrix

4.1 Introduction

Adsorption is an exothermic process and the heat effects associated with adsorption are relatively large. In addition, cracking reactions are highly endothermic. The assumption of isothermal behavior is only valid if the rate of heat dissipation is relatively large or the heat effects of adsorption and reaction are comparable.

Three heat transfer resistances can be distinguished: conduction through micro and macro particles, convection and radiation from external surfaces. An order of magnitude analysis shows that external film resistance is the dominant heat transfer resistance. Experiments measuring intra- and extra-particle temperature prove that [8].

For an endothermic reaction, the particle is cooler than the surrounding fluid. Therefore, the nonisothermal rate is lower than the isothermal rate and nonisothermal behavior is not preferred. Heat transfer controls the reaction if the diffusion is rapid so it is essential to study the heat effects on reaction and diffusion.

This chapter considers nonisothermal diffusion-reaction processes. The chapter adds the thermal effects to the case considered in section 3.6. The main objective of this chapter is to study the effect of heat on diffusion-reaction process and compare isothermal and nonisothermal processes.

4.2 Nonisothermal linear finite volume with external mass fluid film resistance:

This section will refine the assumption of isothermal process to the case discussed in section 3.6. The chapter will include heat effects in the micro particle only. This section assumes negligible external heat transfer resistance.

4.2.1 The model:

A heat balance around the spherical particle gives:

$$\rho C_p \frac{\partial T}{\partial t} = \frac{1}{r^2}\frac{\partial}{\partial r}\left(k\, r^2 \frac{\partial T}{\partial r}\right) + \dot{q} \qquad 4.2.1$$

where k is the thermal conductivity of the particle and $\dot{q}$ is the rate of heat generated inside the particle.

The heat inside the particle is generated by two processes: reaction and adsorption. Therefore,

$$\dot{q} = (-\Delta H_{ad})\frac{\partial q}{\partial t} + (-\Delta H_{rxn}) k_{int}\, \phi_{int} q \qquad 4.2.2$$

where $-\Delta H_{ad}$ is the heat of adsorption and $-\Delta H_{rxn}$ is the heat of reaction. ΔH_{ad} is negative while ΔH_{rxn} for an endothermic reaction is positive.

Substituting equation 4.2.2 into 4.2.1 and assuming k is independent of r:

$$\rho C_p \frac{\partial T}{\partial t} = \frac{k}{r^2}\frac{\partial}{\partial r}\left(r^2 \frac{\partial T}{\partial r}\right) + (-\Delta H_{ad})\frac{\partial q}{\partial t} + (-\Delta H_{rxn}) k_{int}\, \phi_{int} q \qquad 4.2.3$$

Define the thermal diffusivity (α):

$$\alpha = \frac{k}{\rho\, C_p} \qquad 4.2.4$$

Thus,
$$\frac{\partial T}{\partial t} = \frac{\alpha}{r^2}\frac{\partial}{\partial r}\left(r^2 \frac{\partial T}{\partial r}\right) + \frac{\partial q}{\partial t}\left(\frac{-\Delta H_{ad}}{\rho\, C_p}\right) + \left(\frac{-\Delta H_{rxn}}{\rho\, C_p}\right) k_{int}\, \phi_{int} q \qquad 4.2.5$$

The relevant boundary and initial conditions:

$$T(r, 0) = T_i \qquad 4.2.6$$

$$\left(\frac{\partial T}{\partial r}\right)_{r=0} = 0 \qquad 4.2.7$$

$$T(r_c, t) = T_\infty \tag{4.2.8}$$

where T_i is the initial temperature of the particle and it is equal to the temperature of the surrounding fluid (T_∞).

The heat transfer equation should be solved simultaneously with the diffusion-reaction equation. Therefore, Equation 4.2.5 should be coupled with Equation 3.2.4.

4.2.2 Normalization:

Normalization should be performed to simplify and generalize the solution.

Let
$$\bar{T} = \frac{T}{T_0}, \qquad \bar{r} = \frac{r}{r_0}, \qquad \bar{t} = \frac{t}{t_0}, \qquad \bar{q} = \frac{q}{q_0} \tag{4.2.9}$$

Therefore,
$$\frac{\partial T}{\partial t} = \frac{T_0}{t_0}\frac{\partial \bar{T}}{\partial \bar{t}} \tag{4.2.10}$$

$$\frac{\partial T}{\partial r} = \frac{T_0}{r_0}\frac{\partial \bar{T}}{\partial \bar{r}} \tag{4.2.11}$$

$$\frac{\partial q}{\partial r} = \frac{q_0}{r_0}\frac{\partial \bar{q}}{\partial \bar{r}} \tag{4.2.12}$$

Substituting the dimensionless variable into equation 4.2.5:

$$\frac{T_0 \partial \bar{T}}{t_0 \partial \bar{t}} = \frac{\alpha}{r_0^2 \bar{r}^2}\frac{\partial}{r_0 \partial \bar{r}}\left(\frac{r_0^2 T_0}{r_0}\bar{r}^2\frac{\partial \bar{T}}{\partial \bar{r}}\right) + \frac{q_0}{t_0}\frac{\partial \bar{q}}{\partial \bar{t}}\left(\frac{-\Delta H_{ad}}{\rho\, C_p}\right) + q_0 \bar{q} k_{int}\phi_{int}\left(\frac{-\Delta H_{rxn}}{\rho\, C_p}\right) \tag{4.2.13}$$

$$\frac{\partial \bar{T}}{\partial \bar{t}} = \frac{t_0 \alpha}{r_0^2}\frac{1}{\bar{r}^2}\frac{\partial}{\partial \bar{r}}\left(\bar{r}^2\frac{\partial \bar{T}}{\partial \bar{r}}\right) + \frac{\partial \bar{q}}{\partial \bar{t}}\left(\frac{-\Delta H_{ad} q_0}{\rho\, C_p T_0}\right) + \bar{q} k_{int}\phi_{int}\left(\frac{-\Delta H_{rxn} q_0 t_0}{\rho\, C_p T_0}\right) \tag{4.2.14}$$

The dimensionless variables r_0, t_0 and q_0 will have the same values as in section 3.2.

Due to physical significance:

$$T_0 = T_i = T_\infty \tag{4.2.15}$$

Substituting the dimensionless variables in Equation 4.2.14 gives:

$$\frac{\partial \bar{T}}{\partial \bar{t}} = \frac{\alpha}{D_c}\frac{1}{\bar{r}^2}\frac{\partial}{\partial \bar{r}}\left(\bar{r}^2\frac{\partial \bar{T}}{\partial \bar{r}}\right) + \frac{\partial \bar{q}}{\partial t}\left(\frac{-\Delta H_{ad} q_\infty}{\rho\, C_p T_\infty}\right) + \bar{q}\left(\frac{-\Delta H_{rxn} q_\infty \varphi^2}{\rho\, C_p T_\infty}\right) \tag{4.2.16}$$

The term α/D_c is Lewis number (Le) which is the ratio of thermal diffusivity to mass diffusivity.

Define

$$\gamma_{ad} = \frac{-\Delta H_{ad} q_{\infty}}{\rho\, C_p T_{\infty}} \quad 4.2.17$$

$$\gamma_{rxn} = \frac{-\Delta H_{rxn} q_{\infty} \varphi^2}{\rho\, C_p T_{\infty}} \quad 4.2.18$$

$\gamma_{ad}$is positive whereas γ_{rxn} is negative.

Substituting back in equation 4.2.16 gives:

$$\frac{\partial \bar{T}}{\partial \bar{t}} = Le \frac{1}{\bar{r}^2} \frac{\partial}{\partial \bar{r}} \left(\bar{r}^2 \frac{\partial \bar{T}}{\partial \bar{r}} \right) + \gamma_{ad} \frac{\partial \bar{q}}{\partial \bar{t}} + \gamma_{rxn} \bar{q} \quad 4.2.19$$

Performing normalization to the boundary and initial conditions gives:

$$\left(\frac{\partial T}{\partial r} \right)_{r=0} = 0 \rightarrow \left(\frac{\partial \bar{T}}{\partial \bar{r}} \right)_{\bar{r}=0} = 0 \quad 4.2.20$$

$$T(r_c, t) = T_i \rightarrow \bar{T}(1, \bar{t}) = 1 \quad 4.2.21$$

$$\bar{T}(\bar{r}, 0) = 1 \quad 4.2.22$$

Equation 4.2.19 with the conditions 4.2.20-4.1.22 represents the heat balance for a spherical particle.

Coupling the heat balance with the diffusion-reaction Equation 3.2.17 represents the thermal diffusion-reaction system.

4.2.3 Orthogonal collocation

Applying orthogonal collocation to Equation 4.2.19 gives:

For i = 1 to N:

$$\frac{\partial \bar{T}_j}{\partial \bar{t}} = Le \sum_{j=1}^{N+1} B_{ij}\, \bar{T}_j + \gamma_{ad} \frac{\partial \bar{q}_j}{\partial \bar{t}} + \gamma_{rxn} \bar{q}_j \quad 4.2.23$$

where $\partial \bar{q}_j / \partial \bar{t}$ is defined by equation 3.2.23

For i=N+1:

$$\bar{T}_{N+1} = 1 \quad 4.2.24$$

And

$$\left(\frac{\partial \bar{q}}{\partial t}\right)_{N+1} = -\frac{3}{\Lambda}\sum_{j=1}^{N+1} A_{N+1,j}\,\bar{q}_j \qquad 3.5.7$$

where $$\bar{q}_{N+1} = \frac{Bi_m - \sum_{j=1}^{N} A_{ij}\bar{q}_j}{Bi_m + A_{N+1,N+1}} \qquad 3.4.11$$

4.2.4 Results:

The equations representing this system were solved using Matlab. The code is shown in Appendix A.8. Figure 37 illustrates the temperature profile for different values of Lewis number (Le) and for γ_{ad}= 0.01 and γ_{rxn}= -0.015. The Thiele modulus is set to 5.

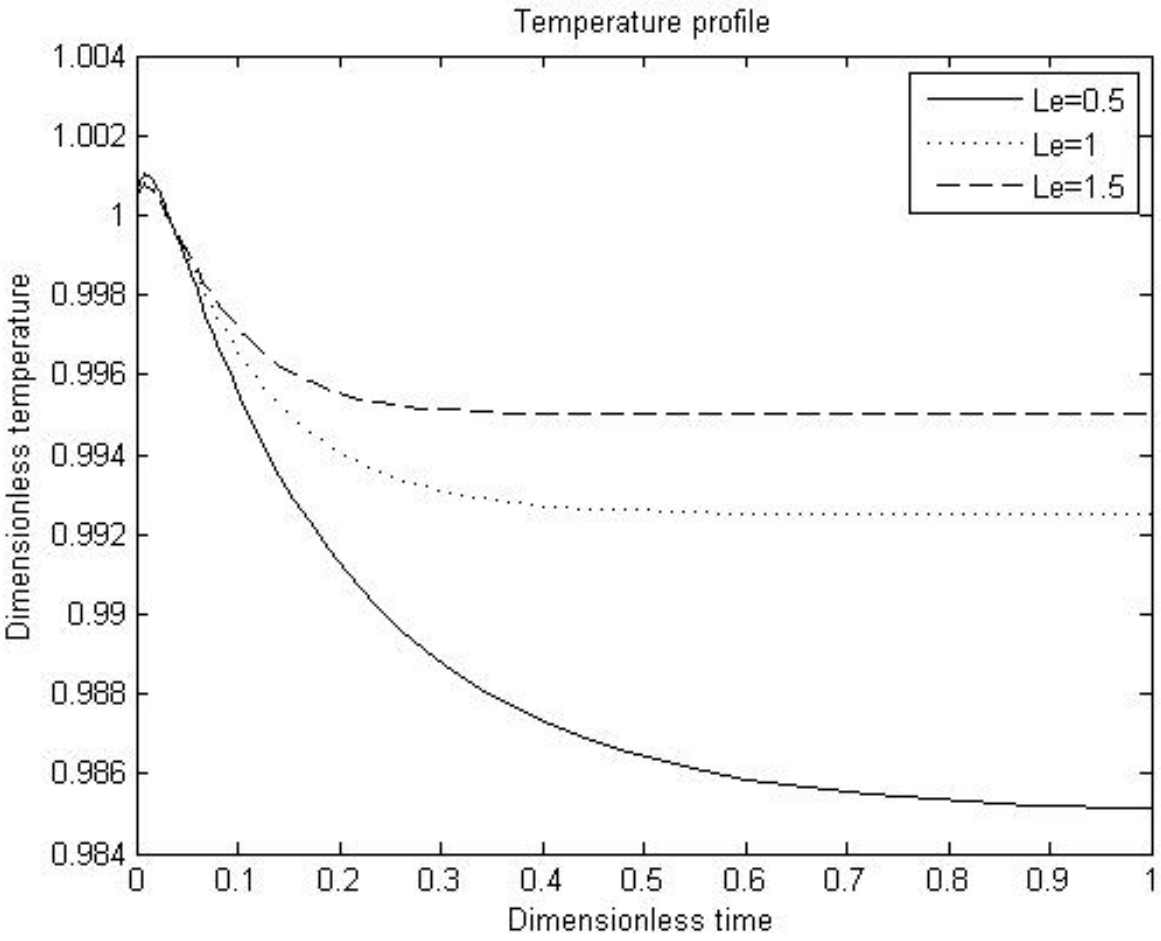

Figure 37: Temperature profile for different values of Le, γ_{ad}= 0.01 and γ_{rxn}= -0.015

Figure 38 shows the short time solution to get a better view of the temperature rise.

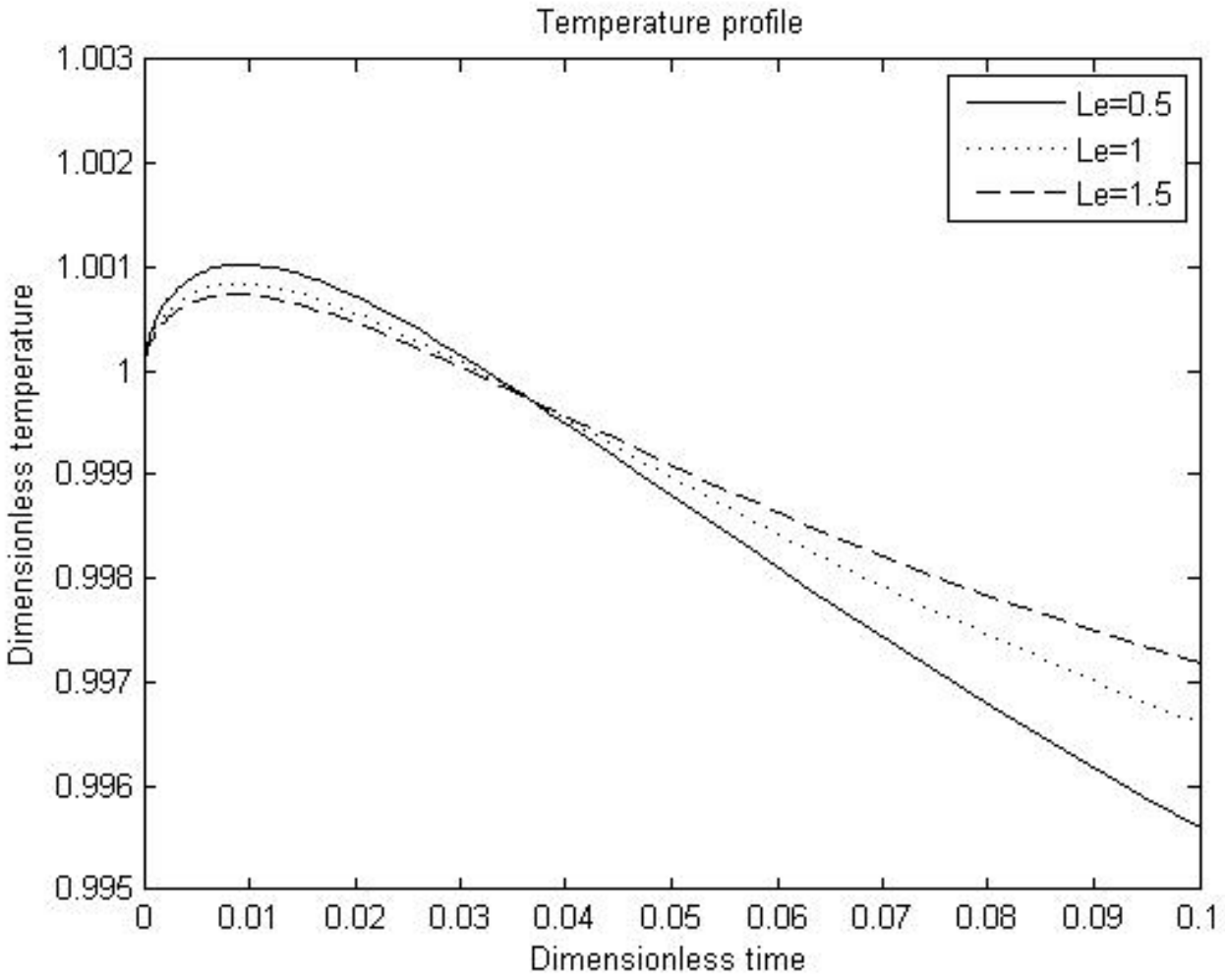

Figure 38: Temperature profile for different values of Le, γ_{ad}= 0.01 and γ_{rxn}= -0.015 (Short time)

As shown in Figure 37 and Figure 38, the temperature initially increases and then rapidly decreases. Initially, the heat of adsorption causes the rise in temperature. Then as the reaction proceed, the term of the heat of reaction dominates and the heat of the endothermic reaction causes the temperature to drop.

As Lewis number increases, the temperate drop decreases because as the Lewis number increases, the thermal diffusivity increases and mass diffusivity limits the system.

Figure 39 shows the temperature profile for different values of Lewis number (Le) and for γ_{ad}= 0.015 and γ_{rxn}= -0.01. The Thiele modulus is set to 5.

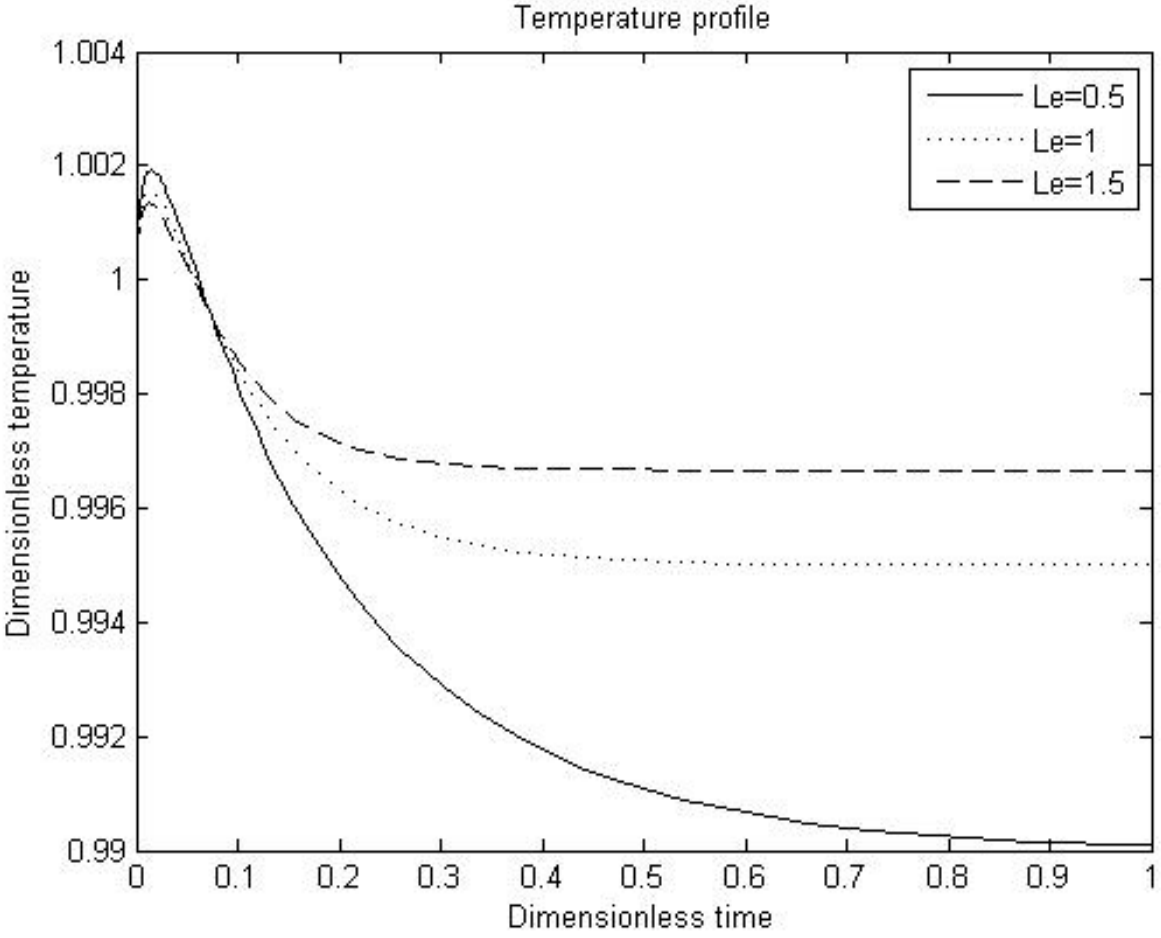

Figure 39: Temperature profile for different values of Le, γ_{ad}= 0.015 and γ_{rxn}= -0.01

Figure 40 shows the short time solution to get a better view.

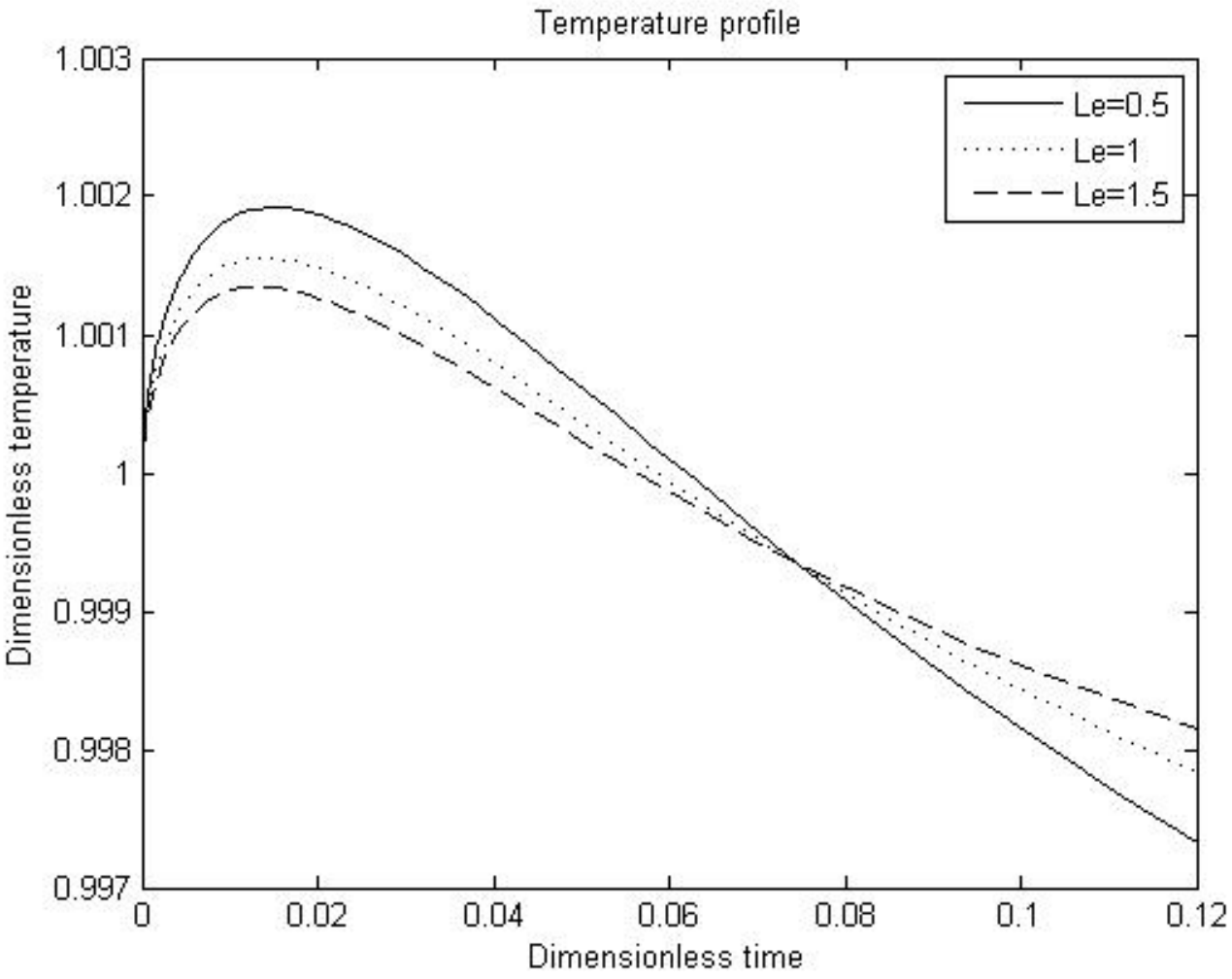

Figure 40: Temperature profile for different values of Le, γ_{ad}= 0.015 and γ_{rxn}= -0.01 (Short time)

As shown in Figure 39 and Figure 40, the temperature initially increases and then decreases. Figure 39 has the same trend as Figure 37; however, the temperature rise is higher for Figure 39 (Higher adsorption term), while the temperature drop is higher for Figure 37 (Higher reaction term)

Figure 41 shows the temperature profile for different values of γ_{rxn} and Lewis number = 0.5 and γ_{ad}=0.01.

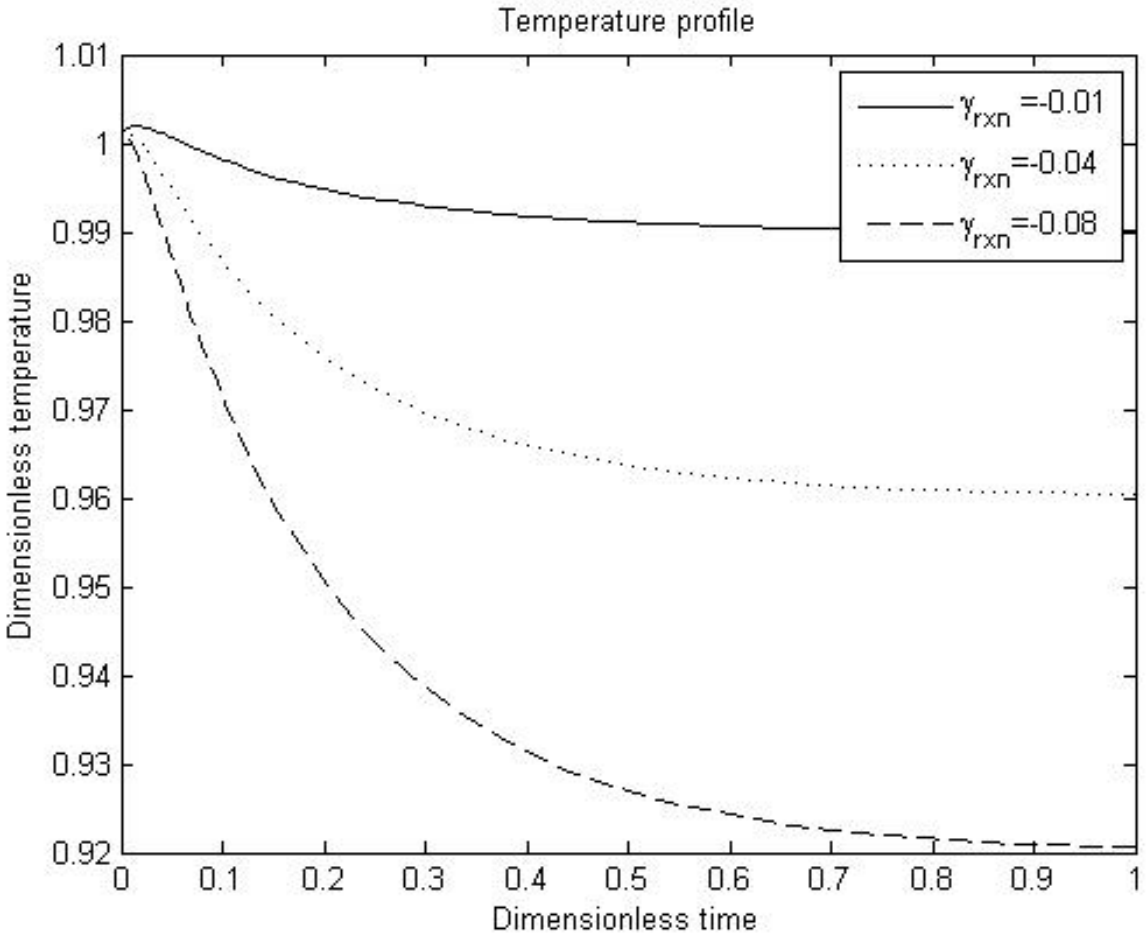

Figure 41: Temperature profile for different positive values of γ_{rxn}, Le 0.5 and γ_{ad}=0.01.

As the absolute value of γ_{rxn} increase, the temperature drop is higher because the heat of reaction is higher. Because the Lewis number is lower than 1, heat transfer is the controlling step.

Figure 42 shows the temperature profile for different values of γ_{ad} and Lewis number = 0.5 and γ_{rxn}= -0.01.

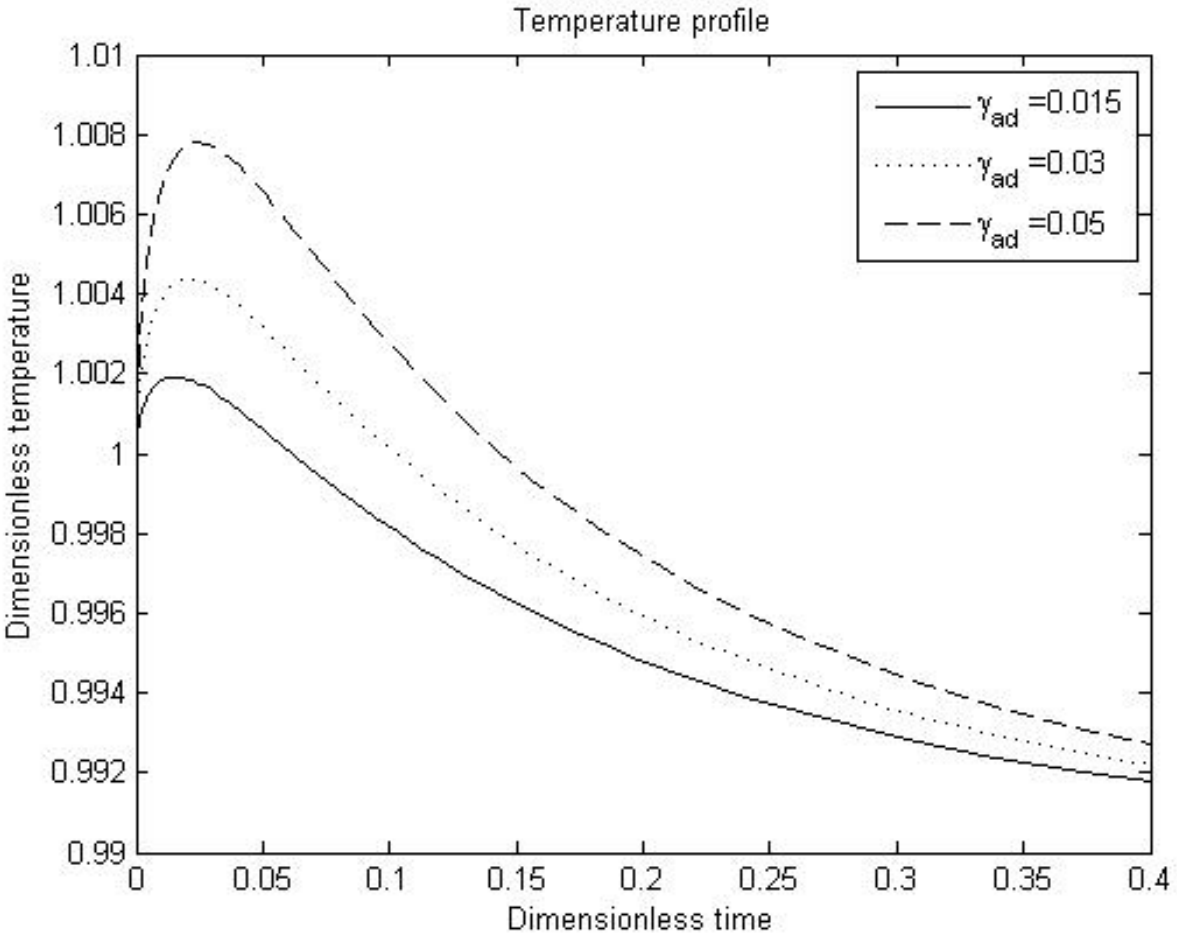

Figure 42: Temperature profile for different negative values of γ_{ad}, Le 0.5 and γ_{rxn}= -0.01

The high heat of adsorption represented by high γ_{ad} cause the rise in temperature. As the value of γ_{ad} increases, the temperature rise is lower.

Figure 43 shows the concentration and temperature profile for a system with no reaction, infinite volume and negligible external fluid film resistance (φ=0, Λ=100 and Bi_m=100). The thermal parameters are chosen as Le = 2, γ_{ad} = 0.02 and $\gamma_{rxn} = 0$.

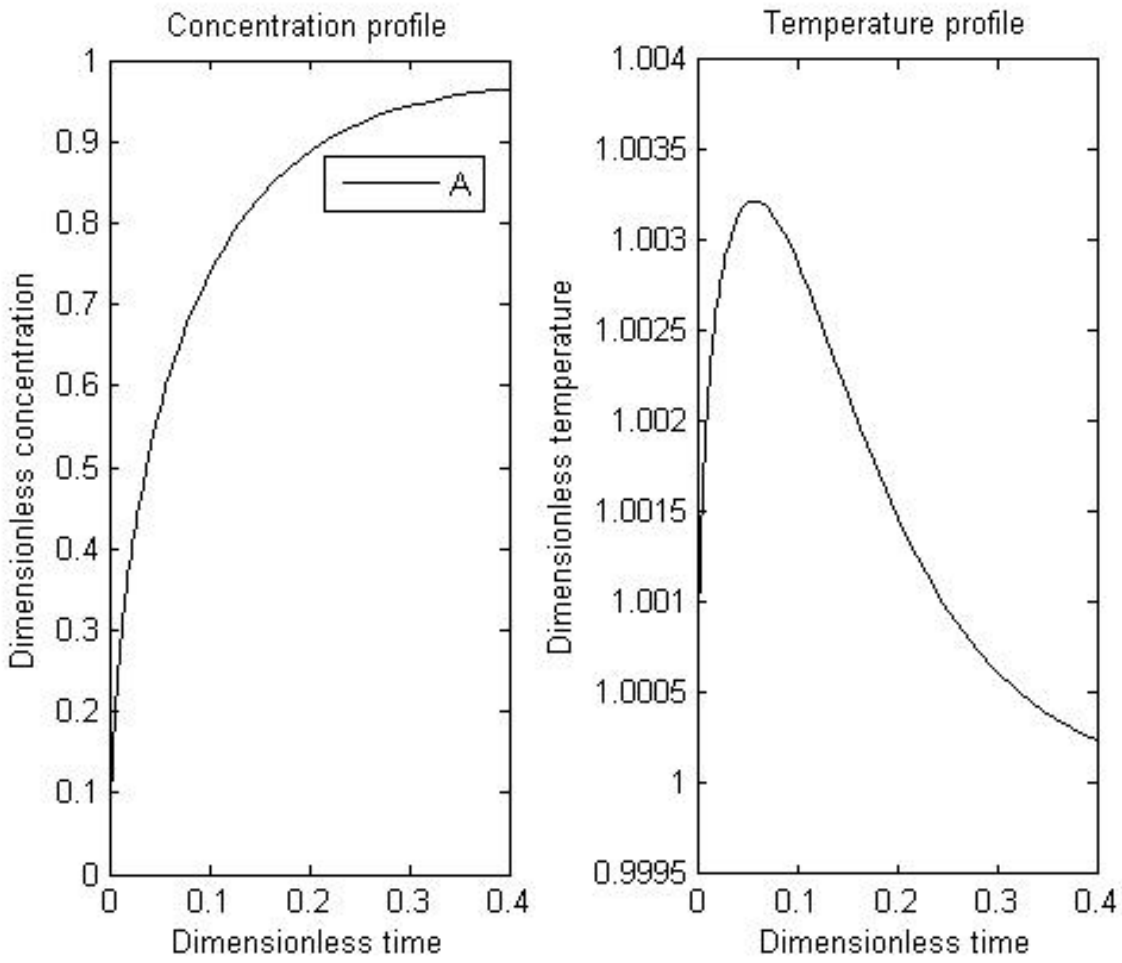

Figure 43: Concentration and Temperature profile for φ=0, Λ=100, Bi_m=100, Le = 2, γ_{ad} = 0.02 and $\gamma_{rxn} = 0$

From Figure 43, the thermal effects caused a small decrease in the concentration of reactant A. For the temperature profile, the temperature increased because of the heat of adsorption.

Figure 44 shows the temperature profile and Figure 45shows the concentration for a reactive system, infinite volume and negligible external fluid film resistance (φ=5, Λ=100 and Bi_m=100). The thermal parameters are chosen as Le = 2, γ_{ad} = 0.02 and γ_{rxn}= -0.001.

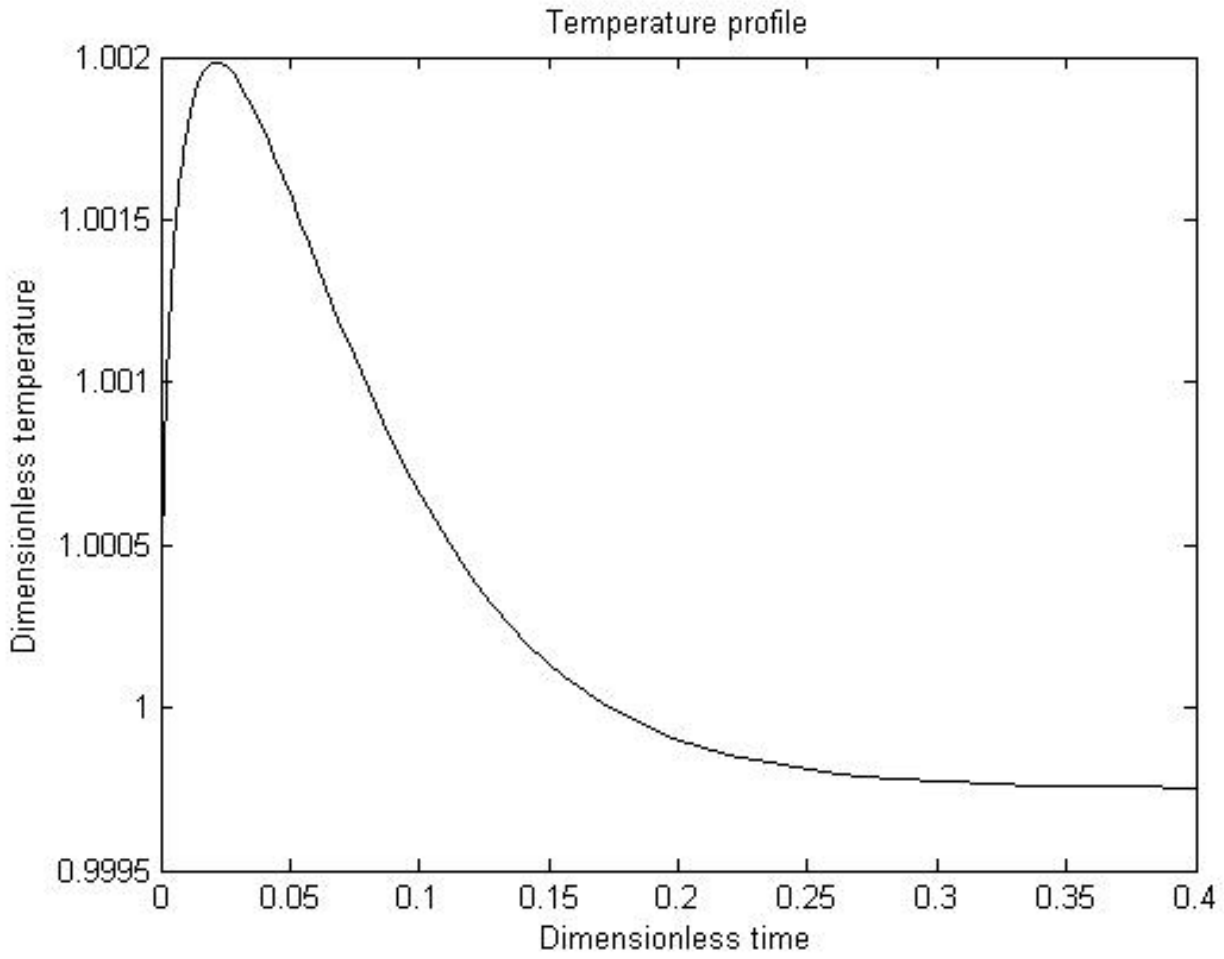

Figure 44: Temperature profile for φ=5, Λ =100, Bi_m=100, Le = 2, γ_{ad} = 0.02 and γ_{rxn}= -0.001

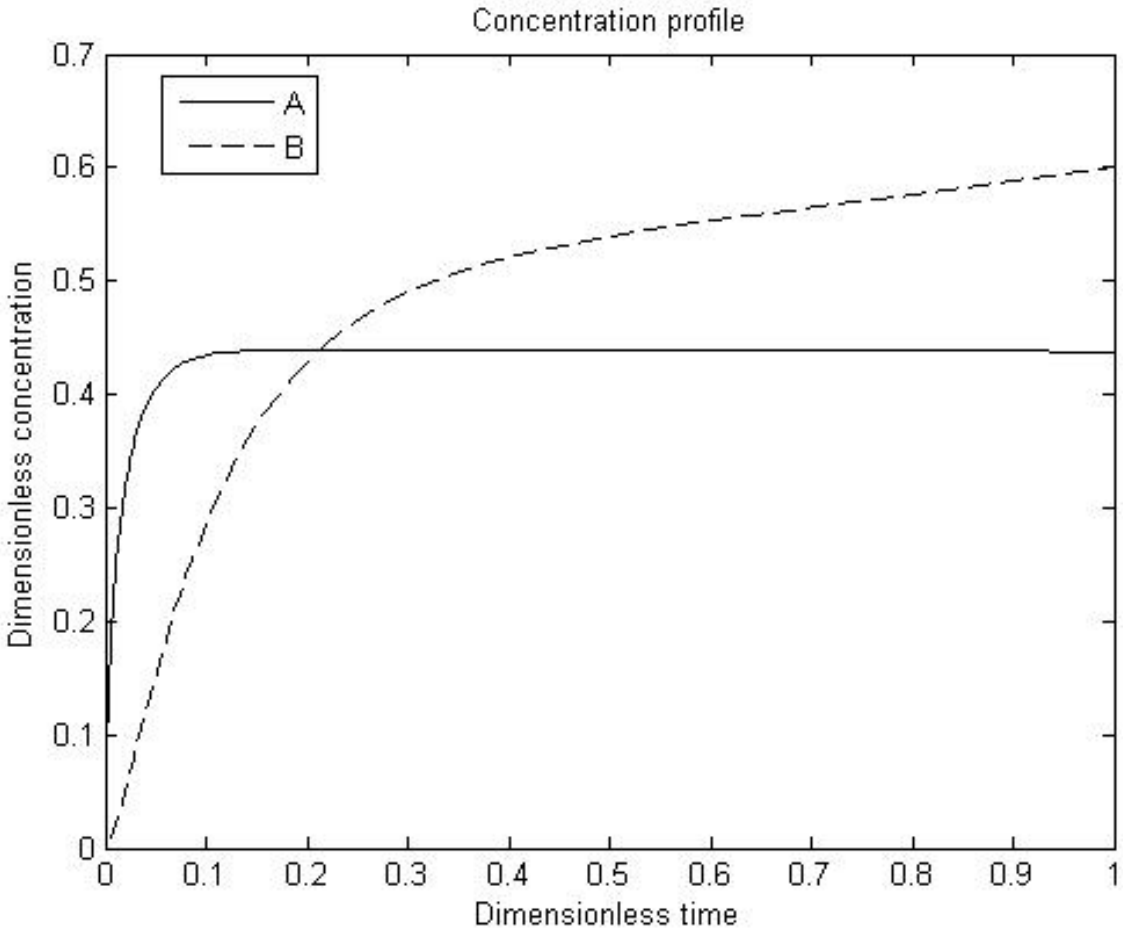

Figure 45: Concentration profile for φ=5, Λ =100, Bi_m=100, Le = 2, γ_{ad} = 0.02 and γ_{rxn}= -0.001

The temperature increased in Figure 44 because γ_{ad} is higher than γ_{rxn}. Comparing Figure 44 with Figure 43, the temperature rise in Figure 44 is lower because the heat of reaction contributes to lower the temperature

Comparing Figure 45 with Figure 28, the thermal effects caused a small decrease in the conversion of reactant B. Therefore, when the heat of adsorption is lower than the heat of reaction, thermal effects should be eliminated if possible.

Figure 46 shows the temperature profile and Figure 47 shows the concentration profile for a reactive system, infinite volume and negligible external fluid film resistance (φ=5, Λ=100 and Bi_m=100). The thermal parameters are chosen as Le = 2, γ_{ad} = 0.002 and γ_{rxn}= - 0.02

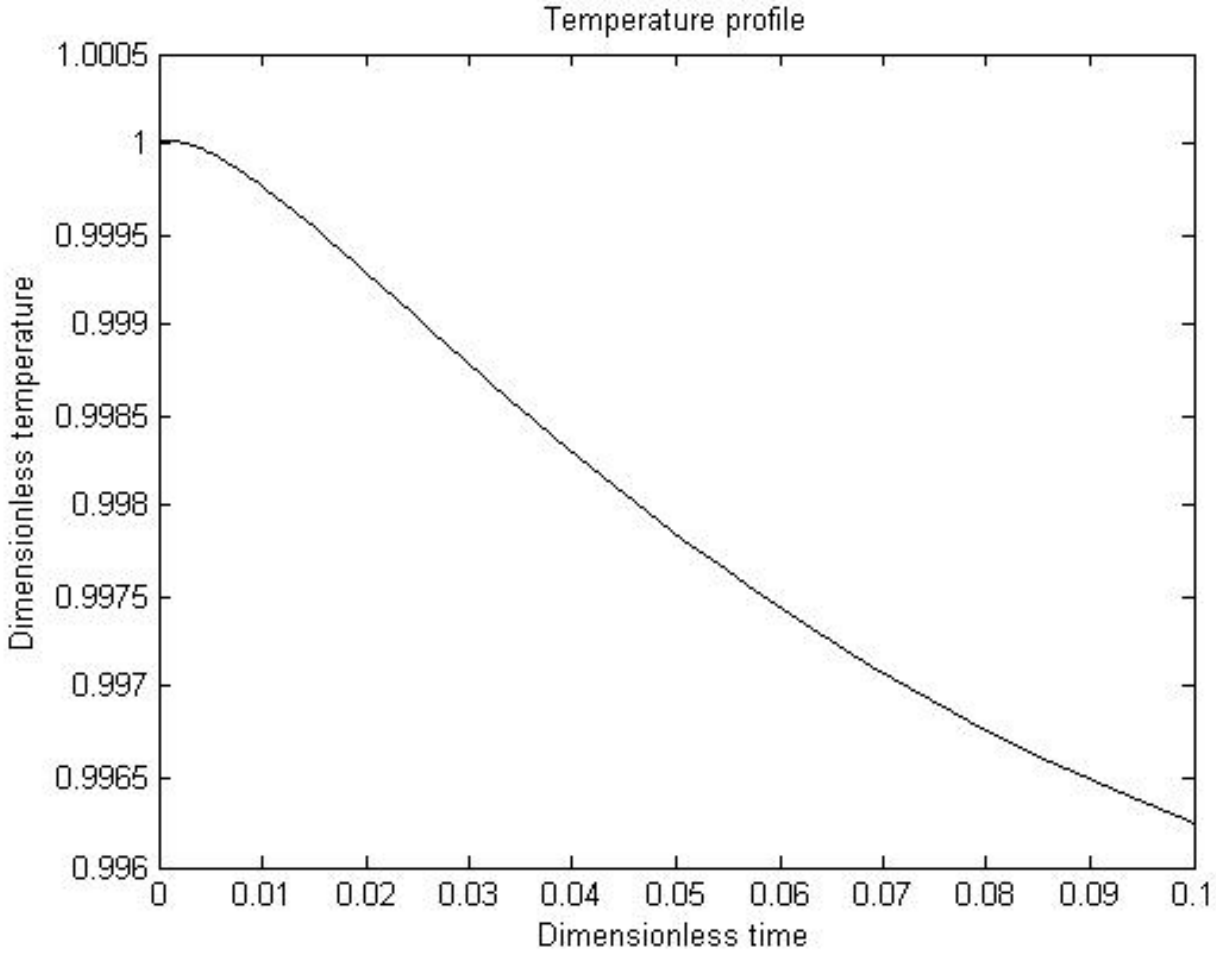

Figure 46: Temperature profile for φ=5, Λ =100, Bi_m=100, Le = 2, γ_{ad} = 0.001 and γ_{rxn}= - 0.02

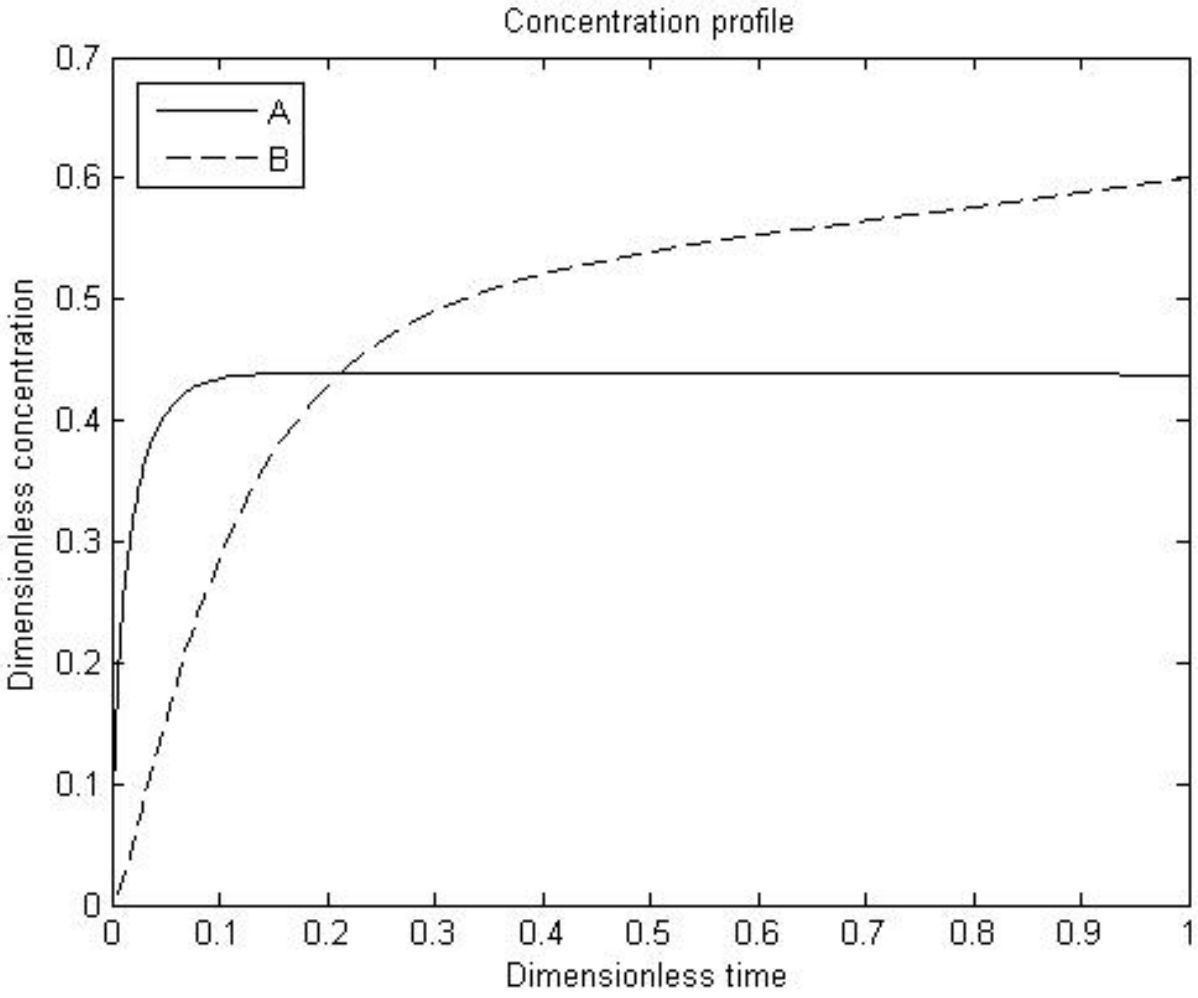

Figure 47: Concentration profile for φ=5, α=100, Bi_m=100, Le = 2, γ_{ad} = 0.001 and γ_{rxn}= - 0.02

For the temperature profile in Figure 46, the temperature decreases because γ_{rxn} is higher. Comparing Figure 47 with Figure 27, the concentration profile is the same.

4.3 Nonisothermal linear finite volume with external mass and heat fluid film resistance:

The previous section assumed the temperature at the surface to be equal to the fluid temperature. This assumption is refined in this section and external heat film resistance is considered.

4.3.1 The model:

Equation 4.2.5 is still valid for this system. However, the boundary condition at the surface is replaced by the following equation:

$$-k\left(\frac{\partial T}{\partial r}\right)_{r=r_c} = h\,(T_{r=r_c} - T_\infty) \qquad 4.3.1$$

where k is the thermal conductivity and h is the heat transfer coefficient.

The system is now governed by the following equations:

$$\frac{\partial T}{\partial t} = \frac{\alpha}{r^2}\frac{\partial}{\partial r}\left(r^2\frac{\partial T}{\partial r}\right) + \frac{\partial q}{\partial t}\left(\frac{-\Delta H_{ad}}{\rho\, C_p}\right) + \left(\frac{-\Delta H_{rxn}}{\rho\, C_p}\right) k_{int}\,\phi_{int} q \qquad 4.2.5$$

$$T(r,0) = T_i \qquad 4.2.6$$

$$\left(\frac{\partial T}{\partial r}\right)_{r=0} = 0 \qquad 4.2.7$$

$$-k\left(\frac{\partial T}{\partial r}\right)_{r=r_c} = h\,(T_{r=r_c} - T_\infty) \qquad 4.3.1$$

4.3.2 Normalization:

The boundary condition at the surface needs to be normalized:

Using the previous dimensionless variables:

$$-k\frac{T_0}{r_0}\left(\frac{\partial \bar{T}}{\partial \bar{r}}\right)_{\bar{r}\,r_c = r_c} = h\,(T_0\bar{T}_{\bar{r}\,r_c = r_c} - T_\infty) \qquad 4.3.2$$

$$\left(\frac{\partial \bar{T}}{\partial \bar{r}}\right)_{\bar{r}=1} = Bi\,(1 - \bar{T}_{\bar{r}=1}) \qquad 4.3.3$$

where Bi is the Biot number defined as the ratio of the heat transfer resistances inside of and at the surface of the particle.

$$Bi = \frac{h\, r_c}{k} \tag{4.3.4}$$

Equation 4.2.19 with the initial condition in Equation 4.2.22 and boundary conditions Equations 4.2.20 and 4.3.3 is the normalized heat transfer equation. To solve the system of nonisothermal diffusion-reaction for finite volume with external film mass and heat resistances, the heat transfer equation should be coupled with Equation 3.2.17 with the initial condition in Equation 3.2.20 and boundary conditions Equations 3.2.18 and 3.6.8.

4.3.3 Orthogonal collocation:

For i = 1 to N:

Equations 4.2.23 and Equation 3.2.23 are still valid

For i=N+1:

$$\bar{T}_{N+1} = \frac{Bi - \sum_{j=1}^{N} A_{ij}\bar{T}_j}{Bi + A_{N+1,N+1}} \tag{4.3.5}$$

and $\bar{q}_{N+1}$ is defined by Equation 3.5.7

These equations were solved using Matlab. The program is shown in Appendix A.9

3.3.4 Results:

Figure 48 demonstrates the effects of the external heat transfer on a non-reactive system with infinite volume and negligible external mass (φ=0, Λ=100, Bi_m=100). The thermal parameters are chosen as Le = 2, γ_{ad} =0.02 and γ_{rxn} =0.

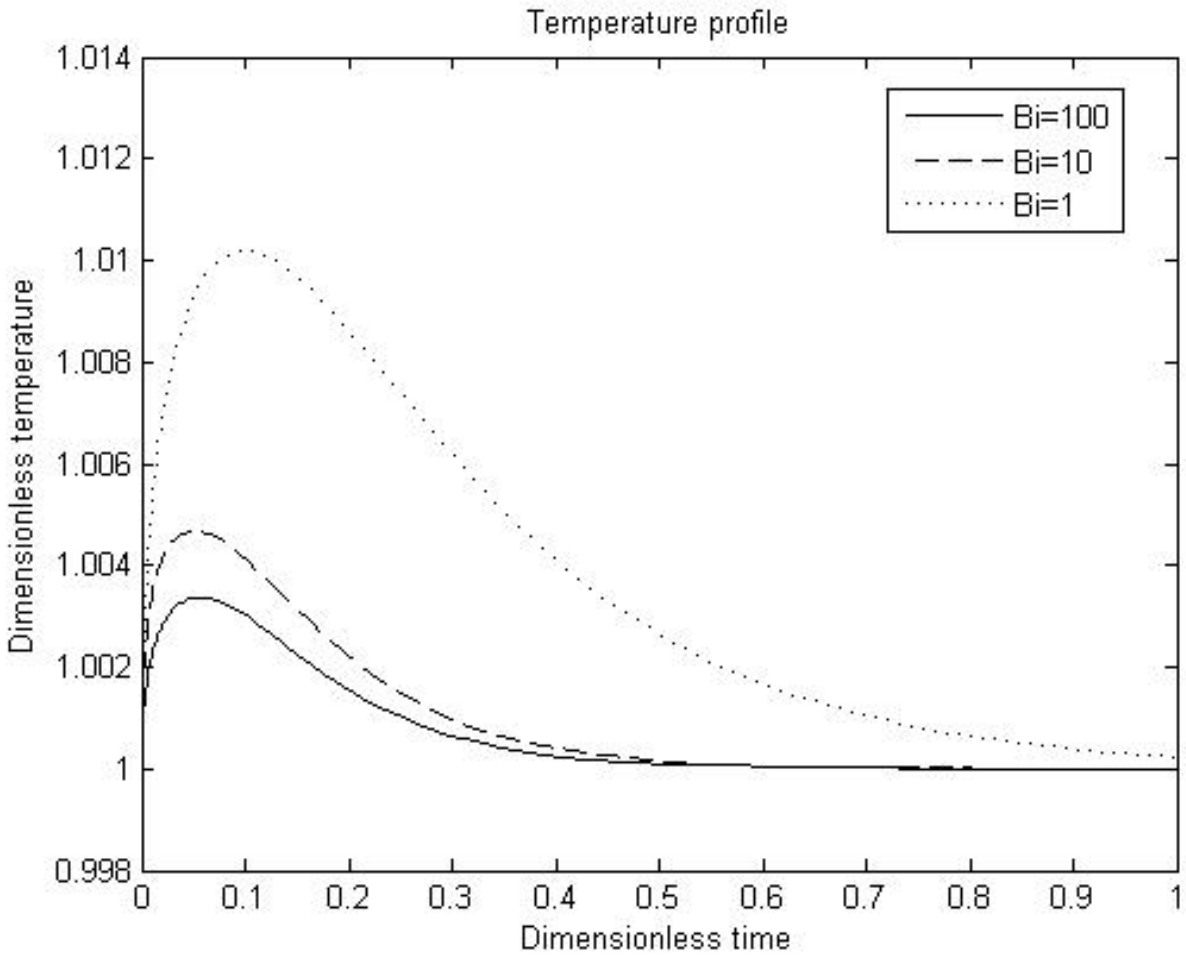

Figure 48: Temperature profile for φ=0, Λ =100, Bi_m=100, Le = 2, γ_{ad} =0.02 and γ_{rxn} =0

From illustrated from Figure 48, as the Biot number increases, the external heat transfer becomes negligible and thus the temperature rise is smaller. Comparing Figure 48 and Figure 43, a large Biot number as 100 gives the same results as when the external heat transfer is negligible.

Figure 49 demonstrates the effects of the external heat transfer on a reactive system with infinite volume and negligible external mass (φ=5, Λ=100, Bi_m=100). The thermal parameters are chosen as Le = 2, γ_{ad} =0.02 and γ_{rxn} = -0.01.

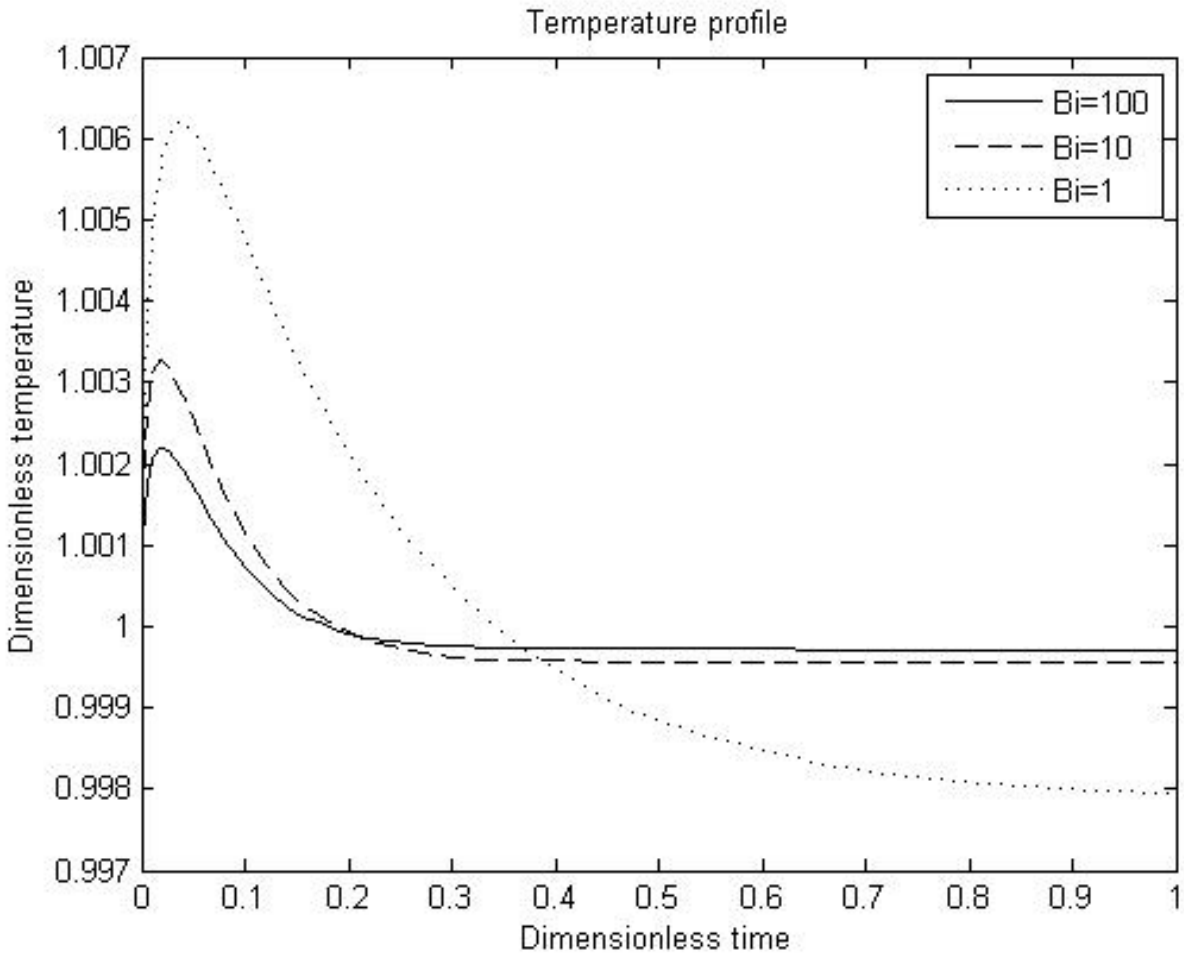

Figure 49: Temperature profile for φ=5, Λ =100, Bi_m=100, Le = 2, γ_{ad} =0.02 and γ_{rxn} = -0.001

As illustrated from Figure 49, as the Biot number increases, initially the temperature rise is smaller and later on the temperature drop is smaller.

Figure 50 demonstrates the effects of the external heat transfer on a reactive system with infinite volume and negligible external mass (φ=5, Λ=100, Bi_m=100). The thermal parameters are chosen as Le = 2, γ_{ad} =0.001 and γ_{rxn} = -0.02

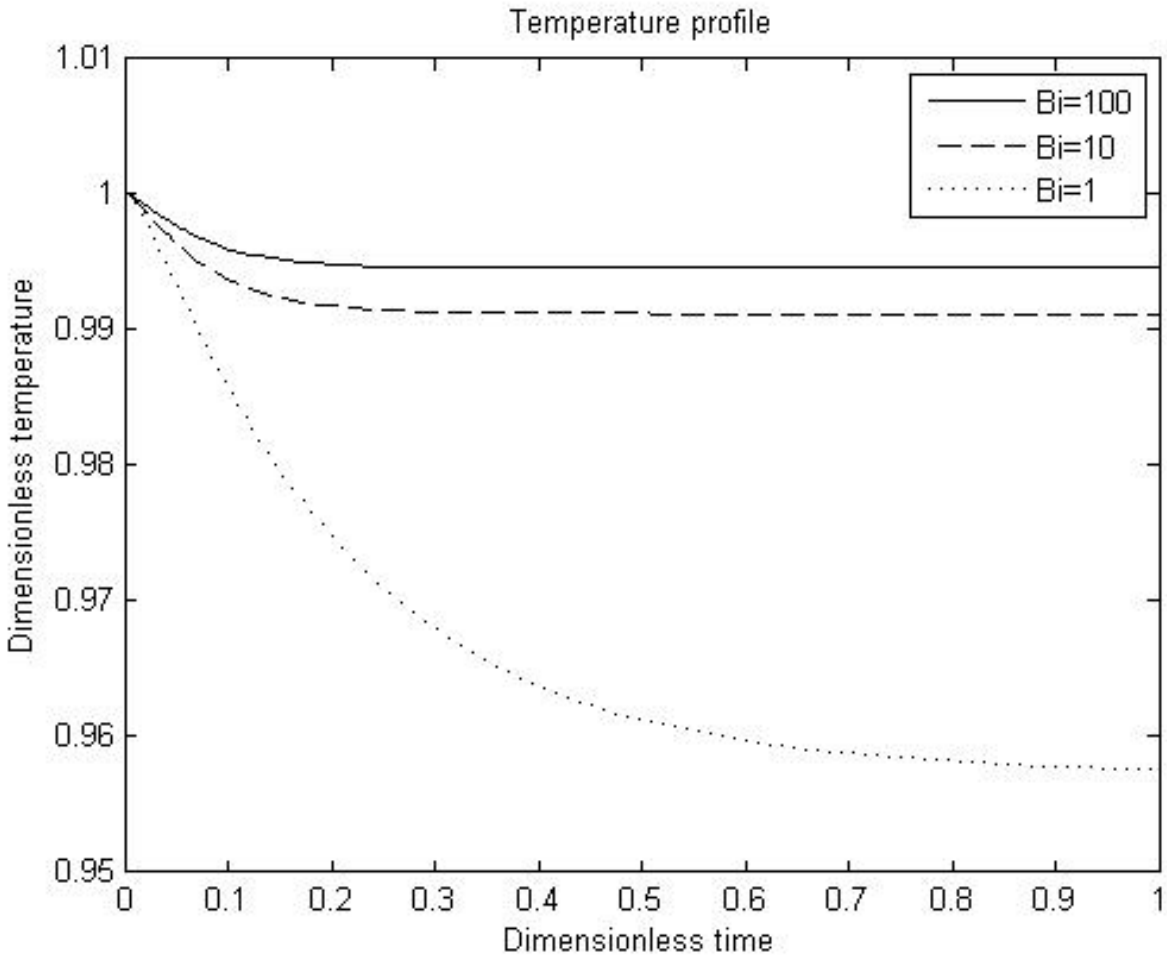

Figure 50: Temperature profile for φ=0, Λ =100, Bi_m=100, Le = 2, γ_{ad} =0.001 and γ_{rxn} = -0.02

The temperature drops because the heat of the endothermic reaction is higher than the heat of adsorption. As illustrated from Figure 50, as the Biot number decreases, the temperature drop is higher.

4.4 Conclusion

Briefly, this chapter considered nonisothermal diffusion-reaction processes. Two cases were considered. The first case is when the surface temperature is equal to the fluid temperature and the second case when external film heat resistance exists. As the Biot number increases, the external film heat resistance is negligible and the first case can be assumed. When the Biot number is less than one, external film heat resistance is the controlling heat transfer resistance. If the heat of adsorption is higher than the heat of reaction, the temperature rise will increase with decreasing Biot number, whereas if the heat of reaction is higher, the temperature drop will increase with decreasing Biot number. The Lewis number is the ratio of the heat to the mass diffusivity. It determines which resistance is controlling. If the heat of reaction is higher than adsorption, the temperature drop decreases with increasing Lewis number. If the heat of adsorption is higher, the temperature rise decreases with increasing Lewis number.

Chapter 5. Modeling Isothermal Reaction, Adsorption and Diffusion in FCC Catalyst with Active Matrix

5.1 Introduction

The FCC catalyst is a biporous catalyst. It consists of zeolite which are micro particles embedded in the alumina matrix which is a macro particle as illustrated in Figure 51.

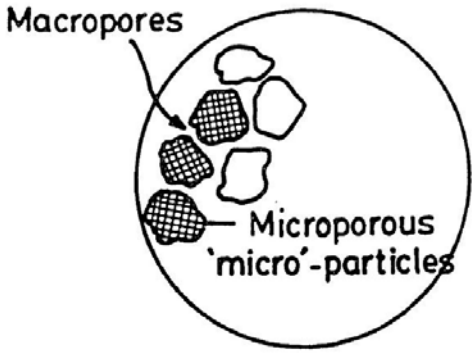

Figure 51: Composite pellet formed from zeolite crystals

The structure of the catalyst offers at least two resistances to mass transfer, micropore and macropore diffusional resistances. Another resistance that could occur is the resistance to mass transfer at the external surface of the micro particle. In addition, external fluid film resistance could exist. The importance of these resistances varies with the system and conditions [33].

As discussed previously, Zaman et al. [6] showed that the matrix of the FCC catalyst has a high adsorption capacity for oil mixtures. That is, diffusion and adsorption occur simultaneously in both macro and micropores. The effects of these competing processes have to be considered to gain a better insight onto the FCC catalyst.

The steps of the heterogeneous catalytic reaction in the case of active matrix are:

1. Transport of reactants from the bulk fluid to the macropore particle.
2. Adsorption of reactants on the macropore particle.

3. Transport of reactants from the macropore particle to the micropore particle.
4. Adsorption of reactants on the micropore particle.
5. Surface chemical reaction between adsorbed molecules.
6. Desorption of products from the micropore particle.
7. Transport of the products from the micropore to the macropore particles.
8. Adsorption/Desorption of products from the macropore particle.
9. Transport of the products from the macropore to the bulk fluid.

The biporous adsorbents were considered in different research papers. Lee[33] considered an isothermal system with the two diffusional resistances with adsorption occurring only in the micropore particles. Ruckenstein et al [35] considered simultaneously diffusion and adsorption in both macropore and micropore particles. The system is assumed to be isothermal and linear equilibrium is assumed.

The purpose of this chapter is to model heterogeneous catalytic reactions in FCC with active matrix. The chapter revises two main assumptions that were assumed in the previous chapters. These assumptions are negligible transport and adsorption within the matrix. The model is then applied to finite volume systems and then external fluid film resistance is considered. The chapter assumes that the rate of heat dissipation is high within the macro and micro particles so that the system can be considered isothermal.

5.2 Infinite linear macro and micropore resistances:

This section considers a spherical macroporous particle that consists of small microporous particles of uniform size. The reactant diffuses into the macropores, adsorbs in the macropores, diffuses into the micropore, adsorbs into the active sites and then reacts. The product is then desorbed from the micropore, diffuses out to the macropore, adsorbed and desorbs from the macropore and then diffuses into the bulk fluid. The volume of the system is assumed to be infinite.

5.2.1 The model

Perform a mass balance around the macroporous spherical particle [35]:

$$\epsilon_p \frac{\partial C}{\partial t} + S_p \frac{\partial C_s}{\partial t} = \frac{D_p \epsilon_p}{R^2} \frac{\partial}{\partial R}\left(R^2 \frac{\partial C}{\partial R}\right) - 4\pi N r_c^2 \epsilon_c D_c \left(\frac{\partial q}{\partial r}\right)_{r=r_c} \qquad 5.2.1$$

where the left-hand side terms represent the accumulation in the macropore volume and surface, respectively, while the right-hand terms represent the diffusional flux in the macropore and at the surface of the micropore, respectively.

Assuming linear equilibrium between the bulk and adsorbed phases in the macropore:

$$C_s = K_p C \qquad 5.2.2$$

Therefore, Equation 5.2.1 becomes:

$$\left[1 + \frac{K_p S_p}{\epsilon_p}\right] \frac{\partial C}{\partial t} = \frac{D_p}{R^2} \frac{\partial}{\partial R}\left(R^2 \frac{\partial C}{\partial R}\right) - \frac{4\pi N r_c^2 \epsilon_c D_c}{\epsilon_p} \left(\frac{\partial q}{\partial r}\right)_{r=r_c} \qquad 5.2.3$$

Defining the effective macropore diffusivity [35]:

$$\mathcal{D}_p = \frac{D_p}{1 + \frac{K_p S_p}{\epsilon_p}} \qquad 5.2.4$$

$$\frac{\partial C}{\partial t} = \frac{\mathcal{D}_p}{R^2} \frac{\partial}{\partial R}\left(R^2 \frac{\partial C}{\partial R}\right) - \frac{4\pi N r_c^2 \epsilon_c D_c}{\epsilon_p \left[1 + \frac{K_p S_p}{\epsilon_p}\right]} \left(\frac{\partial q}{\partial r}\right)_{r=r_c} \qquad 5.2.5$$

Equation 5.2.5 represents the mass balance for an active matrix. For the micropore, Equation 3.2.4 is still valid assuming linear equilibrium.

The relevant initial and boundary conditions for the macropore particle:

$$C\ (0,R) = 0 \qquad 5.2.6$$

$$\left(\frac{\partial C}{\partial R}\right)_{R=0} = 0 \qquad 5.2.7$$

$$C\ \left(t,R_p\right) = C_\infty \qquad 5.2.8$$

And for the micropore particles:

$$q\ (0,r) = 0 \qquad 5.2.9$$

$$\left(\frac{\partial q}{\partial r}\right)_{r=0} = 0 \qquad 5.2.10$$

$$q\ (t,r_c) = C(t,R) \qquad 5.2.11$$

The two equations 5.2.3 and 3.2.4 describe the system when the two resistances, macro and micropore exist.

5.2.2 Normalization:

To normalize Equation 5.2.5, define the following dimensionless variables:

For the macropore particle:

$$\bar{C} = \frac{C}{C_0}\ , \qquad \bar{R} = \frac{R}{R_0}, \qquad \bar{t} = \frac{t}{t_0} \qquad 5.2.12$$

For the micropore particle:

$$\bar{q} = \frac{q}{q_0}\ , \qquad \bar{r} = \frac{r}{r_0} \qquad 5.2.13$$

Therefore:

$$\frac{\partial C}{\partial t} = \frac{C_0}{t_0}\frac{\partial \bar{C}}{\partial \bar{t}} \qquad 5.2.14$$

$$\frac{\partial C}{\partial R} = \frac{R_0}{R_0}\frac{\partial \bar{C}}{\partial \bar{R}} \qquad 5.2.15$$

Substituting these dimensionless variables into Equation 5.2.5:

$$\frac{\partial \bar{C}}{\partial \bar{t}} = \frac{\mathcal{D}_p t_0}{{R_0}^2} \frac{1}{\bar{R}^2} \frac{\partial}{\partial \bar{R}} \left(\bar{R}^2 \frac{\partial \bar{C}}{\partial \bar{R}} \right) - \frac{4\pi N r_c^2 \epsilon_c D_c}{\epsilon_p \left[1 + \frac{K_p S_p}{\epsilon_p} \right]} \frac{t_0 q_0}{C_0 r_0} \left(\frac{\partial \bar{q}}{\partial \bar{r}} \right)_{\bar{r} r_0 = r_c} \quad 5.2.16$$

Because of physical significance, let:

$$R_0 = R_p \quad 5.2.17$$

$$C_0 = C_\infty \quad 5.2.18$$

From Chapter 3:

$$r_0 = r_c \quad 5.2.19$$

$$q_0 = q_\infty = C_\infty \quad 5.2.20$$

For mathematical simplification, let:

$$t_0 = \frac{R_p^2}{\mathcal{D}_p} \quad 5.2.21$$

Define β [35]:

$$\beta = \frac{4\pi N r_c D_c R_p^2}{\epsilon_p D_p} \quad 5.2.22$$

Substitute in Equation 5.2.16:

$$\frac{\partial \bar{C}}{\partial \bar{t}} = \frac{1}{\bar{R}^2} \frac{\partial}{\partial \bar{R}} \left(\bar{R}^2 \frac{\partial \bar{C}}{\partial \bar{R}} \right) - \beta \left(\frac{\partial \bar{q}}{\partial \bar{r}} \right)_{\bar{r}=1} \quad 5.2.23$$

Equation 5.2.23 is the normalized equation for the macropore particle:

Normalizing Equation 3.2.4:

$$\frac{\partial \bar{q}}{\partial \bar{t}} = \frac{\mathcal{D}_c t_0}{{r_0}^2} \frac{1}{\bar{r}^2} \frac{\partial}{\partial \bar{r}} \left(\bar{r}^2 \frac{\partial \bar{q}}{\partial \bar{r}} \right) - \varphi^2 \bar{q} \quad 5.2.24$$

Substitute the values of the dimensionless variables:

$$\frac{\partial \bar{q}}{\partial \bar{t}} = \alpha \frac{1}{\bar{r}^2} \frac{\partial}{\partial \bar{r}} \left(\bar{r}^2 \frac{\partial \bar{q}}{\partial \bar{r}} \right) - \varphi^2 \bar{q} \quad 5.2.25$$

where

$$\alpha = \frac{\mathcal{D}_c}{r_c^2} \frac{R_p^2}{\mathcal{D}_p} \quad 5.2.26$$

$$\varphi^2 = \frac{k_{int}\phi_{int}R_p^2}{\mathcal{D}_p} \quad 5.2.27$$

α is the ratio of the diffusional time constants and it determines the importance of the diffusional resistances.

φ^2 is the Thiele modulus for a first order reaction in biporous particle.

Equation 5.2.25 is the normalized equation for the micropore particles with active matrix.

The normalized initial and boundary conditions for the macropore and micropore particles:

$$\bar{C}\,(0,\bar{R}) = 0 \quad 5.2.28$$

$$\left(\frac{\partial \bar{C}}{\partial \bar{R}}\right)_{\bar{R}=0} = 0 \quad 5.2.29$$

$$\bar{C}\,(\bar{t},1) = 1 \quad 5.2.30$$

$$\bar{q}\,(0,\bar{r}) = 0 \quad 5.2.31$$

$$\left(\frac{\partial \bar{q}}{\partial \bar{r}}\right)_{\bar{r}=0} = 0 \quad 5.2.32$$

$$\bar{q}\,(\bar{t},1) = \bar{C}(\bar{t},\bar{R}) \quad 5.2.33$$

Equation 5.23 and 5.25 with their relevant initial and boundary conditions can be solved to give the concentration profile.

5.2.3 Orthogonal collocation:

Applying orthogonal collocation to Equations 5.23 and 5.25:

For i =1:N

$$\frac{\partial \bar{C}_i}{\partial \bar{t}} = \sum_{j=1}^{N+1} B_{ij}\bar{C}_j - \beta \sum_{j=1}^{N+1} A_{N+1,j}\bar{q}_j \quad 5.2.34$$

$$\frac{\partial \bar{q}_i}{\partial \bar{t}} = \alpha \sum_{j=1}^{N+1} B_{ij}\bar{q}_j - \varphi^2\bar{q} \quad 5.2.35$$

For i = N+1

$$\bar{C}_{N+1} = 1 \quad 5.2.36$$

$$\bar{q}_{N+1} = 3 \sum_{j=1}^{N+1} W_j \bar{C}_j \qquad 5.2.37$$

After solving the set of ordinary differential equations, the concentrations in the macro and micropore particles as a function of time are obtained through the following expressions:

$$M_p = 3 \sum_{j=1}^{N+1} W_j \bar{C}_j \qquad 5.2.38$$

$$M_c = 3 \sum_{j=1}^{N+1} W_j \bar{q}_j \qquad 5.2.39$$

And the total dimensionless concentration in the particle can be obtained as follows [35]:

$$M_t = \frac{M_p + \frac{1}{3}\frac{\beta}{\alpha} M_c}{1 + \frac{1}{3}\frac{\beta}{\alpha}} \qquad 5.2.40$$

The preceding set of equations was solved using Matlab. The code is presented in Appendix A.10

5.2.4 Results:

The total concentration profile was obtained for reactant A for the case of no reaction ($\varphi = 0$). Figure 52 illustrates the concentration profile when micropore diffusion controls ($\alpha = 10^{-4}$) and for different values of β/α. The Figure obtained is similar to Figure 2 obtained by [35].

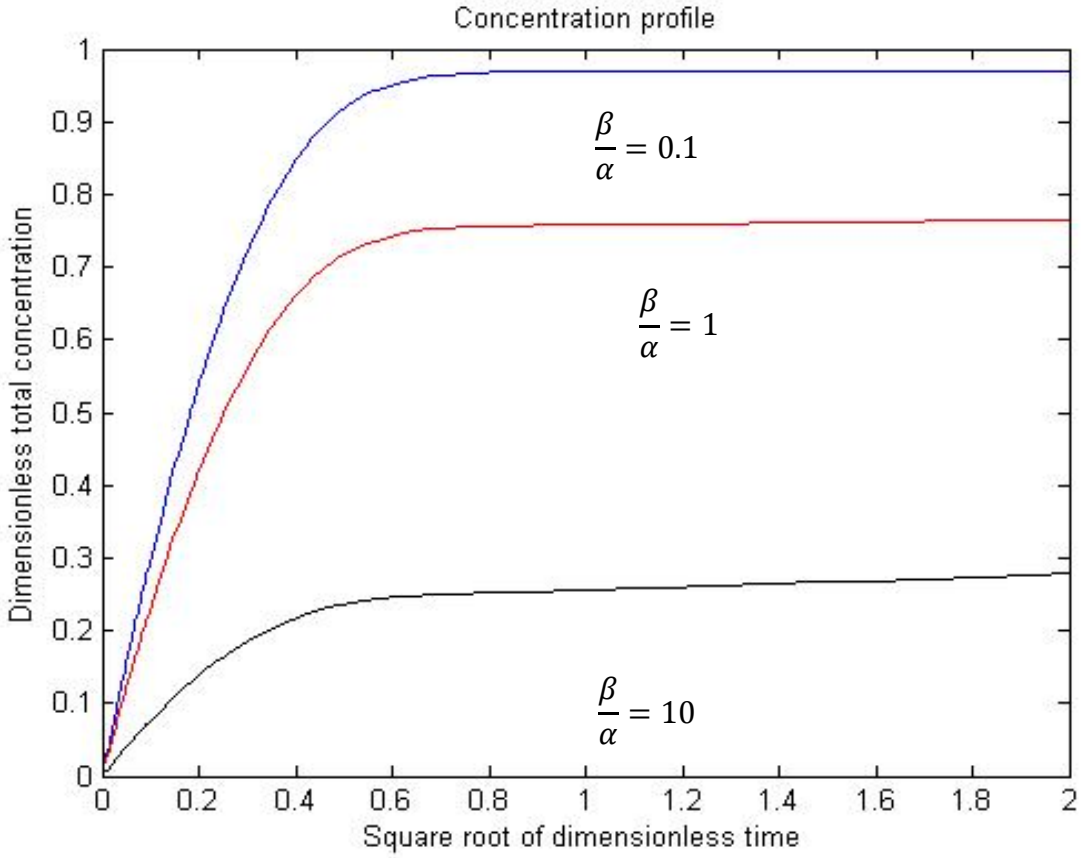

Figure 52: Concentration profile with micropore diffusion controls ($\alpha = 10^{-4}$)

The system illustrated in Figure 52 is controlled by micropore diffusion because the macropore diffusional time constant is smaller than the micropore diffusional time constant. The parameter $\frac{\beta}{\alpha}$ represents the ratio of the micropore to the macropore concentration at equilibrium. Small values of $\frac{\beta}{\alpha}$ represent negligible micropore adsorption, while high values represent negligible macropore adsorption. Figure 52 depicts only the short time solution. All the concentrations will eventually reach equilibrium. Initially the concentration increases rapidly due to macropores until quasi-

equilibrium is reached. Then the concentration slowly approaches equilibrium due to micropores.

Figure 53 shows the total concentration profile when macropore diffusion controls ($\alpha = 10^3$) and for different values of β/α. The Figure obtained is similar to Figure 3 obtained by [35].

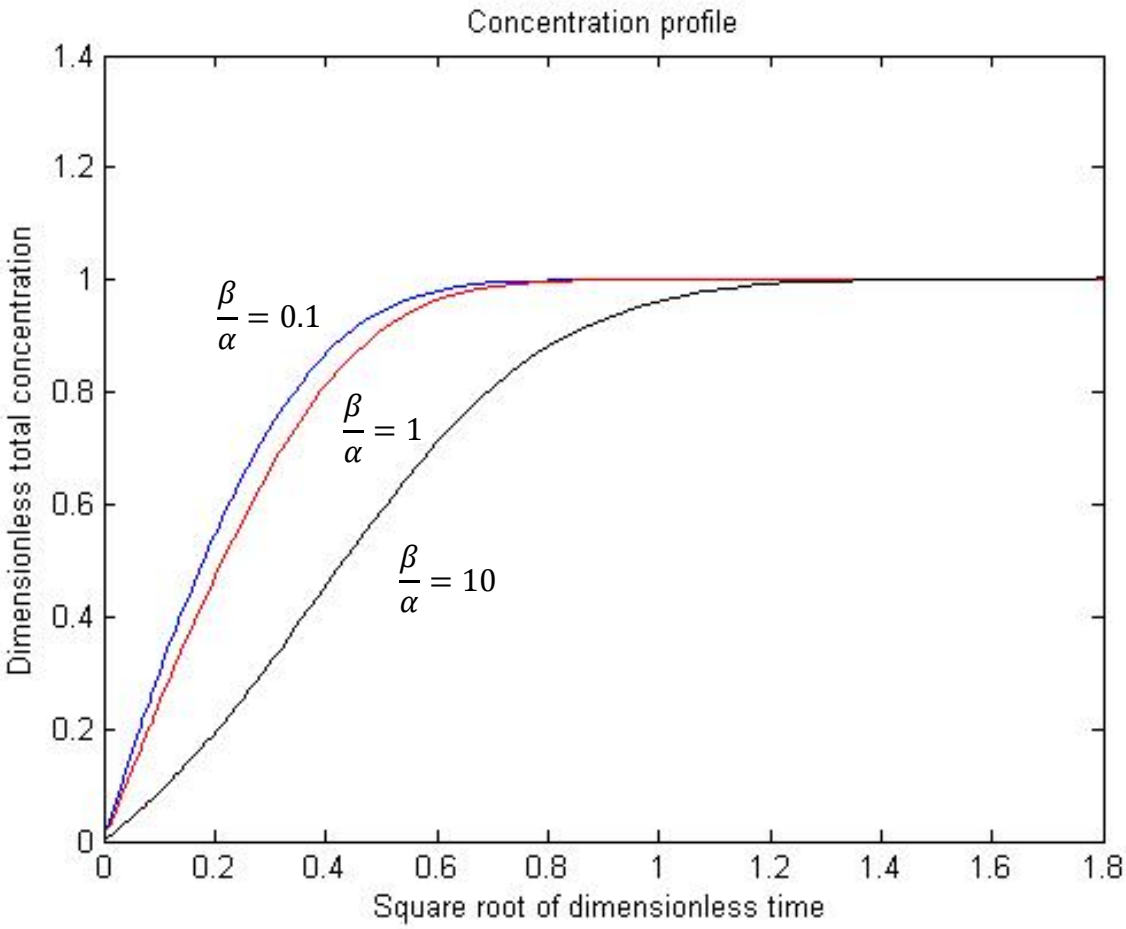

Figure 53: Concentration profile with macropore diffusion controls ($\alpha = 10^3$)

Because the ratio of the diffusional time constants is high, the system shown in Figure 53 is controlled by macropore diffusion. The smaller the value of β/α, the faster the concentration reaches equilibrium. When α equals 10^3 and β/α equals 0.1, the concentration profile is similar to the case when inactive matrix is considered. Comparing Figure 52 with Figure 53 for fixed β/α, the concentration decreases with decreasing α because the micropore adsorption decreases.

Figure 54 shows the total concentration profile for reactant A and product B when micropore diffusion controls ($\alpha = 10^{-4}$) and for β/α equals 0.1. The Thiele modulus is set to 5.

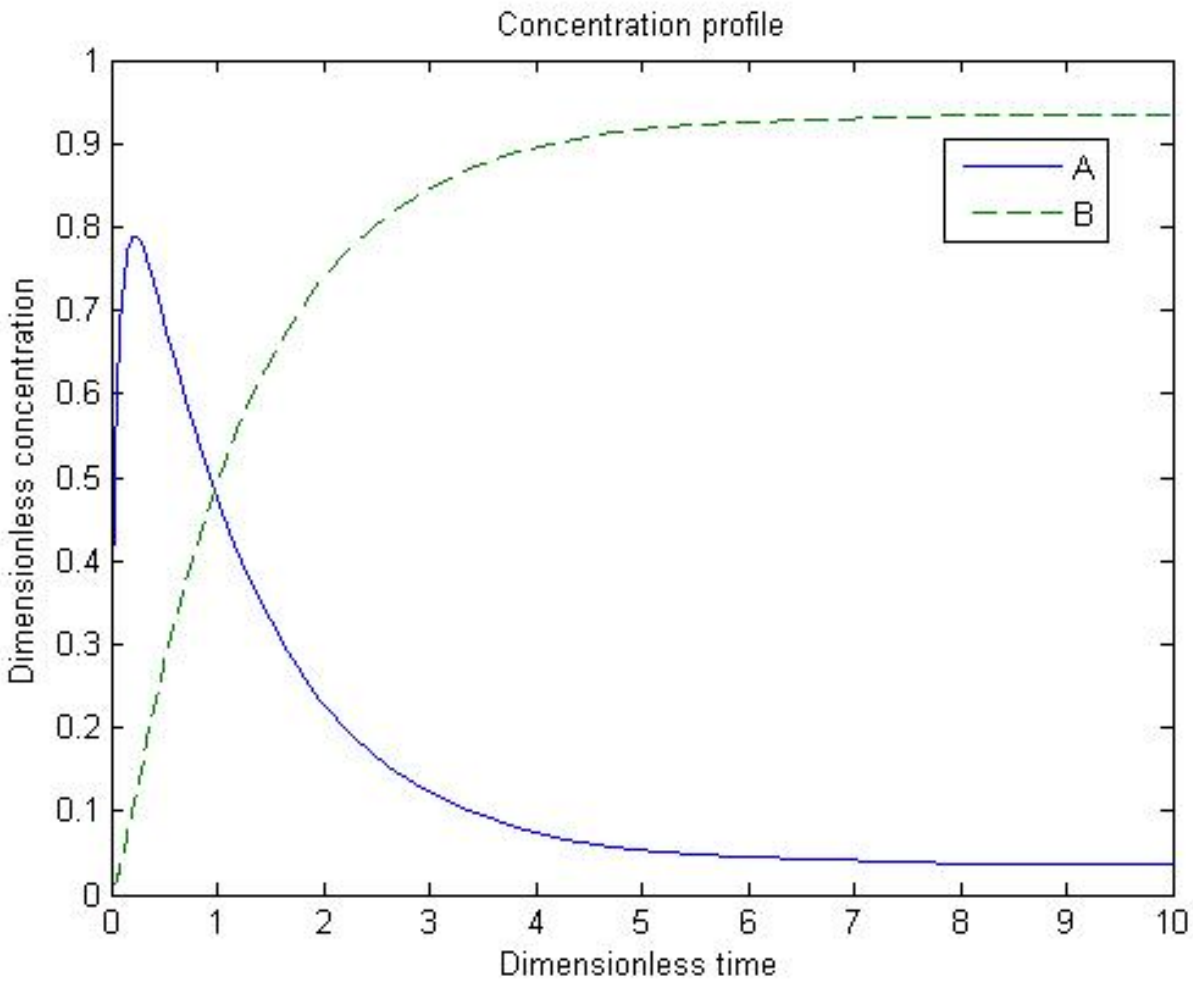

Figure 54: Concentration profile for micropore controlled reaction ($\alpha = 10^{-4}, \beta/\alpha$ =0.1)

As demonstrated in Figure 54, the total concentration of reactant A initially increases in the macropores then as A enters the micropores, it reacts to form B and the concentration of A decreases rapidly until equilibrium is reached between the reactant and product. The total concentration of B increases until equilibrium is reached.

Figure 55 shows the total concentration profile for reactant A and product B when macropore diffusion controls ($\alpha = 10^3$) and for β/α equals 0.1. The Thiele modulus is set to 5.

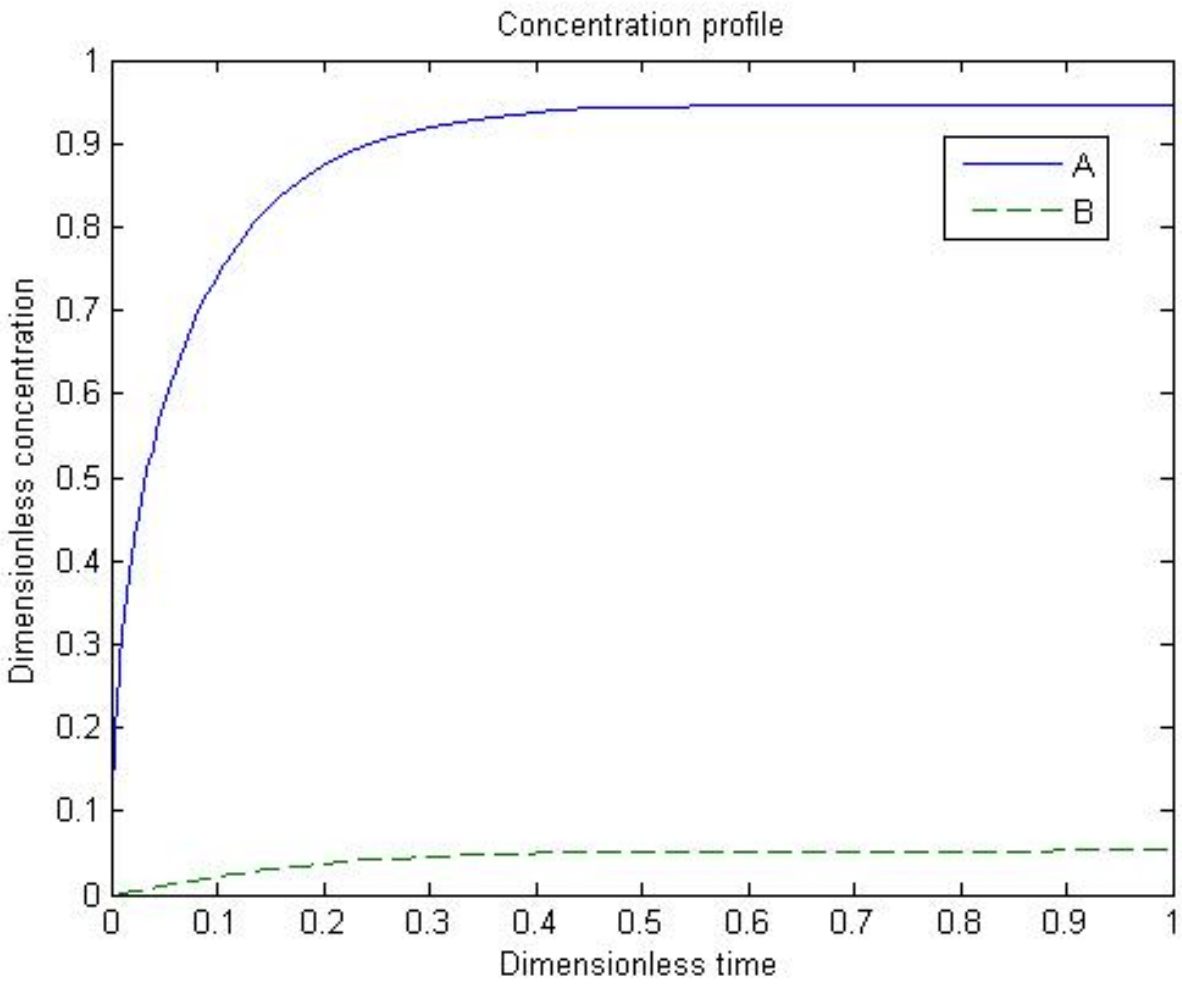

Figure 55: Concentration profile for macropore controlled reaction ($\alpha = 10^3, \beta/\alpha$ =0.1, $\varphi = 5$)

The total concentration of reactant increases with time until equilibrium is reached. Comparing Figure 55 with Figure 54, the conversion is higher when micropore diffusion controls the system.

The following figures illustrate the effects of the active matrix by comparing the concentration achieved with the two diffusion resistances and with micropore only.

Figure 56 demonstrates the concentration profile for reactant A with no reaction. In this Figure, $\alpha = 10^3$ and β/α =0.1

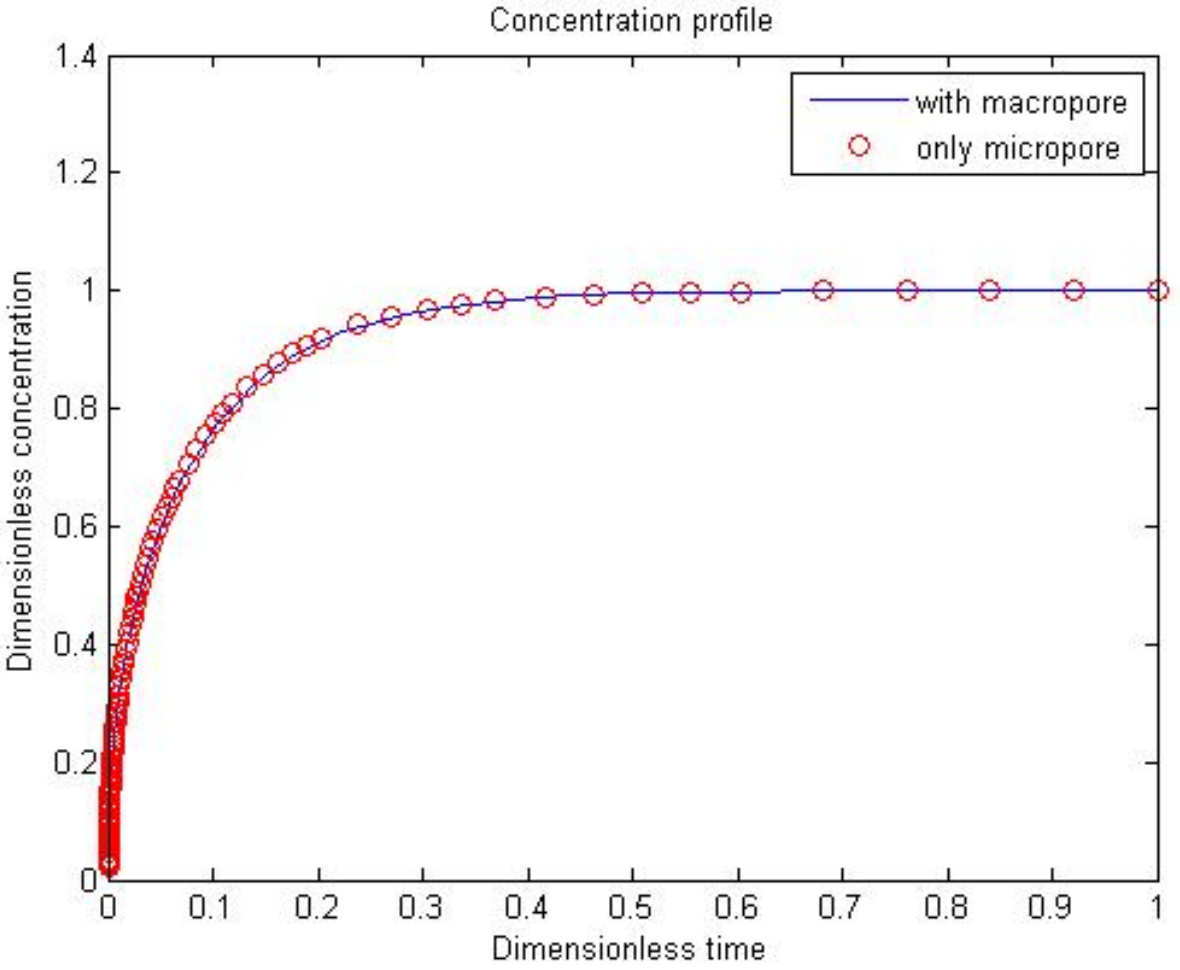

Figure 56: Comparison between active and inactive matrix ($\alpha = 10^3, \beta/\alpha = 0.1$)

The concentration profile is the same for both cases. When macropore diffusion is controlling and macropore adsorption is higher, the resultant total concentration is the same as if only one type of pores is present.

Figure 57 demonstrates the concentration profile for reactant A with no reaction when $\alpha = 10^3$ and $\beta/\alpha = 10$

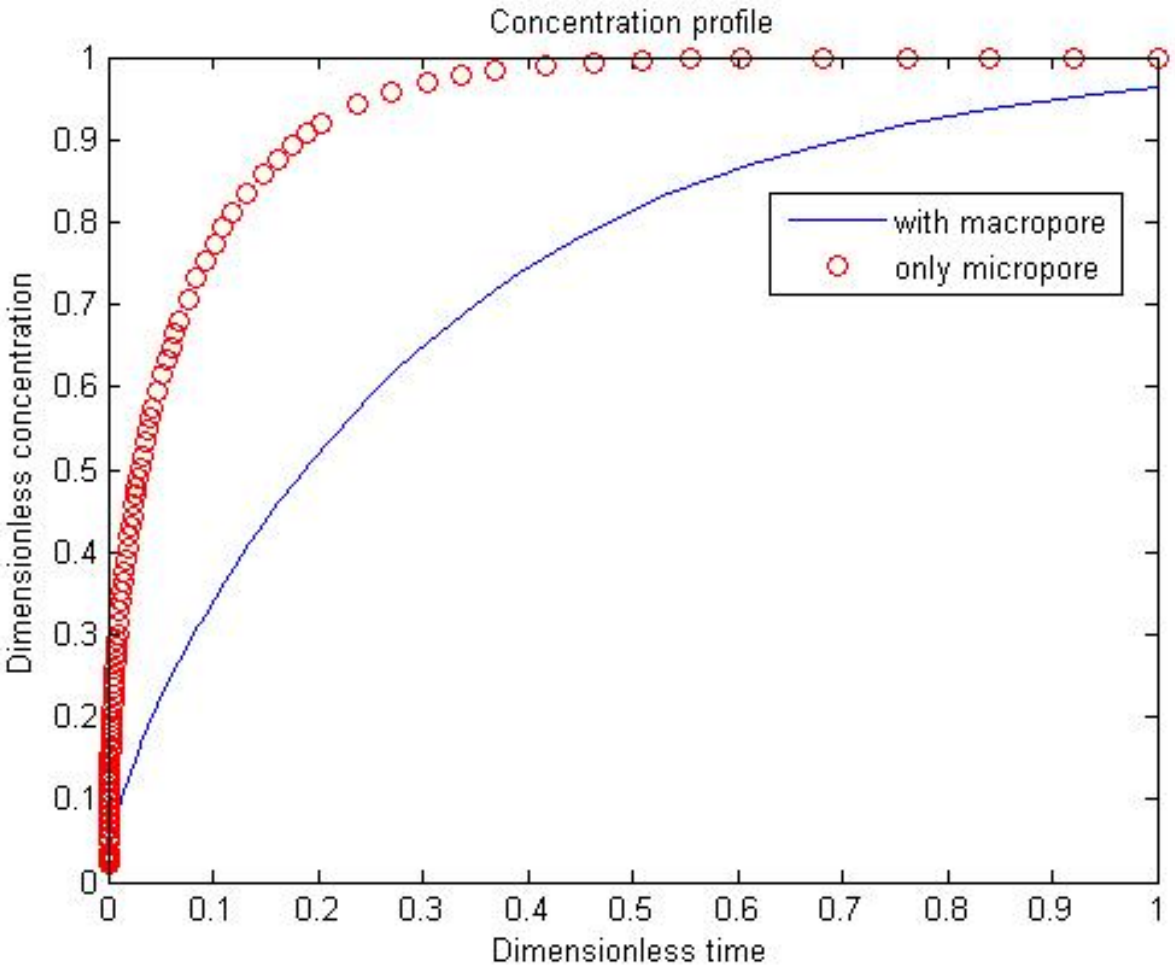

Figure 57: Comparison between active and inactive matrix ($\alpha = 10^3, \beta/\alpha = 10$)

In Figure 57, the active matrix system is controlled by macropore diffusion but micropore adsorption is higher than macropore adsorption. From Figure 57, the concentration of A decreased when the active matrix was considered.

Figure 58 demonstrates the concentration profile for reactant A with no reaction when $\alpha = 10^{-4}$ and β/α =0.1

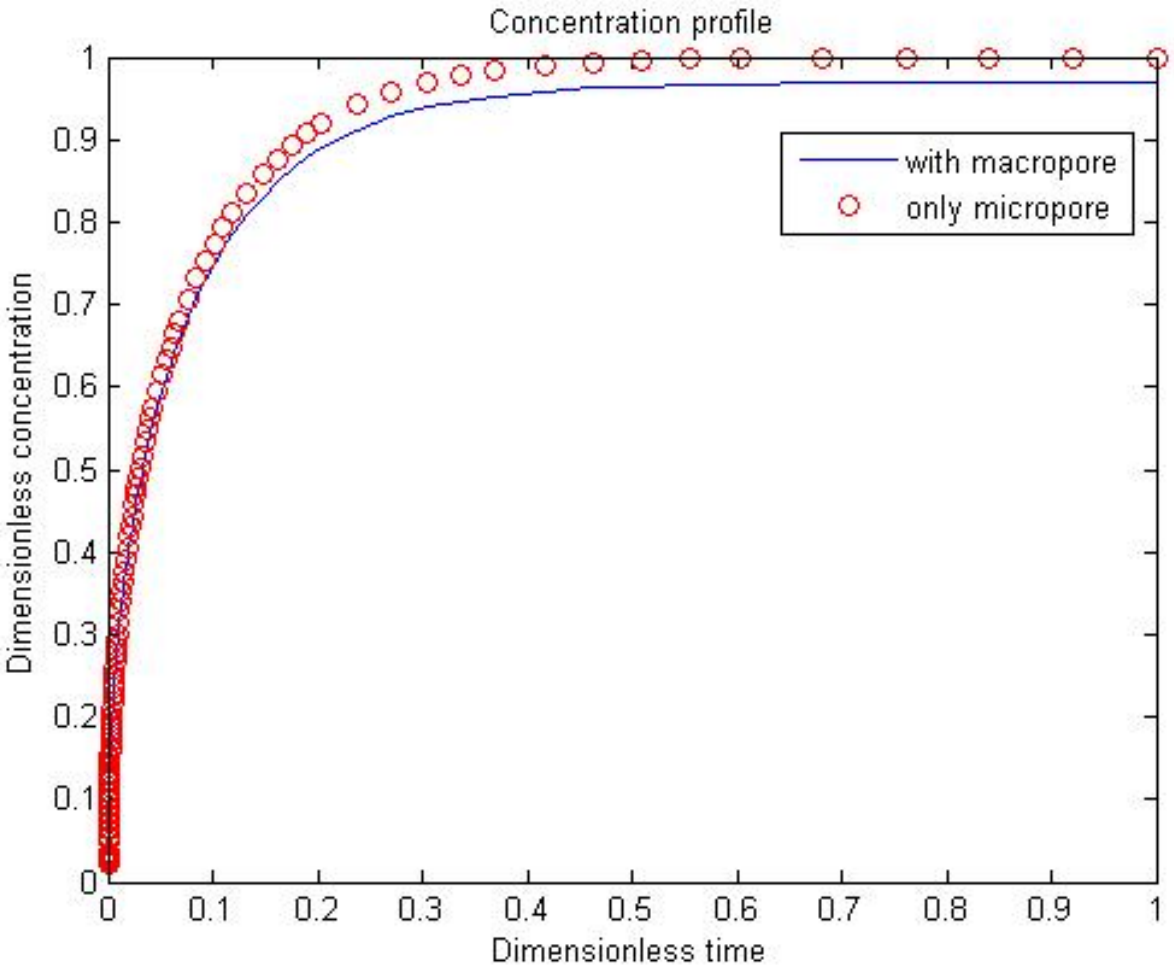

Figure 58: Comparison between active and inactive matrix ($\alpha = 10^{-4}, \beta/\alpha = 0.1$)

In Figure 58, the active matrix system is controlled by micropore diffusion and macropore adsorption is higher than micropore adsorption. Initially the two curves are the same, and then as the reactant in the active matrix system enters the micropores, the rate becomes slower. The difference is due to the adsorption of A in both pores. Comparing Figure 56 to Figure 58, the faster rate is achieved when macropore diffusion controls the system and adsorption is higher in the macropores.

5.3 Finite linear macro and micropore resistances:

The CREC Riser Simulator is a constant volume reactor; therefore, the assumption of infinite volume is invalid. This section releases the assumption of infinite volume.

5.3.1 The model

The derived equations in the previous section are still valid except for the surface boundary conditions. At the surface, Equation 3.5.1 is applied to the macropore particle:

$$-4\,\pi\,N\,R_p^2\,D_p\left(\frac{\partial C_s}{\partial R}\right)_{R=R_p} = V\,\left(\frac{\partial C}{\partial t}\right)_{R=R_p} \qquad 5.3.1$$

Assuming linear equilibrium between the bulk and adsorbed phases:

$$\left(\frac{\partial C}{\partial t}\right)_{R=R_p} = \frac{-4\,K\,\pi\,N\,R_p^2 D_p}{V}\left(\frac{\partial C}{\partial R}\right)_{R=R_p} \qquad 5.3.2$$

So the model for finite macro and micropore resistances is the following set of equations:

$$\frac{\partial C}{\partial t} = \frac{\mathcal{D}_p}{R^2}\frac{\partial}{\partial R}\left(R^2\frac{\partial C}{\partial R}\right) - \frac{4\pi N r_c^2 \epsilon_c D_c}{\epsilon_p\left[1+\frac{K_p S_p}{\epsilon_p}\right]}\left(\frac{\partial q}{\partial r}\right)_{r=r_c} \qquad 5.2.5$$

$$\frac{\partial q}{\partial t} = \frac{\mathcal{D}_c}{r^2}\frac{\partial}{\partial r}\left(r^2\frac{\partial q}{\partial r}\right) - k_{int}\phi_{int}q \qquad 3.2.4$$

$$C\,(0,R) = 0 \qquad 5.2.28$$

$$\left(\frac{\partial C}{\partial R}\right)_{R=0} = 0 \qquad 5.2.29$$

$$\left(\frac{\partial C}{\partial t}\right)_{R=R_p} = \frac{-4\,K\,\pi\,N\,R_p^2 D_p}{V}\left(\frac{\partial C}{\partial R}\right)_{R=R_p} \qquad 5.3.2$$

$$q\,(0,r) = 0 \qquad 5.2.31$$

$$\left(\frac{\partial q}{\partial r}\right)_{r=0} = 0 \qquad 5.2.32$$

$$q\,(t,r_c) = C(t,R) \qquad 5.2.33$$

5.3.2 Normalization:

Equation 5.3.2 is normalized by applying the defined dimensionless variables from the previous section:

$$\left(\frac{\partial C}{\partial t}\right)_{R=R_p} = \frac{-3}{\Lambda}\left(\frac{\partial C}{\partial R}\right)_{R=R_p} \quad 5.3.3$$

where Λ is the ratio of the bulk volume to macropore particles volume and it is defined as:

$$\Lambda = \frac{V}{\frac{4}{3}\ \pi\ N\ R_p^3 K} \quad 5.3.4$$

5.3.3 Orthogonal collocation:

For i = 1 to N:

Equations 5.2.34 and 5.2.35 are applicable.

For i = N+1:

$$\left(\frac{\partial \bar{C}}{\partial \bar{t}}\right)_{N+1} = -\frac{3}{\Lambda}\sum_{j=1}^{N+1} A_{N+1,j}\ \bar{C}_j \quad 5.3.5$$

$$\bar{q}_{N+1} = 3\ \sum_{j=1}^{N+1} W_j \bar{C}_j \quad 5.2.37$$

These equations were solved in Matlab to obtain the total concentration in the particle.

5.3.4 Results:

The following figures illustrate the effect of the finite volume on a non-reactive system. In all the cases, macropore diffusion is the controlling step $\alpha = 10^3$ with higher adsorption in the macropore β/α =0.1.

Figure 59 compares the concentration of reactant A in infinite and finite volume systems with the volume ratios equals to 100

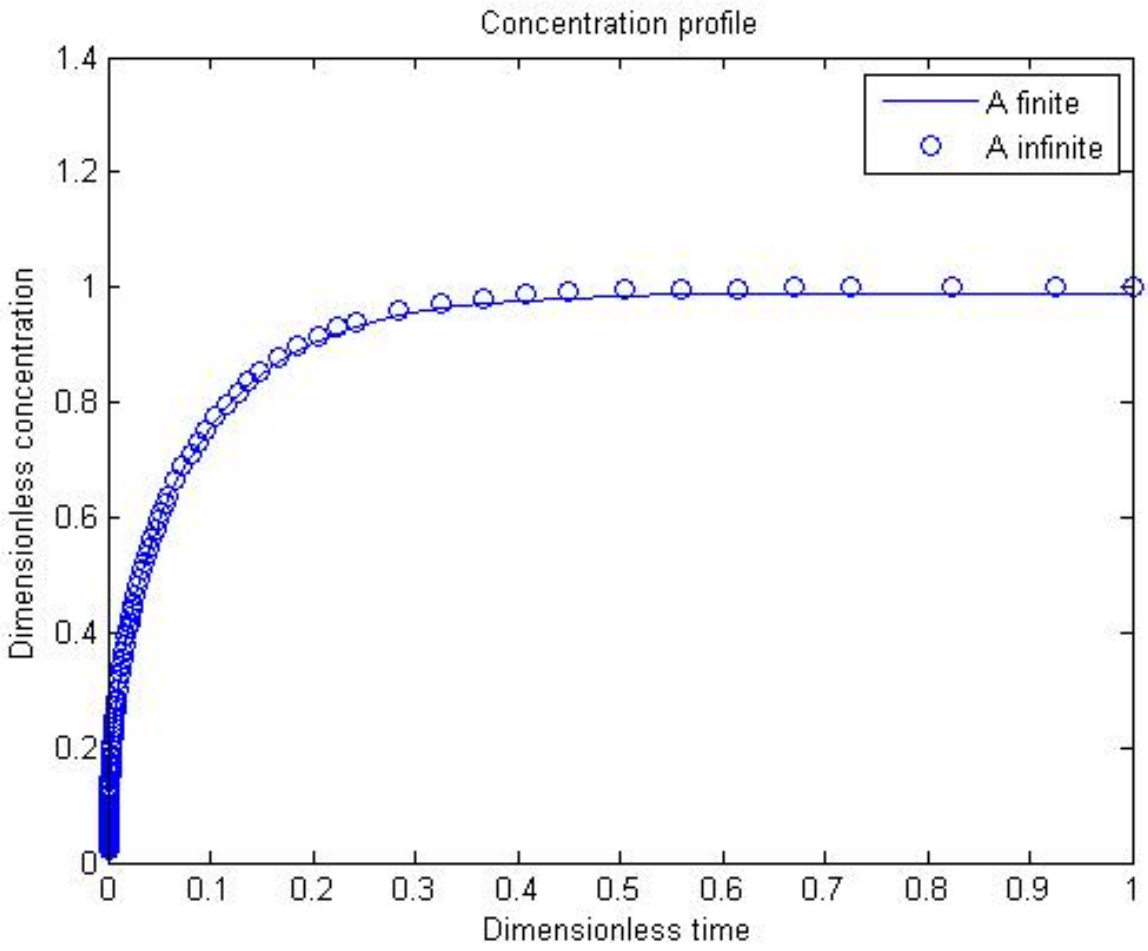

Figure 59: Comparison between infinite and finite volume systems ($\Lambda = 100$)

Figure 60 compares the concentration of reactant A in infinite and finite volume systems with the volume ratios equals to 10

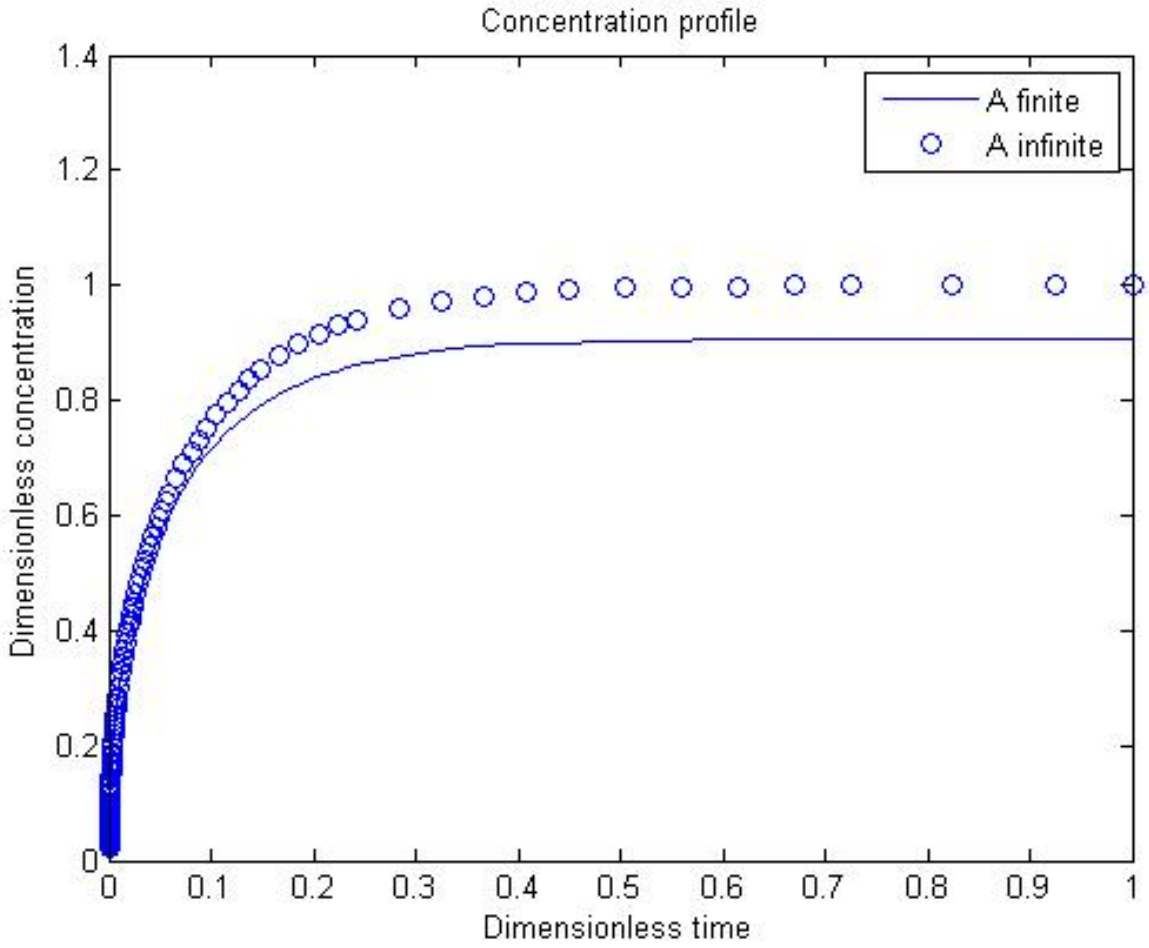

Figure 60: Comparison between infinite and finite volume systems (Λ =10)

Figure 61 compares the concentration of reactant A in infinite and finite volume systems with the volume ratios equals to 1

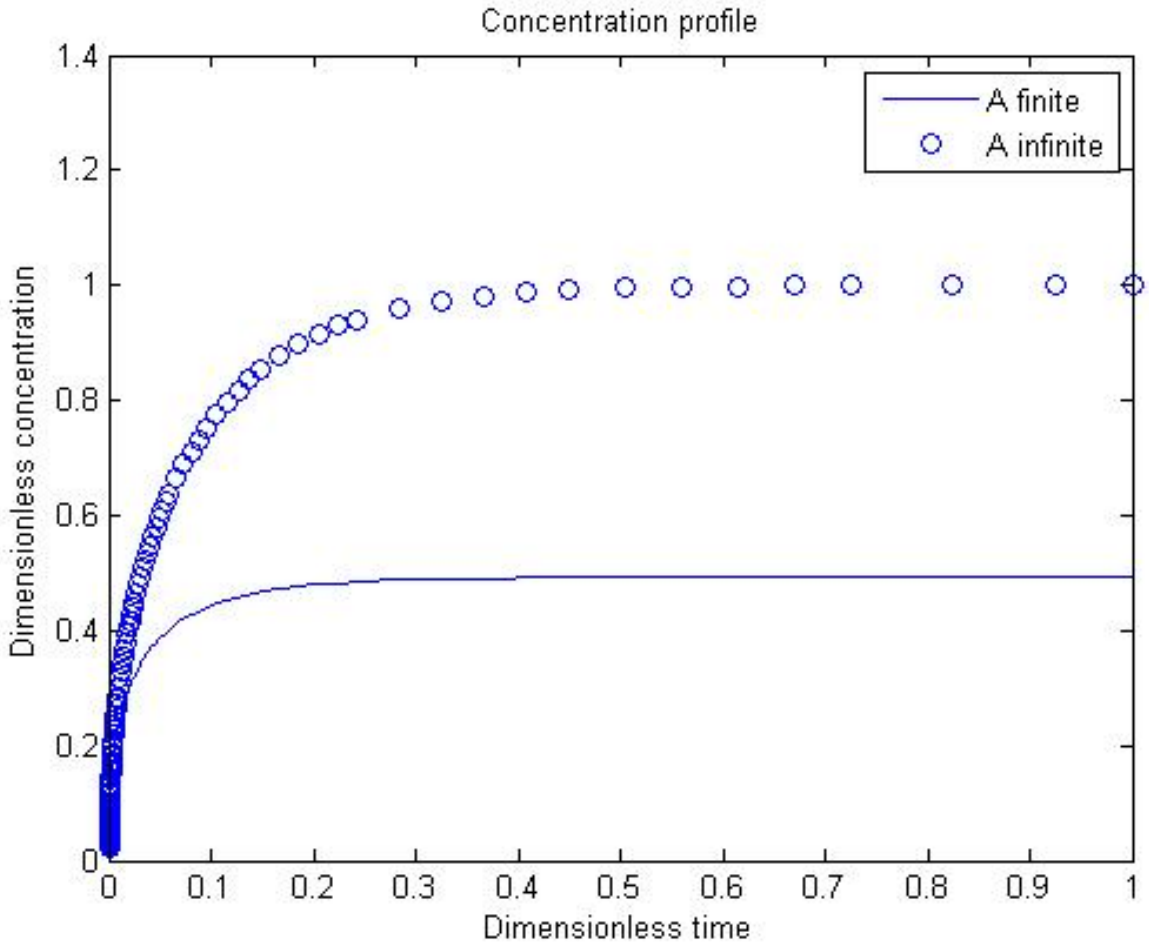

Figure 61: Comparison between infinite and finite volume systems (Λ =1)

Comparing Figure 59 to Figure 61, as the ratio of bulk fluid volume to the solids volume decreases, the concentration decreases. For large ratios, the system can be considered infinite volume system as in Figure 59.

Figure 62 compares the concentration of reactant A and product B in an active matrix with macropore diffusion as the controlling step. The adsorption in the macropore is assumed to be equal to the adsorption in the micropore ($\frac{\beta}{\alpha} = 3$). The figure compares the infinite and finite volume systems with the volume ratios equals to 10 and the Thiele modulus equals to 5.

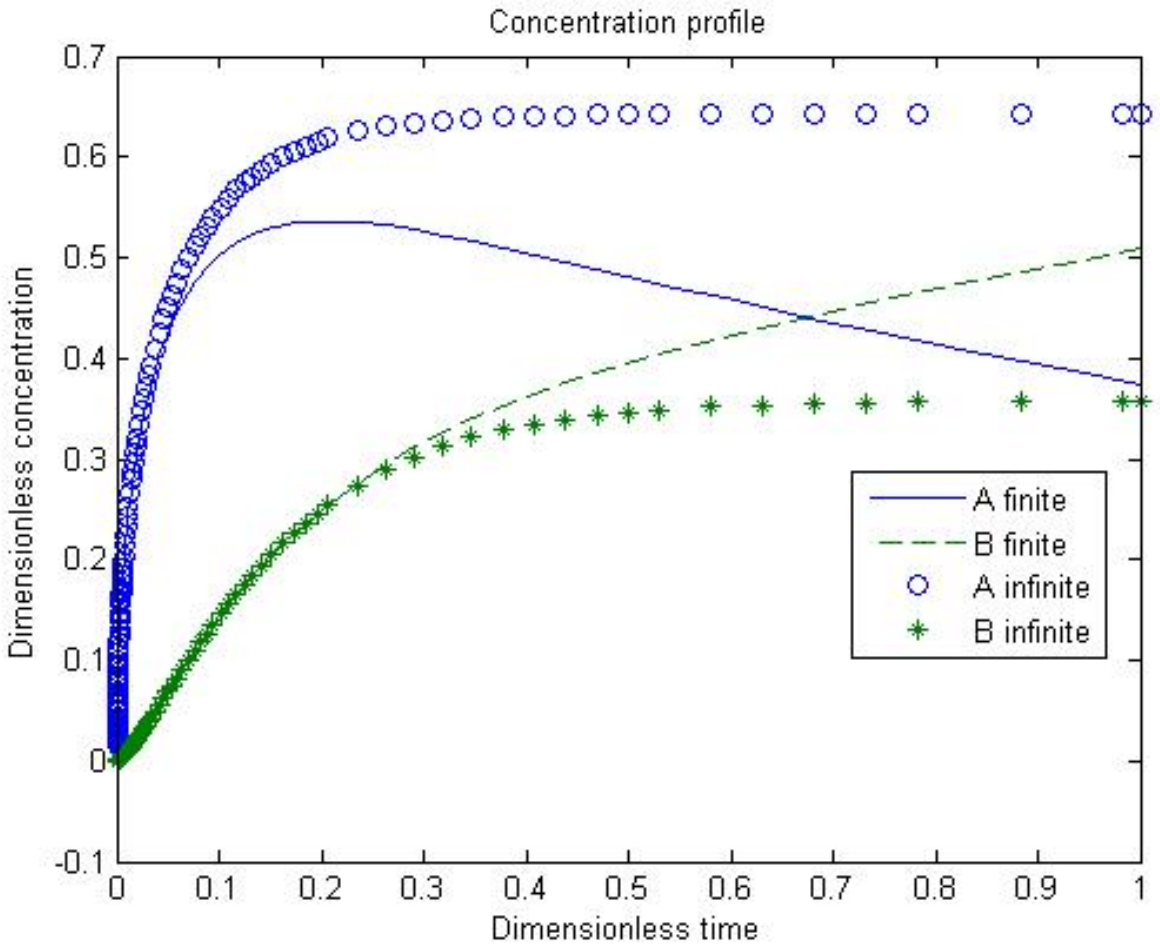

Figure 62: Comparison between infinite and finite volume reactive systems (Λ =10)

As illustrated in Figure 62, the conversion of A is higher for the finite volume system. Figure 62 demonstrates the short time solution. The reaction will proceed until all reactant A is converted to product B for the finite volume case. For the infinite volume case, the concentration of the reactant and product reach equilibrium after a short time.

Figure 63 compares between the concentration of reactant A and product B with active and inactive matrix in a finite volume system. Macropore diffusion is the controlling step with the adsorption in the macropore equals the adsorption in the micropore for the active matrix system. The parameters are set to $\alpha = 10^3, \beta/\alpha = 1, \Lambda = 10\ and\ \varphi = 5$.

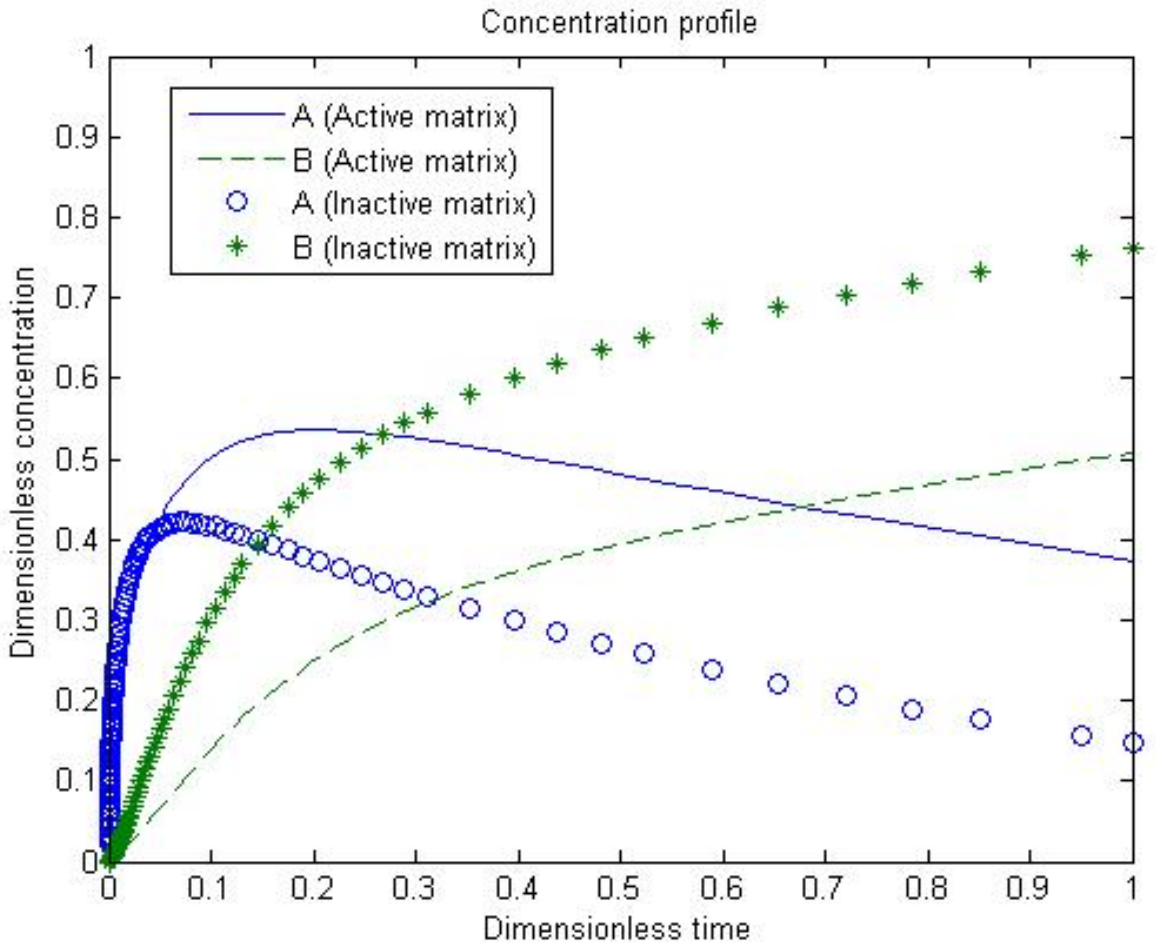

Figure 63: Comparison between active and inactive matrix in finite volume systems (Λ =10)

As illustrated in Figure 63, the conversion of reactant A is higher when inactive matrix is used. The figure depicts the short time solution. The concentration of reactant A will decrease to 0 while the concentration of B will increase to 1 in both cases.

5.4 Finite linear macro and micropore resistances with external fluid film resistance:

This section will include an external fluid film resistance between the macropore and the bulk fluid.

5.4.1 The model:

The external fluid film resistance will only affect the surface boundary condition. Therefore Equations 5.2.5 and 3.2.4 with their relevant initial and boundary conditions at the center are still valid.

The fluid film external resistance can be described by the following equation:

$$D_p\left(\frac{\partial C}{\partial R}\right)_{R_p} = k_f(C_\infty - C_s) \qquad 5.4.1$$

where k_f is the film mass transfer coefficient, C_∞ is the bulk fluid concentration and C_s is the bulk concentration at the surface. Assuming linear equilibrium:

$$D_p\left(\frac{\partial C}{\partial R}\right)_{R_p} = \frac{k_f}{K_p}(C_\infty - C_{R_p}) \qquad 5.4.2$$

Since the system has a limited volume, Equation 5.3.2 is applied:

$$\left(\frac{\partial C}{\partial t}\right)_{R=R_p} = \frac{-4\,K\,\pi\,N\,R_p^2 D_p}{V}\left(\frac{\partial C}{\partial R}\right)_{R=R_p} \qquad 5.3.2$$

Combining the two equation yields,

$$\left(\frac{\partial C}{\partial t}\right)_{R=R_p} = \frac{-4\,K\,\pi\,N\,R_p^2}{V}\frac{k_f}{K_p}(C_\infty - C_{R_p}) \qquad 5.4.3$$

The system with macro and micropore diffusion resistances and external fluid film resistance in a finite volume is described by the following set of equations:

$$\frac{\partial C}{\partial t} = \frac{\mathcal{D}_p}{R^2}\frac{\partial}{\partial R}\left(R^2\frac{\partial C}{\partial R}\right) - \frac{4\pi N r_c^2 \epsilon_c D_c}{\epsilon_p\left[1+\frac{K_p S_p}{\epsilon_p}\right]}\left(\frac{\partial q}{\partial r}\right)_{r=r_c} \qquad 5.2.5$$

$$\frac{\partial q}{\partial t} = \frac{\mathcal{D}_c}{r^2}\frac{\partial}{\partial r}\left(r^2\frac{\partial q}{\partial r}\right) - k_{int}\phi_{int}q \qquad 3.2.4$$

$$C\ (0,R) = 0 \qquad 5.2.28$$

$$\left(\frac{\partial C}{\partial R}\right)_{R=0} = 0 \qquad 5.2.29$$

$$\left(\frac{\partial C}{\partial t}\right)_{R=R_p} = \frac{-4\ K\ \pi\ N\ R_p^2}{V}\frac{k_f}{K_p}(C_\infty - C_{R_p}) \qquad 5.4.3$$

$$q\ (0,r) = 0 \qquad 5.2.31$$

$$\left(\frac{\partial q}{\partial r}\right)_{r=0} = 0 \qquad 5.2.32$$

$$q\ (t,r_c) = C(t,R) \qquad 5.2.33$$

5.4.2 Normalization:

Only the boundary condition at the surface needs to be normalized. Substituting the previous dimensionless variables into equation 5.4.3:

$$\left(\frac{\partial \bar{C}}{\partial \bar{t}}\right)_{\bar{R}=1} = -\frac{3}{\Lambda}\ Bi_m\left(\frac{C_\infty}{C_0} - (\bar{C})_{R=1}\right) \qquad 5.4.4$$

A mass balance around the total volume is performed to find the relation between C_∞ and C_0:

$$V\ C_0 = V\ C_{S_\infty} + V_s\ C_\infty \qquad 5.4.5$$

$$C_0 = C_\infty\left(1 + \frac{V_s K_p}{V}\right) \qquad 5.4.6$$

$$C_\infty = \frac{\Lambda}{1+\ \Lambda}\ C_0 \qquad 5.4.7$$

$$\frac{C_\infty}{C_0} = \frac{\Lambda}{1+\ \Lambda} \qquad 5.4.8$$

Substitute Equation 5.4.8 into Equation 5.4.4:

$$\left(\frac{\partial \bar{C}}{\partial \bar{t}}\right)_{\bar{R}=1} = -\frac{3}{\Lambda}\ Bi_m\left(\frac{\Lambda}{1+\ \Lambda} - (\bar{C})_{R=1}\right) \qquad 5.4.9$$

5.4.3 Orthogonal collocation:

For i = 1 to N:

Equations 5.2.34 and 5.2.35 are applicable.

For i = N+1:

$$\left(\frac{\partial \bar{C}}{\partial t}\right)_{N+1} = -\frac{3}{\Lambda}\sum_{j=1}^{N+1} A_{N+1,j}\,\bar{C}_j \qquad 5.3.5$$

$$\bar{C}_{N+1} = \frac{Bi_m - \sum_{j=1}^{N} A_{ij}\bar{\bar{C}}_j}{Bi_m + A_{N+1,N+1}} \qquad 5.4.10$$

$$\bar{q}_{N+1} = 3\sum_{j=1}^{N+1} W_j \bar{C}_j \qquad 5.2.37$$

These equations were solved in Matlab to obtain the total concentration in the particle. The code is presented in Appendix A.11

5.4.4 Results:

Figure 64 illustrate the effect of the Biot number on an infinite volume non-reactive system. Macropore diffusion is the controlling step $\alpha = 10^3$ with higher adsorption in the macropore β/α =0.1.

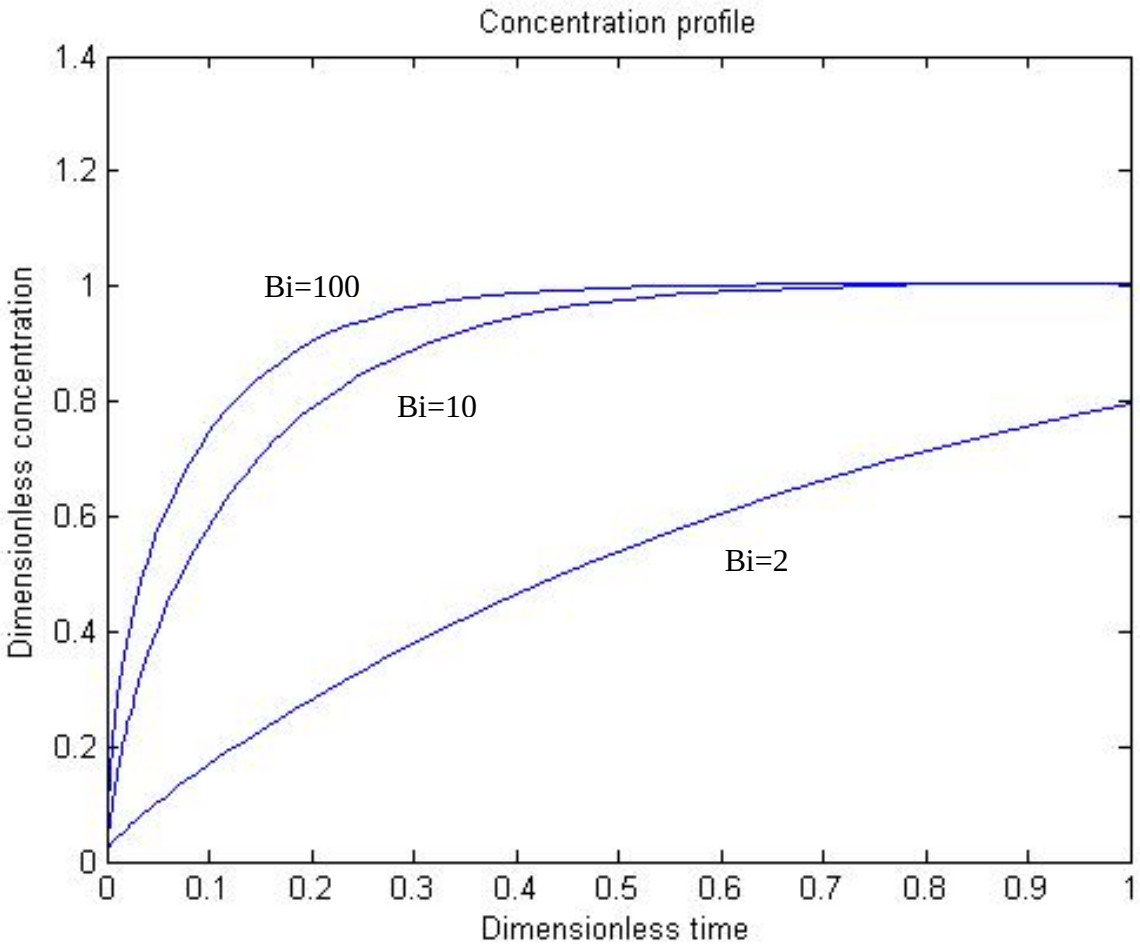

Figure 64: Concentration profile for different Biot number

As demonstrated by Figure 64, the rate of concentration is slower as the value of Biot number decreases. When the Biot number equals 100, the profile obtained is the same as in the case when external mass transfer resistance is neglected as in Figure 53.

Figure 65 illustrate the effect of the Biot number on an infinite volume non-reactive system. Micropore diffusion is the controlling step $\alpha = 10^{-4}$ with higher adsorption in the micropore β/α =10.

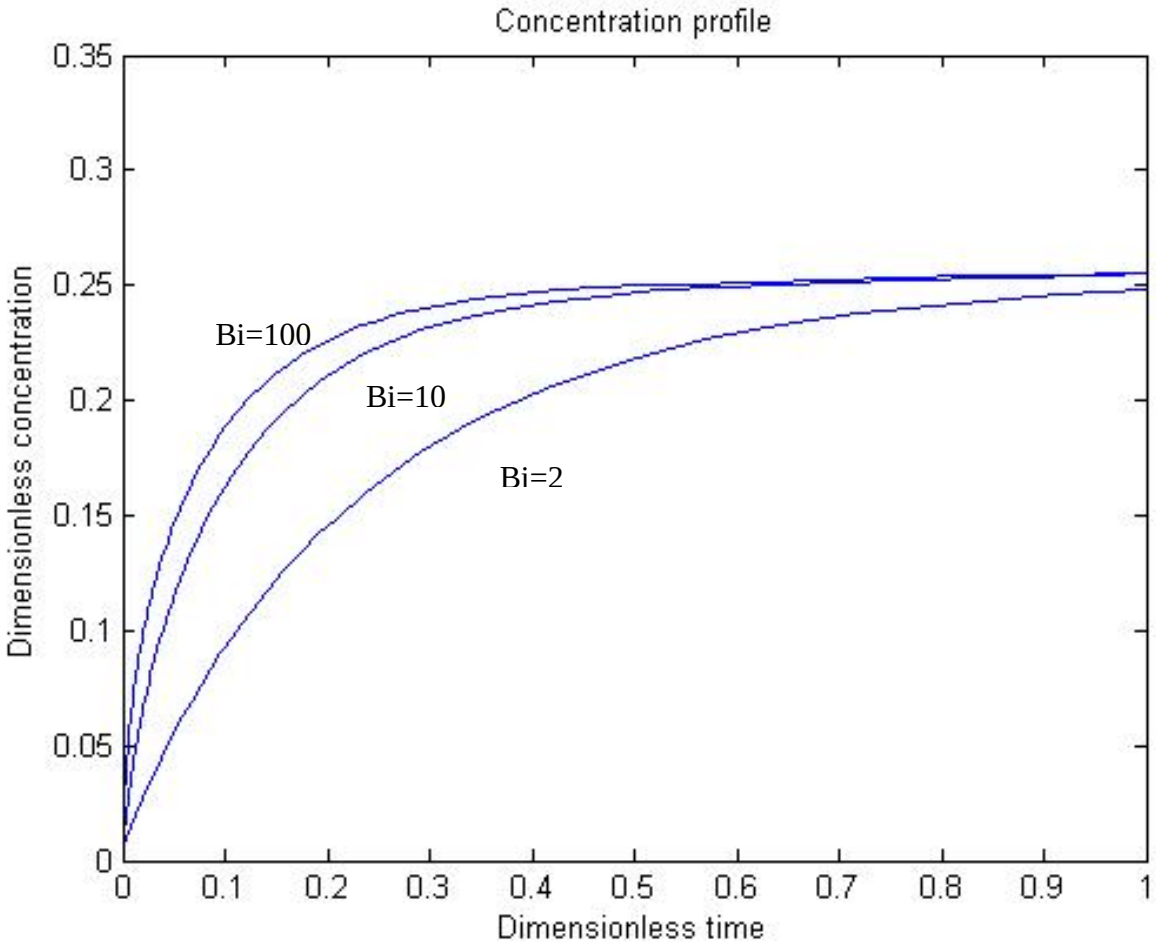

Figure 65: Concentration profile for different Biot number

As demonstrated in Figure 64, as the value of Biot number decreases, the rate of concentration slows. When the Biot number equals 100, the profile obtained is the same as in the case when external mass transfer resistance is neglected as in Figure 53. Comparing Figure 65 with Figure 64, the concentration is slower when micropore diffusion controls for the same Biot number.

Figure 66 illustrates the effect of the Biot number on an infinite volume reactive system ($\varphi = 5$). Macropore diffusion is the controlling step $\alpha = 10^3$ with equal adsorption rates in the macropore and micropore β/α =1.

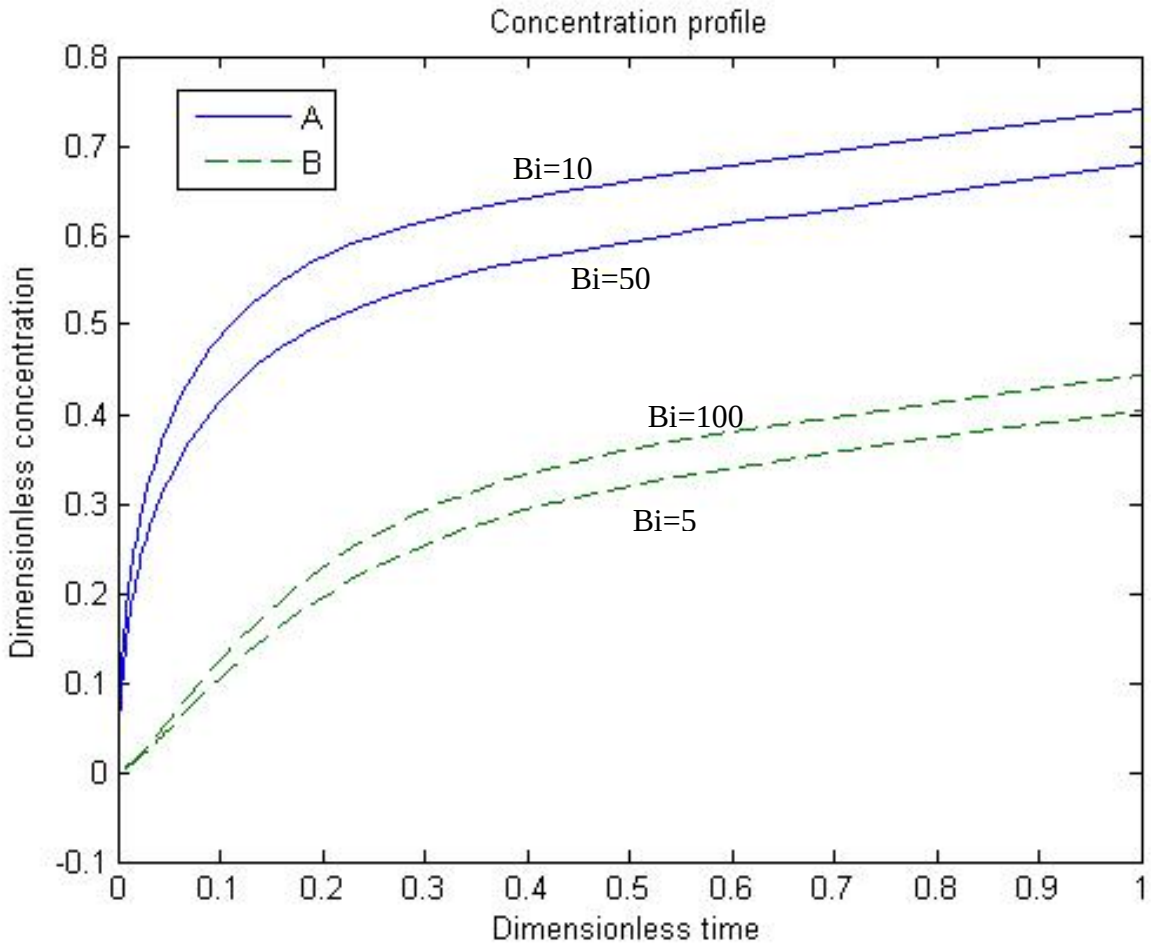

Figure 66: Concentration profile for reactive system with different Biot number

Figure 66 demonstrate the concentration profile for reactant A and product B for two values of Biot number. The smaller Biot number means that external fluid film resistance is the controlling step rather than diffusion and this result in a lower conversion.

5.5 Conclusion

In summary, this chapter considered different systems for diffusion-reaction processes with active matrix. By comparing the results from this chapter with the results from chapter 3, the conversion is higher if only one diffusion resistance is present. When the matrix is active and diffusion and adsorption occur in both micro and macropores, the conversion is higher if macropore is the controlling step and if adsorption in the macropore is higher than adsorption in the micropore. Moreover, it was found that the conversion decreases if external fluid film resistance is controlling and therefore it should be eliminated. Limited volume systems achieve higher conversion than infinite volume systems where equilibrium between the reactant and product are achieved.

Chapter 6: Applications of Modeling Reactions, Adsorption and Diffusion in FCC Catalyst

6.1 Introduction:

The previous chapters developed different models to describe heterogeneous catalytic reaction. The models were applied to simple first order reaction to study the effects of the different parameters. The models were general and could be applicable to different heterogeneous catalytic reactions. The main objective of this thesis is to study the reactions in FCC catalyst; therefore, this chapter applies some of the previous models to the cracking reactions in FCC catalyst.

Two models were used to describe the catalytic cracking of gas oil in FCC catalyst. The first model is the four lump model which consists of gas oil, gasoline, light gases and coke. Although other lumped models can describe the behavior of gas oil better than the four lump model, experimental data and adsorption parameters are not available for the other models in literature. The second model is the reactions of pure components that behave like gas oil. 1,3,5-TIPB was used in this chapter because it is considered a typical gas oil molecule, the reactions pathway of 1,3,5-TIPB can be easily followed and diffusional limitations can be studied using 1,3,5-TIPB.

In this chapter different models were used to fit the data. These models include isothermal reactions, adsorption and diffusion with inactive matrix in infinite volume system, finite volume system and finite volume system with external fluid film resistance. In addition, isothermal reactions, adsorption and diffusion with active matrix in finite volume system was also considered.

The limitations encountered while modeling the experimental data were the lack of experimental data. Moreover, some parameters were not evaluated experimentally such as the diffusivities and adsorption parameters for gas oil and 1,3,5-TIPB in both macro and micropores.

6.2 Modeling Gas oil:

This section applies the different models to the gas oil data in Figure 6. Three models describing the reactions in inactive matrix were used to fit the data: infinite volume, finite volume and finite volume with external fluid film resistance. The reactions in an active matrix with a finite volume system were also considered. The adsorption parameters used in this section were obtained from [2].

6.2.1 Isothermal reactions, adsorption and diffusion with inactive matrix in infinite volume:

The gas oil experimental data were fitted to an infinite volume model.

6.2.1.1 The model

The reaction of gas oil for a lump model is:

$$Gas\ oil \overset{k_1}{\rightarrow} Gasoline$$

$$Gas\ oil \overset{k_2}{\rightarrow} Light\ gases$$

$$Gas\ oil \overset{k_3}{\rightarrow} Coke$$

$$Gasoline \overset{k_4}{\rightarrow} Light\ gases$$

$$Gasoline \overset{k_5}{\rightarrow} Coke$$

Let A, B, C, D correspond to gas oil, gasoline, light gases and coke, respectively. The reaction rates can be written as:

$$r_A = -\phi_{int}(k_1 + k_2 + k_3)q_A^2 \qquad 6.2.1$$

$$r_B = \phi_{int}(k_1 q_A^2 - (k_4 + k_5)q_B) \qquad 6.2.2$$

$$r_C = \phi_{int}(k_2 q_A^2 + k_4 q_B) \qquad 6.2.3$$

$$r_D = \phi_{int}(k_3 q_A^2 + k_5 q_B) \qquad 6.2.4$$

where $$\phi_{int} = \exp(-\lambda y_D) \qquad 6.2.5$$

Applying Equation 3.2.4 to each component gives the following set of diffusion-reaction equations:

$$\frac{\partial q_A}{\partial t} = \frac{D_{c_A}}{r^2}\frac{\partial}{\partial r}\left(r^2\frac{\partial q_A}{\partial r}\right) + r_A \tag{6.2.6}$$

$$\frac{\partial q_B}{\partial t} = \frac{D_{c_B}}{r^2}\frac{\partial}{\partial r}\left(r^2\frac{\partial q_B}{\partial r}\right) + r_B \tag{6.2.7}$$

$$\frac{\partial q_C}{\partial t} = \frac{D_{c_C}}{r^2}\frac{\partial}{\partial r}\left(r^2\frac{\partial q_C}{\partial r}\right) + r_C \tag{6.2.8}$$

$$\frac{\partial q_D}{\partial t} = \frac{D_{c_D}}{r^2}\frac{\partial}{\partial r}\left(r^2\frac{\partial q_D}{\partial r}\right) + r_D \tag{6.2.9}$$

The relevant initial and boundary conditions are:

$$\left(\frac{\partial q_A}{\partial t}\right)_{r=0} = \left(\frac{\partial q_B}{\partial t}\right)_{r=0} = \left(\frac{\partial q_C}{\partial t}\right)_{r=0} = \left(\frac{\partial q_D}{\partial t}\right)_{r=0} = 0 \tag{6.2.10}$$

$$q_A(t, r_C) = K_A\, C_\infty \tag{6.2.11}$$

$$q_B(t, r_c) = q_C(t, r_c) = q_D(t, r_c) = 0 \tag{6.2.12}$$

$$q_A(0, r) = q_B(0, r) = q_C(0, r) = q_D(0, r) = 0 \tag{6.2.13}$$

Equation 6.2.6-6.2.13 needs to be normalized. Normalization results in:

$$\frac{\partial \bar{q}_A}{\partial \bar{t}} = \frac{1}{\bar{r}^2}\frac{\partial}{\partial \bar{r}}\left(\bar{r}^2\frac{\partial \bar{q}_A}{\partial \bar{r}}\right) - \phi_{int}(\varphi_1^2 + \varphi_2^2 + \varphi_3^2)\,\bar{q}_A^2 \tag{6.2.14}$$

$$\frac{\partial \bar{q}_B}{\partial \bar{t}} = \frac{1}{\bar{r}^2}\frac{\partial}{\partial \bar{r}}\left(\bar{r}^2\frac{\partial \bar{q}_B}{\partial \bar{r}}\right) + \phi_{int}\left(\varphi_1^2\,\bar{q}_A^2 - (\varphi_4^2 - \varphi_5^2)\,\bar{q}_B\right) \tag{6.2.15}$$

$$\frac{\partial \bar{q}_C}{\partial \bar{t}} = \frac{1}{\bar{r}^2}\frac{\partial}{\partial \bar{r}}\left(\bar{r}^2\frac{\partial \bar{q}_C}{\partial \bar{r}}\right) + \phi_{int}(\varphi_2^2\,\bar{q}_A^2 + \varphi_4^2\,\bar{q}_B) \tag{6.2.16}$$

$$\frac{\partial \bar{q}_D}{\partial \bar{t}} = \frac{1}{\bar{r}^2}\frac{\partial}{\partial \bar{r}}\left(\bar{r}^2\frac{\partial \bar{q}_D}{\partial \bar{r}}\right) + \phi_{int}\left(\varphi_3^2\,\bar{q}_A^2 + \varphi_5^2\,\bar{q}_B\right) \tag{6.2.17}$$

where,

$$\varphi_1^2 = \frac{k_1 q_0 {r_c}^2}{D_{c_A}} \tag{6.2.18}$$

$$\varphi_2^2 = \frac{k_2 q_0 {r_c}^2}{D_{c_A}} \tag{6.2.19}$$

$$\varphi_3^2 = \frac{k_3 q_0 {r_c}^2}{D_{c_A}} \tag{6.2.20}$$

$$\varphi_4^2 = \frac{k_4 {r_c}^2}{D_{c_A}} \tag{6.2.21}$$

$$\varphi_5^2 = \frac{k_5 {r_c}^2}{D_{c_A}} \quad 6.2.22$$

where the diffusivities of all components were assumed to be equal to the gas oil diffusivity which is 6×10^{-14} m^2/s at 525℃ [17].

The normalized initial and boundary conditions are:

$$\left(\frac{\partial \bar{q}_A}{\partial \bar{t}}\right)_{\bar{r}=0} = \left(\frac{\partial \bar{q}_B}{\partial \bar{t}}\right)_{\bar{r}=0} = \left(\frac{\partial \bar{q}_C}{\partial \bar{t}}\right)_{\bar{r}=0} = \left(\frac{\partial \bar{q}_D}{\partial \bar{t}}\right)_{\bar{r}=0} = 0 \quad 6.2.23$$

$$\bar{q}_A(\bar{t}, 1) = 1 \quad 6.2.24$$

$$\bar{q}_B(\bar{t}, 1) = \bar{q}_C(\bar{t}, 1) = \bar{q}_D(\bar{t}, 1) = 0 \quad 6.2.25$$

$$\bar{q}_A(0, \bar{r}) = \bar{q}_B(0, \bar{r}) = \bar{q}_C(0, \bar{r}) = \bar{q}_D(0, \bar{r}) = 0 \quad 6.2.26$$

The preceding set of equations was solved using orthogonal collocation as outlined in section 3.2.

The values of the Thiele moduli were optimized for the data in Figure 6 to minimize the sum of squares of errors. The steps for optimizations are as follows:

1. Start with initial guesses for the values of Thiele modulus.
2. Solve the differential equations for the normalized time ($\bar{t}$) and adsorbed concentrations ($\bar{q}_A$).
3. Find the time ($t = \bar{t}\, r^2/D_{C_A}$)
4. Find the adsorbed concentration ($q_A = \bar{q}_A q_0 = \bar{q}_A K_A C_\infty$)
5. Find the bulk concentration ($C_A = q_A/K_A$)
6. Find the mass ($m_A = C_A M w_A V$)
7. Find the sum of squares of errors:

$$Error_A^2 = \left(\sum_{i=1}^{N} \frac{m_A - m_{A_{exp}}}{m_{A_{exp}}}\right)^2 \quad 6.2.27$$

$$Error_B^2 = \left(\sum_{i=1}^{N} \frac{m_B - m_{B_{exp}}}{m_{B_{exp}}}\right)^2 \quad 6.2.28$$

$$Error_C^2 = \left(\sum_{i=1}^{N} \frac{m_C - m_{C_{exp}}}{m_{C_{exp}}}\right)^2 \quad 6.2.29$$

$$Error_D^2 = \left(\sum_{i=1}^{N} \frac{m_D - m_{D_{exp}}}{m_{D_{exp}}} \right)^2 \quad 6.2.30$$

$$Error = \sqrt{Error_A^2 + Error_B^2 + Error_C^2 + Error_D^2} \quad 6.2.31$$

7. The sum of squares of errors was minimized using the function fmincon in Matlab which finds a constrained minimum of multivariable function.

6.2.1.2 Results

The diffusion-reaction equations that describe the 4 lumps model were optimized using Matlab. Figure 67 demonstrates the results:

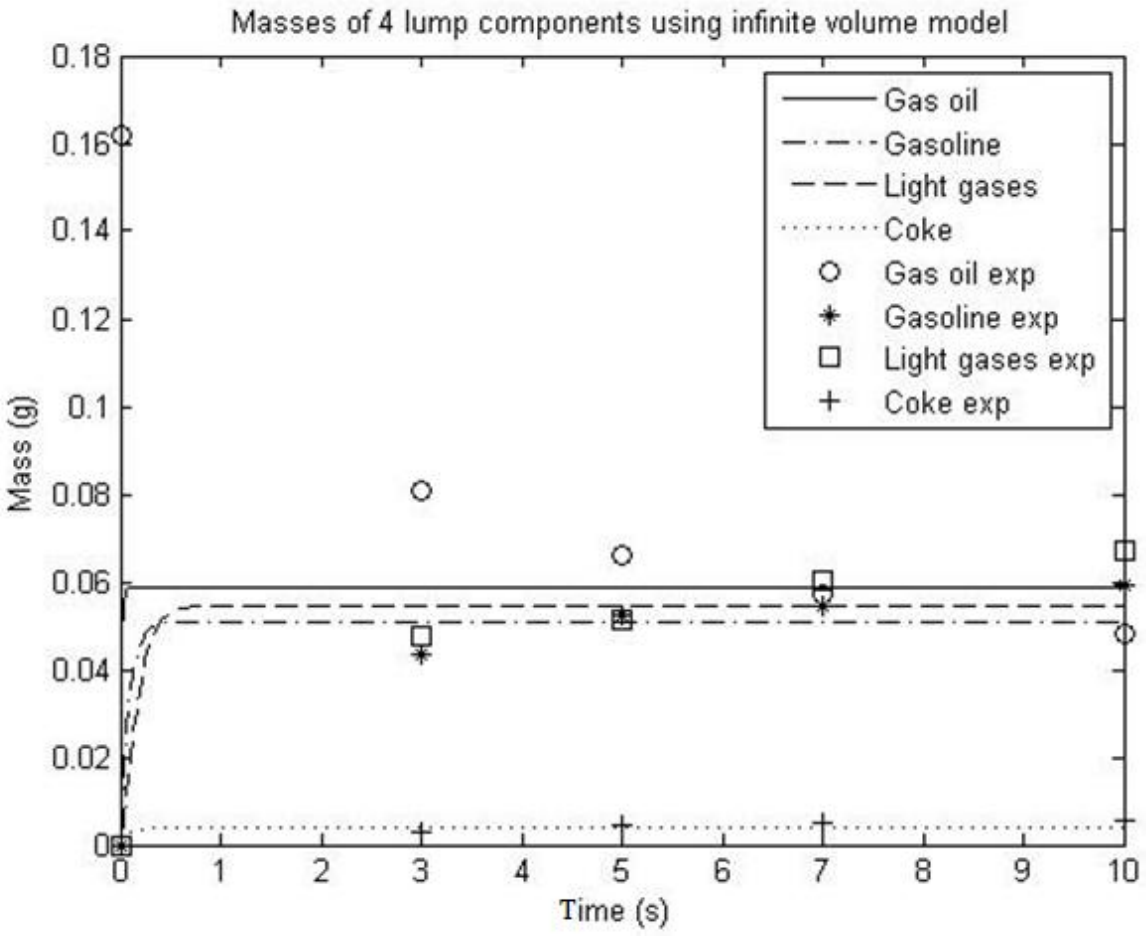

Figure 67: Application of infinite volume model to gas oil data
Experimental data obtained from Al-Khattaf [28]

Figure 67 clearly shows that the infinite volume model dose not describe the gas oil experimental data. For an infinite volume system, the reactant and products concentration reaches equilibrium, however, the experimental data shows a continuous decrease in the reactant concentration and a continuous increase in the products concentration. Table 11 summarizes the values of Thiele moduli obtained from the optimization. The diffusivities of the products are not available in literature; therefore, the kinetics parameters cannot be found.

Table 11: Values of Thiele modulus for infinite volume model

φ_1	15.0913
φ_2	11.8746
φ_3	1.5203
φ_4	4.8570
φ_5	0.0204

6.2.2 Isothermal reactions, adsorption and diffusion with inactive matrix in finite volume:

From the previous section, the infinite volume system did not describe the data properly. This suggests that a finite volume model should be used. Moreover, the CREC reactor where the experiments were carried out is a constant volume reactor. Thus the infinite volume model was a poor approximation.

6.2.2.1 The model

The diffusion-reaction equations are still applicable except for the boundary conditions at the surface. Equations 6.2.26 and 6.2.27 are replaced with the following set of normalized equations:

$$\left(\frac{\partial \bar{q}_A}{\partial \bar{t}}\right)_{\bar{r}=1} = -\frac{3}{\Lambda}\left(\frac{\partial \bar{q}_A}{\partial \bar{r}}\right)_{\bar{r}=1} \quad 6.2.32$$

$$\left(\frac{\partial \bar{q}_B}{\partial \bar{t}}\right)_{\bar{r}=1} = -\frac{3}{\Lambda}\left(\frac{\partial \bar{q}_B}{\partial \bar{r}}\right)_{\bar{r}=1} \quad 6.2.33$$

$$\left(\frac{\partial \bar{q}_C}{\partial \bar{t}}\right)_{\bar{r}=1} = -\frac{3}{\Lambda}\left(\frac{\partial \bar{q}_C}{\partial \bar{r}}\right)_{\bar{r}=1} \quad 6.2.34$$

$$\left(\frac{\partial \bar{q}_D}{\partial \bar{t}}\right)_{\bar{r}=1} = -\frac{3}{\Lambda}\left(\frac{\partial \bar{q}_D}{\partial \bar{r}}\right)_{\bar{r}=1} \quad 6.2.35$$

The new set of equations was solved using orthogonal collocation and optimized for the values of Thiele moduli and the value of the ratio of the bulk and solids volumes. The code is presented in Appendix A.12

6.2.2.2 Results:

Figure 68 demonstrates the application of the finite volume model to the experimental data of the four lump model.

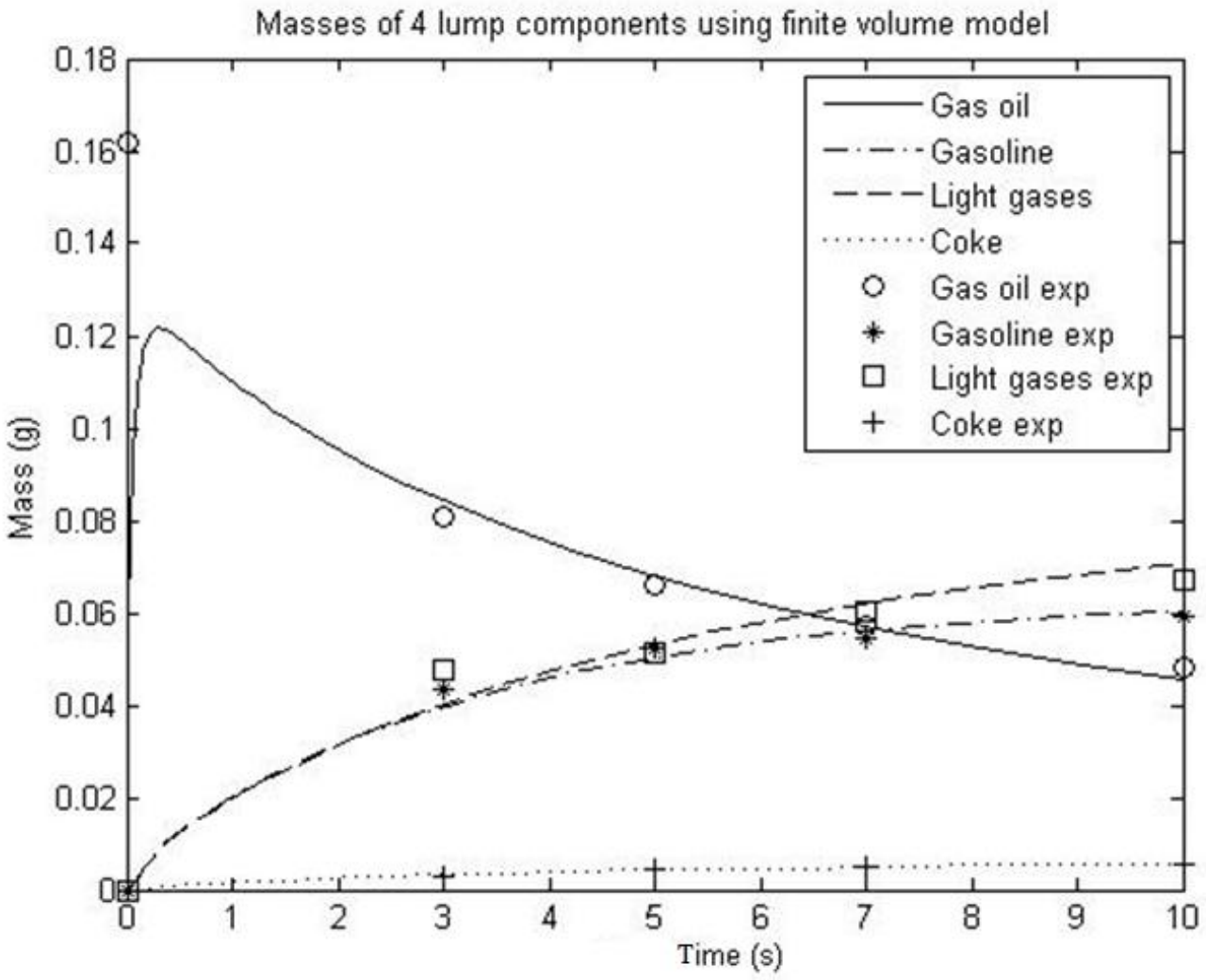

Figure 68: Application of finite volume model to gas oil data

Experimental data obtained from Al-Khattaf [28]

According to Figure 67 the finite volume model fit the gas oil experimental data. This result emphasizes that treating the CREC as an infinite volume system is a poor approximation. Table 12 summarizes the values of Thiele moduli obtained from the optimization. It also provides the optimized value for the ratio of bulk to solids volumes. The small ratio corresponds to a finite volume system.

Table 12: Values of Thiele moduli for finite volume model

φ_1	1.8773
φ_2	2.8389
φ_3	0.1971
φ_4	0.0058
φ_5	0.0020
Λ	5.003

6.2.3 Isothermal reactions, adsorption and diffusion with inactive matrix in finite volume with external fluid film resistance:

Although the finite volume system fit the experimental data, the external fluid film resistance model was used to fit the data to check the existence of such resistance.

6.2.3.1 The model:

Adding the effect of the external fluid film resistance will change the boundary condition of the reactant (Gas oil) at the surface. Equation 6.2.34 will be replaced by the following equation:

$$\left(\frac{\partial \bar{q}_A}{\partial \bar{t}}\right)_{\bar{r}=1} = -\frac{3}{\Lambda}\, Bi_m \left(\frac{\Lambda}{1+\Lambda} - (\bar{q}_A)_{\bar{r}=1}\right) \qquad 6.2.36$$

The new model is solved using orthogonal collocation and optimized for the Thiele modulus values, the ratio of the bulk to solids volume and the mass Biot number.

6.2.3.2 Results:

Figure 69 demonstrates the application of the external fluid film resistance with a finite volume model to the gas oil data.

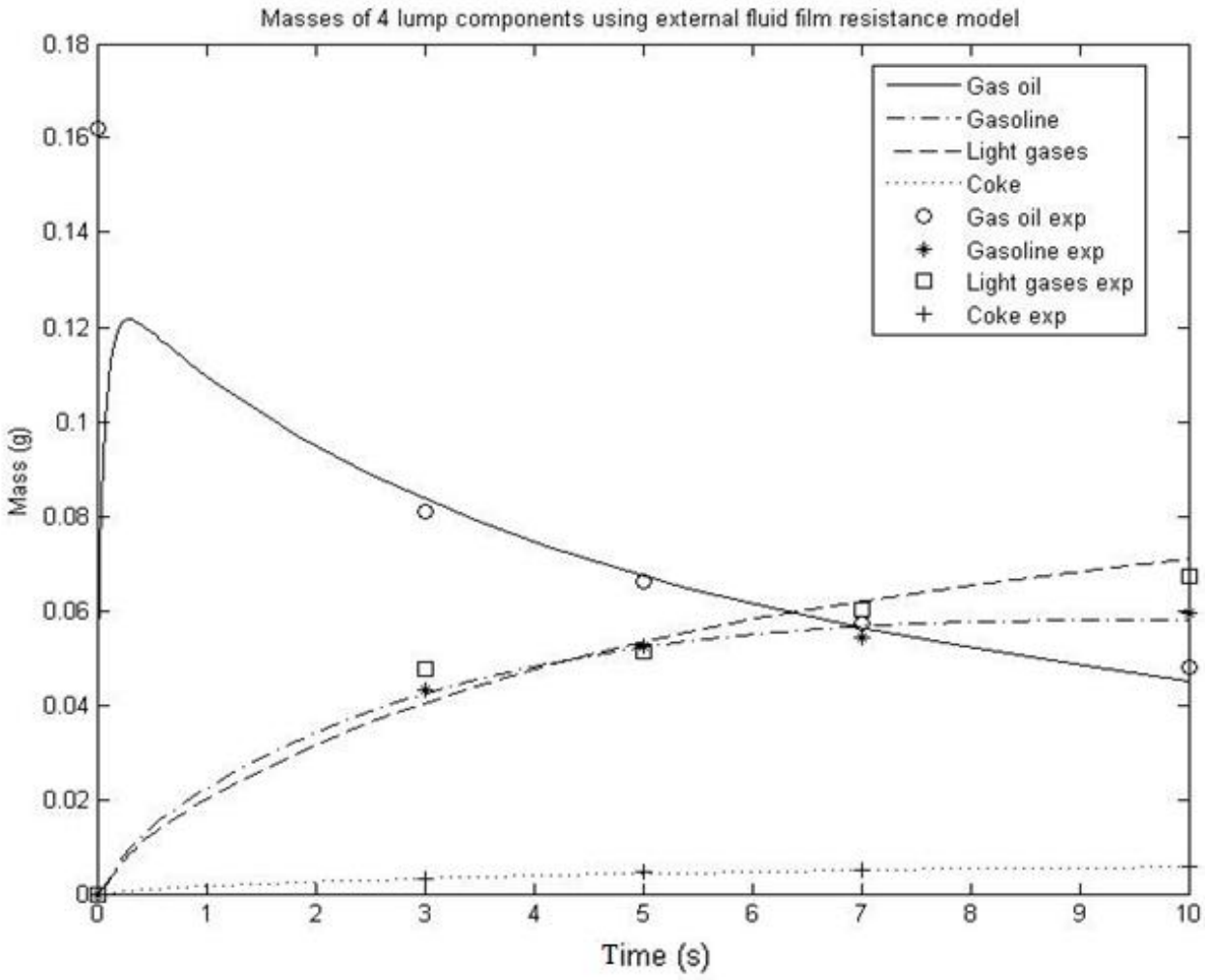

Figure 69: Application of external fluid film resistance model to gas oil data

Experimental data obtained from Al-Khattaf [28]

Comparing Figure 68 with Figure 69, adding the effect of the external fluid film resistance does not affect or enhance the fit by much. This suggests that the external fluid film resistance is not a controlling step for the gas oil reaction under the experiments' conditions. This is further proved by the value of the Biot number obtained from the optimization and shown in Table 13. The values of the Thiele moduli changes slightly. The small differences between the values in Table 12 and Table 13 suggest that the effects of the external fluid film resistance can be neglected.

Table 13: Values of Thiele moduli for external fluid film resistance model

φ_1	1.9940
φ_2	2.8557
φ_3	0.1974
φ_4	0.0013
φ_5	0.0113
Λ	5.003
Bi	10

6.2.4 Isothermal reactions, adsorption and diffusion with active matrix in finite volume:

The effects of the active matrix were studied in this section by fitting the data to a finite volume model. From the previous sections, infinite volume system cannot describe the data and the external fluid film resistance can be neglected so the only finite volume system will be applied with the active matrix. The diffusion and adsorption parameters of the macropore are not available in the literature so some assumption were made to be able to use the active matrix model. First, the macropore adsorption parameters were assumed to be equal for all components. Second, the macropore diffusivities were assumed equal for all components and the micropore diffusivities were also assumed equal for all components. This means that the macropore parameters α and β/α are equal for all components.

6.2.4.1 The model:

Applying Equations 5.2.23 and 5.2.25 to different components results in the following set of equations:

$$\frac{\partial \bar{C}_A}{\partial \bar{t}} = \frac{1}{\bar{R}^2}\frac{\partial}{\partial \bar{R}}\left(\bar{R}^2\frac{\partial \bar{C}_A}{\partial \bar{R}}\right) - \beta\left(\frac{\partial \bar{q}_A}{\partial \bar{r}}\right)_{\bar{r}=1} \tag{6.2.37}$$

$$\frac{\partial q_A}{\partial t} = \frac{\alpha}{\bar{r}^2}\frac{\partial}{\partial \bar{r}}\left(\bar{r}^2\frac{\partial \bar{q}_A}{\partial \bar{r}}\right) + r_A \tag{6.2.38}$$

$$\bar{m}_A = \frac{\bar{C}_A + \frac{1}{3}\frac{\beta}{\alpha}\,\bar{q}_A}{1 + \frac{1}{3}\frac{\beta}{\alpha}} \tag{6.2.39}$$

$$\frac{\partial \bar{C}_B}{\partial \bar{t}} = \frac{1}{\bar{R}^2}\frac{\partial}{\partial \bar{R}}\left(\bar{R}^2\frac{\partial \bar{C}_B}{\partial \bar{R}}\right) - \beta\left(\frac{\partial \bar{q}_B}{\partial \bar{r}}\right)_{\bar{r}=1} \tag{6.2.40}$$

$$\frac{\partial q_B}{\partial t} = \frac{\alpha}{\bar{r}^2}\frac{\partial}{\partial \bar{r}}\left(\bar{r}^2\frac{\partial \bar{q}_B}{\partial \bar{r}}\right) + r_B \tag{6.2.41}$$

$$\bar{m}_B = \frac{\bar{C}_B + \frac{1}{3}\frac{\beta}{\alpha}\,\bar{q}_B}{1 + \frac{1}{3}\frac{\beta}{\alpha}} \tag{6.2.42}$$

$$\frac{\partial \bar{C}_C}{\partial \bar{t}} = \frac{1}{\bar{R}^2}\frac{\partial}{\partial \bar{R}}\left(\bar{R}^2\frac{\partial \bar{C}_C}{\partial \bar{R}}\right) - \beta\left(\frac{\partial \bar{q}_C}{\partial \bar{r}}\right)_{\bar{r}=1} \tag{6.2.43}$$

$$\frac{\partial q_C}{\partial t} = \frac{\alpha}{\bar{r}^2}\frac{\partial}{\partial \bar{r}}\left(\bar{r}^2\frac{\partial \bar{q}_C}{\partial \bar{r}}\right) + r_C \tag{6.2.44}$$

$$\bar{m}_C = \frac{\bar{C}_C + \frac{1}{3}\frac{\beta}{\alpha}\,\bar{q}_C}{1 + \frac{1}{3}\frac{\beta}{\alpha}} \tag{6.2.45}$$

$$\frac{\partial \bar{C}_D}{\partial \bar{t}} = \frac{1}{\bar{R}^2}\frac{\partial}{\partial \bar{R}}\left(\bar{R}^2\frac{\partial \bar{C}_D}{\partial \bar{R}}\right) - \beta\left(\frac{\partial \bar{q}_D}{\partial \bar{r}}\right)_{\bar{r}=1} \tag{6.2.46}$$

$$\frac{\partial q_D}{\partial t} = \frac{\alpha}{\bar{r}^2}\frac{\partial}{\partial \bar{r}}\left(\bar{r}^2\frac{\partial \bar{q}_D}{\partial \bar{r}}\right) + r_D \tag{6.2.47}$$

$$\bar{m}_D = \frac{\bar{C}_D + \frac{1}{3}\frac{\beta}{\alpha}\,\bar{q}_D}{1 + \frac{1}{3}\frac{\beta}{\alpha}} \tag{6.2.48}$$

where

$$r_A = \varphi_1^2\,\bar{m}_A^2 \tag{6.2.49}$$

$$r_B = \varphi_2^2\,\bar{m}_A^2 - \varphi_3^2\,\bar{m}_B \tag{6.2.50}$$

$$r_C = \varphi_4^2\,\bar{m}_A^2 + \varphi_5^2\,\bar{m}_B \tag{6.2.51}$$

$$r_D = \varphi_6^2\,\bar{m}_A^2 + \varphi_7^2\,\bar{m}_B \tag{6.2.52}$$

The Thiele moduli are defined as in Equations 6.2.18 to 6.2.24 but in terms of the pore diffusivity and radius instead of the crystal diffusivity and radius.

The relevant initial and boundary conditions are:

$$\bar{C}_A\,(0,\bar{R}) = \bar{C}_B\,(0,\bar{R}) = \bar{C}_C\,(0,\bar{R}) = \bar{C}_D\,(0,\bar{R}) = 0 \tag{6.2.53}$$

$$\left(\frac{\partial \bar{C}_A}{\partial \bar{R}}\right)_{\bar{R}=0} = \left(\frac{\partial \bar{C}_B}{\partial \bar{R}}\right)_{\bar{R}=0} = \left(\frac{\partial \bar{C}_C}{\partial \bar{R}}\right)_{\bar{R}=0} = \left(\frac{\partial \bar{C}_D}{\partial \bar{R}}\right)_{\bar{R}=0} = 0 \tag{6.2.54}$$

$$\left(\frac{\partial \bar{C}_A}{\partial \bar{t}}\right)_{\bar{R}=1} = \frac{-3}{\Lambda}\left(\frac{\partial \bar{C}_A}{\partial \bar{R}}\right)_{\bar{R}=1} \tag{6.2.55}$$

$$\left(\frac{\partial \bar{C}_B}{\partial \bar{t}}\right)_{\bar{R}=1} = \frac{-3}{\Lambda}\left(\frac{\partial \bar{C}_B}{\partial \bar{R}}\right)_{\bar{R}=1} \tag{6.2.56}$$

$$\left(\frac{\partial \bar{C}_C}{\partial \bar{t}}\right)_{\bar{R}=1} = \frac{-3}{\Lambda}\left(\frac{\partial \bar{C}_C}{\partial \bar{R}}\right)_{\bar{R}=1} \tag{6.2.57}$$

$$\left(\frac{\partial \bar{C}_D}{\partial \bar{t}}\right)_{\bar{R}=1} = \frac{-3}{\Lambda}\left(\frac{\partial \bar{C}_D}{\partial \bar{R}}\right)_{\bar{R}=1} \tag{6.2.58}$$

$$\bar{q}_A\,(0,\bar{r}) = \bar{q}_B\,(0,\bar{r}) = \bar{q}_C\,(0,\bar{r}) = \bar{q}_D\,(0,\bar{r}) = 0 \qquad 6.2.59$$

$$\left(\frac{\partial \bar{q}_A}{\partial \bar{r}}\right)_{\bar{r}=0} = \left(\frac{\partial \bar{q}_B}{\partial \bar{r}}\right)_{\bar{r}=0} = \left(\frac{\partial \bar{q}_C}{\partial \bar{r}}\right)_{\bar{r}=0} = \left(\frac{\partial \bar{q}_D}{\partial \bar{r}}\right)_{\bar{r}=0} = 0 \qquad 6.2.60$$

$$\bar{q}_A\,(\bar{t},1) = \bar{C}_A(\bar{t},\bar{R}) \qquad 6.2.61$$

$$\bar{q}_B\,(\bar{t},1) = \bar{C}_B(\bar{t},\bar{R}) \qquad 6.2.62$$

$$\bar{q}_C\,(\bar{t},1) = \bar{C}_C(\bar{t},\bar{R}) \qquad 6.2.63$$

$$\bar{q}_D\,(\bar{t},1) = \bar{C}_D(\bar{t},\bar{R}) \qquad 6.2.64$$

where Λ is the ratio of the bulk to macro solids volumes.

This model was solved using orthogonal collocation and optimized for the Thiele moduli, the ratio of volumes and the macropore parameters (α and β/α).

6.2.4.2 Results:

Figure 70 demonstrates the application of the active matrix model with finite volume system to the gas oil data.

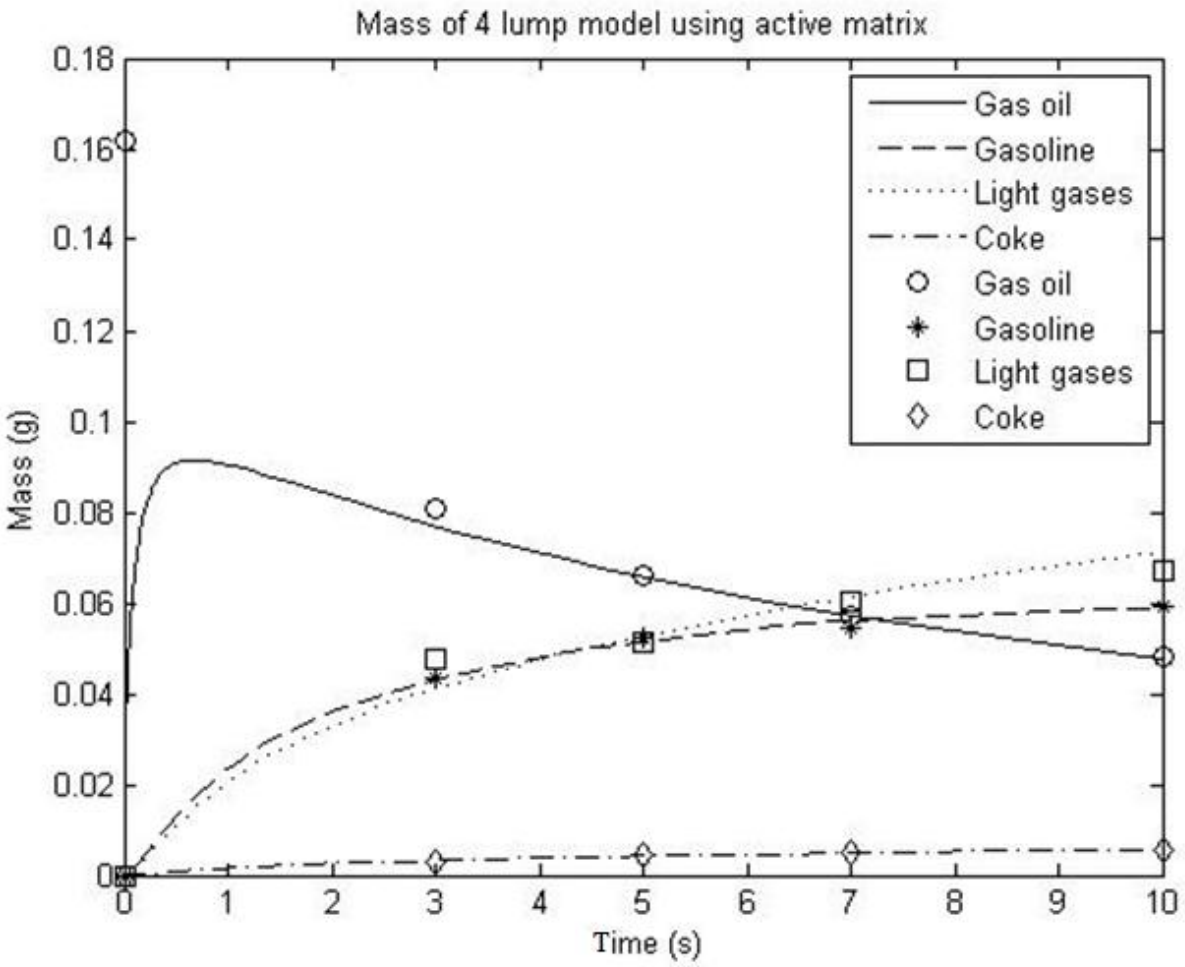

Figure 70: Application of the active matrix model with finite volume system

Experimental data obtained from Al-Khattaf [28]

From Figure 70 adding the effect of the active matrix does not enhance the fit significantly. Since assumptions were made regarding the macropore parameters, it cannot be determined whether the matrix is active or inactive. The optimization values are summarized in Table 14. The values of the Thiele modulus are close to those in Table 12. The value of α obtained shows that both macropore and micropore diffusion are important. Moreover, the value of β/α obtained shows that the rates of adsorption in the macropore and micropore are comparable. Therefore, the active matrix model should be considered for gas oil reactions in FCC catalyst.

Table 14: Values of Thiele moduli for active matrix model

φ_1	2.5624
φ_2	3.5756
φ_3	0.2433
φ_4	0.1807
φ_5	0.0276
Λ	5.003
α	0.1334
β/α	2.4343

6.2.5 Discussion:

Four models were used to describe the gas oil data in Figure 6. Table 15 summarizes the sum of squares of errors of the models. From the table the best model to describe the data is the finite volume with external fluid film resistance, although finite volume model and active matrix model are comparable. If more information about the diffusion and adsorption parameters in the macropore were available, the active matrix model may describe the data better.

Table 15: Sum of squares of error for the gas oil data

Model	Sum of squares of errors
Inactive matrix with infinite volume	1.2025
Inactive matrix with finite volume	1.0038
Inactive matrix with external fluid film resistance in finite volume	1.0002
Active matrix with finite volume	1.007

In this chapter the Thiele moduli were found. If the diffusivities of the different components were available, the kinetic parameters would be easily calculated from the definitions of the Thiele moduli. Moreover, the diffusivity could be used to calculate the film mass transfer coefficient from the mass Biot number. If the diffusivities are assumed to be equal to that of gas oil at 525℃ which equals 6×10^{-14} m^2/s [28], then the reaction constants are calculated and compared to the values obtained by Al-Khattaf [28] in Table 16. The initial adsorbed concentration (q_0) can be calculated as follows:

$$q_0 = \frac{m_0 K_{gas\ oil\ @\ 525℃}}{Mw_{gas\ oil} V_{reactor}} \tag{6.2.65}$$

$$q_0 = \frac{(0.162\ g)(9 \times 10^{-6})}{\left(330 \frac{g}{mol}\right)(53.94 \times 10^{-6} m^3)} = 8.2 \times 10^{-5} \frac{mol}{m^3} \tag{6.2.66}$$

Table 16: Comparison between the reaction constants

Reaction constant	This thesis	Al-Khattaf [28]
k_1 (m^3/mol.s)	7.36×10^4	2.94×10^2
k_2 (m^3/mol.s)	1.51×10^5	1.49×10^2
k_3 (m^3/mol.s)	7.22×10^2	1.41×10^1
k_4 (s^{-1})	2.54×10^{-6}	5.79
k_5 (s^{-1})	1.92×10^{-4}	2.48×10^1

The differences between the reaction constants obtained in this thesis and the results obtained by Al-Khattaf are due to the different models used and to the assumed diffusivities. If the diffusivity of gasoline was available, k_4 and k_5 can be corrected. If the diffusivity of gasoline is assumed to be 10^{-8} m/s^2, then the new reaction constants are summarized in Table 17 :

Table 17: Comparison between the reaction constants (Corrected diffusivities)

Reaction constant	This thesis	Al-Khattaf [28]
k_1 (m^3/mol.s)	7.36×10^4	2.94×10^2
k_2 (m^3/mol.s)	1.51×10^5	1.49×10^2
k_3 (m^3/mol.s)	7.22×10^2	1.41×10^1
k_4 (s^{-1})	0.423	5.79
k_5 (s^{-1})	3.20×10^1	2.48×10^1

From Table 17, if the diffusivity of gasoline is corrected, the values of the reaction constants are closer to the values obtained by Al-Khattaf [28].

In deriving Equations 6.2.14-6.2.17, the diffusivities of all components were assumed to be the same which is not a valid assumption since the components differ in their critical diameter. If the diffusivity of each component was known, the equations can be optimized for the reaction constants directly after applying the necessary changes to the equations. Optimizing for the reaction constants directly would result in more accurate results.

6.3 Modeling 1,3,5-TIPB:

This section applies different models to the 1,3,5-TIPB data. Two sets of data were considered, the data in Figure 7 at 400℃ and in Figure 8 at 550℃. From the results of gas oil, the data of 1,3,5-TIPB were fitted to the finite volume model only as infinite volume will not represent the system and external fluid film resistance can be neglected. The adsorption parameters for the products are not available in the literature; therefore, it was assumed that the adsorption constants for the products equals the adsorption constant for 1,3,5-TIPB obtained from [2].

6.3.1 Finite volume model with reaction set 1

The 1,3,5-TIPB experimental data were fitted to the finite volume model because the CREC is a constant volume reactor.

6.3.1.1 The model

The main reactions of 1,3,5-TIPB according to [2] are:

$$A \overset{k_1}{\rightarrow} B + E$$

$$B \overset{k_2}{\rightarrow} C + E$$

$$C \overset{k_3}{\rightarrow} D + E$$

Let A, B, C, D and E correspond to 1,3,5-TIPB, 1,3-DIPB, cumene, benzene and propylene respectively. The reaction rates can be written as:

$$r_A = -\phi_{int} k_1 q_A \quad 6.3.1$$

$$r_B = \phi_{int}(k_1 q_A - k_2 q_B) \quad 6.3.2$$

$$r_C = \phi_{int}(k_2 q_B - k_3 q_C) \quad 6.3.3$$

$$r_D = \phi_{int}(k_3 q_C) \quad 6.3.4$$

$$r_E = \phi_{int}(k_1 q_A + k_2 q_B + k_3 q_C) \quad 6.3.5$$

Applying Equation 3.2.4 to each component gives the following set of diffusion-reaction equations:

$$\frac{\partial q_A}{\partial t} = \frac{D_{c_A}}{r^2}\frac{\partial}{\partial r}\left(r^2\frac{\partial q_A}{\partial r}\right) + r_A \quad 6.3.6$$

$$\frac{\partial q_B}{\partial t} = \frac{D_{c_B}}{r^2}\frac{\partial}{\partial r}\left(r^2\frac{\partial q_B}{\partial r}\right) + r_B \quad 6.3.7$$

$$\frac{\partial q_C}{\partial t} = \frac{D_{c_C}}{r^2}\frac{\partial}{\partial r}\left(r^2\frac{\partial q_C}{\partial r}\right) + r_C \quad 6.3.8$$

$$\frac{\partial q_D}{\partial t} = \frac{D_{c_D}}{r^2}\frac{\partial}{\partial r}\left(r^2\frac{\partial q_D}{\partial r}\right) + r_D \quad 6.3.9$$

$$\frac{\partial q_E}{\partial t} = \frac{D_{c_E}}{r^2}\frac{\partial}{\partial r}\left(r^2\frac{\partial q_E}{\partial r}\right) + r_E \quad 6.3.10$$

The relevant initial and boundary conditions for a finite volume system are:

$$\left(\frac{\partial q_A}{\partial t}\right)_{r=0} = \left(\frac{\partial q_B}{\partial t}\right)_{r=0} = \left(\frac{\partial q_C}{\partial t}\right)_{r=0} = \left(\frac{\partial q_D}{\partial t}\right)_{r=0} = \left(\frac{\partial q_E}{\partial t}\right)_{r=0} = 0 \quad 6.3.11$$

$$q_A(0,r) = q_B(0,r) = q_C(0,r) = q_D(0,r) = q_E(0,r) = 0 \quad 6.3.12$$

$$-4\,\pi\,N\,r_c^2\,D_c\left(\frac{\partial q_A}{\partial r}\right)_{r=rc} = \frac{V}{K_A}\left(\frac{\partial q_A}{\partial t}\right)_{r=r_c} \quad 6.3.13$$

$$-4\,\pi\,N\,r_c^2\,D_c\left(\frac{\partial q_B}{\partial r}\right)_{r=rc} = \frac{V}{K_B}\left(\frac{\partial q_B}{\partial t}\right)_{r=r_c} \quad 6.3.14$$

$$-4\,\pi\,N\,r_c^2\,D_c\left(\frac{\partial q_C}{\partial r}\right)_{r=rc} = \frac{V}{K_C}\left(\frac{\partial q_C}{\partial t}\right)_{r=r_c} \quad 6.3.15$$

$$-4\,\pi\,N\,r_c^2\,D_c\left(\frac{\partial q_D}{\partial r}\right)_{r=rc} = \frac{V}{K_D}\left(\frac{\partial q_D}{\partial t}\right)_{r=r_c} \quad 6.3.16$$

$$-4\,\pi\,N\,r_c^2\,D_c\left(\frac{\partial q_E}{\partial r}\right)_{r=rc} = \frac{V}{K_E}\left(\frac{\partial q_E}{\partial t}\right)_{r=r_c} \quad 6.3.17$$

Equation 6.3.6 to 6.3.10 needs to be normalized.

$$\frac{\partial \bar{q}_A}{\partial \bar{t}} = \frac{1}{\bar{r}^2}\frac{\partial}{\partial \bar{r}}\left(\bar{r}^2\frac{\partial \bar{q}_A}{\partial \bar{r}}\right) - \varphi_1^2\,\bar{q}_A \quad 6.3.18$$

$$\frac{\partial \bar{q}_B}{\partial \bar{t}} = \frac{1}{\bar{r}^2}\frac{\partial}{\partial \bar{r}}\left(\bar{r}^2\frac{\partial \bar{q}_B}{\partial \bar{r}}\right) + \varphi_1^2\,\bar{q}_A - \varphi_2^2\,\bar{q}_B \quad 6.3.19$$

$$\frac{\partial \bar{q}_C}{\partial \bar{t}} = \frac{1}{\bar{r}^2}\frac{\partial}{\partial \bar{r}}\left(\bar{r}^2\frac{\partial \bar{q}_C}{\partial \bar{r}}\right) + \varphi_2^2\,\bar{q}_B - \varphi_3^2\,\bar{q}_C \quad 6.3.20$$

$$\frac{\partial \bar{q}_D}{\partial \bar{t}} = \frac{1}{\bar{r}^2}\frac{\partial}{\partial \bar{r}}\left(\bar{r}^2\frac{\partial \bar{q}_D}{\partial \bar{r}}\right) + \varphi_3^2\,\bar{q}_C \quad 6.3.21$$

$$\frac{\partial \bar{q}_E}{\partial \bar{t}} = \frac{1}{\bar{r}^2}\frac{\partial}{\partial \bar{r}}\left(\bar{r}^2\frac{\partial \bar{q}_E}{\partial \bar{r}}\right) + \varphi_1^2\,\bar{q}_A + \varphi_2^2\,\bar{q}_B + \varphi_3^2\,\bar{q}_C \quad 6.3.22$$

where,

$$\varphi_1^2 = \frac{k_1 {r_c}^2}{D_c} \quad 6.3.23$$

$$\varphi_2^2 = \frac{k_2 {r_c}^2}{D_c} \quad 6.3.24$$

$$\varphi_3^2 = \frac{k_3 {r_c}^2}{D_c} \quad 6.3.25$$

where the diffusivities of all components were assumed to be equal to the diffusivity of 1,3,5-TIPB given in Table 9 at 450℃:

$$D_{TIPB} = 2 \times 10^{-13} \exp\left(-20\left(\frac{1}{T} - \frac{1}{723}\right)\right)$$

where T is in K and D_{TIPB} is in m^2/s.

The deactivation function is assumed to be negligible because the amount of coke formed is small.

The normalized initial and boundary conditions are:

$$\left(\frac{\partial \bar{q}_A}{\partial \bar{t}}\right)_{\bar{r}=0} = \left(\frac{\partial \bar{q}_B}{\partial \bar{t}}\right)_{\bar{r}=0} = \left(\frac{\partial \bar{q}_C}{\partial \bar{t}}\right)_{\bar{r}=0} = \left(\frac{\partial \bar{q}_D}{\partial \bar{t}}\right)_{\bar{r}=0} = \left(\frac{\partial \bar{q}_E}{\partial \bar{t}}\right)_{\bar{r}=0} = 0 \quad 6.3.26$$

$$\bar{q}_A(0,\bar{r}) = \bar{q}_B(0,\bar{r}) = \bar{q}_C(0,\bar{r}) = \bar{q}_D(0,\bar{r}) = \bar{q}_E(0,\bar{r}) = 0 \quad 6.3.27$$

$$\left(\frac{\partial \bar{q}_A}{\partial \bar{t}}\right)_{\bar{r}=1} = -\frac{3}{\Lambda}\left(\frac{\partial \bar{q}_A}{\partial \bar{r}}\right)_{\bar{r}=1} \quad 6.3.28$$

$$\left(\frac{\partial \bar{q}_B}{\partial \bar{t}}\right)_{\bar{r}=1} = -\frac{3}{\Lambda}\left(\frac{\partial \bar{q}_B}{\partial \bar{r}}\right)_{\bar{r}=1} \quad 6.3.29$$

$$\left(\frac{\partial \bar{q}_C}{\partial \bar{t}}\right)_{\bar{r}=1} = -\frac{3}{\Lambda}\left(\frac{\partial \bar{q}_C}{\partial \bar{r}}\right)_{\bar{r}=1} \quad 6.3.30$$

$$\left(\frac{\partial \bar{q}_D}{\partial \bar{t}}\right)_{\bar{r}=1} = -\frac{3}{\Lambda}\left(\frac{\partial \bar{q}_D}{\partial \bar{r}}\right)_{\bar{r}=1} \quad 6.3.31$$

$$\left(\frac{\partial \bar{q}_E}{\partial \bar{t}}\right)_{\bar{r}=1} = -\frac{3}{\Lambda}\left(\frac{\partial \bar{q}_E}{\partial \bar{r}}\right)_{\bar{r}=1} \quad 6.3.32$$

where Λ is the ratio of the bulk to micropore volumes. Since the diffusivities and adsorption constants were assumed to be the same for all components, Λ is the same for all components.

The preceding set of equations was solved using orthogonal collocation and optimized for the values of the Thiele moduli and the volumes ratio that minimize the sum of squares of errors for the data in Figure 7 at 400℃ and Figure 8 at 550℃.

6.3.1.2 Results at 400℃

Figure 71 demonstrates the application of the finite volume model for the experimental data of 1,3,5-TIPB at 400℃ .

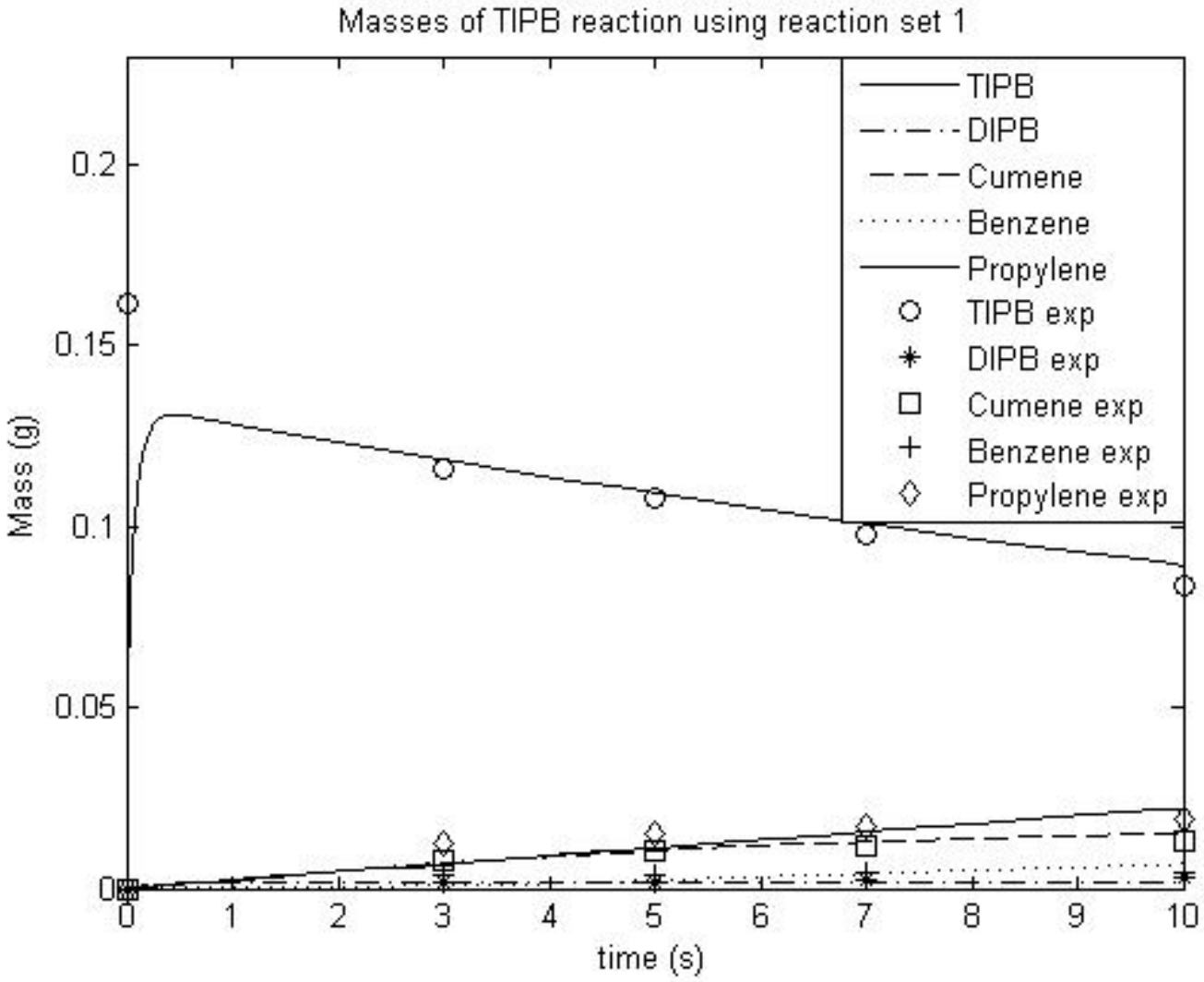

Figure 71: Application of finite volume model to 1,3,5-TIPB at 400℃

Experimental data obtained from Al-Khattaf [28]

Figure 72 shows the same figure but for a different scale to get a better view of the fitting.

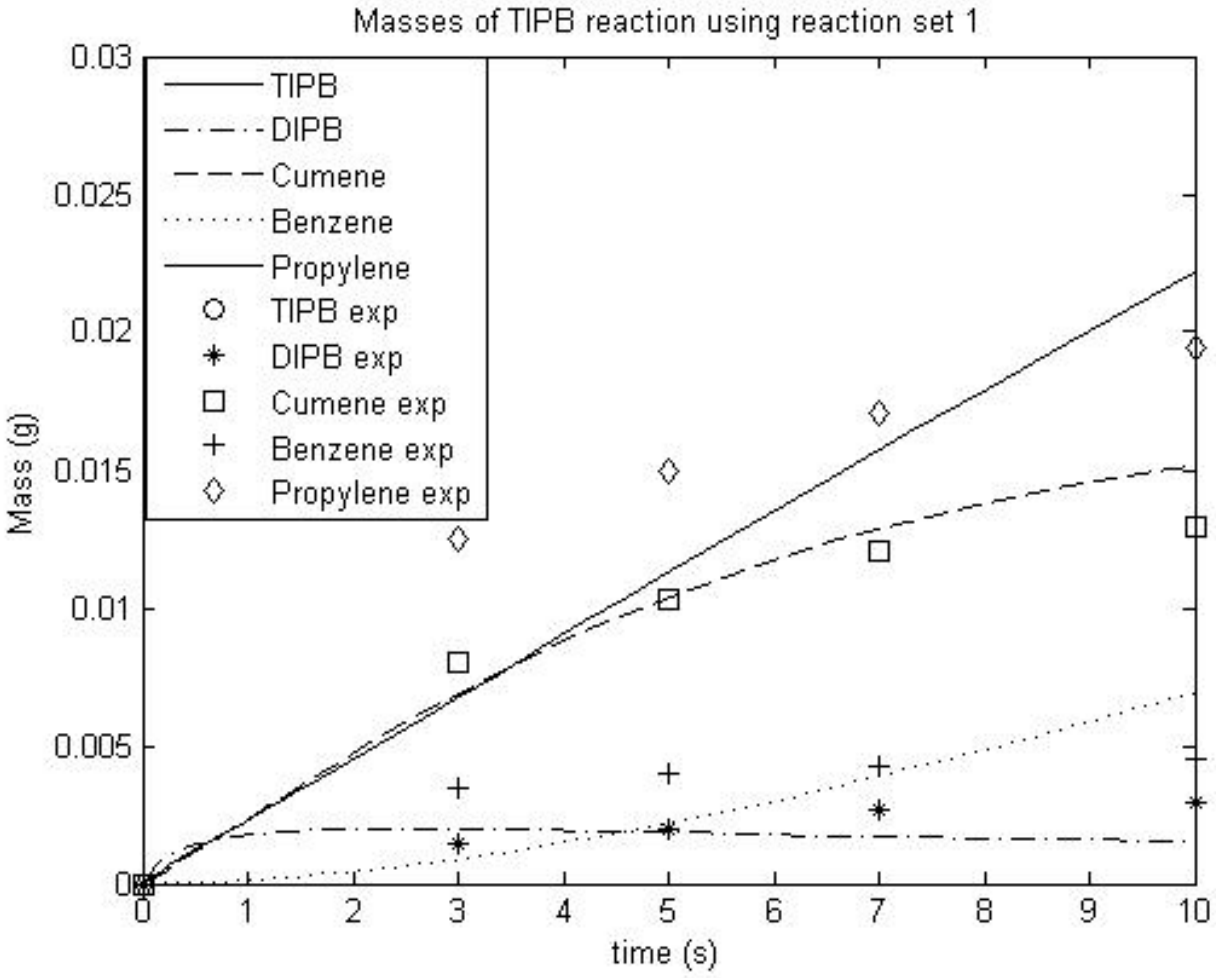

Figure 72: Application of finite volume model to 1,3,5-TIPB at 400℃ (Smaller scale)

From Figure 71 and Figure 72, the finite volume model provides a reasonable fit for the data. The model does not fit benzene and 1,3-DIPB as good as it fits the other components which also affects the fit to propylene. Table 18 summarizes the Thiele moduli obtained from optimization.

Table 18: Values of Thiele moduli for finite volume model at 400℃

φ_1	0.4960
φ_2	3.4289
φ_3	0.8082
Λ	5.0215

The poor fit to benzene and 1,3-DIPB can be due to the assumed diffusivities and adsorption constants. It can also be due to the existence of other resistances. Another cause for the poor fit may be the reactions considered.

6.3.1.3 Results at 550 ℃

Figure 73 demonstrates the application of finite volume model for the experimental data of 1,3,5-TIPB at 550℃ .

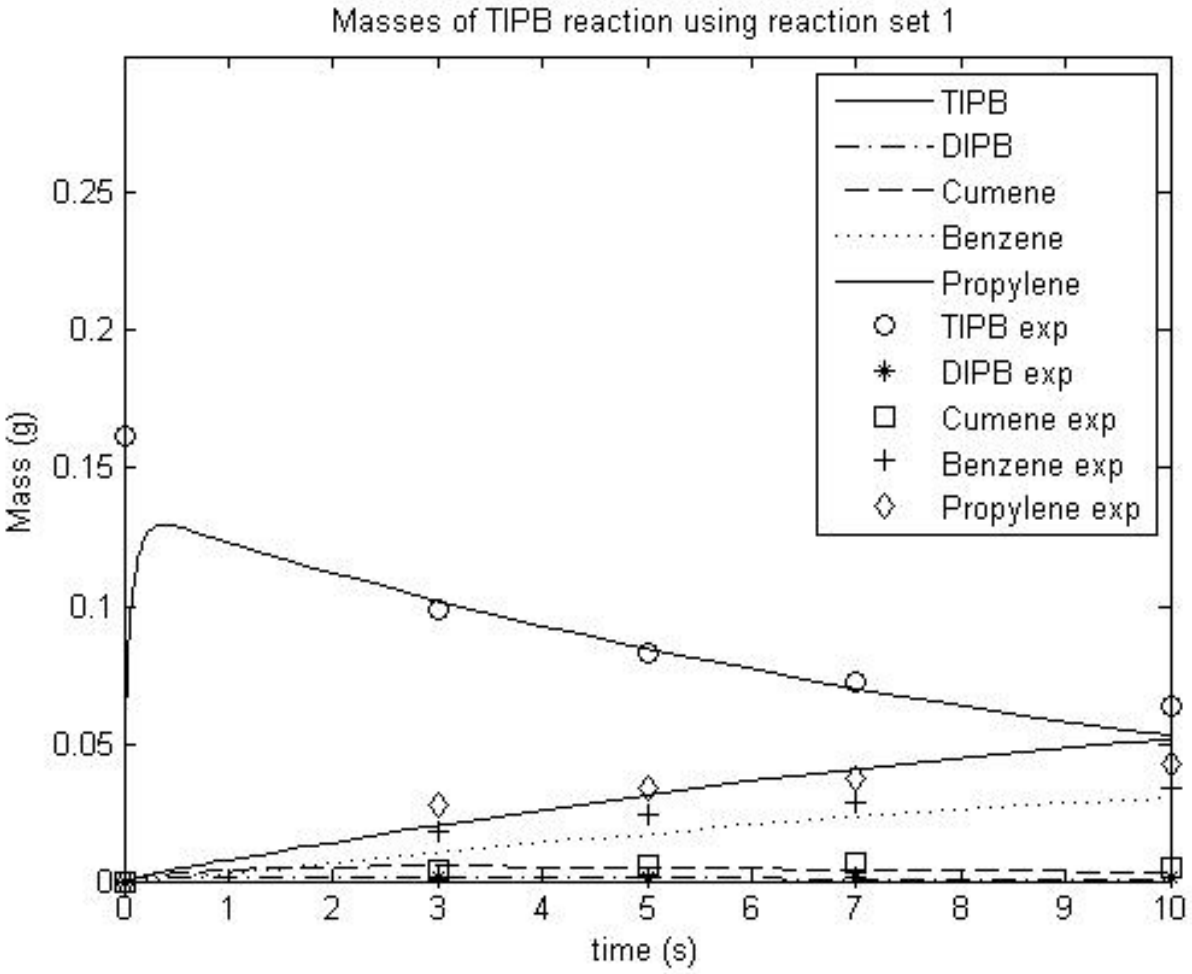

Figure 73: Application of finite volume model to 1,3,5-TIPB at 550℃

Experimental data obtained from Al-Khattaf [28]

Figure 74 illustrate the same Figure but for a smaller scale.

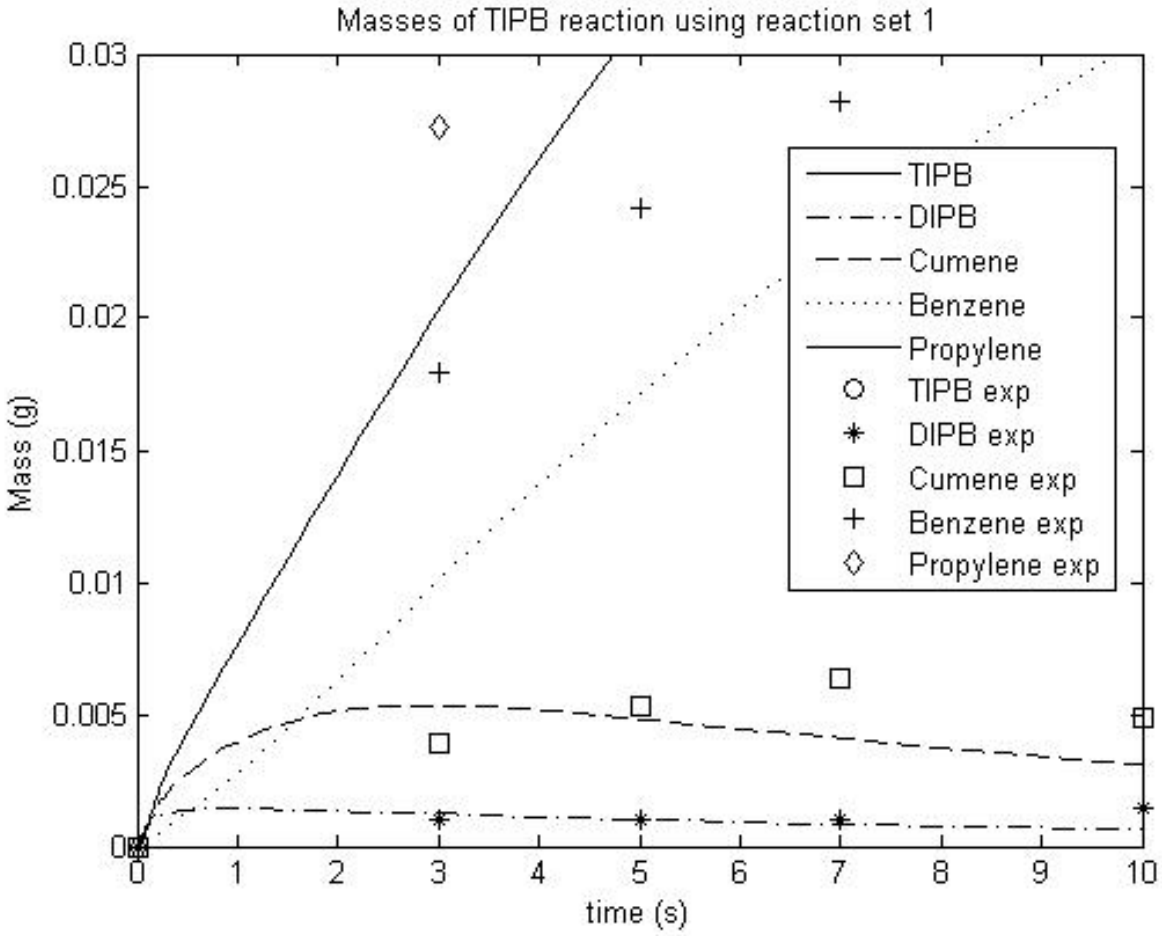

Figure 74: Application of reaction set 1 model to 1,3,5-TIPB at 550℃ (Smaller scale)

From Figure 73 and Figure 74, the model gives a poor fit for cumene and benzene and as a result to propylene. The Thiele moduli obtained are summarized in Table 19.

Table 19: Values of Thiele moduli for finite volume model at 550℃

φ_1	0.8230
φ_2	6.7451
φ_3	2.7540
Λ	5.9993

Again, the poor fit can be due to the assumed values, reactions or resistances.

6.3.2 Finite volume model with reaction set 2

In order to achieve a better fit, different reaction sets were considered. This section assumes that 1,3,5-TIPB reacts to form cumene in addition to 1,3-DIPB.

$$A \overset{k_1}{\rightarrow} B + E$$

$$A \overset{k_2}{\rightarrow} C + 2\,E$$

$$B \overset{k_3}{\rightarrow} C + E$$

$$C \overset{k_4}{\rightarrow} D + E$$

where A, B, C, D and E correspond to 1,3,5-TIPB, 1,3-DIPB, cumene, benzene and propylene respectively.

6.3.2.1 The model

The reaction rates can be written as:

$$r_A = -\phi_{int}(k_1 + k_2)q_A \qquad 6.3.33$$

$$r_B = \phi_{int}(k_1 q_A - k_3 q_B) \qquad 6.3.34$$

$$r_C = \phi_{int}(k_2 q_A + k_3 q_B - k_4 q_C) \qquad 6.3.35$$

$$r_D = \phi_{int}(k_4 q_C) \qquad 6.3.36$$

$$r_E = \phi_{int}(k_1 q_A + \frac{1}{2} k_2 q_A + k_3 q_B + k_4 q_C) \quad 6.3.37$$

The normalized equations that describe this system are:

$$\frac{\partial \bar{q}_A}{\partial \bar{t}} = \frac{1}{\bar{r}^2}\frac{\partial}{\partial \bar{r}}\left(\bar{r}^2 \frac{\partial \bar{q}_A}{\partial \bar{r}}\right) - (\varphi_1^2 + \varphi_2^2)\, \bar{q}_A \quad 6.3.38$$

$$\frac{\partial \bar{q}_B}{\partial \bar{t}} = \frac{1}{\bar{r}^2}\frac{\partial}{\partial \bar{r}}\left(\bar{r}^2 \frac{\partial \bar{q}_B}{\partial \bar{r}}\right) + \varphi_1^2\, \bar{q}_A - \varphi_3^2\, \bar{q}_B \quad 6.3.39$$

$$\frac{\partial \bar{q}_C}{\partial \bar{t}} = \frac{1}{\bar{r}^2}\frac{\partial}{\partial \bar{r}}\left(\bar{r}^2 \frac{\partial \bar{q}_C}{\partial \bar{r}}\right) + \varphi_2^2\, \bar{q}_A + \varphi_3^2\, \bar{q}_B - \varphi_4^2\, \bar{q}_C \quad 6.3.40$$

$$\frac{\partial \bar{q}_D}{\partial \bar{t}} = \frac{1}{\bar{r}^2}\frac{\partial}{\partial \bar{r}}\left(\bar{r}^2 \frac{\partial \bar{q}_D}{\partial \bar{r}}\right) + \varphi_4^2\, \bar{q}_C \quad 6.3.41$$

$$\frac{\partial \bar{q}_E}{\partial \bar{t}} = \frac{1}{\bar{r}^2}\frac{\partial}{\partial \bar{r}}\left(\bar{r}^2 \frac{\partial \bar{q}_E}{\partial \bar{r}}\right) + \varphi_1^2\, \bar{q}_A + \frac{1}{2}\varphi_2^2\, \bar{q}_A + \varphi_3^2\, \bar{q}_B + \varphi_4^2\, \bar{q}_C \quad 6.3.42$$

where

$$\varphi_1^2 = \frac{k_1 {r_c}^2}{D_c} \quad 6.3.43$$

$$\varphi_2^2 = \frac{k_2 {r_c}^2}{D_c} \quad 6.3.44$$

$$\varphi_3^2 = \frac{k_3 {r_c}^2}{D_c} \quad 6.3.45$$

$$\varphi_4^2 = \frac{k_4 {r_c}^2}{D_c} \quad 6.3.46$$

These equations were solved for the initial and boundary conditions in Equations 6.3.26-6.3.32 and optimized for the Thiele moduli.

6.3.2.2 Results at 400 ℃

Figure 75 demonstrates the application of reaction set 2 model for the experimental data of 1,3,5-TIPB at 400℃ .

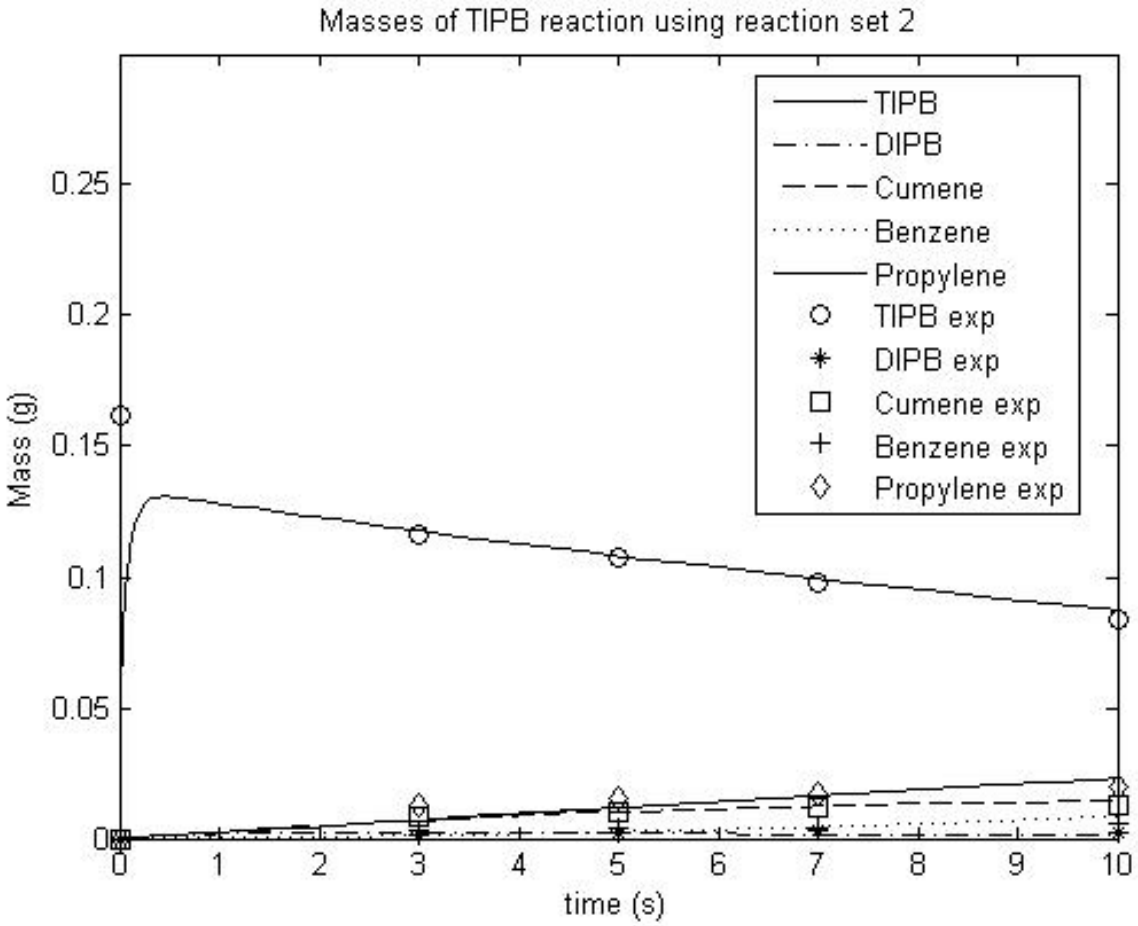

Figure 75: Application of reaction set 2 model to 1,3,5-TIPB at 400℃

Experimental data obtained from Al-Khattaf [28]

Figure 76 illustrate the same figure but for a smaller scale.

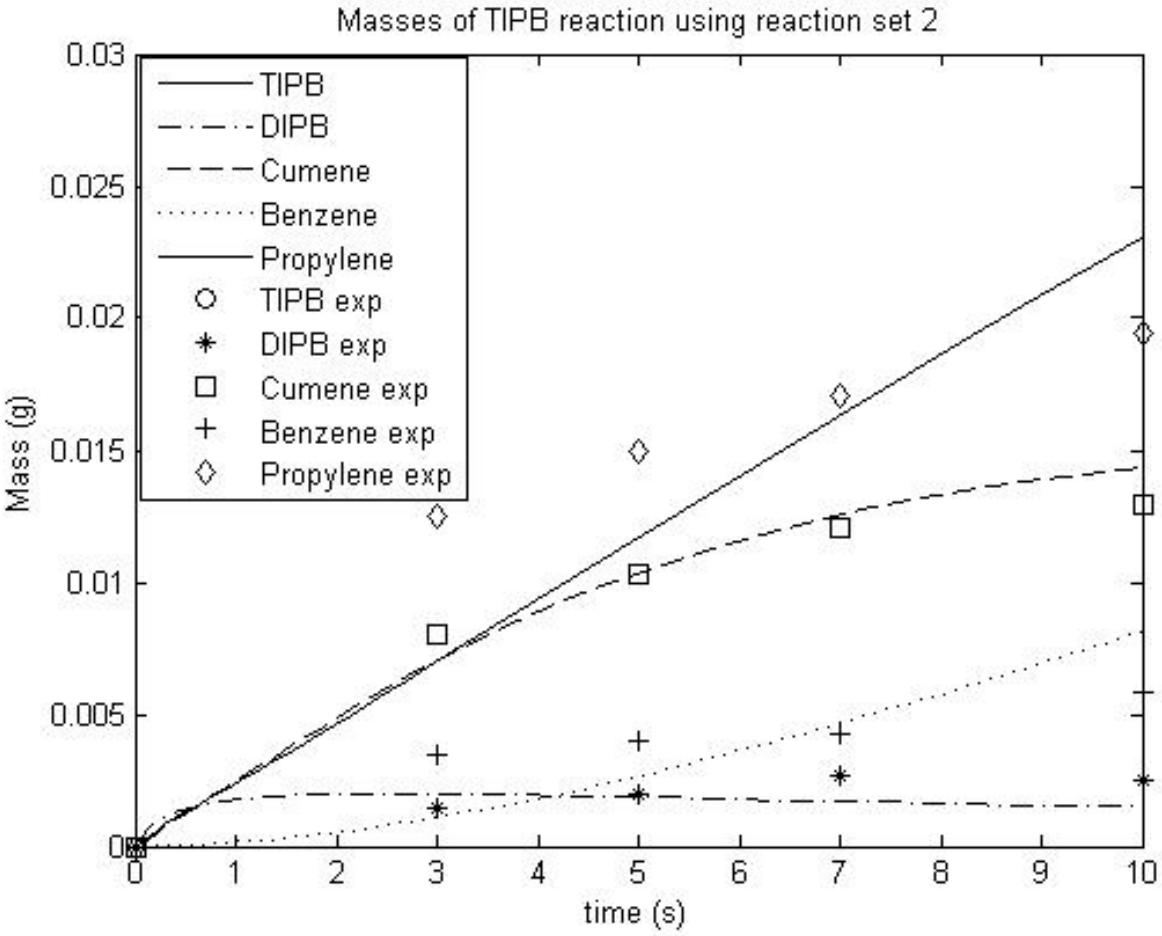

Figure 76: Application of reaction set 2 model to 1,3,5-TIPB at 400℃ (Smaller scale)

From Figure 75 and Figure 76, the fit is slightly better than in Figure 71. The model still cannot fit the experimental data for benzene at 400℃. The Thiele moduli obtained are summarized in

Table 20: Values of Thiele moduli for reaction set 2 model at 400℃

φ_1	0.4986
φ_2	0.1001
φ_3	3.434
φ_4	0.8843
Λ	5.0084

Comparing Table 18 and Table 20, the corresponding Thiele moduli are comparable.

6.3.2.3 Results at 550 ℃

Figure 77 demonstrates the application of reaction set 2 model for the experimental data of 1,3,5-TIPB at 550℃ .

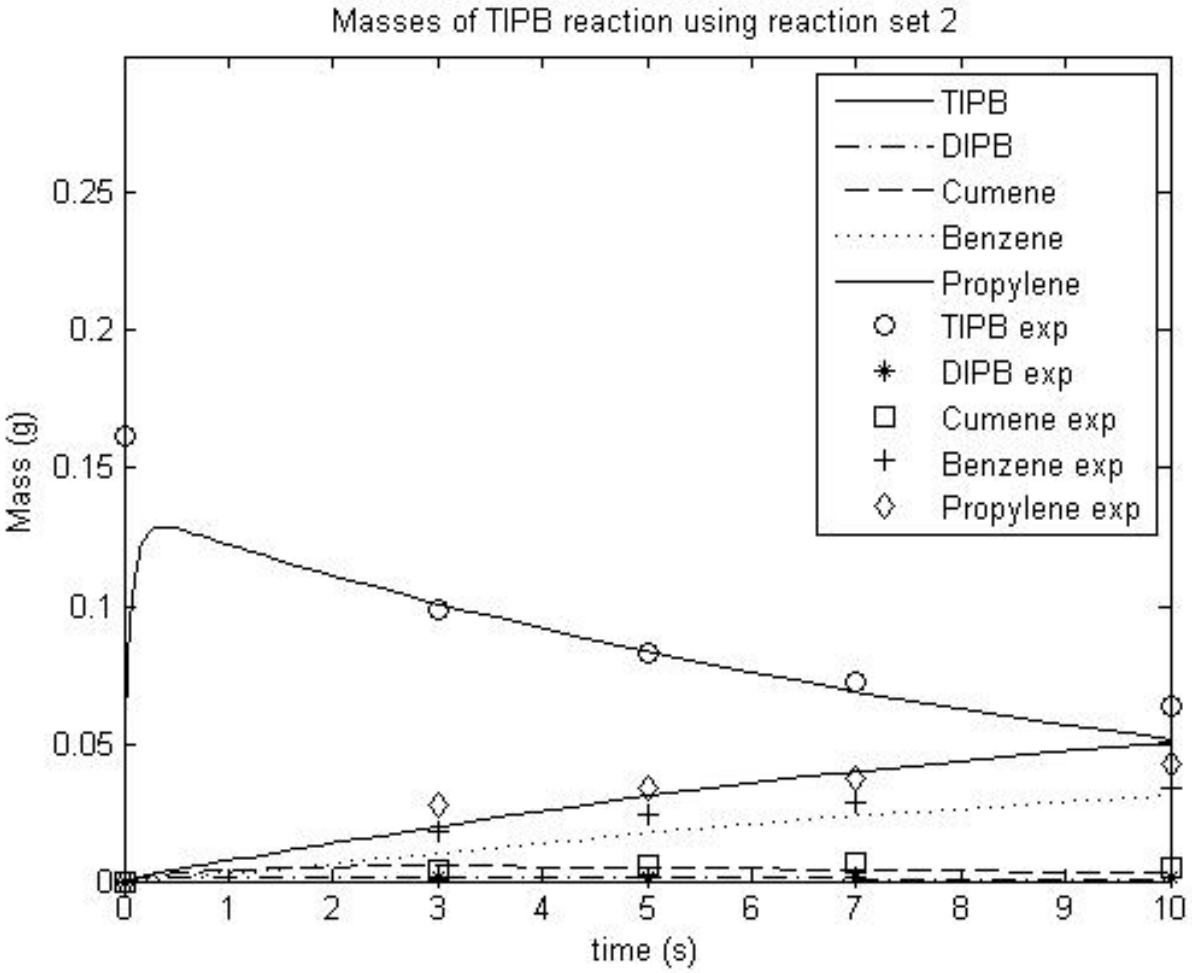

Figure 77: Application of reaction set 2 model to 1,3,5-TIPB at 550℃

Experimental data obtained from Al-Khattaf [28]

Figure 78 illustrate the same figure but for a smaller scale.

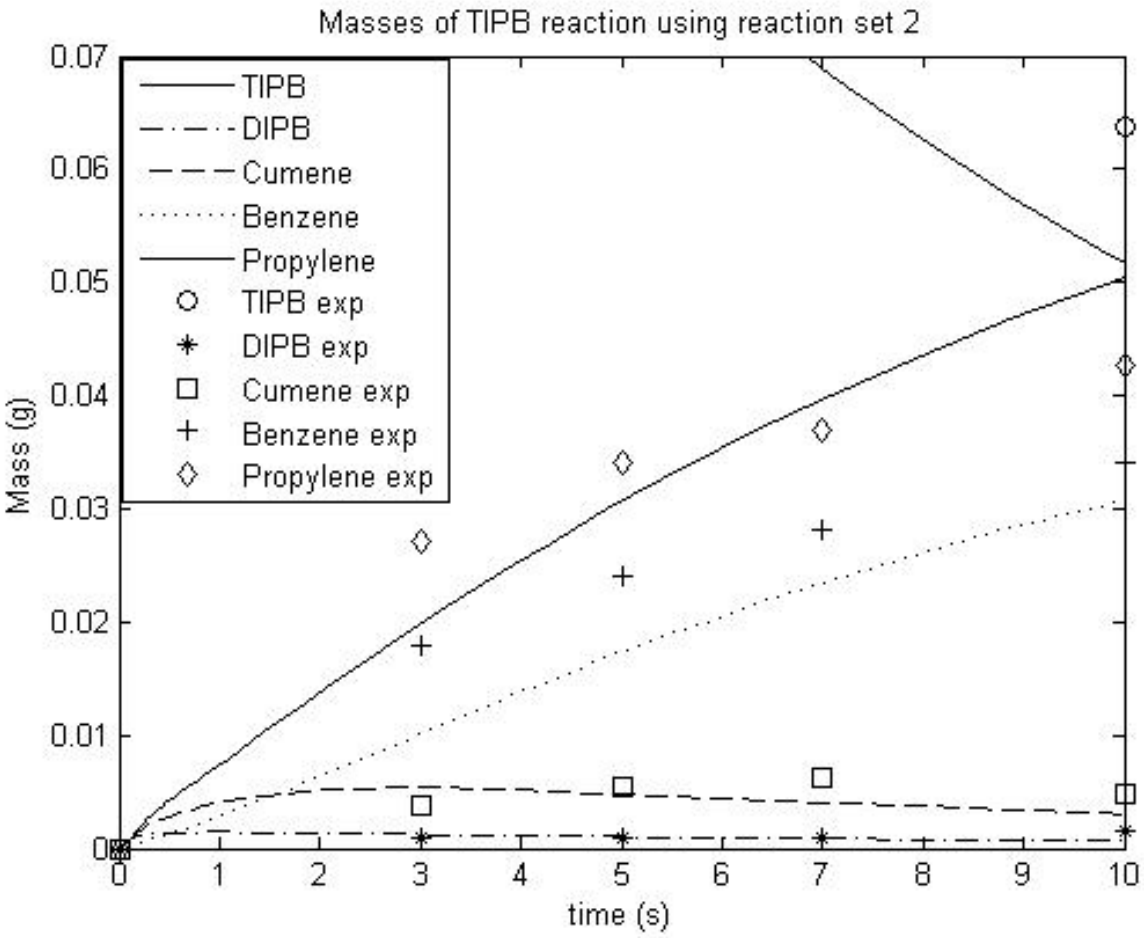

Figure 78: Application of reaction set 2 model to 1,3,5-TIPB at 550℃ (Smaller scale)

From Figure 77 and Figure 78, the fit is comparable to that in Figure 73. The model still cannot fit the experimental data for benzene at 550℃. The Thiele moduli obtained are summarized in Table 21.

Table 21: Values of Thiele moduli for reaction set 2 model at 550℃

φ_1	0.7960
φ_2	0.1996
φ_3	6.4789
φ_4	2.7319
Λ	5.8184

Comparing Table 21 and Table 19, the corresponding values are comparable.

6.3.3 Finite volume model with reaction set 3

This section assumes that 1,3-DIPB reacts to form benzene in addition to cumene.

$$A \overset{k_1}{\rightarrow} B + E$$

$$B \overset{k_2}{\rightarrow} C + E$$

$$B \overset{k_3}{\rightarrow} D + 2E$$

$$C \overset{k_4}{\rightarrow} D + E$$

where A, B, C, D and E correspond to 1,3,5-TIPB, 1,3-DIPB, cumene, benzene and propylene respectively.

6.3.3.1 The model

The reaction rates can be written as:

$$r_A = -\phi_{int} k_1 q_A \quad 6.3.47$$

$$r_B = \phi_{int}(k_1 q_A - k_2 q_B - k_3 q_B) \quad 6.3.48$$

$$r_C = \phi_{int}(k_2 q_B - k_4 q_C) \quad 6.3.49$$

$$r_D = \phi_{int}(k_3 q_B + k_4 q_C) \tag{6.3.50}$$

$$r_E = \phi_{int}(k_1 q_A + k_2 q_B + \frac{1}{2} k_3 q_B + k_4 q_C) \tag{6.3.51}$$

The normalized equations that describe this system are:

$$\frac{\partial \bar{q}_A}{\partial \bar{t}} = \frac{1}{\bar{r}^2}\frac{\partial}{\partial \bar{r}}\left(\bar{r}^2 \frac{\partial \bar{q}_A}{\partial \bar{r}}\right) - \varphi_1^2 \, \bar{q}_A \tag{6.3.52}$$

$$\frac{\partial \bar{q}_B}{\partial \bar{t}} = \frac{1}{\bar{r}^2}\frac{\partial}{\partial \bar{r}}\left(\bar{r}^2 \frac{\partial \bar{q}_B}{\partial \bar{r}}\right) + \varphi_1^2 \, \bar{q}_A - (\varphi_2^2 + \varphi_3^2) \, \bar{q}_B \tag{6.3.53}$$

$$\frac{\partial \bar{q}_C}{\partial \bar{t}} = \frac{1}{\bar{r}^2}\frac{\partial}{\partial \bar{r}}\left(\bar{r}^2 \frac{\partial \bar{q}_C}{\partial \bar{r}}\right) + \varphi_2^2 \, \bar{q}_B - \varphi_4^2 \, \bar{q}_C \tag{6.3.54}$$

$$\frac{\partial \bar{q}_D}{\partial \bar{t}} = \frac{1}{\bar{r}^2}\frac{\partial}{\partial \bar{r}}\left(\bar{r}^2 \frac{\partial \bar{q}_D}{\partial \bar{r}}\right) + \varphi_3^2 \, \bar{q}_B + \varphi_4^2 \, \bar{q}_C \tag{6.3.55}$$

$$\frac{\partial \bar{q}_E}{\partial \bar{t}} = \frac{1}{\bar{r}^2}\frac{\partial}{\partial \bar{r}}\left(\bar{r}^2 \frac{\partial \bar{q}_E}{\partial \bar{r}}\right) + \varphi_1^2 \, \bar{q}_A + \varphi_2^2 \, \bar{q}_B + \frac{1}{2}\varphi_3^2 \, \bar{q}_B + \varphi_4^2 \, \bar{q}_C \tag{6.3.56}$$

where

$$\varphi_1^2 = \frac{k_1 {r_c}^2}{D_c} \tag{6.3.57}$$

$$\varphi_2^2 = \frac{k_2 {r_c}^2}{D_c} \tag{6.3.58}$$

$$\varphi_3^2 = \frac{k_3 {r_c}^2}{D_c} \tag{6.3.59}$$

$$\varphi_4^2 = \frac{k_4 {r_c}^2}{D_c} \tag{6.3.60}$$

These equations were solved for the initial and boundary conditions in Equations 6.3.26-6.3.32 and optimized for the Thiele moduli.

6.3.3.2 Results at 400 ℃

Figure 79 demonstrates the application of reaction set 3 model for the experimental data of 1,3,5-TIPB at 400℃ .

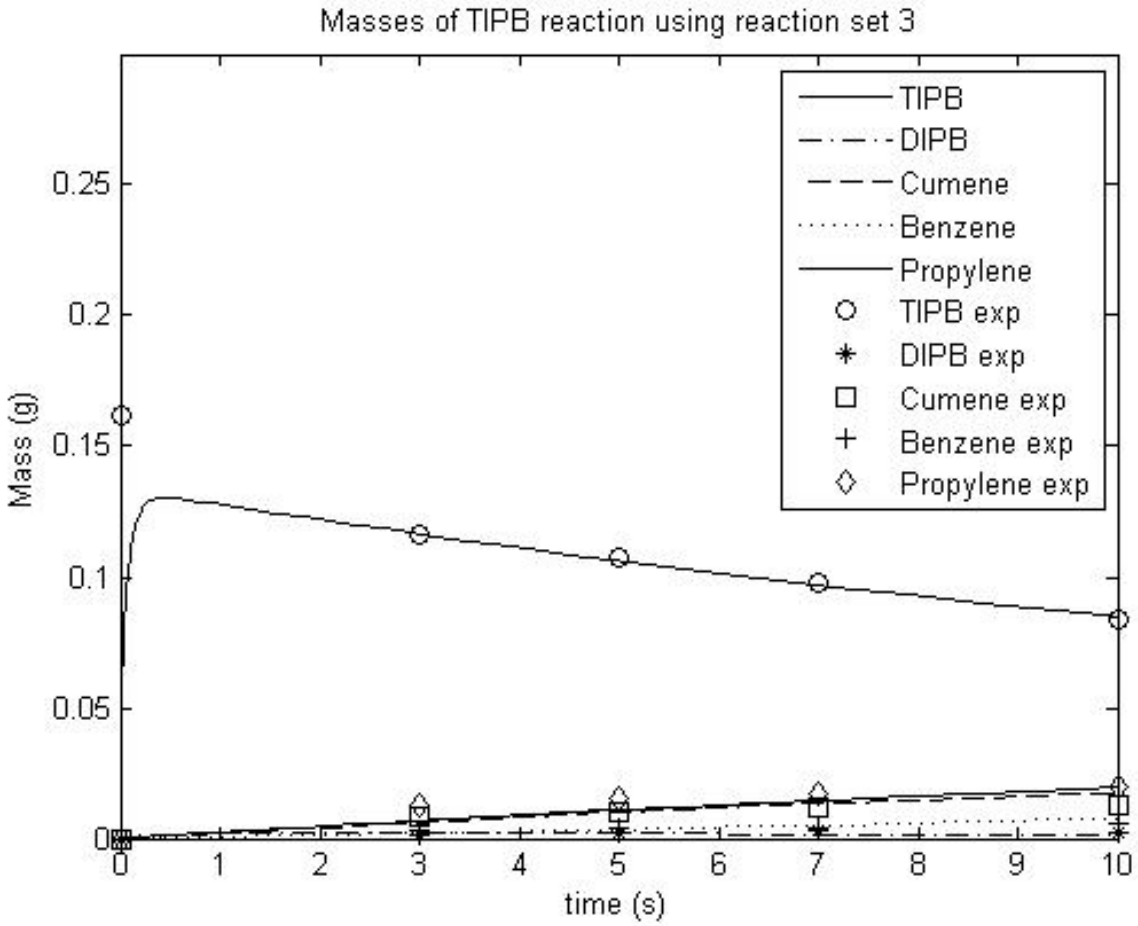

Figure 79: Application of reaction set 3 model to 1,3,5-TIPB at 400℃

Experimental data obtained from Al-Khattaf [28]

Figure 80 illustrates the same figure but for a smaller scale.

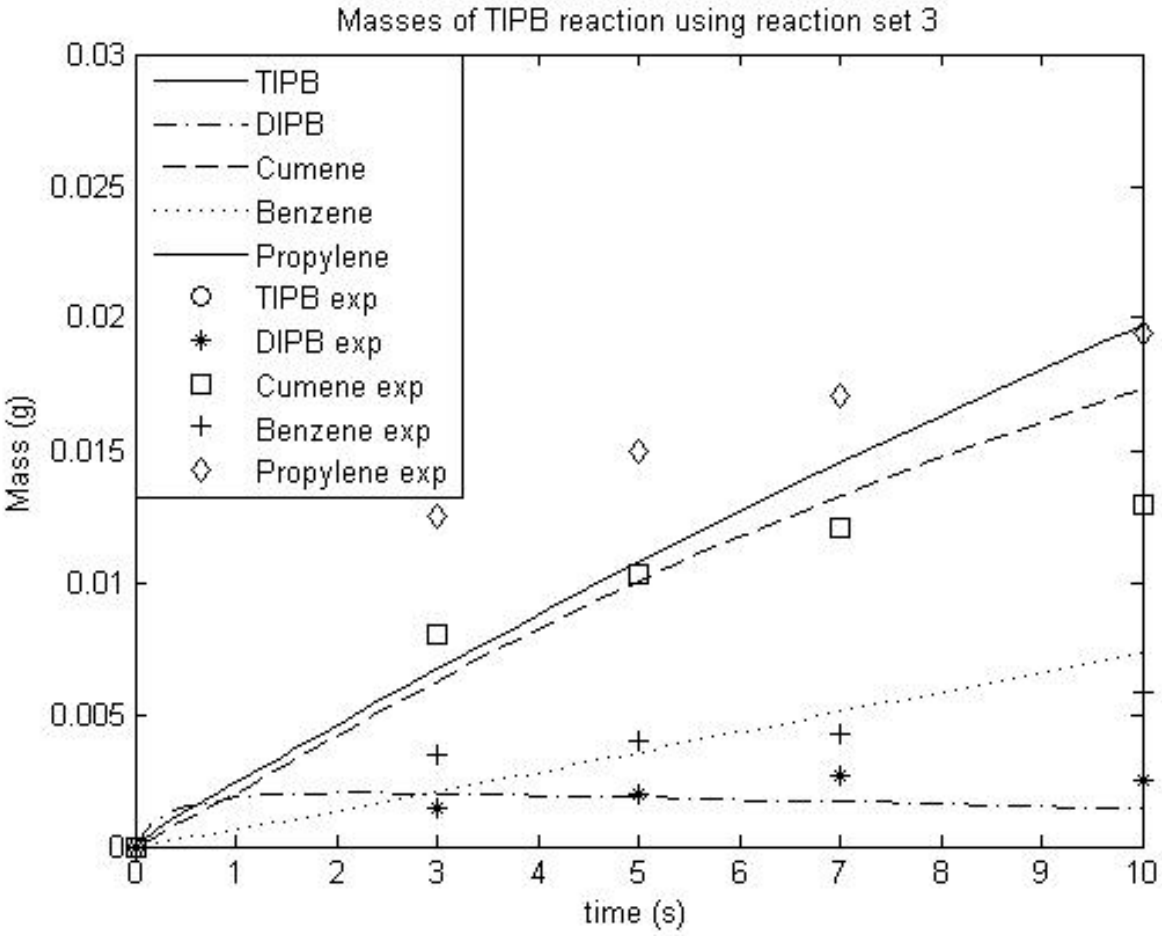

Figure 80: Application of reaction set 3 model to 1,3,5-TIPB at 400℃ (Smaller scale)

From Figure 79 and Figure 80, the fit is slightly better for propylene. The Thiele moduli obtained are summarized in Table 22.

Table 22: Values of Thiele moduli for reaction set 3 model at 400℃

φ_1	0.5272
φ_2	3.0001
φ_3	2.0019
φ_4	0.3862
Λ	5.0003

Comparing Table 22 and Table 20, the corresponding values are fairly different.

6.3.3.3 Results at 550 ℃

Figure 81 demonstrates the application of reaction set 3 model for the experimental data of 1,3,5-TIPB at 550℃ .

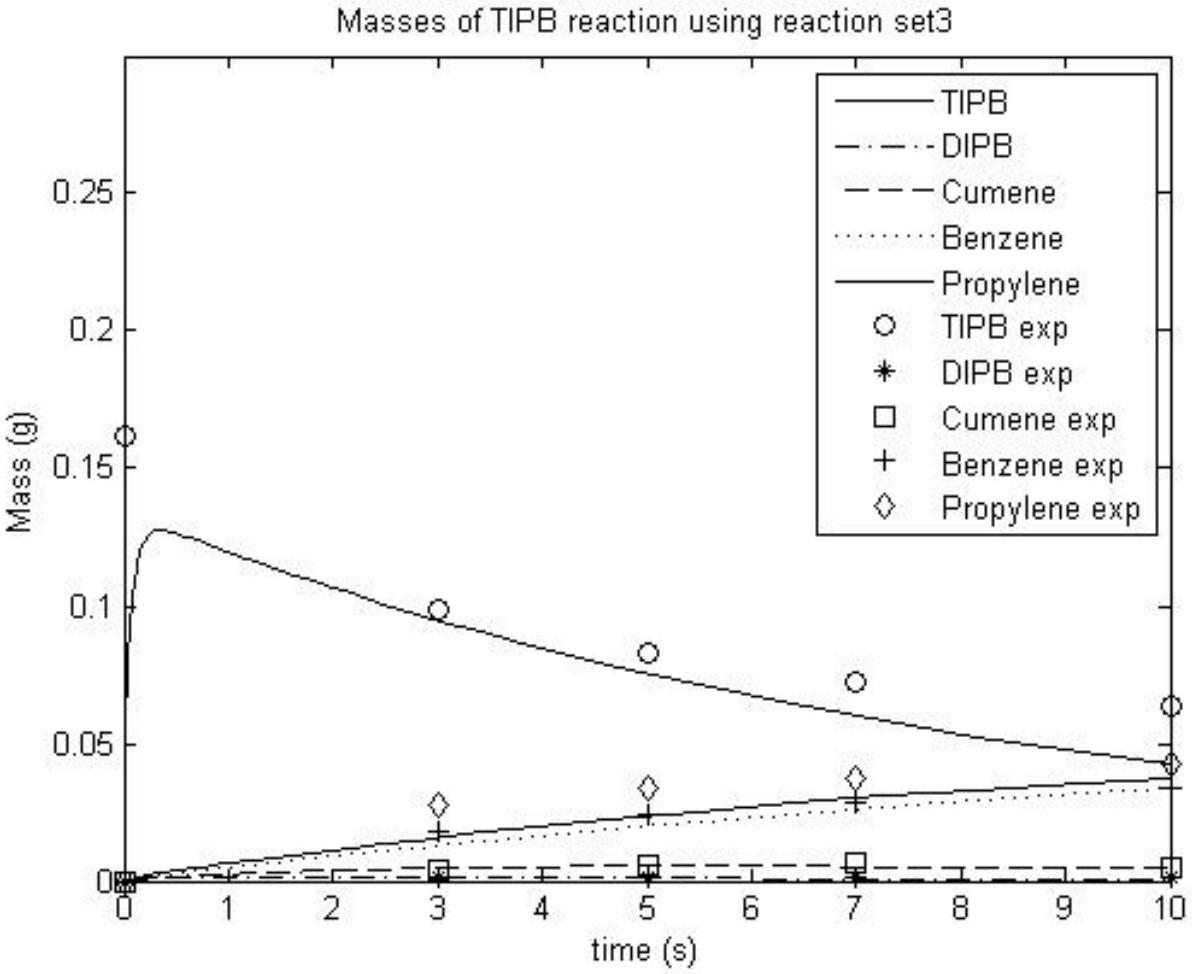

Figure 81: Application of reaction set 3 model to 1,3,5-TIPB at 550℃

Experimental data obtained from Al-Khattaf [28]

Figure 82 illustrates the same figure but for a smaller scale.

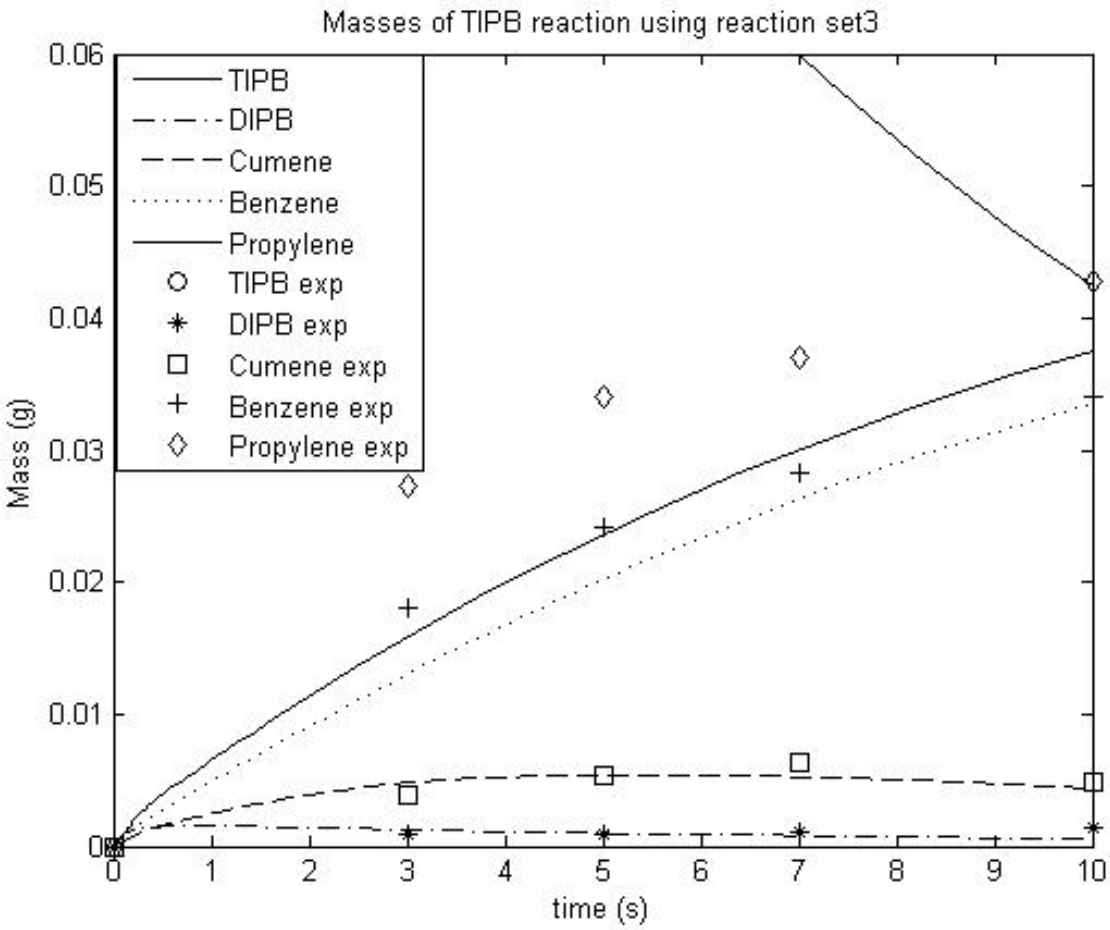

Figure 82: Application of reaction set 3 model to 1,3,5-TIPB at 550℃ (Smaller scale)

From Figure 81 and Figure 82, the fit is better for benzene. The Thiele moduli obtained are summarized in Table 22.

Table 23: Values of Thiele moduli for reaction set 3 model at 550℃

φ_1	0.9089
φ_2	4.0225
φ_3	5.8616
φ_4	1.4256
Λ	5.9049

6.3.4 Finite volume model with reaction set 4

This section assumes that the reaction of cumene to form benzene is a second order reaction.

$$A \overset{k_1}{\rightarrow} B + E$$

$$B \overset{k_2}{\rightarrow} C + E$$

$$C \overset{k_3}{\rightarrow} D + E$$

where A, B, C, D and E correspond to 1,3,5-TIPB, 1,3-DIPB, cumene, benzene and propylene respectively.

6.3.4.1 The model

The reaction rates can be written as:

$$r_A = -\phi_{int} k_1 q_A \quad 6.3.61$$

$$r_B = \phi_{int}(k_1 q_A - k_2 q_B) \quad 6.3.62$$

$$r_C = \phi_{int}(k_2 q_B - k_3 q_C^2) \quad 6.3.63$$

$$r_D = \phi_{int}(k_3 q_C^2) \quad 6.3.64$$

$$r_E = \phi_{int}(k_1 q_A + k_2 q_B + k_3 q_C^2) \quad 6.3.65$$

The normalized equations that describe this system are:

$$\frac{\partial \bar{q}_A}{\partial \bar{t}} = \frac{1}{\bar{r}^2}\frac{\partial}{\partial \bar{r}}\left(\bar{r}^2 \frac{\partial \bar{q}_A}{\partial \bar{r}}\right) - \varphi_1^2\ \bar{q}_A \tag{6.3.66}$$

$$\frac{\partial \bar{q}_B}{\partial \bar{t}} = \frac{1}{\bar{r}^2}\frac{\partial}{\partial \bar{r}}\left(\bar{r}^2 \frac{\partial \bar{q}_B}{\partial \bar{r}}\right) + \varphi_1^2\ \bar{q}_A - \varphi_2^2\ \bar{q}_B \tag{6.3.67}$$

$$\frac{\partial \bar{q}_C}{\partial \bar{t}} = \frac{1}{\bar{r}^2}\frac{\partial}{\partial \bar{r}}\left(\bar{r}^2 \frac{\partial \bar{q}_C}{\partial \bar{r}}\right) + \varphi_2^2\ \bar{q}_B - \varphi_3^2\ \bar{q}_C^2 \tag{6.3.68}$$

$$\frac{\partial \bar{q}_D}{\partial \bar{t}} = \frac{1}{\bar{r}^2}\frac{\partial}{\partial \bar{r}}\left(\bar{r}^2 \frac{\partial \bar{q}_D}{\partial \bar{r}}\right) + \varphi_3^2\ \bar{q}_C^2 \tag{6.3.69}$$

$$\frac{\partial \bar{q}_E}{\partial \bar{t}} = \frac{1}{\bar{r}^2}\frac{\partial}{\partial \bar{r}}\left(\bar{r}^2 \frac{\partial \bar{q}_E}{\partial \bar{r}}\right) + \varphi_1^2\ \bar{q}_A + \varphi_2^2\ \bar{q}_B + \varphi_3^2\ \bar{q}_C^2 \tag{6.3.70}$$

where

$$\varphi_1^2 = \frac{k_1 {r_c}^2}{D_c} \tag{6.3.71}$$

$$\varphi_2^2 = \frac{k_2 {r_c}^2}{D_c} \tag{6.3.72}$$

$$\varphi_3^2 = \frac{k_3 {r_c}^2 q_0}{D_c} \tag{6.3.73}$$

These equations were solved for the initial and boundary conditions in Equations 6.3.26-6.3.32 and optimized for the Thiele moduli.

6.3.4.2 Results at 400 ℃

Figure 83 demonstrates the application of reaction set 4 model for the experimental data of 1,3,5-TIPB at 400℃ .

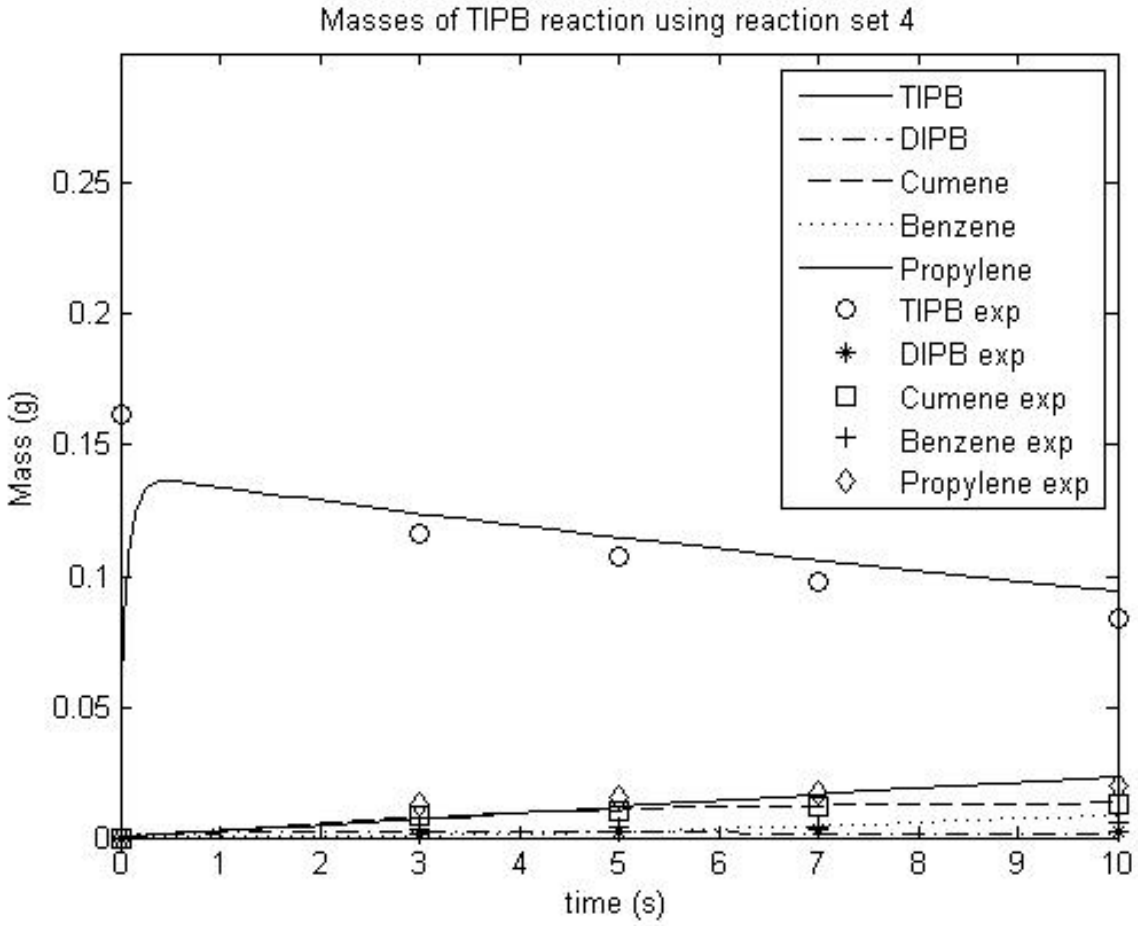

Figure 83: Application of reaction set 4 model to 1,3,5-TIPB at 400℃

Experimental data obtained from Al-Khattaf [28]

Figure 84 illustrate the same figure but for a smaller scale.

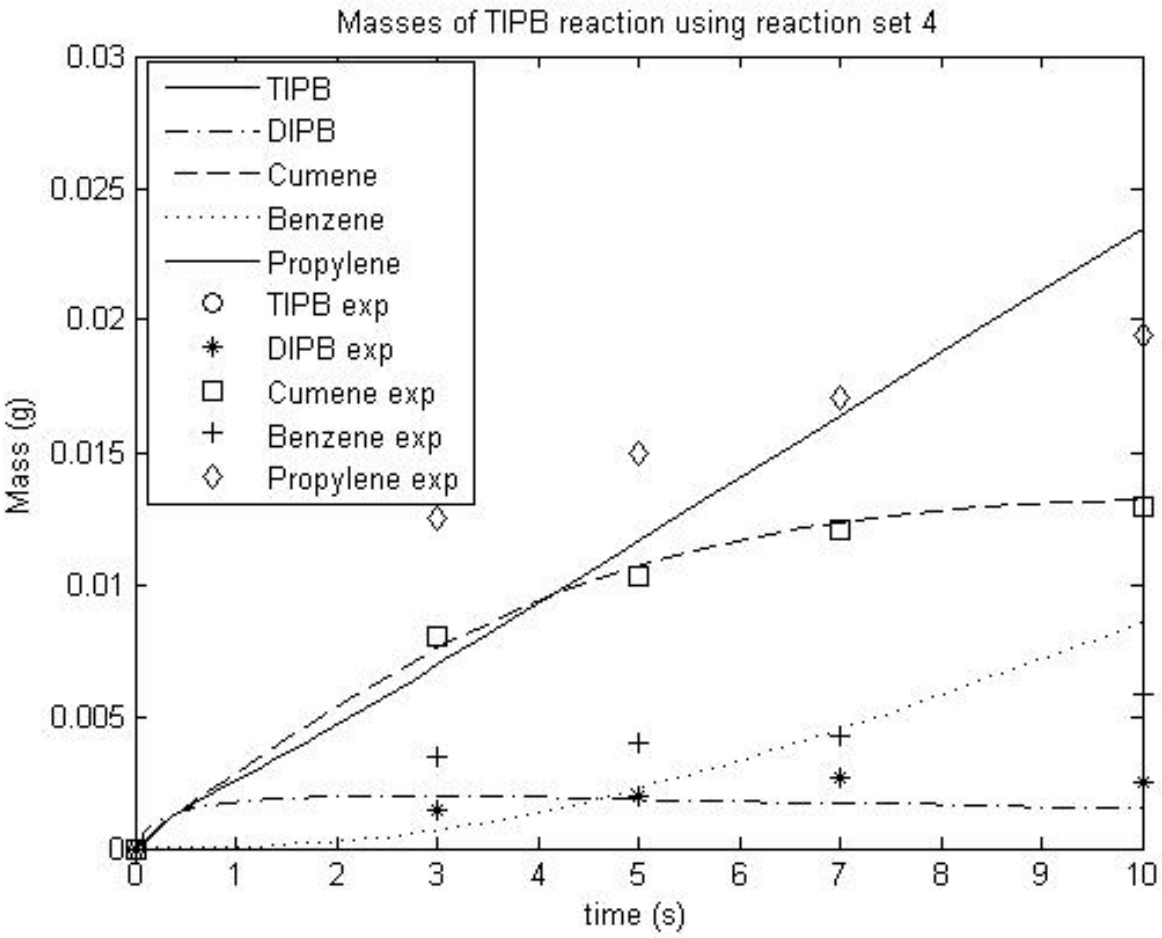

Figure 84: Application of reaction set 4 model to 1,3,5-TIPB at 400℃ (Smaller scale)

From Figure 83 and Figure 84, the fit is worse than reaction sets 2 and 3. The Thiele moduli obtained are summarized in Table 24.

Table 24: Values of Thiele moduli for reaction set 4 model at 400℃

φ_1	0.5544
φ_2	3.9189
φ_3	3.0129
Λ	6.7892

6.3.4.3 Results at 550 ℃

Figure 85 demonstrates the application of reaction set 4 model for the experimental data of 1,3,5-TIPB at 550℃ .

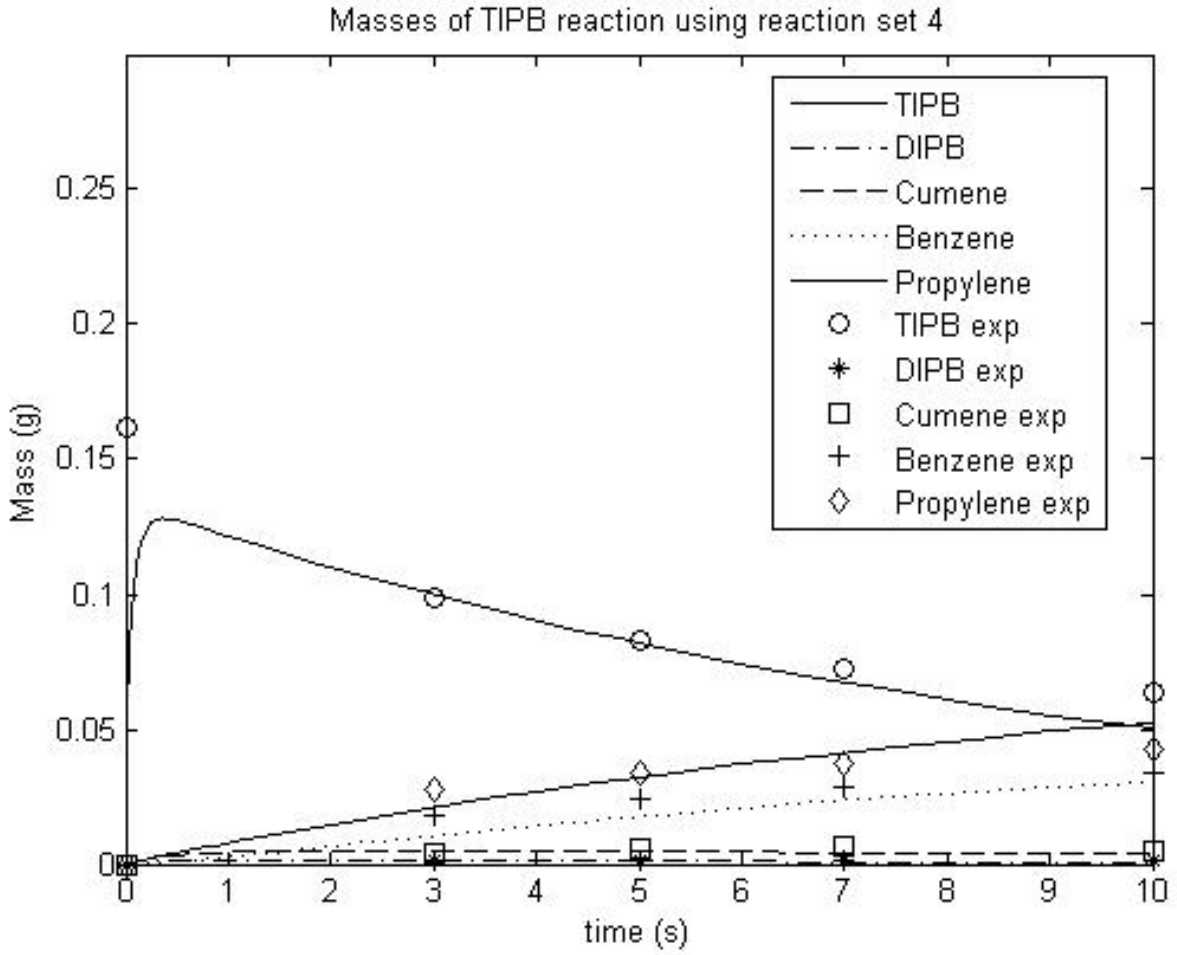

Figure 85: Application of reaction set 4 model to 1,3,5-TIPB at 550℃

Experimental data obtained from Al-Khattaf [28]

Figure 86 illustrates the same figure but for a smaller scale.

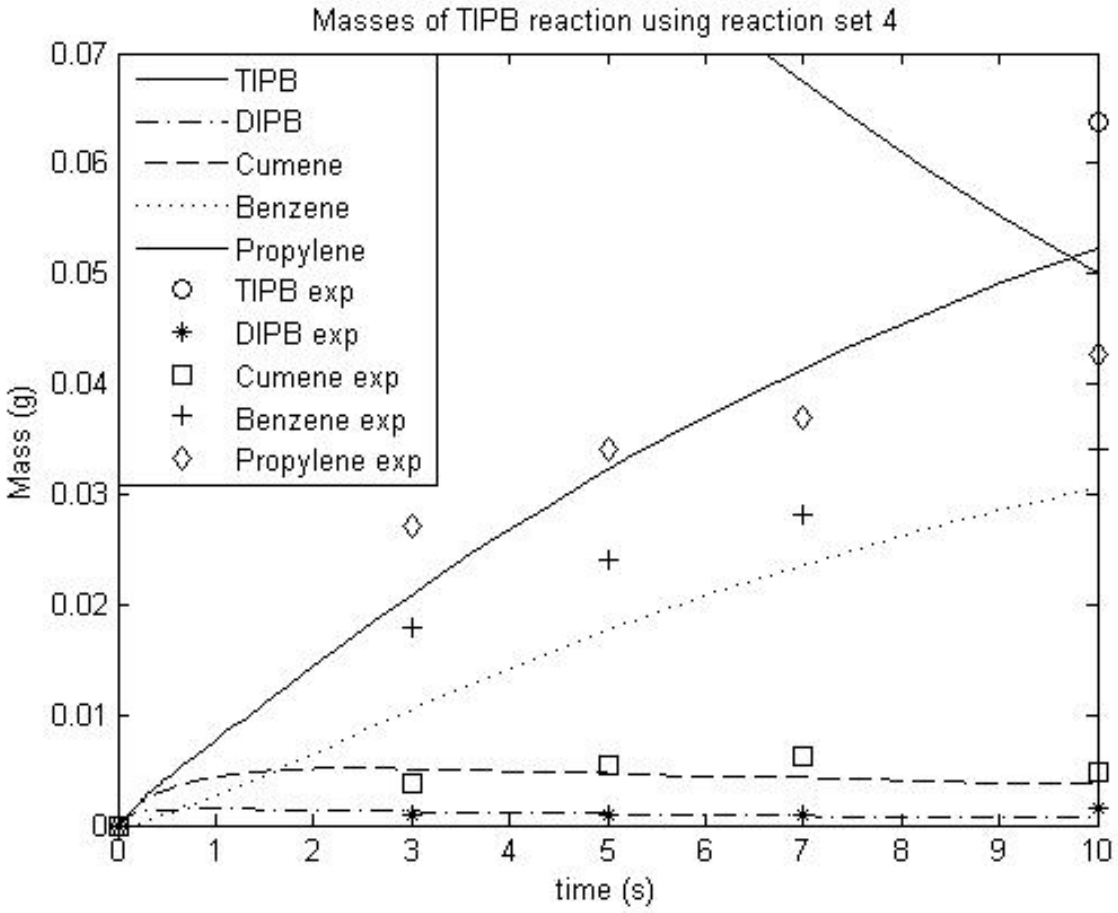

Figure 86: Application of reaction set 4 model to 1,3,5-TIPB at 550℃ (Smaller scale)

From Figure 86, the fit is slightly better. The Thiele moduli obtained are summarized in Table 25.

Table 25: Values of Thiele moduli for reaction set 4 model at 550℃

φ_1	0.8180
φ_2	6.6139
φ_3	12.1646
Λ	5.5997

The values of Thiele moduli are higher than the previous reaction sets.

6.3.5 Finite volume model with reaction set 5

This section assumes that 1,3-DIPB reaction to form cumene is a second order reaction.

$$A \overset{k_1}{\rightarrow} B + E$$

$$B \overset{k_2}{\rightarrow} C + E$$

$$C \overset{k_3}{\rightarrow} D + E$$

where A, B, C, D and E correspond to 1,3,5-TIPB, 1,3-DIPB, cumene, benzene and propylene respectively.

6.3.5.1 The model

The reaction rates can be written as:

$$r_A = -\phi_{int} k_1 q_A \quad 6.3.74$$

$$r_B = \phi_{int}(k_1 q_A - k_2 q_B^2) \quad 6.3.75$$

$$r_C = \phi_{int}(k_2 q_B^2 - k_3 q_C) \quad 6.3.76$$

$$r_D = \phi_{int}(k_4 q_C) \quad 6.3.77$$

$$r_E = \phi_{int}(k_1 q_A + k_2 q_B^2 + k_3 q_C) \quad 6.3.78$$

The normalized equations that describe this system are:

$$\frac{\partial \bar{q}_A}{\partial \bar{t}} = \frac{1}{\bar{r}^2}\frac{\partial}{\partial \bar{r}}\left(\bar{r}^2 \frac{\partial \bar{q}_A}{\partial \bar{r}}\right) - \varphi_1^2\, \bar{q}_A \quad 6.3.79$$

$$\frac{\partial \bar{q}_B}{\partial \bar{t}} = \frac{1}{\bar{r}^2}\frac{\partial}{\partial \bar{r}}\left(\bar{r}^2 \frac{\partial \bar{q}_B}{\partial \bar{r}}\right) + \varphi_1^2\, \bar{q}_A - \varphi_2^2\, \bar{q}_B^2 \quad 6.3.80$$

$$\frac{\partial \bar{q}_C}{\partial \bar{t}} = \frac{1}{\bar{r}^2}\frac{\partial}{\partial \bar{r}}\left(\bar{r}^2 \frac{\partial \bar{q}_C}{\partial \bar{r}}\right) + \varphi_2^2\, \bar{q}_B^2 - \varphi_3^2\, \bar{q}_C \quad 6.3.81$$

$$\frac{\partial \bar{q}_D}{\partial \bar{t}} = \frac{1}{\bar{r}^2}\frac{\partial}{\partial \bar{r}}\left(\bar{r}^2 \frac{\partial \bar{q}_D}{\partial \bar{r}}\right) + \varphi_4^2\, \bar{q}_C \quad 6.3.82$$

$$\frac{\partial \bar{q}_E}{\partial \bar{t}} = \frac{1}{\bar{r}^2}\frac{\partial}{\partial \bar{r}}\left(\bar{r}^2 \frac{\partial \bar{q}_E}{\partial \bar{r}}\right) + \varphi_1^2\, \bar{q}_A + \varphi_2^2\, \bar{q}_B^2 + \varphi_3^2\, \bar{q}_C \quad 6.3.83$$

where

$$\varphi_1^2 = \frac{k_1 {r_c}^2}{D_c} \quad 6.3.84$$

$$\varphi_2^2 = \frac{k_2 {r_c}^2 q_0}{D_c} \quad 6.3.85$$

$$\varphi_3^2 = \frac{k_3 {r_c}^2}{D_c} \quad 6.3.86$$

These equations were solved for the initial and boundary conditions in Equations 6.3.26-6.3.32 and optimized for the Thiele moduli.

6.3.5.2 Results at 400 ℃

Figure 87 demonstrates the application of reaction set 5 model for the experimental data of 1,3,5-TIPB at 400℃ .

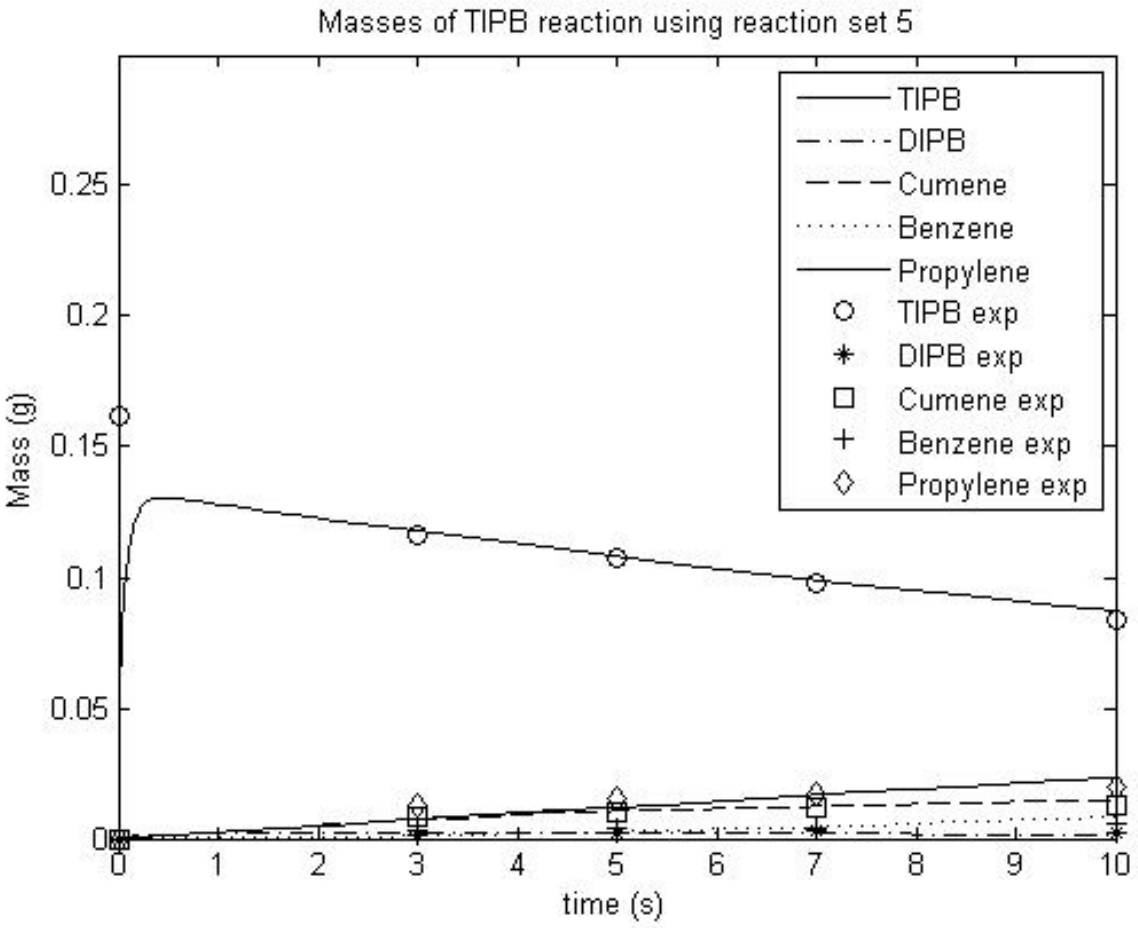

Figure 87: Application of reaction set 5 model to 1,3,5-TIPB at 400℃

Experimental data obtained from Al-Khattaf [28]

Figure 88 illustrate the same figure but for a smaller scale.

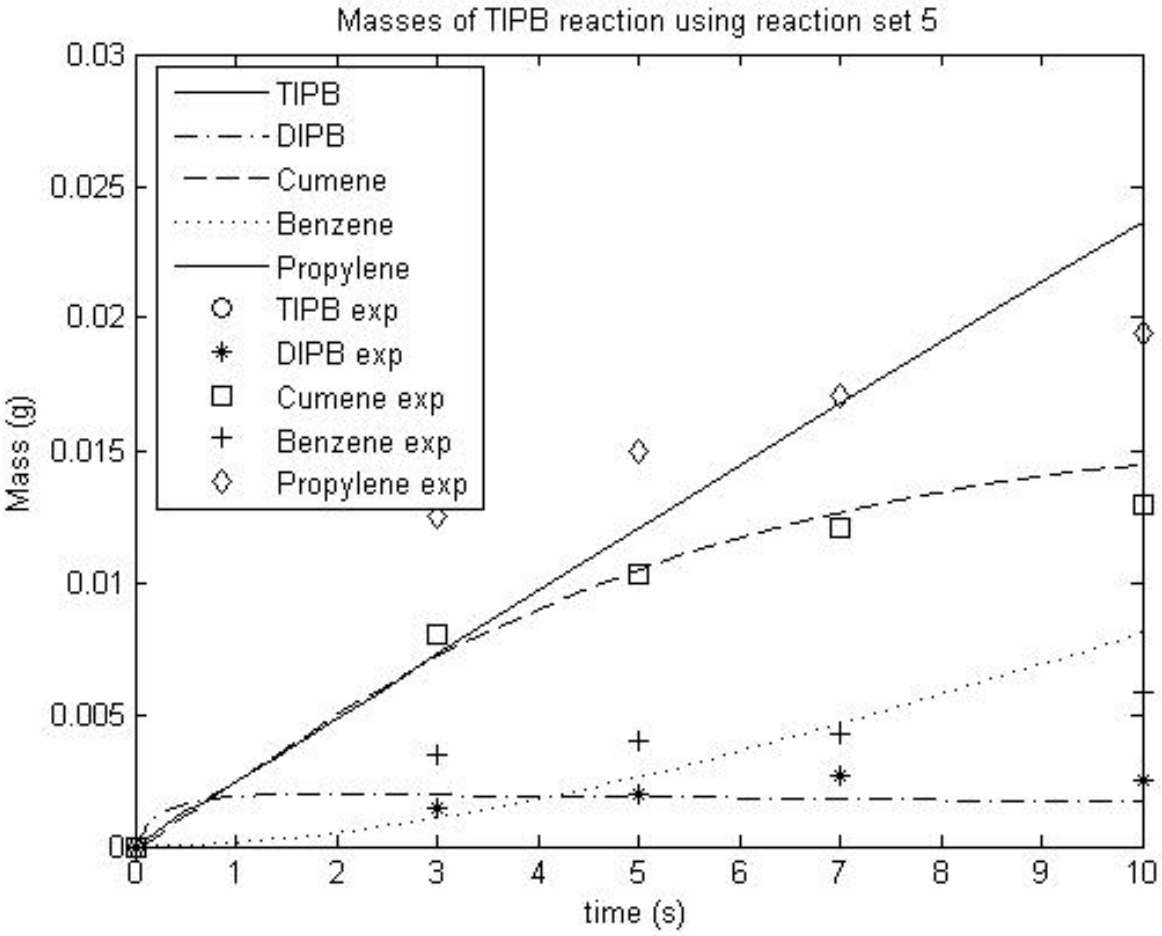

Figure 88: Application of reaction set 5 model to 1,3,5-TIPB at 400℃ (Smaller scale)

From Figure 87 and Figure 88, the fit is better than in reaction set 4. The Thiele moduli obtained are summarized in Table 26.

Table 26: Values of Thiele moduli for reaction set 5 model at 400℃

φ_1	0.5097
φ_2	28.9101
φ_3	0.8757
Λ	5.0004

6.3.5.3 Results at 550 ℃

Figure 89 demonstrates the application of reaction set 5 model for the experimental data of 1,3,5-TIPB at 550℃ .

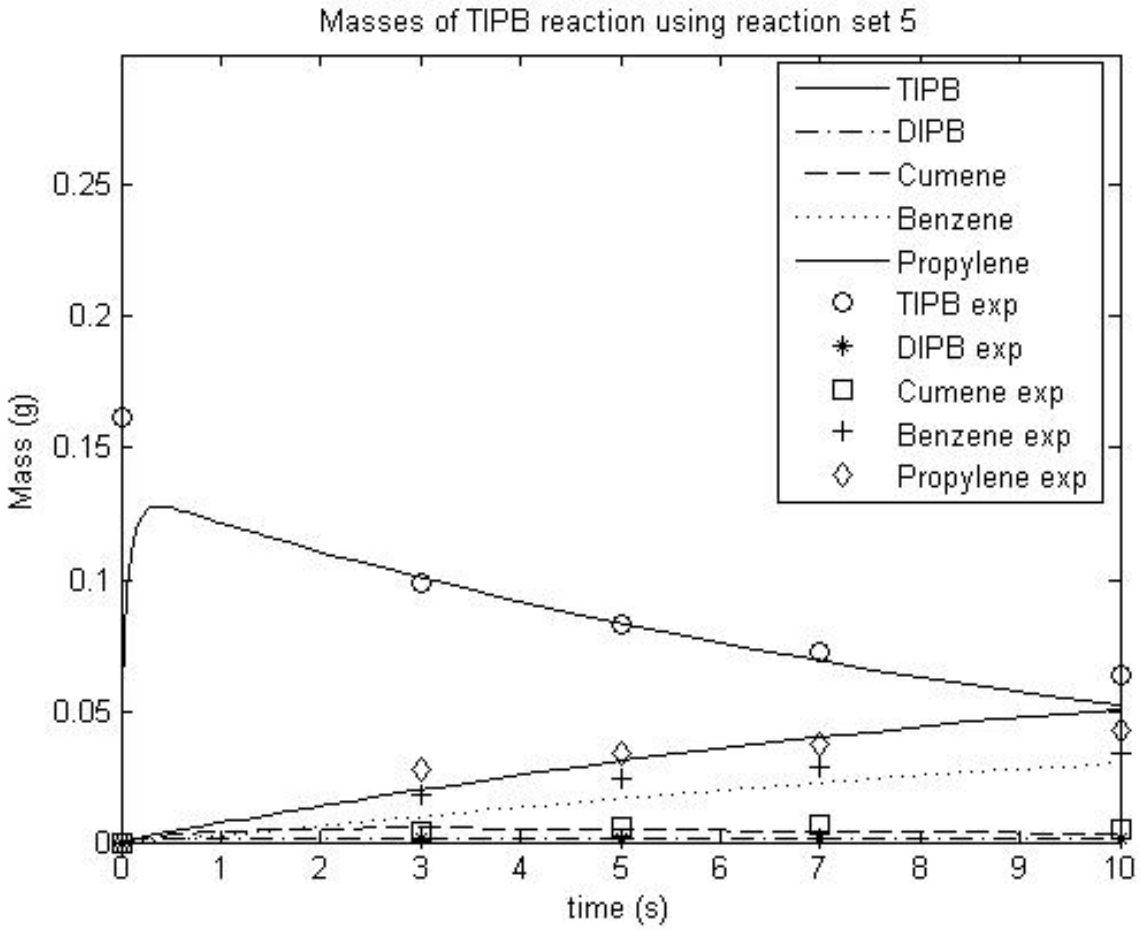

Figure 89: Application of reaction set 5 model to 1,3,5-TIPB at 550℃

Experimental data obtained from Al-Khattaf [28]

Figure 90 illustrates the same figure but for a smaller scale.

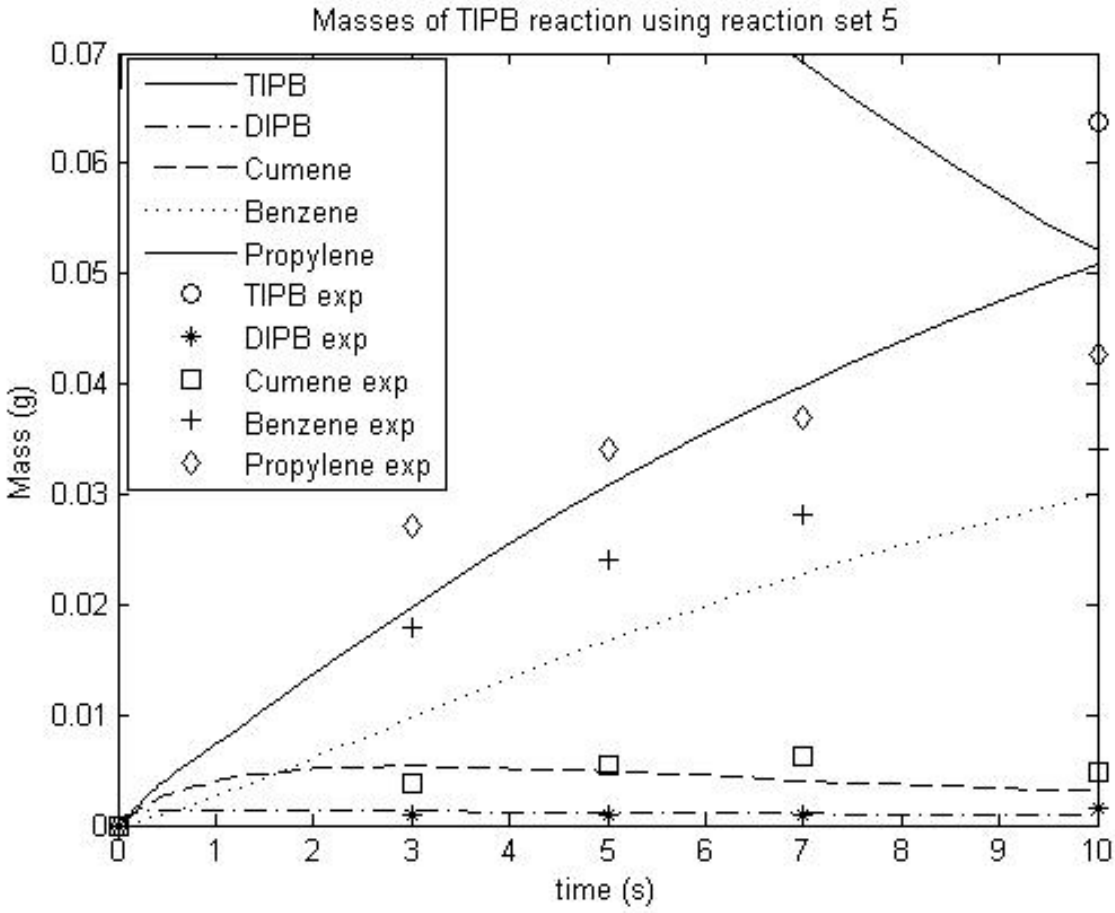

Figure 90: Application of reaction set 5 model to 1,3,5-TIPB at 550℃ (Smaller scale)

From Figure 89 and Figure 90, the fit is comparable to the previous case. The Thiele moduli obtained are summarized in Table 27.

Table 27: Values of Thiele moduli for reaction set 5 model at 550℃

φ_1	0.7900
φ_2	64.4171
φ_3	2.6215
Λ	5.4327

The value of the second Thiele modulus is relatively high.

6.3.6 Finite volume model with reaction set 6

This section assumes that benzene will react to form light gases.

$$A \overset{k_1}{\rightarrow} B + E$$

$$B \overset{k_2}{\rightarrow} C + E$$

$$C \overset{k_3}{\rightarrow} D + E$$

$$D \overset{k_4}{\rightarrow} Light\ gases$$

where A, B, C, D and E correspond to 1,3,5-TIPB, 1,3-DIPB, cumene, benzene and propylene respectively.

6.3.6.1 The model

The reaction rates can be written as:

$$r_A = -\phi_{int} k_1 q_A \quad 6.3.87$$

$$r_B = \phi_{int}(k_1 q_A - k_2 q_B) \quad 6.3.88$$

$$r_C = \phi_{int}(k_2 q_B - k_3 q_C) \quad 6.3.89$$

$$r_D = \phi_{int}(k_3 q_C - k_4 q_D) \quad 6.3.90$$

$$r_E = \phi_{int}(k_1 q_A + k_2 q_B + k_3 q_C) \quad 6.3.91$$

The normalized equations that describe this system are:

$$\frac{\partial \bar{q}_A}{\partial \bar{t}} = \frac{1}{\bar{r}^2}\frac{\partial}{\partial \bar{r}}\left(\bar{r}^2 \frac{\partial \bar{q}_A}{\partial \bar{r}}\right) - \varphi_1^2\ \bar{q}_A \tag{6.3.92}$$

$$\frac{\partial \bar{q}_B}{\partial \bar{t}} = \frac{1}{\bar{r}^2}\frac{\partial}{\partial \bar{r}}\left(\bar{r}^2 \frac{\partial \bar{q}_B}{\partial \bar{r}}\right) + \varphi_1^2\ \bar{q}_A - \varphi_2^2\ \bar{q}_B \tag{6.3.93}$$

$$\frac{\partial \bar{q}_C}{\partial \bar{t}} = \frac{1}{\bar{r}^2}\frac{\partial}{\partial \bar{r}}\left(\bar{r}^2 \frac{\partial \bar{q}_C}{\partial \bar{r}}\right) + \varphi_2^2\ \bar{q}_B - \varphi_3^2\ \bar{q}_C \tag{6.3.94}$$

$$\frac{\partial \bar{q}_D}{\partial \bar{t}} = \frac{1}{\bar{r}^2}\frac{\partial}{\partial \bar{r}}\left(\bar{r}^2 \frac{\partial \bar{q}_D}{\partial \bar{r}}\right) + \varphi_3^2\ \bar{q}_C - \varphi_4^2\ \bar{q}_D \tag{6.3.95}$$

$$\frac{\partial \bar{q}_E}{\partial \bar{t}} = \frac{1}{\bar{r}^2}\frac{\partial}{\partial \bar{r}}\left(\bar{r}^2 \frac{\partial \bar{q}_E}{\partial \bar{r}}\right) + \varphi_1^2\ \bar{q}_A + \varphi_2^2\ \bar{q}_B + \varphi_3^2\ \bar{q}_C \tag{6.3.96}$$

where,

$$\varphi_1^2 = \frac{k_1 {r_c}^2}{D_c} \tag{6.3.97}$$

$$\varphi_2^2 = \frac{k_2 {r_c}^2}{D_c} \tag{6.3.98}$$

$$\varphi_3^2 = \frac{k_3 {r_c}^2}{D_c} \tag{6.3.99}$$

$$\varphi_4^2 = \frac{k_4 {r_c}^2}{D_c} \tag{6.3.100}$$

These equations were solved for the initial and boundary conditions in Equations 6.3.26-6.3.32 and optimized for the Thiele moduli.

6.3.6.2 Results at 400 ℃

Figure 91 demonstrates the application of reaction set 6 model for the experimental data of 1,3,5-TIPB at 400℃ .

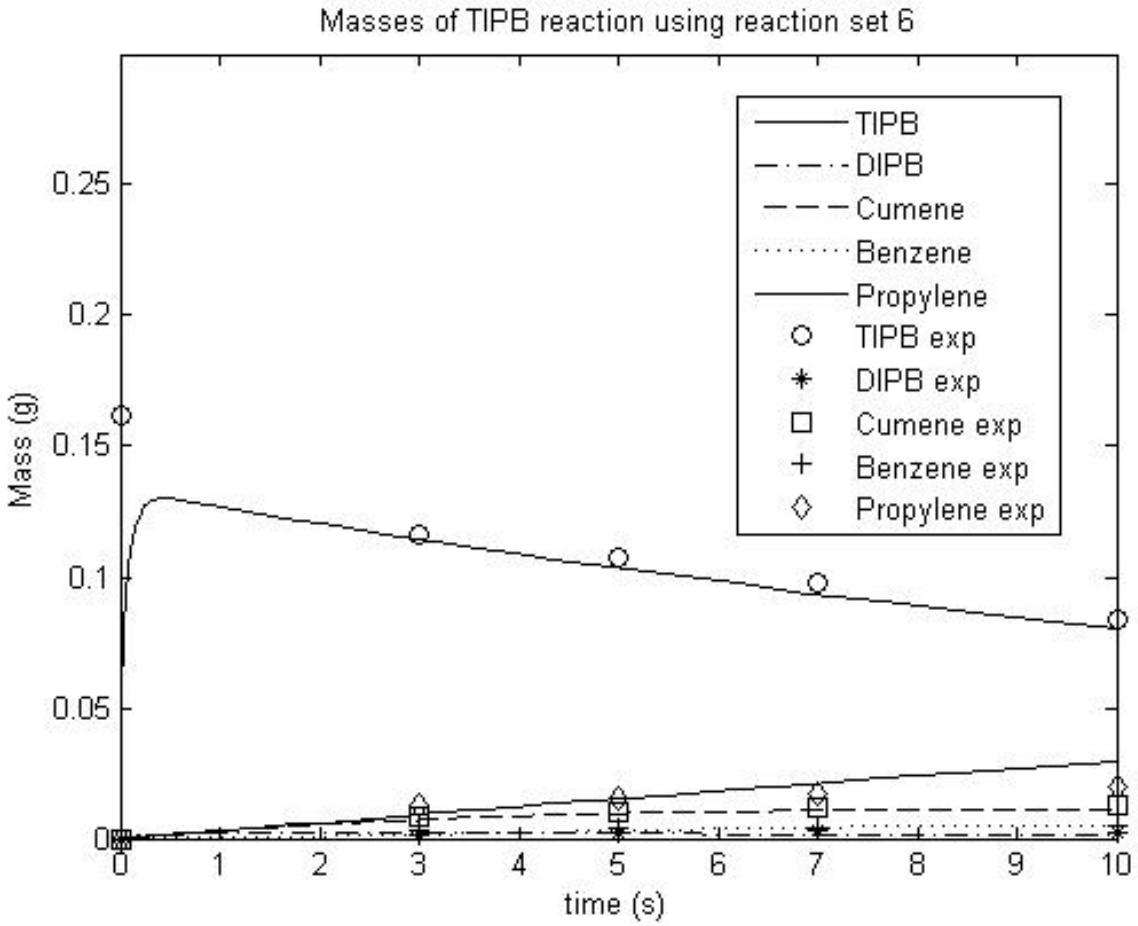

Figure 91: Application of reaction set 6 model to 1,3,5-TIPB at 400℃

Experimental data obtained from Al-Khattaf [28]

Figure 92 illustrates the same figure but for a smaller scale.

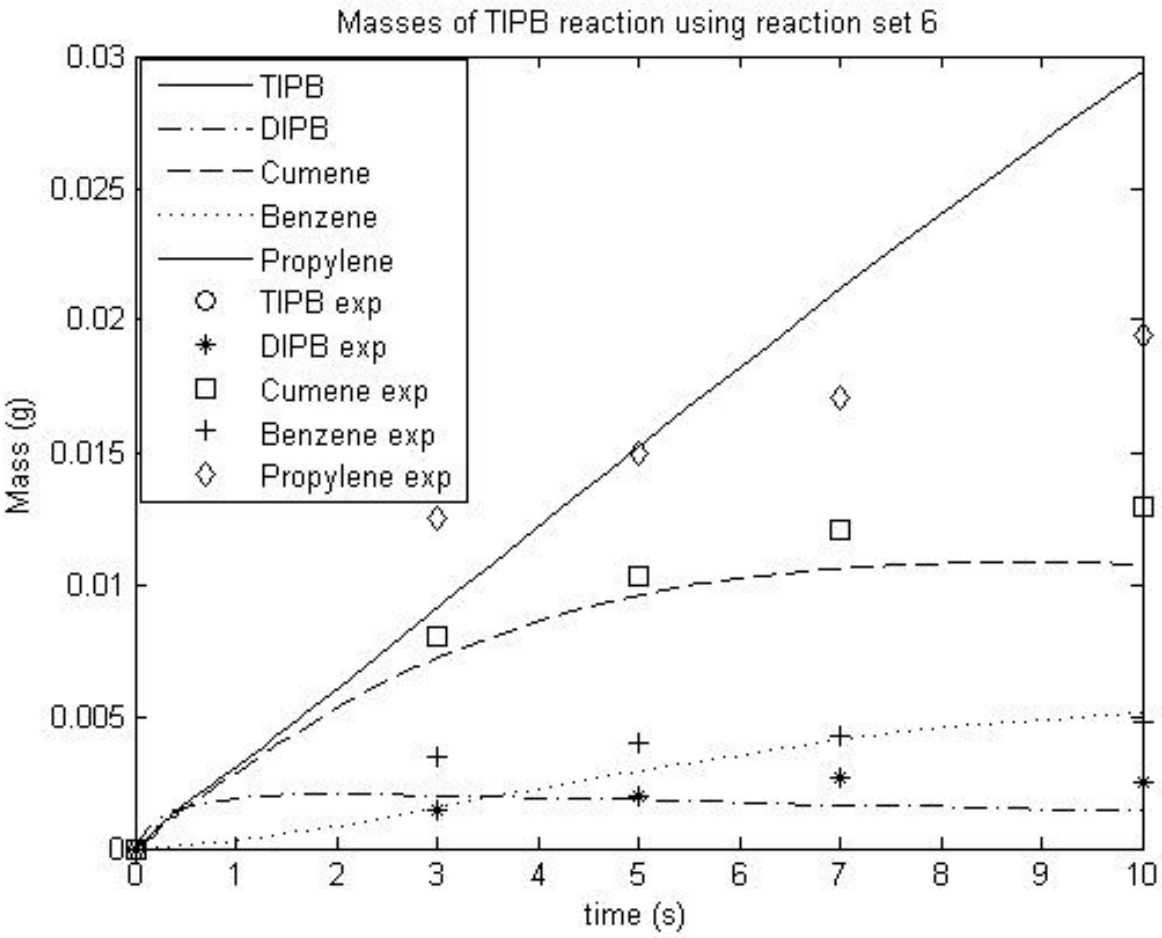

Figure 92: Application of reaction set 6 model to 1,3,5-TIPB at 400℃ (Smaller scale)

From Figure 91 and Figure 92, the model fits benzene experimental data better than the previous models. The Thiele moduli obtained are summarized in Table 28.

Table 28: Values of Thiele moduli for reaction set 6 model at 400℃

φ_1	0.5576
φ_2	3.7879
φ_3	1.2046
φ_4	1.3000
Λ	5.0089

6.3.6.3 Results at 550 ℃

Figure 93 demonstrates the application of reaction set 6 model for the experimental data of 1,3,5-TIPB at 550℃ .

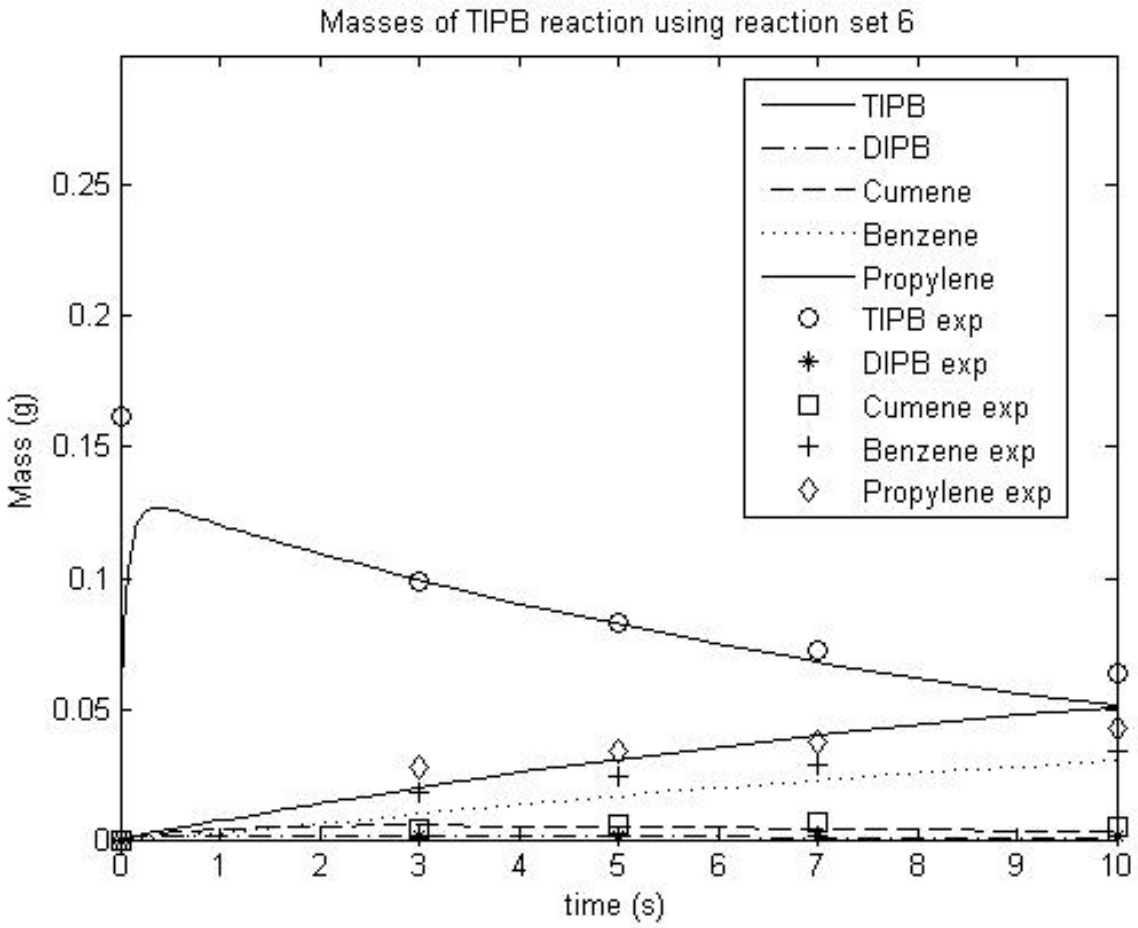

Figure 93: Application of reaction set 6 model to 1,3,5-TIPB at 550℃

Experimental data obtained from Al-Khattaf [28]

Figure 94 illustrates the same figure but for a smaller scale.

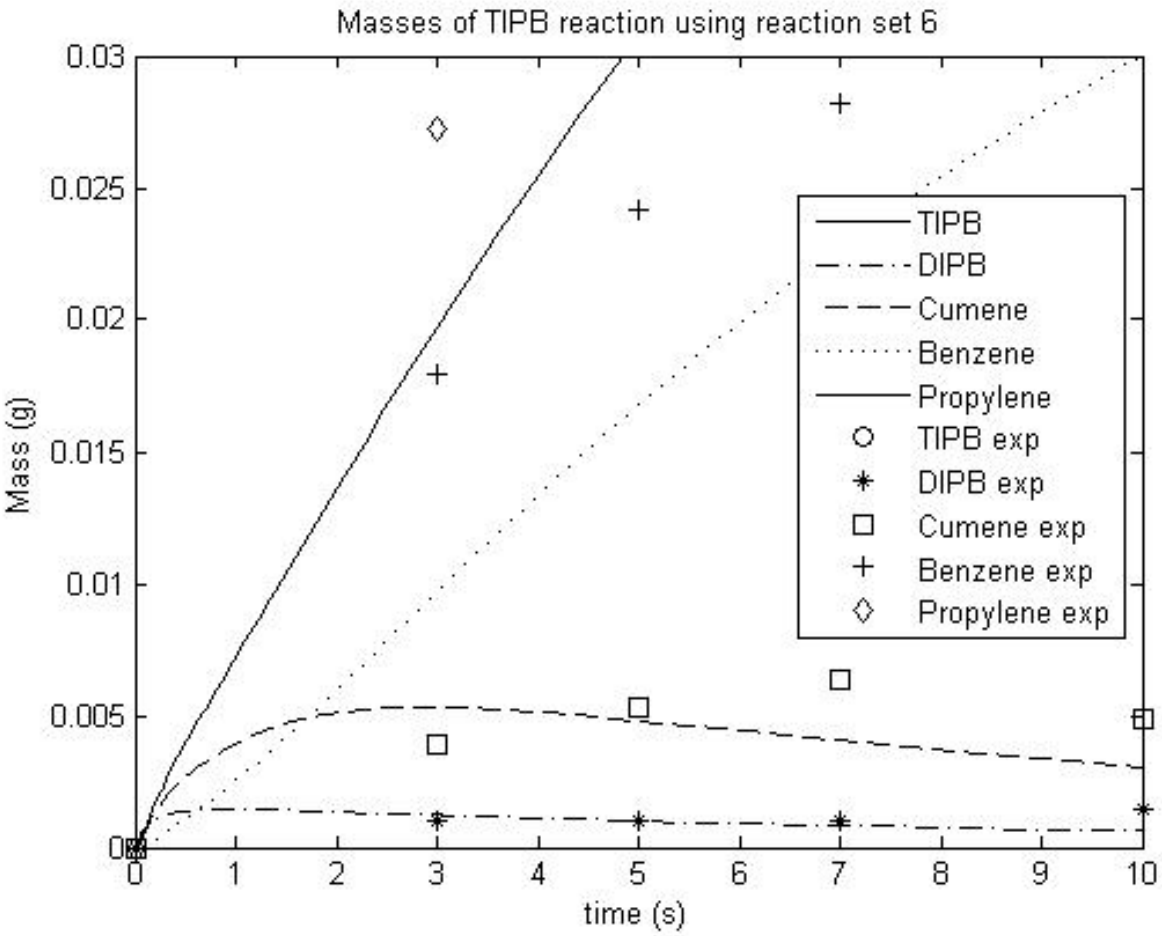

Figure 94: Application of reaction set 6 model to 1,3,5-TIPB at 550℃ (Smaller scale)

From Figure 93 and Figure 94, the fit to benzene did not enhance and the fit to cumene got worse. The Thiele moduli obtained are summarized in Table 29.

Table 29: Values of Thiele moduli for reaction set 6 model at 550℃

φ_1	0.7743
φ_2	6.2679
φ_3	2.5649
φ_4	0.0012
Λ	5.1020

6.3.7 Finite volume model with reaction set 7

This section assumes that the reaction of 1,3,5-TIPB is second order reaction.

$$A \xrightarrow{k_1} B + E$$

$$B \xrightarrow{k_2} C + E$$

$$C \xrightarrow{k_3} D + E$$

where A, B, C, D and E correspond to 1,3,5-TIPB, 1,3-DIPB, cumene, benzene and propylene respectively.

6.3.7.1 The model

The reaction rates can be written as:

$$r_A = -\phi_{int} k_1 q_A^2 \quad 6.3.101$$

$$r_B = \phi_{int}(k_1 q_A^2 - k_2 q_B) \quad 6.3.102$$

$$r_C = \phi_{int}(k_2 q_B - k_3 q_C) \quad 6.3.103$$

$$r_D = \phi_{int}(k_3 q_C) \quad 6.3.104$$

$$r_E = \phi_{int}(k_1 q_A^2 + k_2 q_B + k_3 q_C) \quad 6.3.105$$

The normalized equations that describe this system are:

$$\frac{\partial \bar{q}_A}{\partial \bar{t}} = \frac{1}{\bar{r}^2}\frac{\partial}{\partial \bar{r}}\left(\bar{r}^2 \frac{\partial \bar{q}_A}{\partial \bar{r}}\right) - \varphi_1^2\, \bar{q}_A^2 \quad 6.3.106$$

$$\frac{\partial \bar{q}_B}{\partial \bar{t}} = \frac{1}{\bar{r}^2}\frac{\partial}{\partial \bar{r}}\left(\bar{r}^2 \frac{\partial \bar{q}_B}{\partial \bar{r}}\right) + \varphi_1^2\, \bar{q}_A^2 - \varphi_2^2\, \bar{q}_B \quad 6.3.107$$

$$\frac{\partial \bar{q}_C}{\partial \bar{t}} = \frac{1}{\bar{r}^2}\frac{\partial}{\partial \bar{r}}\left(\bar{r}^2 \frac{\partial \bar{q}_C}{\partial \bar{r}}\right) + \varphi_2^2\, \bar{q}_B - \varphi_3^2\, \bar{q}_C \quad 6.3.108$$

$$\frac{\partial \bar{q}_D}{\partial \bar{t}} = \frac{1}{\bar{r}^2}\frac{\partial}{\partial \bar{r}}\left(\bar{r}^2 \frac{\partial \bar{q}_D}{\partial \bar{r}}\right) + \varphi_3^2\, \bar{q}_C \quad 6.3.109$$

$$\frac{\partial \bar{q}_E}{\partial \bar{t}} = \frac{1}{\bar{r}^2}\frac{\partial}{\partial \bar{r}}\left(\bar{r}^2 \frac{\partial \bar{q}_E}{\partial \bar{r}}\right) + \varphi_1^2\, \bar{q}_A^2 + \varphi_2^2\, \bar{q}_B + \varphi_3^2\, \bar{q}_C \quad 6.3.110$$

where,

$$\varphi_1^2 = \frac{k_1 {r_c}^2}{D_c} \quad 6.3.111$$

$$\varphi_2^2 = \frac{k_2 {r_c}^2}{D_c} \qquad 6.3.112$$

$$\varphi_3^2 = \frac{k_3 {r_c}^2}{D_c} \qquad 6.3.113$$

These equations were solved for the initial and boundary conditions in Equations 6.3.26-6.3.32 and optimized for the Thiele moduli.

6.3.7.2 Results at 400 ℃

Figure 95 demonstrates the application of reaction set 7 model for the experimental data of 1,3,5-TIPB at 400℃ .

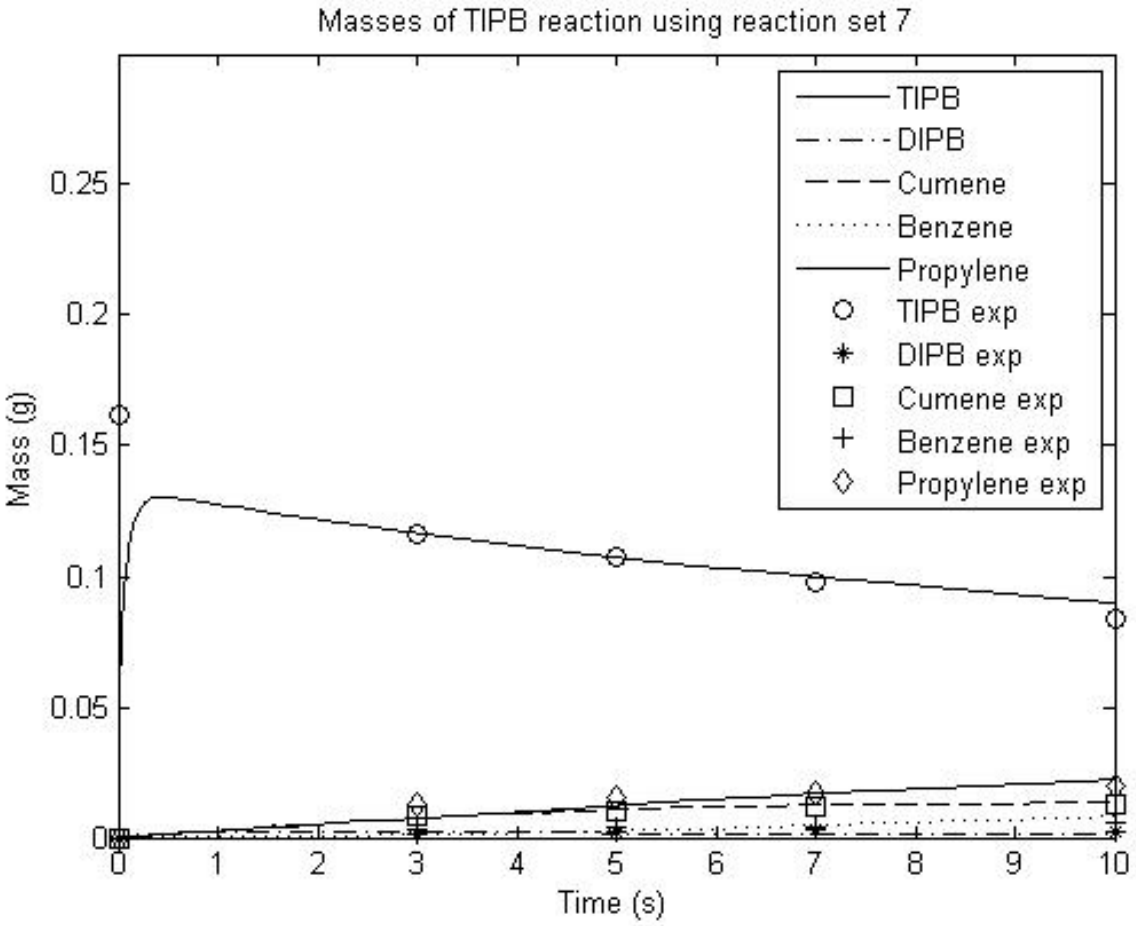

Figure 95: Application of reaction set 7 model to 1,3,5-TIPB at 400℃

Experimental data obtained from Al-Khattaf [28]

Figure 96 illustrates the same figure but for a smaller scale.

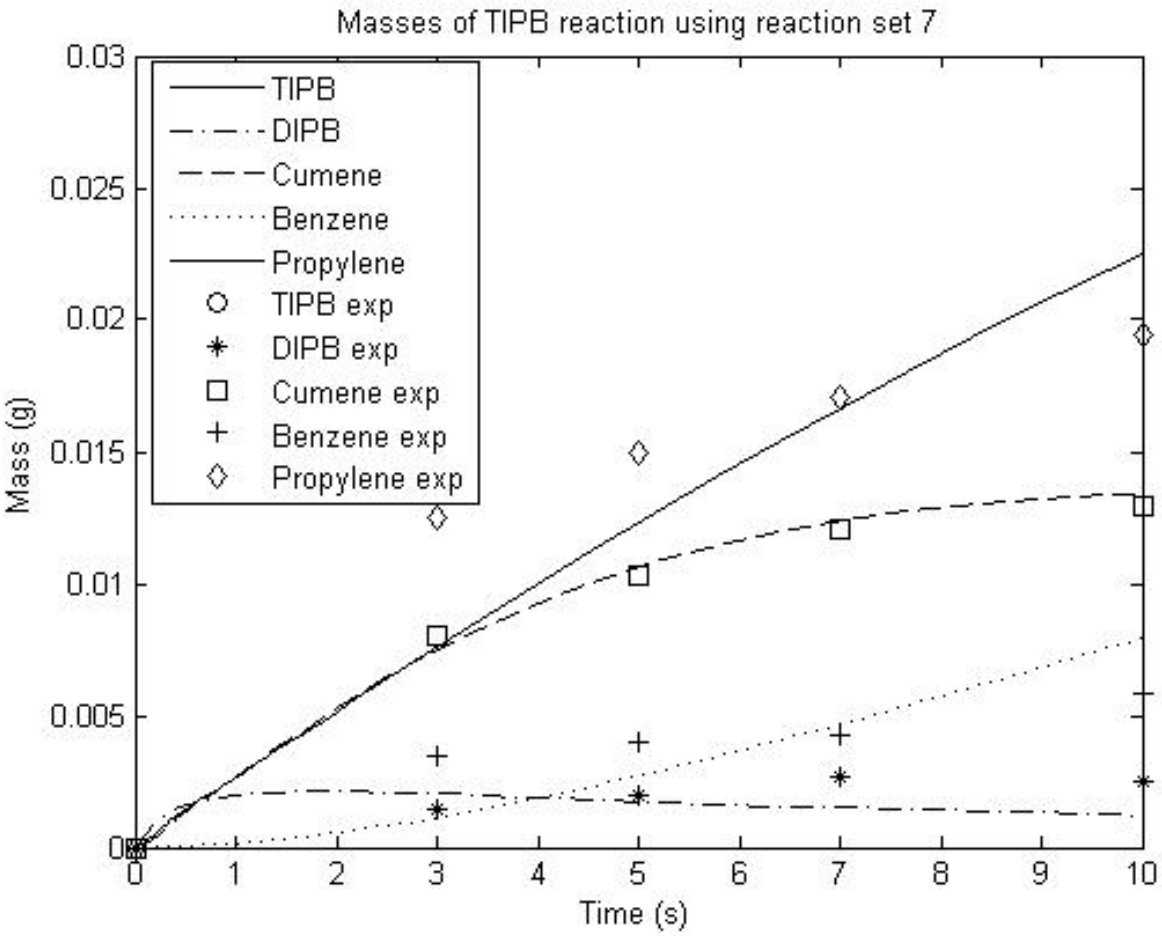

Figure 96: Application of reaction set 7 model to 1,3,5-TIPB at 400℃ (Smaller scale)

From Figure 95 and Figure 96, the model provides a bad fit for benzene. The Thiele moduli obtained are summarized in Table 30.

Table 30: Values of Thiele moduli for reaction set 7 model at 400℃

φ_1	0.6015
φ_2	3.4926
φ_3	0.8738
Λ	5.0000

6.3.7.3 Results at 550 ℃

Figure 97 demonstrates the application of reaction set 7 model for the experimental data of 1,3,5-TIPB at 550℃ .

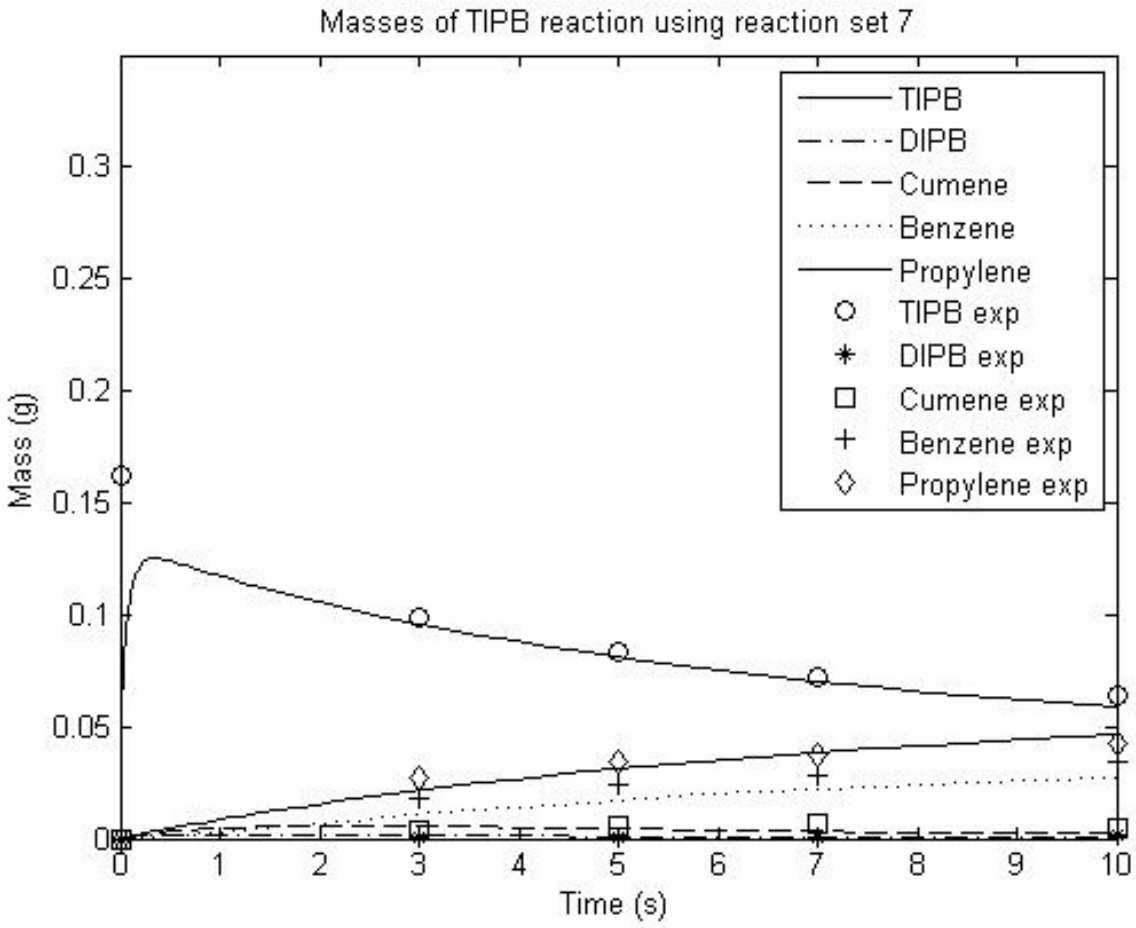

Figure 97: Application of reaction set 7 model to 1,3,5-TIPB at 550℃

Experimental data obtained from Al-Khattaf [28]

Figure 98 illustrates the same figure but for a smaller scale.

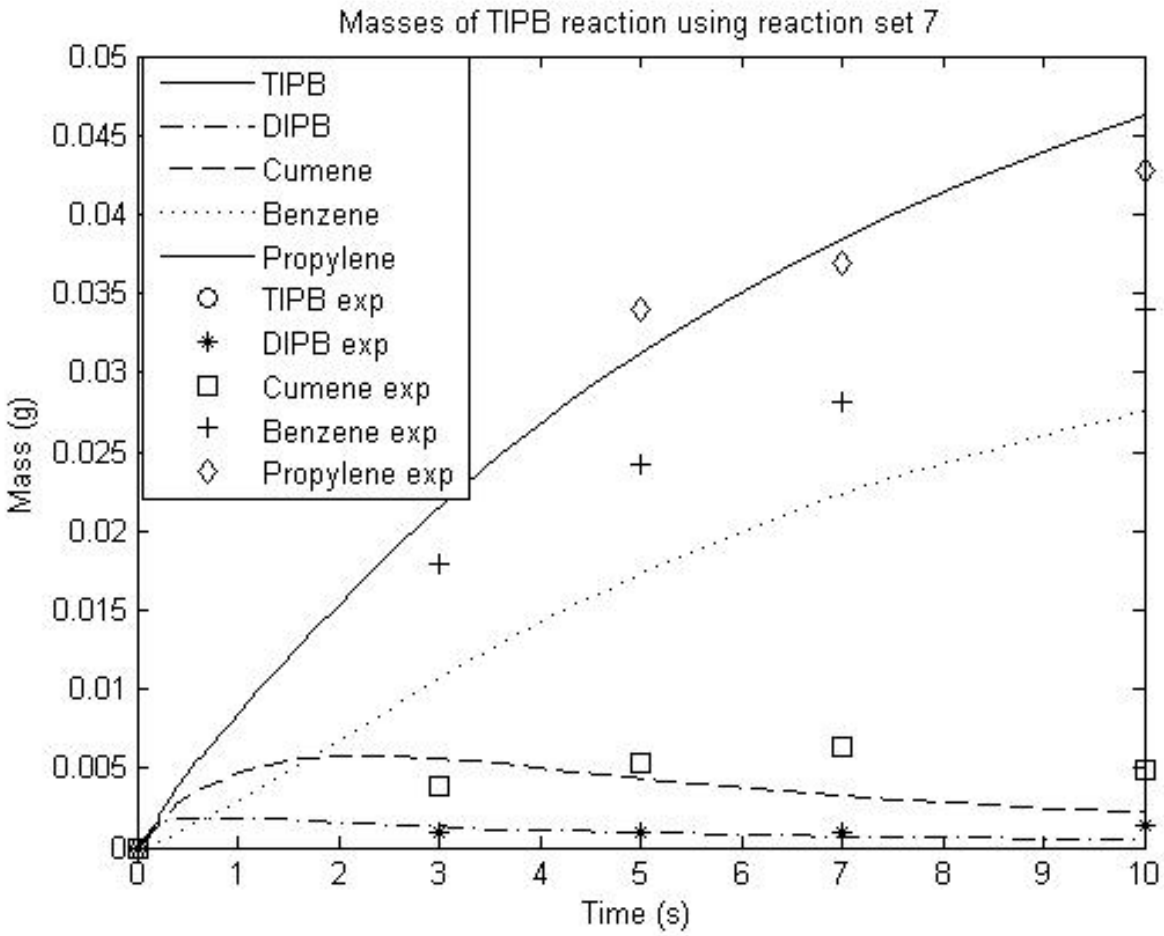

Figure 98: Application of reaction set 7 model to 1,3,5-TIPB at 550℃ (Smaller scale)

From Figure 97 and Figure 98, the model does not fit benzene and cumene. The Thiele moduli obtained are summarized in Table 31.

Table 31: Values of Thiele moduli for reaction set 7 model at 550℃

φ_1	0.9834
φ_2	5.8982
φ_3	2.5172
Λ	5.0001

6.3.6 Discussion:

Seven different reaction set were used to describe the 1,3,5-TIPB data in Figure 7 at 400℃ and in Figure 8 at 550℃. Table 32 summarizes the sum of squares of errors of the models at 400℃. From Table 32 the best model to describe the data is reaction set 3 which assumes that 1,3-DIPB reacts to form benzene in addition to cumene. Reaction set 6 also provides a good fit.

Table 32: Sum of squares of error for the 1,3,5-TIPB data at 400℃

Model	Sum of squares of errors
Finite volume with reaction set 1	1.696
Finite volume with reaction set 2	1.5652
Finite volume with reaction set 3	1.4768
Finite volume with reaction set 4	1.656
Finite volume with reaction set 5	1.5279
Finite volume with reaction set 6	1.5144
Finite volume with reaction set 7	1.5820

Table 33 summarizes the sum of squares of errors of the models at 550℃. From the table, reaction sets 3, 4 and 5 are comparable but reaction set 4 which assumes a second order reaction for cumene gives the best results.

Table 33: Sum of squares of error for the 1,3,5-TIPB data at 550℃

Model	Sum of squares of errors
Finite volume with reaction set 1	1.5020
Finite volume with reaction set 2	1.5057
Finite volume with reaction set 3	1.4634
Finite volume with reaction set 4	1.4574
Finite volume with reaction set 5	1.4624
Finite volume with reaction set 6	1.5260
Finite volume with reaction set 7	1.6701

In general, the models fit all the components except benzene. The reaction sets where higher benzene is formed gave better results. The concavity of benzene can be corrected by letting benzene reacts to form light gases but this results in insufficient benzene. Other reaction sets should be examined to determine the best reaction set. The poor fit of benzene may also be a result of the assumed adsorption constant. If the adsorption parameters and the diffusivities were available, better fit may be obtained.

This chapter the Thiele moduli were found. If the diffusivities of the different components were available, the kinetic parameters would be easily calculated from the definitions of the Thiele moduli. The ratio of the bulk to solids volumes could be calculated if more information about the system were available. The optimized values for Λ were in the same range for all the reaction sets which suggests that the actual value is approximately 5.

According to Arrhenius equation, plotting ln k versus 1/T should give a straight line with negative slope. Figure 99 demonstrates the plot of ln φ versus 1/T for reaction set 1 which is equivalent to the plot of ln k versus 1/T. From the figure, the optimized Thiele moduli follow Arrhenius equation with E_1 = 15545.5 J/mol, E_2 = 20770.9 J/mol and E_3 = 37637.5 J/mol.

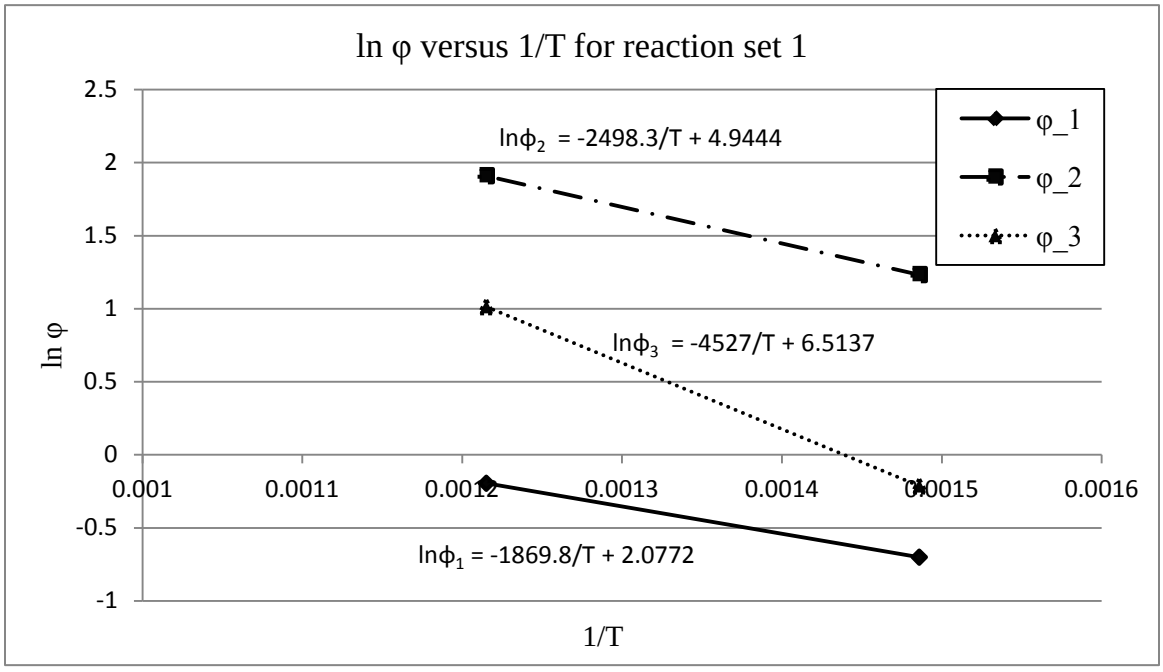

Figure 99: Plot of ln φ versus 1/T for reaction set 1

Chapter 7. Conclusions

The objective of this thesis was to study the reactions, adsorption and diffusion processes in FCC catalyst. The effects of different parameters on catalytic cracking were studied. First, the isothermal reactions, adsorption and diffusion were studied for different resistances. Second, the nonisothermal reactions, adsorption and diffusion were considered for two cases, negligible and controlling external heat resistance. Finally, isothermal reactions, adsorption and diffusion in active matrix were studied. Different resistances were applied to the system and the effect of each parameter was studied.

It was found that for an isothermal process the conversion is higher for higher Thiele modulus, lower degree of nonlinearity, higher Biot number and lower ratio of bulk to solids volumes. Moreover, it was concluded that thermal resistances affect the conversion and thermal effects should be consider. Diffusion and adsorption processes occur simultaneously in the macropore and micropore. Macropore processes slow the diffusion and thus reducing the conversion. If external fluid film resistance exists simultaneously with macropore and micropore diffusion, the conversion will be further reduced.

The models developed were applied to a four lump gas oil data and to 1,3,5-TIPB data at two different temperatures. The finite volume model with external fluid film resistance fits the gas oil data. For 1,3,5-TIPB, different reaction sets were considered but all sets did not give a satisfactory fit. Other reaction sets should be examined.

To obtain better fits and model the catalytic cracking of 1,3,5-TIPB, the diffusivities and the adsorption constants should be measured experimentally.

References

[1] J. H. Gary, G. E. Handwerk and M. J. Kaiser, Petroleum Refining: Technology and Economics, 5th ed., New York: CRC Press, 2007.

[2] J. Atias, *Adsorption, Diffusion and Reaction in FCC Catalysts*, PhD, The university of Westren Ontario, Ontario, Canada, 2004.

[3] L. Lee, Y. Chen and T. Huang, "Four-lump Kinetic Model for Fluid Catalytic Cracking Process," *The Canadian Journal of Chemical Engineering* , vol. 67, pp. 615-619, 1989.

[4] J. Ancheyta-Juarez, F. Lopez-Isunza, E. Aguilar-Rodriguez and J. Moreno-Mayorga, "A Strategy for Kinetic Parameter Estimation in the FluidCatalytic Cracking Process," *Industrial & Engineering Chemistry Research* , vol. 36, pp. 5170-5174, 1997.

[5] P. B. Venuto and T. Habib, Fluid Catalytic Cracking with Zeolite Catalysts, vol. 1, New York: Marcel Dekker, 1979.

[6] S. Zaman, K. F. Loughlin and S. A. Al-Khattaf, "Kinetics of desorption of 1,3 di-isopropyl benzene and 1,3,5 tri-isopropyl benzene. 2. Diffusion in FCC Catalyst Particles by Zero Length Column Method," *Industrial Engineering and Chemistry Research,* 2012.

[7] J. Scherzer, Octane-Enhancing Zeolitic FCC Catalysts, New York: Marcel Dekker, 1990.

[8] D. M. Ruthven, Principles of Adsorption and Adsorption Processes, New York: Wiely-Interscience, 1984.

[9] S. Bhatia, Zeolite Catalysis: Principles and Applications, Boca Raton: CRC Press Inc., 1990.

[10] J. W. Wilson, Fluid Catalytic Cracking, Tulsa, Oklahoma: Pennwell Books, 1997.

[11] A. Corma and F. Ortega, "Influence of Adsorption Parameters on Catalytic Cracking and Catalyst Decay," *Journal of Catalysis*, vol. 233, pp. 257-265, 2005.

[12] J. A. Atias and H. de Lasa, "Adsorption and Catalytic Reaction in FCC Catalysts Using a Novel Fluidized CREC Riser Simulator," *Chemical Engineering Science*, vol. 59, pp. 5663-5669, 2004.

[13] C. M. Bidabehere and U. Sedran, "Simultaneous Diffusion, Adsorption, and Reaction in Fluid Catalytic," *Industrial & Engineering Chemistry Research*, vol. 40, pp. 530-535, 2001.

[14] P. J. Barrie, C. K. Lee and L. F. Gladden, "Adsorption and desorption kinetics of hydrocarbons in FCC catalysts studiedusing a taperedelement oscillating microbalance (TEOM). Part 2: numerical simulations," *Chemical Engineering Science*, vol. 59, p. 1139 – 1151, 2004.

[15] A. Shichi, A. Satsuma, M. Iwase, K. Shimizu, S. Komai and T. Hatorri, "Catalyst Effectiveness Factor of Cobalt-Exchanged Modenites for the Selective Catalytic Reduction of NO with Hydrocarbons," *Applied Catalysis* , vol. 17, pp. 107-113, 1998.

[16] B. Gates, J. Katzer and G. Schuit, Chemistry of Catalytic Processes, New York: Mc-Graw-Hill, 1979.

[17] S. Al-Khattaf and H. I. de Lasa, "Diffusion and Reactivity of Gas Oil in FCC Catalysts," *The Canadian Journal of Chemical Engineering* , vol. 79, pp. 341-348, 2001.

[18] S. Al-Khattaf and H. I. de Lasa, "Activity and Selectivity of Fluidized Catalytic Cracking in a Riser Simulator: The role of Y-Zeolite Crystal Size," *Industrial & Engineering Chemistry Research* , vol. 38, pp. 1350-1356, 1999.

[19] J. Garcia-Martinez, M. Johnson, J. Valla, K. Li and J. Y. Ying, "Mesostructured Zeolite Y—High Hydrothermal Stability and Superior FCC Catalytic Performance," *Catalysis Science & Technology,* vol. 2, no. 5, pp. 987-994, 2012.

[20] V. W. Weekman and D. M. Nace, "Kinetics of Catalytic Cracking Selectivity in Fixed, Moving and Fluid Bed reactors," *AlCHE,* vol. 16, no. 3, pp. 397-404, 1970.

[21] G. M. Bollas, A. A. Lappas, D. K. Iatridis and I. A. Vasalos, "Five-lupm Kinetics Model with Selective Catalyst Deactviation for the Prediction of the Product Selectivity in the fluid Catalytic Cracking Process," *Catalysis Today,* vol. 127, pp. 31-43, 2007.

[22] G. Puente, A. AÄ vila, G. Chiovetta, W. Martignoni, H. Cerqueira and U. Sedran, "Adsorption of Hydrocarbons on FCC Catalysts under Reaction Conditions," *Industrial & Engineering Chemistry Research* , vol. 44, pp. 3879-3886, 2005.

[23] A. M. Avila, C. M. Bidabehere and U. Sedran, "Diffusion and adsorption selectivities of hydrocarbons over FCC catalysts," *Chemical Engineering Journal,* vol. 132, pp. 67-75, 2007.

[24] S. Al-Khattaf, J. A. Atias, K. Jarosch and H. de Lasa, "Diffusion and Catalytic Cracking of 1,3,5 tri-iso-propyl-benzene in FCC Catalysts," *Chemical Engineering Science,* vol. 57, pp. 4909-4920, 2002.

[25] J. A. Atias, G. Tonetto and H. de Lasa, "Catalytic Conversion of 1,2,4-Trimethylbenzene in a CREC Riser Simulator. A Heterogeneous Model with Adsorption and Reaction Phenomena," *Industrial & Engineering Chemistry Research* , vol. 42, pp. 4162-4173, 2003.

[26] M. Al-Sabawi and H. de Lasa, "Kinetic Modeling of Catalytic Conversion of Methylcyclohexane over USY zeolites: Adsorption and Reaction Phenomena," *AICHE ,* vol. 55, no. 6, pp. 1538 - 1558, 2009.

[27] K. Pashikanti and Y. A. Liu, "Predictive Modeling of Large-Scale Integrated Refinery Reaction and Fractionation Systems from Plant Data: Part 2: Fluid Catalytic Cracking (FCC) Process," *American Chemical Society*, vol. 25, pp. 5298-5319, 2011.

[28] S. Al-Khattaf, *Diffusion and reaction of hydrocarbons in FCC catalysts*, PhD, The university of Westren Ontario, Ontario, Canada, 2000.

[29] H. Fogler, Elements of Chemical Reaction Engineering, 4th ed., New Jersey: Pearson Education International, 2006.

[30] G. F. Froment and K. B. Bischoff, Chemical Reactor Analysis and Design, New York: John Wiley & Sons, 1979.

[31] E. Kikuchi, T. Matsuda, Y. Morita and H. Fujiki, "Disproportionation of 1,2,4-trimethylbenzene Over Montmorillonite Pillared by Aluminium Oxide," *Applied Catalysis*, vol. 11, pp. 331-340, 1984.

[32] A. Ko and C. Kuo, "Isomerization and Disproportionation of 1,2,4-Trimethylbenzene over HY Zeolite," *Journal of the Chinese Chemical Society*, vol. 41, pp. 141-150, 1994.

[33] K. J. and D. Ruthven, Diffusion in Zeolites and Other Microporous Solids, New York: John Wiley & Sons, 1992.

[34] W. F. Ramirez, Computational Methods for Process Simulation, Boston: Butterworths, 1989.

[35] E. Ruckenstein, A. Vaidyanathan and G. Youngquist, "Sorption by solids with bidisperse pore structures," *Chemical Engineering Science*, vol. 26, pp. 1305-1318, 1971.

[36] S. Al-Khattaf and H. de Lasa, "The role of diffusion in alkyl-benzenes catalytic cracking," *Applied Catalysis, in press*, 2001.

Appendix A: Matlab files

A.1 Orthogonal collocation matrices:

A.1.1 N = 7:

```
A( 1, 1)= -.7915067E+01;
A( 2, 1)= -.1934611E+01;
A( 3, 1)=  .5573536E+00;
A( 4, 1)= -.2741722E+00;
A( 5, 1)=  .1820224E+00;
A( 6, 1)= -.1527397E+00;
A( 7, 1)=  .1653947E+00;
A( 8, 1)= -.3759492E+00;
A( 1, 2)=  .1385362E+02;
A( 2, 2)= -.4030368E+01;
A( 3, 2)= -.3477346E+01;
A( 4, 2)=  .1339336E+01;
A( 5, 2)= -.8155276E+00;
A( 6, 2)=  .6578083E+00;
A( 7, 2)= -.6989540E+00;
A( 8, 2)=  .1577742E+01;
A( 1, 3)= -.1113234E+02;
A( 2, 3)=  .9699160E+01;
A( 3, 3)= -.2770669E+01;
A( 4, 3)= -.4959143E+01;
A( 5, 3)=  .2324861E+01;
A( 6, 3)= -.1706730E+01;
A( 7, 3)=  .1740738E+01;
A( 8, 3)= -.3873008E+01;
A( 1, 4)=  .9797133E+01;
A( 2, 4)= -.6683369E+01;
A( 3, 4)=  .8872100E+01;
A( 4, 4)= -.2170676E+01;
A( 5, 4)= -.6962483E+01;
A( 6, 4)=  .3929682E+01;
A( 7, 4)= -.3663855E+01;
A( 8, 4)=  .7918509E+01;
A( 1, 5)= -.8574007E+01;
A( 2, 5)=  .5364485E+01;
A( 3, 5)= -.5482771E+01;
A( 4, 5)=  .9177989E+01;
A( 5, 5)= -.1838920E+01;
A( 6, 5)= -.1050468E+02;
A( 7, 5)=  .7618631E+01;
```

```
A( 8, 5)= -.1542207E+02;
A( 1, 6)=  .7174594E+01;
A( 2, 6)= -.4314945E+01;
A( 3, 6)=  .4013790E+01;
A( 4, 6)= -.5165678E+01;
A( 5, 6)=  .1047537E+02;
A( 6, 6)= -.1646759E+01;
A( 7, 6)= -.1930504E+02;
A( 8, 6)=  .3197945E+02;
A( 1, 7)= -.5373311E+01;
A( 2, 7)=  .3171022E+01;
A( 3, 7)= -.2831379E+01;
A( 4, 7)=  .3331064E+01;
A( 5, 7)= -.5254583E+01;
A( 6, 7)=  .1335198E+02;
A( 7, 7)= -.1541414E+01;
A( 8, 7)= -.8830468E+02;
A( 1, 8)=  .2169385E+01;
A( 2, 8)= -.1271375E+01;
A( 3, 8)=  .1118922E+01;
A( 4, 8)= -.1278719E+01;
A( 5, 8)=  .1889257E+01;
A( 6, 8)= -.3928556E+01;
A( 7, 8)=  .1568450E+02;
A( 8, 8)=  .6650000E+02;
B( 1, 1)= -.8012240E+02;
B( 2, 1)=  .2807094E+02;
B( 3, 1)= -.4693042E+01;
B( 4, 1)=  .1716107E+01;
B( 5, 1)= -.9435288E+00;
B( 6, 1)=  .7010818E+00;
B( 7, 1)= -.7066446E+00;
B( 8, 1)= -.4956928E+02;
B( 1, 2)=  .1023568E+03;
B( 2, 2)= -.1016347E+03;
B( 3, 2)=  .4871346E+02;
B( 4, 2)= -.1092035E+02;
B( 5, 2)=  .5050600E+01;
B( 6, 2)= -.3467560E+01;
B( 7, 2)=  .3365234E+01;
B( 8, 2)=  .2072473E+03;
B( 1, 3)= -.3281258E+02;
B( 2, 3)=  .9340608E+02;
B( 3, 3)= -.1265533E+03;
B( 4, 3)=  .7432725E+02;
B( 5, 3)= -.2037682E+02;
B( 6, 3)=  .1158863E+02;
```

```
B( 7, 3)= -.1036244E+02;
B( 8, 3)= -.5048137E+03;
B( 1, 4)=  .1681746E+02;
B( 2, 4)= -.2934898E+02;
B( 3, 4)=  .1041785E+03;
B( 4, 4)= -.1724846E+03;
B( 5, 4)=  .1209389E+03;
B( 6, 4)= -.4065484E+02;
B( 7, 4)=  .3037853E+02;
B( 8, 4)=  .1016295E+04;
B( 1, 5)= -.1032577E+02;
B( 2, 5)=  .1515830E+02;
B( 3, 5)= -.3189464E+02;
B( 4, 5)=  .1350571E+03;
B( 5, 5)= -.2701868E+03;
B( 6, 5)=  .2328926E+03;
B( 7, 5)= -.1053019E+03;
B( 8, 5)= -.1913059E+04;
B( 1, 6)=  .6851564E+01;
B( 2, 6)= -.9293627E+01;
B( 3, 6)=  .1619821E+02;
B( 4, 6)= -.4054313E+02;
B( 5, 6)=  .2079742E+03;
B( 6, 6)= -.5317986E+03;
B( 7, 6)=  .6407142E+03;
B( 8, 6)=  .3598063E+04;
B( 1, 7)= -.4470809E+01;
B( 2, 7)=  .5839029E+01;
B( 3, 7)= -.9376939E+01;
B( 4, 7)=  .1961263E+02;
B( 5, 7)= -.6087714E+02;
B( 6, 7)=  .4147902E+03;
B( 7, 7)= -.1709720E+04;
B( 8, 7)= -.5346663E+04;
B( 1, 8)=  .1705760E+01;
B( 2, 8)= -.2197010E+01;
B( 3, 8)=  .3427736E+01;
B( 4, 8)= -.6764920E+01;
B( 5, 8)=  .1842053E+02;
B( 6, 8)= -.8405150E+02;
B( 7, 8)=  .1151633E+04;
B( 8, 8)=  .2992500E+04;
```

A.1.2 N = 14:

```
A( 1, 1)= -.1458258E+02
A( 2, 1)= -.3331056E+01
A( 3, 1)=  .8669763E+00
A( 4, 1)= -.3671157E+00
A( 5, 1)=  .1977144E+00
A( 6, 1)= -.1239342E+00
A( 7, 1)=  .8664427E-01
A( 8, 1)= -.6600350E-01
A( 9, 1)=  .5406808E-01
A(10, 1)= -.4730611E-01
A(11, 1)=  .4414784E-01
A(12, 1)= -.4417165E-01
A(13, 1)=  .4825160E-01
A(14, 1)= -.6098845E-01
A(15, 1)=  .1476574E+00
A( 1, 2)=  .2580921E+02
A( 2, 2)= -.7330142E+01
A( 3, 2)= -.5505422E+01
A( 4, 2)=  .1821581E+01
A( 5, 2)= -.8971415E+00
A( 6, 2)=  .5383448E+00
A( 7, 2)= -.3671711E+00
A( 8, 2)=  .2754461E+00
A( 9, 2)= -.2233764E+00
A(10, 2)=  .1941055E+00
A(11, 2)= -.1802896E+00
A(12, 2)=  .1797991E+00
A(13, 2)= -.1959816E+00
A(14, 2)=  .2473956E+00
A(15, 2)= -.5986466E+00
A( 1, 3)= -.2148371E+02
A( 2, 3)=  .1760759E+02
A( 3, 3)= -.4930360E+01
A( 4, 3)= -.6935732E+01
A( 5, 3)=  .2616266E+01
A( 6, 3)= -.1418314E+01
A( 7, 3)=  .9187526E+00
A( 8, 3)= -.6688191E+00
A( 9, 3)=  .5321659E+00
A(10, 3)= -.4566254E+00
A(11, 3)=  .4204912E+00
A(12, 3)= -.4169001E+00
A(13, 3)=  .4526728E+00
A(14, 3)= -.5701279E+00
A(15, 3)=  .1378306E+01
```

```
A( 1, 4)=  .1997877E+02
A( 2, 4)= -.1279445E+02
A( 3, 4)=  .1523197E+02
A( 4, 4)= -.3744241E+01
A( 5, 4)= -.8121176E+01
A( 6, 4)=  .3345478E+01
A( 7, 4)= -.1947411E+01
A( 8, 4)=  .1341475E+01
A( 9, 4)= -.1033114E+01
A(10, 4)=  .8682405E+00
A(11, 4)= -.7886139E+00
A(12, 4)=  .7747305E+00
A(13, 4)= -.8361945E+00
A(14, 4)=  .1049477E+01
A(15, 4)= -.2533542E+01
A( 1, 5)= -.1901553E+02
A( 2, 5)=  .1113623E+02
A( 3, 5)= -.1015430E+02
A( 4, 5)=  .1435235E+02
A( 5, 5)= -.3044162E+01
A( 6, 5)= -.9288276E+01
A( 7, 5)=  .4093361E+01
A( 8, 5)= -.2527342E+01
A( 9, 5)=  .1838591E+01
A(10, 5)= -.1493897E+01
A(11, 5)=  .1328211E+01
A(12, 5)= -.1286868E+01
A(13, 5)=  .1376722E+01
A(14, 5)= -.1719049E+01
A(15, 5)=  .4141341E+01
A( 1, 6)=  .1817228E+02
A( 2, 6)= -.1018793E+02
A( 3, 6)=  .8392449E+01
A( 4, 6)= -.9013853E+01
A( 5, 6)=  .1416065E+02
A( 6, 6)= -.2587749E+01
A( 7, 6)= -.1058316E+02
A( 8, 6)=  .4938390E+01
A( 9, 6)= -.3216482E+01
A(10, 6)=  .2467274E+01
A(11, 6)= -.2120586E+01
A(12, 6)=  .2011868E+01
A(13, 6)= -.2124478E+01
A(14, 6)=  .2633121E+01
A(15, 6)= -.6324550E+01
A( 1, 7)= -.1731613E+02
A( 2, 7)=  .9470799E+01
```

```
A( 3, 7)= -.7409816E+01
A( 4, 7)=  .7151592E+01
A( 5, 7)= -.8505912E+01
A( 6, 7)=  .1442474E+02
A( 7, 7)= -.2271289E+01
A( 8, 7)= -.1214543E+02
A( 9, 7)=  .5975018E+01
A(10, 7)= -.4102994E+01
A(11, 7)=  .3330347E+01
A(12, 7)= -.3056995E+01
A(13, 7)=  .3165424E+01
A(14, 7)= -.3880803E+01
A(15, 7)=  .9281252E+01
A( 1, 8)=  .1638925E+02
A( 2, 8)= -.8827463E+01
A( 3, 8)=  .6701911E+01
A( 4, 8)= -.6120808E+01
A( 5, 8)=  .6525081E+01
A( 6, 8)= -.8362941E+01
A( 7, 8)=  .1509016E+02
A( 8, 8)= -.2043096E+01
A( 9, 8)= -.1415763E+02
A(10, 8)=  .7345724E+01
A(11, 8)= -.5342107E+01
A(12, 8)=  .4637518E+01
A(13, 8)= -.4655887E+01
A(14, 8)=  .5614634E+01
A(15, 8)= -.1334198E+02
A( 1, 9)= -.1535738E+02
A( 2, 9)=  .8188809E+01
A( 3, 9)= -.6099878E+01
A( 4, 9)=  .5392108E+01
A( 5, 9)= -.5429893E+01
A( 6, 9)=  .6230735E+01
A( 7, 9)= -.8491899E+01
A( 8, 9)=  .1619480E+02
A( 9, 9)= -.1874620E+01
A(10, 9)= -.1691271E+02
A(11, 9)=  .9306488E+01
A(12, 9)= -.7253978E+01
A(13, 9)=  .6908638E+01
A(14, 9)= -.8113788E+01
A(15, 9)=  .1908924E+02
A( 1,10)=  .1419173E+02
A( 2,10)= -.7515585E+01
A( 3,10)=  .5528095E+01
A( 4,10)= -.4786206E+01
```

```
A( 5,10)=  .4659801E+01
A( 6,10)= -.5047955E+01
A( 7,10)=  .6158939E+01
A( 8,10)= -.8874798E+01
A( 9,10)=  .1786288E+02
A(10,10)= -.1748960E+01
A(11,10)= -.2095749E+02
A(12,10)=  .1239839E+02
A(13,10)= -.1064923E+02
A(14,10)=  .1194168E+02
A(15,10)= -.2763270E+02
A( 1,11)= -.1285875E+02
A( 2,11)=  .6777462E+01
A( 3,11)= -.4942475E+01
A( 4,11)=  .4220739E+01
A( 5,11)= -.4022421E+01
A( 6,11)=  .4212394E+01
A( 7,11)= -.4853674E+01
A( 8,11)=  .6266336E+01
A( 9,11)= -.9543384E+01
A(10,11)=  .2034786E+02
A(11,11)= -.1655484E+01
A(12,11)= -.2748373E+02
A(13,11)=  .1803301E+02
A(14,11)= -.1841586E+02
A(15,11)=  .4133061E+02
A( 1,12)=  .1130829E+02
A( 2,12)= -.5940836E+01
A( 3,12)=  .4307067E+01
A( 4,12)= -.3644475E+01
A( 5,12)=  .3425407E+01
A( 6,12)= -.3512592E+01
A( 7,12)=  .3915870E+01
A( 8,12)= -.4781198E+01
A( 9,12)=  .6537929E+01
A(10,12)= -.1058012E+02
A(11,12)=  .2415566E+02
A(12,12)= -.1587582E+01
A(13,12)= -.3971571E+02
A(14,12)=  .3146670E+02
A(15,12)= -.6607241E+02
A( 1,13)= -.9448341E+01
A( 2,13)=  .4952974E+01
A( 3,13)= -.3577065E+01
A( 4,13)=  .3008756E+01
A( 5,13)= -.2803009E+01
A( 6,13)=  .2837161E+01
```

```
A( 7,13)= -.3101508E+01
A( 8,13)=  .3671679E+01
A( 9,13)= -.4762902E+01
A(10,13)=  .6951233E+01
A(11,13)= -.1212361E+02
A(12,13)=  .3037987E+02
A(13,13)= -.1540518E+01
A(14,13)= -.7044942E+02
A(15,13)=  .1209659E+03
A( 1,14)=  .7059351E+01
A( 2,14)= -.3695869E+01
A( 3,14)=  .2663101E+01
A( 4,14)= -.2232162E+01
A( 5,14)=  .2068883E+01
A( 6,14)= -.2078598E+01
A( 7,14)=  .2247647E+01
A( 8,14)= -.2617262E+01
A( 9,14)=  .3306459E+01
A(10,14)= -.4607519E+01
A(11,14)=  .7318328E+01
A(12,14)= -.1422754E+02
A(13,14)=  .4164187E+02
A(14,14)= -.1511951E+01
A(15,14)= -.3108305E+03
A( 1,15)= -.2846478E+01
A( 2,15)=  .1489467E+01
A( 3,15)= -.1072253E+01
A( 4,15)=  .8974623E+00
A( 5,15)= -.8300909E+00
A( 6,15)=  .8315093E+00
A( 7,15)= -.8952661E+00
A( 8,15)=  .1035823E+01
A( 9,15)= -.1295596E+01
A(10,15)=  .1775693E+01
A(11,15)= -.2735491E+01
A(12,15)=  .4975581E+01
A(13,15)= -.1190860E+02
A(14,15)=  .5176898E+02
A(15,15)=  .2310000E+03
B( 1, 1)= -.2660592E+03;
B( 2, 1)=  .8712673E+02;
B( 3, 1)= -.1286985E+02;
B( 4, 1)=  .3924229E+01;
B( 5, 1)= -.1678128E+01;
B( 6, 1)=  .8830355E+00;
B( 7, 1)= -.5378322E+00;
B( 8, 1)=  .3668056E+00;
```

```
B( 9, 1)= -.2748273E+00;
B(10, 1)=  .2238594E+00;
B(11, 1)= -.1974358E+00;
B(12, 1)=  .1893026E+00;
B(13, 1)= -.2005267E+00;
B(14, 1)=  .2485945E+00;
B(15, 1)=  .6806319E+02;
B( 1, 2)=  .3393299E+03;
B( 2, 2)= -.3116085E+03;
B( 3, 2)=  .1321852E+03;
B( 4, 2)= -.2460865E+02;
B( 5, 2)=  .8800615E+01;
B( 6, 2)= -.4243843E+01;
B( 7, 2)=  .2460065E+01;
B( 8, 2)= -.1627112E+01;
B( 9, 2)=  .1194799E+01;
B(10, 2)= -.9599679E+00;
B(11, 2)=  .8386706E+00;
B(12, 2)= -.7988686E+00;
B(13, 2)=  .8425721E+00;
B(14, 2)= -.1041884E+01;
B(15, 2)= -.2758693E+03;
B( 1, 3)= -.1078250E+03;
B( 2, 3)=  .2843533E+03;
B( 3, 3)= -.3362187E+03;
B( 4, 3)=  .1636078E+03;
B( 5, 3)= -.3432287E+02;
B( 6, 3)=  .1350864E+02;
B( 7, 3)= -.7063747E+01;
B( 8, 3)=  .4399361E+01;
B( 9, 3)= -.3109874E+01;
B(10, 3)=  .2436280E+01;
B(11, 3)= -.2092157E+01;
B(12, 3)=  .1969575E+01;
B(13, 3)= -.2061358E+01;
B(14, 3)=  .2537490E+01;
B(15, 3)=  .6348324E+03;
B( 1, 4)=  .5483393E+02;
B( 2, 4)= -.8829013E+02;
B( 3, 4)=  .2728681E+03;
B( 4, 4)= -.3661488E+03;
B( 5, 4)=  .1944769E+03;
B( 6, 4)= -.4419707E+02;
B( 7, 4)=  .1866225E+02;
B( 8, 4)= -.1040753E+02;
B( 9, 4)=  .6892169E+01;
B(10, 4)= -.5179572E+01;
```

```
B(11, 4)=  .4327347E+01;
B(12, 4)= -.3999417E+01;
B(13, 4)=  .4136030E+01;
B(14, 4)= -.5056061E+01;
B(15, 4)= -.1166017E+04;
B( 1, 5)= -.3369211E+02;
B( 2, 5)=  .4536756E+02;
B( 3, 5)= -.8225086E+02;
B( 4, 5)=  .2794320E+03;
B( 5, 5)= -.4073433E+03;
B( 6, 5)=  .2310720E+03;
B( 7, 5)= -.5592531E+02;
B( 8, 5)=  .2505588E+02;
B( 9, 5)= -.1480572E+02;
B(10, 5)=  .1040042E+02;
B(11, 5)= -.8325884E+01;
B(12, 5)=  .7484065E+01;
B(13, 5)= -.7604073E+01;
B(14, 5)=  .9201000E+01;
B(15, 5)=  .1903834E+04;
B( 1, 6)=  .2297648E+02;
B( 2, 6)= -.2835268E+02;
B( 3, 6)=  .4195376E+02;
B( 4, 6)= -.8230077E+02;
B( 5, 6)=  .2994675E+03;
B( 6, 6)= -.4653790E+03;
B( 7, 6)=  .2791462E+03;
B( 8, 6)= -.7143401E+02;
B( 9, 6)=  .3383569E+02;
B(10, 6)= -.2118331E+02;
B(11, 6)=  .1584762E+02;
B(12, 6)= -.1365840E+02;
B(13, 6)=  .1352055E+02;
B(14, 6)= -.1611922E+02;
B(15, 6)= -.2902800E+04;
B( 1, 7)= -.1674152E+02;
B( 2, 7)=  .1966184E+02;
B( 3, 7)= -.2624444E+02;
B( 4, 7)=  .4157356E+02;
B( 5, 7)= -.8670689E+02;
B( 6, 7)=  .3339448E+03;
B( 7, 7)= -.5486474E+03;
B( 8, 7)=  .3467279E+03;
B( 9, 7)= -.9369584E+02;
B(10, 7)=  .4700961E+02;
B(11, 7)= -.3136630E+02;
B(12, 7)=  .2530465E+02;
```

```
B(13, 7)= -.2408627E+02;
B(14, 7)=  .2809753E+02;
B(15, 7)=  .4249920E+04;
B( 1, 8)=  .1276084E+02;
B( 2, 8)= -.1453417E+02;
B( 3, 8)=  .1826784E+02;
B( 4, 8)= -.2591175E+02;
B( 5, 8)=  .4341613E+02;
B( 6, 8)= -.9550900E+02;
B( 7, 8)=  .3875121E+03;
B( 8, 8)= -.6715556E+03;
B( 9, 8)=  .4476009E+03;
B(10, 8)= -.1282092E+03;
B(11, 8)=  .6867200E+02;
B(12, 8)= -.4954894E+02;
B(13, 8)=  .4433744E+02;
B(14, 8)= -.5004144E+02;
B(15, 8)= -.6088222E+04;
B( 1, 9)= -.1003496E+02;
B( 2, 9)=  .1120160E+02;
B( 3, 9)= -.1355353E+02;
B( 4, 9)=  .1801013E+02;
B( 5, 9)= -.2692665E+02;
B( 6, 9)=  .4748158E+02;
B( 7, 9)= -.1099075E+03;
B( 8, 9)=  .4697875E+03;
B( 9, 9)= -.8609489E+03;
B(10, 9)=  .6086882E+03;
B(11, 9)= -.1866590E+03;
B(12, 9)=  .1085736E+03;
B(13, 9)= -.8743163E+02;
B(14, 9)=  .9359407E+02;
B(15, 9)=  .8664217E+04;
B( 1,10)=  .8054045E+01;
B( 2,10)= -.8868019E+01;
B( 3,10)=  .1046221E+02;
B( 4,10)= -.1333658E+02;
B( 5,10)=  .1863788E+02;
B( 6,10)= -.2929138E+02;
B( 7,10)=  .5433652E+02;
B( 8,10)= -.1325957E+03;
B( 9,10)=  .5997844E+03;
B(10,10)= -.1171701E+04;
B(11,10)=  .8896512E+03;
B(12,10)= -.2980970E+03;
B(13,10)=  .1952455E+03;
B(14,10)= -.1905418E+03;
```

```
B(15,10)= -.1243116E+05;
B( 1,11)= -.6528729E+01;
B( 2,11)=  .7120702E+01;
B( 3,11)= -.8257508E+01;
B( 4,11)=  .1024063E+02;
B( 5,11)= -.1371275E+02;
B( 6,11)=  .2013976E+02;
B( 7,11)= -.3332029E+02;
B( 8,11)=  .6527207E+02;
B( 9,11)= -.1690381E+03;
B(10,11)=  .8176258E+03;
B(11,11)= -.1730821E+04;
B(12,11)=  .1446308E+04;
B(13,11)= -.5528016E+03;
B(14,11)=  .4474336E+03;
B(15,11)=  .1829534E+05;
B( 1,12)=  .5274099E+01;
B( 2,12)= -.5714874E+01;
B( 3,12)=  .6550076E+01;
B( 4,12)= -.7975214E+01;
B( 5,12)=  .1038716E+02;
B( 6,12)= -.1462766E+02;
B( 7,12)=  .2265411E+02;
B( 8,12)= -.3969142E+02;
B( 9,12)=  .8286732E+02;
B(10,12)= -.2308986E+03;
B(11,12)=  .1218966E+04;
B(12,12)= -.2890633E+04;
B(13,12)=  .2800797E+04;
B(14,12)= -.1364483E+04;
B(15,12)= -.2825877E+05;
B( 1,13)= -.4147025E+01;
B( 2,13)=  .4474197E+01;
B( 3,13)= -.5088715E+01;
B( 4,13)=  .6122344E+01;
B( 5,13)= -.7834170E+01;
B( 6,13)=  .1074877E+02;
B( 7,13)= -.1600692E+02;
B( 8,13)=  .2636478E+02;
B( 9,13)= -.4953561E+02;
B(10,13)=  .1122626E+03;
B(11,13)= -.3458515E+03;
B(12,13)=  .2079085E+04;
B(13,13)= -.5961463E+04;
B(14,13)=  .7703550E+04;
B(15,13)=  .4694333E+05;
B( 1,14)=  .2982976E+01;
```

```
B( 2,14)= -.3210042E+01;
B( 3,14)=  .3634329E+01;
B( 4,14)= -.4342000E+01;
B( 5,14)=  .5499339E+01;
B( 6,14)= -.7434063E+01;
B( 7,14)=  .1083210E+02;
B( 8,14)= -.1726170E+02;
B( 9,14)=  .3076061E+02;
B(10,14)= -.6355365E+02;
B(11,14)=  .1623842E+03;
B(12,14)= -.5875628E+03;
B(13,14)=  .4468752E+04;
B(14,14)= -.1973948E+05;
B(15,14)= -.6536470E+05;
B( 1,15)= -.1183707E+01;
B( 2,15)=  .1272471E+01;
B( 3,15)= -.1437978E+01;
B( 4,15)=  .1713087E+01;
B( 5,15)= -.2160719E+01;
B( 6,15)=  .2903542E+01;
B( 7,15)= -.4194394E+01;
B( 8,15)=  .6598863E+01;
B( 9,15)= -.1152701E+02;
B(10,15)=  .2303830E+02;
B(11,15)= -.5537316E+02;
B(12,15)=  .1753841E+03;
B(13,15)= -.8919824E+03;
B(14,15)=  .1308210E+05;
B(15,15)=  .3572800E+05;
```

A.2 Linear infinite volume:

Function file:

```
function dq=Linearinfinitevolume(t,q,h)
qa=q(1:7);
qb=q(8:14);
for i=1:7
    for j=1:7
    n=8; m=8;
    qa(8)=1;
    dqa(i)=(sum(B(i,1:n).*qa(1:n)'))-h^2*qa(i);
    qb(8)=0;
    dqb(j)=(sum(B(j,1:m).*qb(1:m)'))+h^2*qa(j);
    end
end
dqa=dqa';
dqb=dqb';
dq=[dqa;dqb];
```

Script File:

```
tspan=[0 1];
q0=zeros(1,14);
h=0.1;
[t,q]=ode15s(@Linearinfinitevolume,tspan,q0,[],h);
% weight frations:
          W(1)=  .6723835E-02;
          W(2)=  .2451753E-01;
          W(3)=  .4701138E-01;
          W(4)=  .6589205E-01;
          W(5)=  .7358414E-01;
          W(6)=  .6571099E-01;
          W(7)=  .4254046E-01;
          W(8)=  .7352941E-02;
n=7;
W8=W(8);
W1=W(1:n);
q1=q(:,1:7);
m1=3*(W1*q1'+W8);
q2=q(:,8:14);
m2=3*(W1*q2');
plot(t,m1,'-k')
```

A.3 Nonlinear infinite volume:

Function file:

```
function dq=Nonlinearinfinitevolume(t,q,h,L)
qa=q(1:7);
qb=q(8:14);
for i=1:7
    for j=1:7
    n=8; m=8;
    qa(8)=1;
    dqa(i)=(1/(1-
(L*qa(i)))).*(sum(B(i,1:n).*qa(1:n)'))+(L/((1-
(L*qa(i)))^2)).*(sum(A(i,1:n).*qa(1:n)')).^2-h^2*qa(i);
    qb(8)=0;
    dqb(j)=(1/(1-
(L*qb(j)))).*(sum(B(j,1:m).*qb(1:m)'))+(L/((1-
(L*qb(j)))^2)).*(sum(A(j,1:m).*qb(1:m)')).^2+h^2*qa(j);
    end
end
dqa=dqa';
dqb=dqb';
dq=[dqa;dqb];
```

Script file:

```
tspan=[0 1];

q0=zeros(1,14);
h=5;
L =0.5;
[t,q]=ode15s(@Nonlinearinfinitevolume,tspan,q0,[],h,L);
%weight fractions
          W( 1)=  .6723835E-02;
          W( 2)=  .2451753E-01;
          W( 3)=  .4701138E-01;
          W( 4)=  .6589205E-01;
          W( 5)=  .7358414E-01;
          W( 6)=  .6571099E-01;
          W( 7)=  .4254046E-01;
          W( 8)=  .7352941E-02;
n=7;
W8=W(8);
W1=W(1:n);
q1=q(:,1:7);
m1=3*(W1*q1'+W8);
```

```
q2=q(:,8:14);
m2=3*(W1*q2');
plot(t,m1,'-k')
```

A.4 Linear infinite with Biot number

Function file:

```
function dq=Biotinfinitevolume(t,q,h,Bi)
qa=q(1:8);
qb=q(9:15);
for i=1:8
    for j=1:7
    n=7; m=8;
    dqa(i)=(sum(B(i,1:n).*qa(1:n)')+B(i,n+1)*(Bi-
(sum(A(n+1,1:n).*qa(1:n)')))/(A(n+1,n+1)+Bi))-qa(i)*h^2;
    qb(8)=0;
    dqb(j)=(sum(B(j,1:m).*qb(1:m')))+h^2*qa(j);
    end
end
dqa=dqa';
dqb=dqb';
dq=[dqa;dqb];
```

Script file:

```
tspan=[0 1];
q0=zeros(1,15);
h=5;
Bi=100;
[t,q]=ode15s(@Biotinfinitevolume,tspan,q0,[],h,Bi);
% weight frations:
          W(1)=  .6723835E-02;
          W(2)=  .2451753E-01;
          W(3)=  .4701138E-01;
          W(4)=  .6589205E-01;
          W(5)=  .7358414E-01;
          W(6)=  .6571099E-01;
          W(7)=  .4254046E-01;
          W(8)=  .7352941E-02;
n=7;
W8=W(8);
W1=W(1:n);
q1=q(:,1:7);
```

```
global A
q8=(Bi-((A(8,1:7)*q1(:,1:7)')))/(A(8,8)+Bi);
m1=3*(W1*q1'+W8*q8);
q2=q(:,8:14);
m2=3*(W1*q2');
plot(t,m1,'-k');
```

A.5 Linear finite volume:

Function file:

```
function dq=limitingvolume(t,q,h,alpha)


qai=q(1:7);
qa8=q(8);
qa=q(1:8);
qbi=q(9:15);
qb8=q(16);
qb=q(9:16);
for i=1:7
    n=8;
% reactant A
         dqa8=-(3/alpha)*(sum(A(n,1:n).* qa(1:n)'));
           if t==0
               qa8=1;
           else

qa8=(dqa8+(3/alpha)*(sum(A(n,1:i).*qai(1:i)')))/(-
3*A(8,8)/alpha)
           end
           dqai(i)=(sum(B(i,1:n).*qa(1:n'))-h^2*qai(i);
% product B
         dqb8=-(3/alpha)*(sum(A(n,1:n).* qb(1:n)'));
           if t==0
               qb(8)=0;
           else

qb8=(dqb8+(3/alpha)*(sum(A(n,1:i).*qbi(1:i)')))/(-
3*A(8,8)/alpha);
           end
           dqbi(i)=(sum(B(i,1:n).*qb(1:n'))+h^2*qai(i);
end
dqai=dqai';
dqa8=dqa8';
```

```
dqbi=dqbi';
dqb8=dqb8';
dq=[dqai;dqa8;dqbi;dqb8];
```

Script file:

```
tspan=[0 1];
q0=[zeros(1,7),1,zeros(1,8)];
h=0;
alpha=10;
[t,q]=ode15s(@limitingvolume,tspan,q0,[],h,alpha);
% weight frations:
          W(1)=  .6723835E-02;
          W(2)=  .2451753E-01;
          W(3)=  .4701138E-01;
          W(4)=  .6589205E-01;
          W(5)=  .7358414E-01;
          W(6)=  .6571099E-01;
          W(7)=  .4254046E-01;
          W(8)=  .7352941E-02;
n=8;
W1=W(1:7);
W=W(1:n);
q1=q(:,1:8);
m1=3*(W*q1');
q2=q(:,9:16);
m2=3*(W*q2');
plot(t,m1,'-k')
```

A.6 Finite volume with Biot number:

Function file:

```
function dq=limitingvolumewithproductBi23(t,q,h,alpha,Bi)
qa=q(1:8);
qai=qa(1:7);
qa8=qa(8);
qbj=q(9:15);
qb8=q(16);
qb=q(9:16);
for i=1:7
    for j=1:7
        n=8; m=8;
           if t==0
               qa(8)=1;
```

```
            else
            qa(8)=(Bi-
(sum(A(8,1:7).*qa(1:7)'')))/(A(8,8)+Bi);
            end
          dqa8=(-3/alpha)*(sum(A(n,1:n).* qa(1:n)''));
            dqai(i)=(sum(B(i,1:n).*qa(1:n)''))-h^2*qai(i);
% product b
             dqb8=-(3/alpha)*(sum(A(m,1:m).* qb(1:m)''));
            if t==0
                qb(8)=0;
            else

qb(8)=(dqb8+(3/alpha)*(sum(A(m,1:j).*qbj(1:j)'')))/(-
3*A(8,8)/alpha);
            end
            dqbj(j)=(sum(B(j,1:m).*qb(1:m)''))+h^2*qai(j);
    end
end
dqai=dqai';
dqa8=dqa8';
dqbj=dqbj';
dqb8=dqb8';
dq=[dqai;dqa8;dqbj;dqb8];
```

Script file:

```
tspan=[0 1];
q0=[zeros(1,7),1,zeros(1,8)];
alpha=100;
h=5;
[t,q]=ode15s(@limitingvolumewithproductwthphi,tspan,q0,[],h
,alpha);
% weight frations:
          W(1)=  .6723835E-02;
          W(2)=  .2451753E-01;
          W(3)=  .4701138E-01;
          W(4)=  .6589205E-01;
          W(5)=  .7358414E-01;
          W(6)=  .6571099E-01;
          W(7)=  .4254046E-01;
          W(8)=  .7352941E-02;
n=8;
W=W(1:n);
q1=q(:,1:8);
m1=3*(W*q1');
q2=q(:,9:16);
m2=3*(W*q2');
```

```
plot(t,m2,'-k')
```

A.7 Deactivation function:

Function file:

```
function dq=limitingvolumewithproductwthphi(t,q,h,alpha)
qai=q(1:7);
qa8=q(8);
qa=q(1:8);
qbi=q(9:15);
qb8=q(16);
qb=q(9:16);
for i=1:7
        n=8;
% reactant A
            dqa8=-(3/alpha)*(sum(A(n,1:n).* qa(1:n)'));
            dqb8=-(3/alpha)*(sum(A(n,1:n).* qb(1:n)'));
           if t==0
               qa8=1;
               qb8=0;
               ya(i)=1;
           else

qa8=(dqa8+(3/alpha)*(sum(A(n,1:i).*qai(1:i)')))/(-
3*A(8,8)/alpha);

qb8=(dqb8+(3/alpha)*(sum(A(n,1:i).*qbi(1:i)')))/(-
3*A(8,8)/alpha);
                ya(i)=qa(i)/(qa(i)+qb(i));
           end
           phi(i)=exp(-6.03*(1-ya(i)));
           dqai(i)=(sum(B(i,1:n).*qa(1:n)'))-
h^2*phi(i)*qai(i);

dqbi(i)=(sum(B(i,1:n).*qb(1:n)'))+h^2*phi(i)*qai(i);
end
dqai=dqai';
dqa8=dqa8';
dqbi=dqbi';
dqb8=dqb8';
dq=[dqai;dqa8;dqbi;dqb8];
```

Script file:

```
tspan=[0 1];
q0=[zeros(1,7),1,zeros(1,8)];
alpha=100;
h=5;
[t,q]=ode15s(@limitingvolumewithproductwthphi,tspan,q0,[],h
,alpha);
% weight frations:
          W(1)=  .6723835E-02;
          W(2)=  .2451753E-01;
          W(3)=  .4701138E-01;
          W(4)=  .6589205E-01;
          W(5)=  .7358414E-01;
          W(6)=  .6571099E-01;
          W(7)=  .4254046E-01;
          W(8)=  .7352941E-02;
n=8;
W=W(1:n);
q1=q(:,1:8);
m1=3*(W*q1');
q2=q(:,9:16);
m2=3*(W*q2');
plot(t,m2,'-k')
```

A.8 Nonisothermal linear infinite volume:

Function file:

```
function dq=nonisothermal(t,q,h,alpha,Bi,Le,yad,yrxn)
qa=q(1:8);
qb=q(9:16);
T=q(17:23);
        n=8; m=8;
        for i=1:7
           if t==0
               qa(8)=1;
           else
           qa(8)=(Bi-
(sum(A(8,1:7).*qa(1:7)')))/(A(8,8)+Bi);
           end
         dqa(8)=(-3/alpha)*(sum(A(n,1:n).* qa(1:n)'));
           dqa(i)=(sum(B(i,1:n).*qa(1:n)'))-h^2*qa(i);
        end
% product b
        for j=1:7
            dqb(8)=-(3/alpha)*(sum(A(m,1:m).* qb(1:m)'));
```

```
            if t==0
                qb(8)=0;
            else

qb(8)=(dqb(8)+(3/alpha)*(sum(A(m,1:7).*qb(1:7)')))/(-
3*A(8,8)/alpha);
            end
            dqb(j)=(sum(B(j,1:m).*qb(1:m)'))+h^2*qa(j);
        end
    for g=1:7
% Temperature
             T(8)=1;

dT(g)=Le*(sum(B(g,1:8).*T(1:8)'))+yad*dqa(g)+yrxn*h^2*qa(g)
;
    end
dq=[dqa';dqb';dT'];
```

Script file:

```
clc;
tspan=[0 0.1];
q0=[zeros(1,16),ones(1,7)];
h=5;
Bi=100;
yad=0.001;
yrxn=-0.02;
alpha=100;
Le=2;
[t,q]=ode15s(@nonisothermal,tspan,q0,[],h,alpha,Bi,Le,yad,y
rxn);
          W(1)=  .6723835E-02;
          W(2)=  .2451753E-01;
          W(3)=  .4701138E-01;
          W(4)=  .6589205E-01;
          W(5)=  .7358414E-01;
          W(6)=  .6571099E-01;
          W(7)=  .4254046E-01;
          W(8)=  .7352941E-02;
n=8;
W8=W(8);
W1=W(1:n);
W2=W(1:7);
qa=q(:,1:8);
m1=3*(W1*qa');
qb=q(:,9:16);
```

```
m2=3*(W1*qb');
T=q(:,17:23);
T1=3*(W2*T'+W8);
plot(t,m1,'-k',t,m2,'--k');
```

A.9 Nonisothermal with Biot number:

Function file:

```
function
dq=nonisothermalwithBi(t,q,h,alpha,Bim,Le,yad,yrxn,Bi)
qa=q(1:8);
qb=q(9:16);
T=q(17:23);
        n=8; m=8;
        for i=1:7
           if t==0
               qa(8)=1;
           else
           qa(8)=(Bim-
(sum(A(8,1:7).*qa(1:7)')))/(A(8,8)+Bim);
           end
         dqa(8)=(-3/alpha)*(sum(A(n,1:n).* qa(1:n)'));
           dqa(i)=(sum(B(i,1:n).*qa(1:n)'))-h^2*qa(i);
        end
% product b
        for j=1:7
            dqb(8)=-(3/alpha)*(sum(A(m,1:m).* qb(1:m)'));
           if t==0
               qb(8)=0;
           else

qb(8)=(dqb(8)+(3/alpha)*(sum(A(m,1:7).*qb(1:7)')))/(-
3*A(8,8)/alpha);
           end
           dqb(j)=(sum(B(j,1:m).*qb(1:m)'))+h^2*qa(j);
        end
    for g=1:7
% Temperature
            T(8)=(Bi-sum(A(8,1:7).*T(1:7)'))/(A(8,8)+Bi);

dT(g)=Le*(sum(B(g,1:8).*T(1:8)'))+yad*dqa(g)+yrxn*h^2*qa(g)
;
    end
dq=[dqa';dqb';dT'];
```

Script file:

```
tspan=[0 1];
q0=[zeros(1,16),ones(1,7)];
h=5;
Bim=100;
yad=0.001;
yrxn=-0.02;
Le=2;
alpha=100;
Bi=100;
[t,q]=ode15s(@nonisothermalwithBi,tspan,q0,[],h,alpha,Bim,L
e,yad,yrxn,Bi);
          W(1)=  .6723835E-02;
          W(2)=  .2451753E-01;
          W(3)=  .4701138E-01;
          W(4)=  .6589205E-01;
          W(5)=  .7358414E-01;
          W(6)=  .6571099E-01;
          W(7)=  .4254046E-01;
          W(8)=  .7352941E-02;
n=8;
W8=W(8);
W1=W(1:n);
W2=W(1:7);
qa=q(:,1:8);
m1=3*(W1*qa');
qb=q(:,9:16);
m2=3*(W1*qb');
T8=(Bi-A(8,1:7)*T(:,1:7)')/(A(8,8)+Bi);
T=q(:,17:23);
T1=3*(W2*T'+W8*T8);
%subplot(1,2,1);plot(t,m1,'b',t,m2,'r');
title('Concentration profile')
xlabel('Dimensionless time')
ylabel('Dimensionless concentration')
plot(t,T1,'-k');
```

A.10 Active matrix with infinite volume

Function file:

```
function dq=macrorxn(t,q,alpha,Beta,ba,h)
qa=q(1:7);
Ca=q(8:14);
qb=q(15:21);
Cb=q(22:28);
       Ca(8)=1;
       Cb(8)=0;
for i=1:7
        qa(8)=3*(sum(W(1:8).*Ca(1:8)'));
        qb(8)=3*(sum(W(1:8).*Cb(1:8)'));
        mt(i)=(Ca(i)+1/3*ba*qa(i))/(1+1/3*ba);
        dqa(i)=alpha*(sum(B(i,1:8).*qa(1:8)'))-h^2*mt(i);
        dqb(i)=alpha*(sum(B(i,1:8).*qb(1:8)'))+h^2*mt(i);
        dCa(i)=sum(B(i,1:8).*Ca(1:8)')-
Beta*(sum(A(8,1:8).*qa(1:8)'));
        dCb(i)=sum(B(i,1:8).*Cb(1:8)')-
Beta*(sum(A(8,1:8).*qb(1:8)'));
end
dq=[dqa';dCa';dqb';dCb'];
```

Script file:

```
clc;
tspan=[0 1];
alpha=1e3;
ba=0.1;
Beta=ba*alpha;
h=5;
q0=zeros(1,28);
[t,q]=ode15s(@macrorxn,tspan,q0,[],alpha,Beta,ba,h);
% weight frations:
          W(1)=  .6723835E-02;
          W(2)=  .2451753E-01;
          W(3)=  .4701138E-01;
          W(4)=  .6589205E-01;
          W(5)=  .7358414E-01;
          W(6)=  .6571099E-01;
          W(7)=  .4254046E-01;
          W(8)=  .7352941E-02;
W8=W(8);
W2=W(1:7);
Ca=q(:,8:14);
m2=3*(W2*Ca'+W8);
qa=q(:,1:7);
m1=3*(W2*qa'+W8*m2);
ma=(m2+1/3*ba*m1)/(1+1/3*ba);
```

```
qb=q(:,15:21);
Cb=q(:,22:28);
m4=3*(W2*Cb');
m3=3*(W2*qb'+W8*m4);
mb=(m4+1/3*ba*m3)/(1+1/3*ba);
plot(t,ma,t,mb,'--')
```

A.11 Active matrix with finite volume and Biot number

Function file:

```
function dq=macrorxnlimitedBi(t,q,alpha,Beta,ba,h,v,Bi)
qa=q(1:7);
Ca=q(8:15);
Cai=q(8:14);
Ca8=q(15);
qb=q(16:22);
Cb=q(23:30);
Cbi=q(23:29);
Cb8=q(30);
for i=1:7
    %Reactant A
        qa(8)=3*(sum(W(1:8).*Ca(1:8)'));
           if t==0
               Ca(8)=1;
           else
           Ca(8)=(Bi-
(sum(A(8,1:7).*Ca(1:7')))/(A(8,8)+Bi);
           end
         dCa8=(-3/v)*(sum(A(8,1:8).* Ca(1:8)'));
           dCai(i)=(sum(B(i,1:8).*Ca(1:8)'));
        mt(i)=(Ca(i)+1/3*ba*qa(i))/(1+1/3*ba);
        dqa(i)=alpha*(sum(B(i,1:8).*qa(1:8)'))-h^2*mt(i);
        dCai(i)=sum(B(i,1:8).*Ca(1:8)')-
Beta*(sum(A(8,1:8).*qa(1:8)'));
            % product B
        qb(8)=3*(sum(W(1:8).*Cb(1:8)'));
        dCb8=-(3/v)*(sum(A(8,1:8).* Cb(1:8)'));
           if t==0
               Cb8=0;
           else
           Cb8=(dCb8+(3/v)*(sum(A(8,1:7).*Cbi(1:7')))/(-
3*A(8,8)/v);
           end
```

```
dqb(i)=alpha*(sum(B(i,1:8).*qb(1:8)'))+h^2*mt(i);
        dCbi(i)=sum(B(i,1:8).*Cb(1:8)')-
Beta*(sum(A(8,1:8).*qb(1:8)'));
end
dq=[dqa';dCai';dCa8';dqb';dCbi';dCb8'];
```

Script file:

```
clc;
tspan=[0 1];
alpha=1e3;
ba=1;
Beta=ba*alpha;
h=5;
v=10;
Bi=10;
q0=[zeros(1,14),1,zeros(1,15)];
[t,q]=ode15s(@macrorxnlimitedBi,tspan,q0,[],alpha,Beta,ba,h
,v,Bi);
% weight frations:
          W(1)=  .6723835E-02;
          W(2)=  .2451753E-01;
          W(3)=  .4701138E-01;
          W(4)=  .6589205E-01;
          W(5)=  .7358414E-01;
          W(6)=  .6571099E-01;
          W(7)=  .4254046E-01;
          W(8)=  .7352941E-02;
W8=W(8);
W2=W(1:7);
W1=W(1:8);
Ca=q(:,8:15);
m2=3*(W1*Ca');
qa=q(:,1:7);
m1=3*(W2*qa'+W8*m2);
ma=(m2+1/3*ba*m1)/(1+1/3*ba);
Cb=q(:,23:30);
m4=3*(W1*Cb');
qb=q(:,16:22);
m3=3*(W2*qb'+W8*m4);
mb=(m4+1/3*ba*m3)/(1+1/3*ba);
plot(t,ma,t,mb,'--')
```

A.12 Optimization of gas oil data using finite volume model:

Function file:

```
function
dq=limitingvolumewithproductsgasoil(t,q,h1,h2,h3,h4,h5,h6,h
7,alpha,Bi)
qai=q(1:7);
qa8=q(8);
qa=q(1:8);
qbi=q(9:15);
qb8=q(16);
qb=q(9:16);
qci=q(17:23);
qc8=q(24);
qc=q(17:24);
qdi=q(25:31);
qd8=q(32);
qd=q(25:32);
for i=1:7
        n=8;
        if t==0
            yd(i)=0;
        else
            yd(i)=qd(i)/(qa(i)+qb(i)+qc(i)+qd(i));
        end
        phi(i)=exp(-3.85*yd(i));
        rA=-h1^2*qai(i)^2;
        rB=h2^2*qai(i)^2-h3^2*qbi(i);
        rC=h4^2*qai(i)^2+h5^2*qbi(i);
        rD=h6^2*qai(i)^2+h7^2*qbi(i);
% reactant A
         dqa8=-(3/alpha)*(sum(A(n,1:n).* qa(1:n)'));
           if t==0
               qa8=1;
           else

%qa8=(dqa8+(3/alpha)*(sum(A(n,1:i).*qai(1:i)')))/(-
3*A(8,8)/alpha);
           qa8=(Bi-(sum(A(8,1:7).*qa(1:7'))))/(A(8,8)+Bi);
           end
           dqai(i)=(sum(B(i,1:n).*qa(1:n)'))+rA*phi(i);
% product B
         dqb8=-(3/alpha)*(sum(A(n,1:n).* qb(1:n)'));
           if t==0
               qb8=0;
```

```
            else

qb8=(dqb8+(3/alpha)*(sum(A(n,1:i).*qbi(1:i)')))/(-
3*A(8,8)/alpha);
            end
            dqbi(i)=(sum(B(i,1:n).*qb(1:n)'))+rB*phi(i);
% product C
          dqc8=-(3/alpha)*(sum(A(n,1:n).* qc(1:n)'));
            if t==0
                qc8=0;
            else

qc8=(dqc8+(3/alpha)*(sum(A(n,1:i).*qci(1:i)')))/(-
3*A(8,8)/alpha);
            end
            dqci(i)=(sum(B(i,1:n).*qc(1:n)'))+rC*phi(i);
% product D
          dqd8=-(3/alpha)*(sum(A(n,1:n).* qd(1:n)'));
            if t==0
                qd8=0;
            else

qd8=(dqd8+(3/alpha)*(sum(A(n,1:i).*qdi(1:i)')))/(-
3*A(8,8)/alpha);
            end
            dqdi(i)=(sum(B(i,1:n).*qd(1:n)'))+rD*phi(i);
end
dqai=dqai';
dqa8=dqa8';
dqbi=dqbi';
dqb8=dqb8';
dqci=dqci';
dqc8=dqc8';
dqdi=dqdi';
dqd8=dqd8';
dq=[dqai;dqa8;dqbi;dqb8;dqci;dqc8;dqdi;dqd8];
```

Optimization file:

```
function val=File2SSE(k)
h1=k(1);
h2=k(2);
h3=k(3);
h4=k(4);
h5=k(5);
h6=k(6);
h7=k(7);
```

```
%alpha=k(8);
alpha=5.003;
Bi=k(8);
texp=[0 3 5 7 10];
m1exp=[0.162 0.081 0.0660474 0.0573156 0.0479844];
m2exp=[0 0.0432054 0.0524556 0.0543834 0.0594054];
m3exp=[0 0.0474498 0.0513054 0.0601668 0.0671166];
m4exp=[0 0.003078 0.004617 0.005022 0.0055566];
tspan=texp;
V=53.94*10^-6; %Reactor volume in m^3
r=0.2*10^-6; %r in m for small catalyst
Mw1=330;
Mw2=115;
Mw3=48;
Mw4=800;
T0=450+273;
T1=525+273;
H1=-69.32e3;
H2=-54.32e3;
H3=-29.46e3;
R=8.314;
K10=26.56e-6;
K20=8.03e-6;
K30=3.426e-6;
K1=K10*exp(-H1/R*(1/T1-1/T0));
K2=K20*exp(-H2/R*(1/T1-1/T0));
K3=K30*exp(-H3/R*(1/T1-1/T0));
Vs=0.81*10^-3/827; % V of all catalysts in m3
N=Vs/((4/3)*pi*r^3);
%=(K1*V)/(N*(4/3)*pi*r^3);
q0=[zeros(1,7),1,zeros(1,24)];
[t,q]=ode15s(@limitingvolumewithproductsgasoil,tspan,q0,[],
h1,h2,h3,h4,h5,h6,h7,alpha,Bi);
          W(1)=  .6723835E-02;
          W(2)=  .2451753E-01;
          W(3)=  .4701138E-01;
          W(4)=  .6589205E-01;
          W(5)=  .7358414E-01;
          W(6)=  .6571099E-01;
          W(7)=  .4254046E-01;
          W(8)=  .7352941E-02;
n=8;
W=W(1:n);
C0=0.162/(Mw1*V);
m0=K1*C0;
q1=q(:,1:8);
m1=3*(W*q1');
```

```
q2=q(:,9:16);
m2=3*(W*q2');
q3=q(:,17:24);
m3=3*(W*q3');
q4=q(:,25:32);
m4=3*(W*q4');
m11=m1*Mw1*V*m0/K1;
m22=m2*Mw2*V*m0/K1;
m33=m3*Mw3*V*m0/K1;
m44=m4*Mw4*V*m0/K1;
resid1=((m11(1)-m1exp(1))./m1exp(1))^2+((m11(2)-
m1exp(2))./m1exp(2))^2+((m11(3)-
m1exp(3))./m1exp(3))^2+((m11(4)-
m1exp(4))./m1exp(4))^2+((m11(5)-m1exp(5))./m1exp(5))^2;
resid2=((m22(1)-m2exp(1)))^2+((m22(2)-
m2exp(2))./m2exp(2))^2+((m22(3)-
m2exp(3))./m2exp(3))^2+((m22(4)-
m2exp(4))./m2exp(4))^2+((m22(5)-m2exp(5))./m2exp(5))^2;
resid3=((m33(1)-m3exp(1)))^2+((m33(2)-
m3exp(2))./m3exp(2))^2+((m33(3)-
m3exp(3))./m3exp(3))^2+((m33(4)-
m3exp(4))./m3exp(4))^2+((m33(5)-m3exp(5))./m3exp(5))^2;
resid4=((m44(1)-m4exp(1)))^2+((m44(2)-
m4exp(2))./m4exp(2))^2+((m44(3)-
m4exp(3))./m4exp(3))^2+((m44(4)-
m4exp(4))./m4exp(4))^2+((m44(5)-m4exp(5))./m4exp(5))^2;
val=sqrt(resid1+resid2+resid3+resid4)
```

Script file:

```
% limting volume, 4 products
clc;
T0=450+273;
T1=525+273;
H1=-69.32e3;
H2=-54.32e3;
H3=-29.46e3;
R=8.314;
K10=26.56e-6;
K20=8.03e-6;
K30=3.426e-6;
K1=K10*exp(-H1/R*(1/T1-1/T0));
K2=K10*exp(-H2/R*(1/T1-1/T0));
K3=K10*exp(-H3/R*(1/T1-1/T0));
texp=[0 3 5 7 10];
m1exp=[0.162 0.081 0.0660474 0.0573156 0.0479844];
```

```
m2exp=[0 0.0432054 0.0524556 0.0543834 0.0594054];
m3exp=[0 0.0474498 0.0513054 0.0601668 0.0671166];
m4exp=[0 0.003078 0.004617 0.005022 0.0055566];
tspan=[0 10];
V=53.94*10^-6; %Reactor volume in m^3
r=0.2*10^-6; %r in m for small catalyst
D=6e-14; %diffusivity of gas oil at 525
Mw1=330;
Mw2=115;
Mw3=48;
Mw4=800;
C0=0.162/(Mw1*V);
m0=K1*C0
q0=[zeros(1,7),1,zeros(1,24)];
h1=1; %initial  guess
h2=2; %initial  guess
h3=0.5; %initial  guess
h4=3;
h5=0.2;
h6=0.2;
h7=0.02;
alpha=5.003;
Bi=10;
k=[h1 h2 h3 h4 h5 h6 h7 Bi];
options=optimset('MaxFunEvals',10000000,'MaxIter',10000000)
;
[k SEEmin]=fmincon(@File2SSE,k,[],[],[],[],[0 0 0 0 0 0 0
5],[]);
h1=k(1)
h2=k(2)
h3=k(3)
h4=k(4)
h5=k(5)
h6=k(6)
h7=k(7)
Bi=k(8)
%alpha=k(8)
[t,q]=ode15s(@limitingvolumewithproductsgasoil,tspan,q0,[],
h1,h2,h3,h4,h5,h6,h7,alpha,Bi);
% weight frations:
          W(1)=  .6723835E-02;
          W(2)=  .2451753E-01;
          W(3)=  .4701138E-01;
          W(4)=  .6589205E-01;
          W(5)=  .7358414E-01;
          W(6)=  .6571099E-01;
          W(7)=  .4254046E-01;
```

```
          W(8)=  .7352941E-02;
n=8;
W=W(1:n);
C0=0.162/(Mw1*V);
m0=K1*C0
q1=q(:,1:8);
m1=3*(W*q1');
q2=q(:,9:16);
m2=3*(W*q2');
q3=q(:,17:24);
m3=3*(W*q3');
q4=q(:,25:32);
m4=3*(W*q4');
m11=m1*Mw1*V*m0/K1;
m22=m2*Mw2*V*m0/K1;
m33=m3*Mw3*V*m0/K1;
m44=m4*Mw4*V*m0/K1;
plot(t,m11,'-k',t,m22,'-.k',t,m33,'--k',t,m44,':k')
hold on
plot(texp,m1exp,'ok',texp,m2exp,'*k',texp,m3exp,'sk',texp,m
4exp,'+k')
legend('Gas oil','Gasoline','Light gases','Coke','Gas oil
exp','Gasoline exp','Light gases exp','Coke exp')
title('Masses of 4 lump components using external fluid
film resistance model')
xlabel('time (s)')
ylabel('Mass (g)')
```

Appendix B: Checking the Numerical Solution

The numerical solution using orthogonal collocation depends on the number of orthogonal points. As the number of points increases, the solution reaches the exact solution. After this point adding more orthogonal points will not enhance the solution.

In this thesis, the number of collocation points were chose to be 7 points. This Appendix will compare the solution using 7 points with the solution using 14 points to check if the solutions obtained were the exact solutions. Although all cases were checked, only few cases are shown here as a sample.

Figures B.1 through B.3 shows that the solution obtained using 7 orthogonal points is exact.

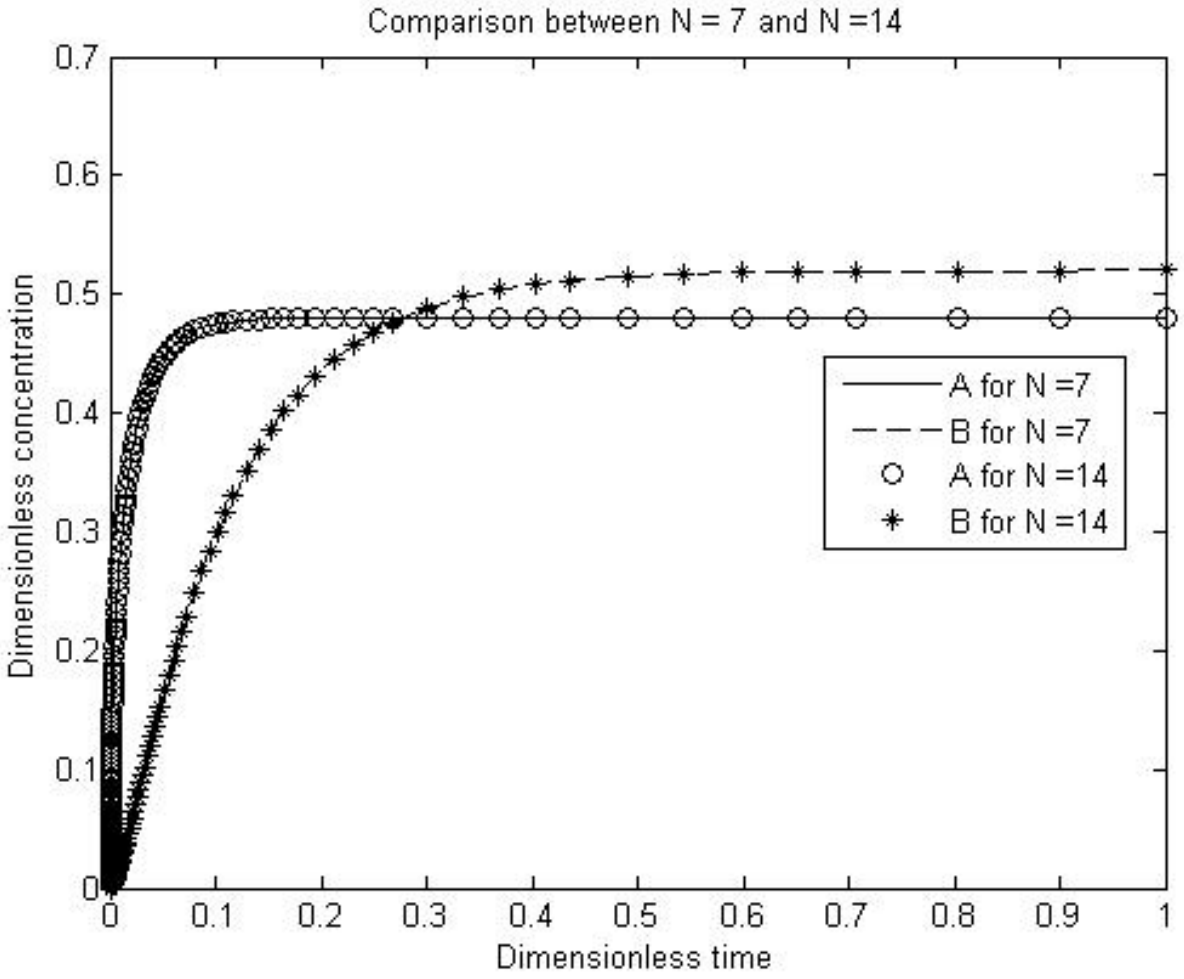

Figure B.1: Comparison between N =7 and N =14 for linear infinite volume system

($\varphi = 5$)

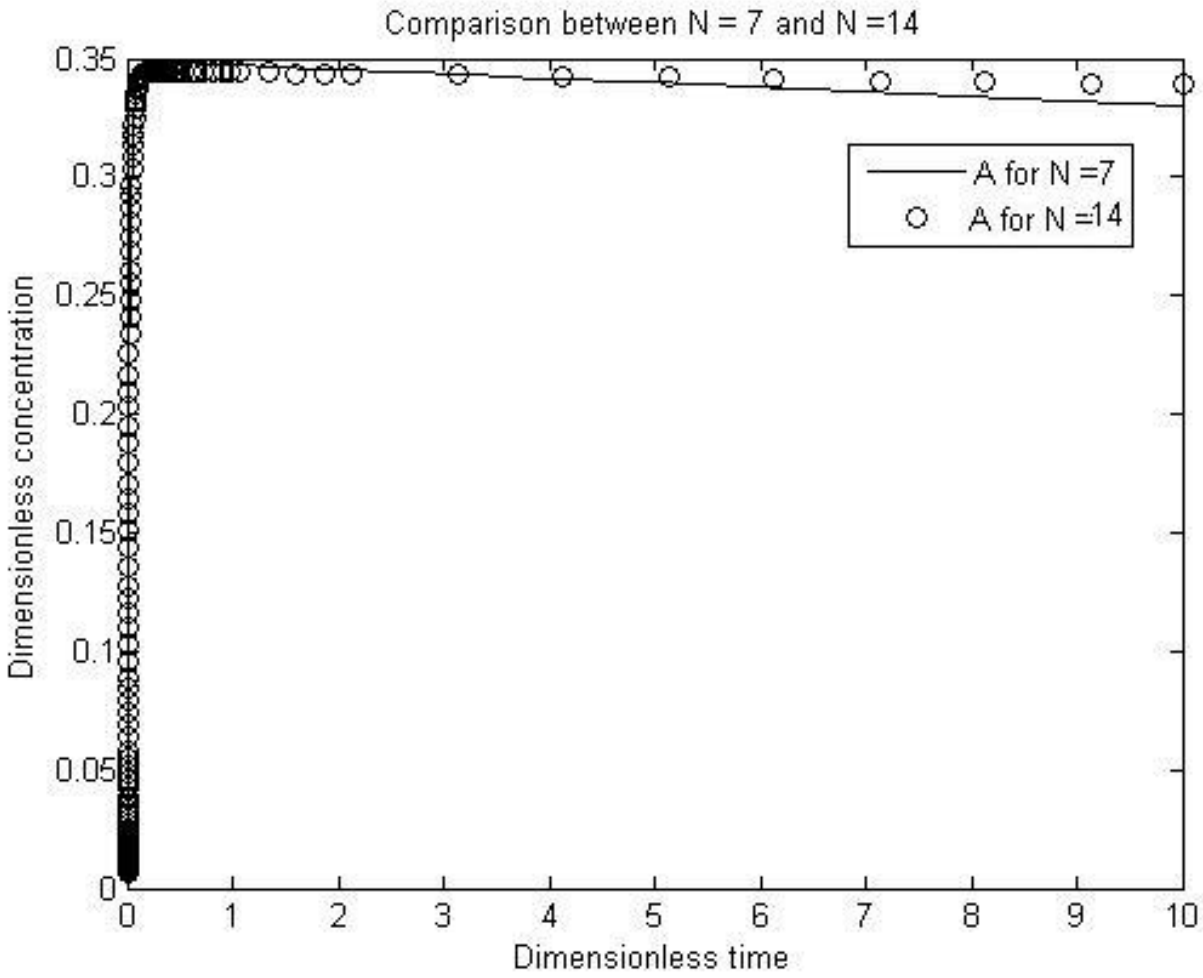

Figure B.2: Comparison between N =7 and N =14 for linear finite volume system

($\varphi = 5,\ \Lambda = 100\ and\ Bi_m = 10$)

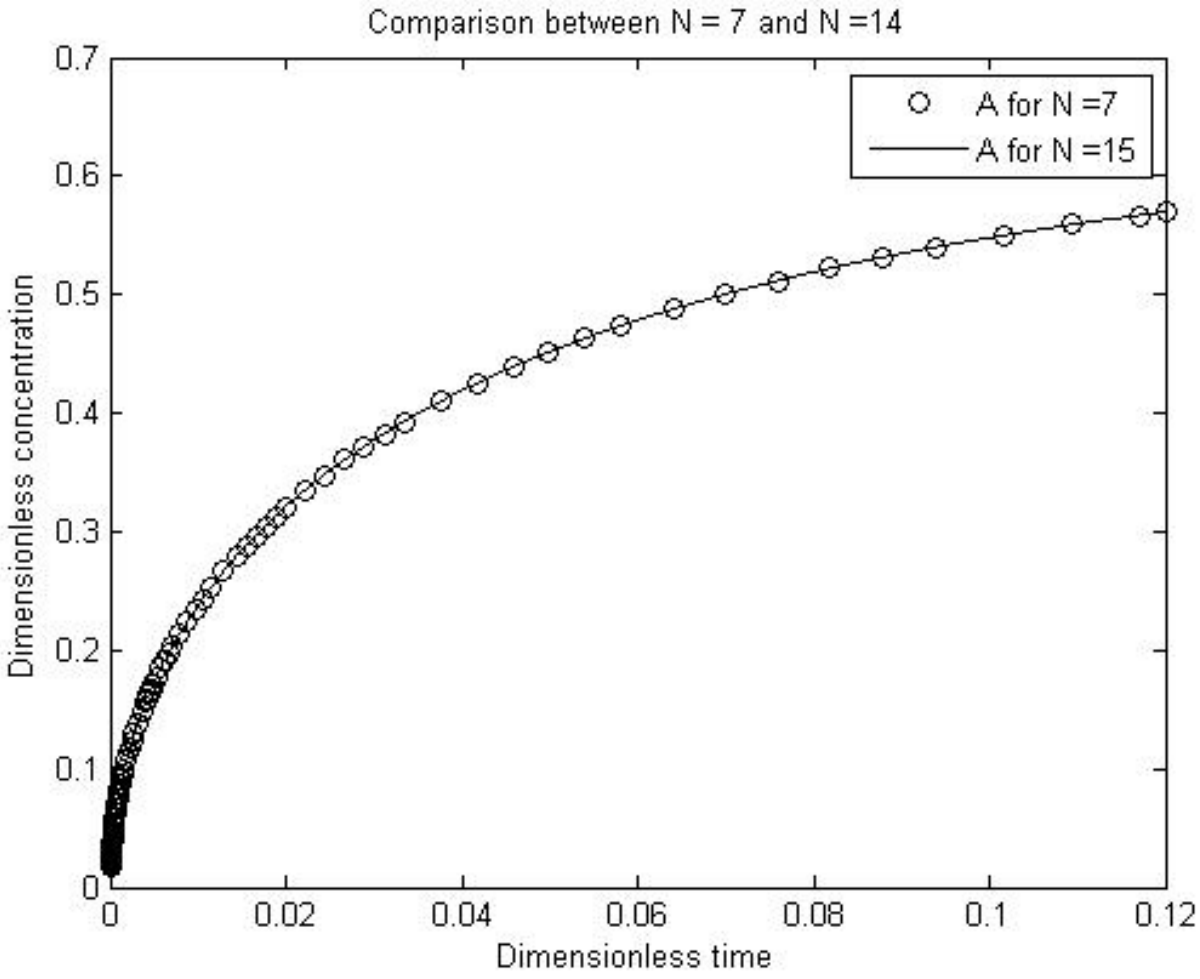

Figure B.3: Comparison between N =7 and N =14 for linear infinite volume system with active matrix

$$\left(\varphi = 5, \alpha = 10^3, \frac{\beta}{\alpha} = 1\right)$$

Vita

Wafa Mahaly, originally from Yemen, was born on July, 30, 1989 in Abu Dhabi, UAE. She was educated in public schools and graduated from Al-Wahdah secondary school in 2007 with an average of 99.3%. She received a scholarship from Abu Dhabi crown prince office to attend the American University of Sharjah. She graduated in 2011 with Magna cum laude. Her degree is a Bachelor of Science in Chemical Engineering with a minor in Petroleum Engineering.

In 2012, she was awarded full scholarship from the American University of Sharjah to continue her studies in Chemical Engineering. She worked as a teaching assistant during her master studies.